



Delft University of Technology

Wave-induced vibrations of flood gates modelling, experimentation and design

Tieleman, O.C.

DOI

[10.4233/uuid:ca37004a-ef93-4d31-b451-35b7079f0ec9](https://doi.org/10.4233/uuid:ca37004a-ef93-4d31-b451-35b7079f0ec9)

Publication date

2022

Document Version

Final published version

Citation (APA)

Tieleman, O. C. (2022). *Wave-induced vibrations of flood gates: modelling, experimentation and design*. [Dissertation (TU Delft), Delft University of Technology]. <https://doi.org/10.4233/uuid:ca37004a-ef93-4d31-b451-35b7079f0ec9>

Important note

To cite this publication, please use the final published version (if applicable).
Please check the document version above.

Copyright

Other than for strictly personal use, it is not permitted to download, forward or distribute the text or part of it, without the consent of the author(s) and/or copyright holder(s), unless the work is under an open content license such as Creative Commons.

Takedown policy

Please contact us and provide details if you believe this document breaches copyrights.
We will remove access to the work immediately and investigate your claim.

An abstract graphic at the top of the cover featuring overlapping, wavy shapes in various shades of blue, creating a sense of movement and depth, reminiscent of water or waves.

WAVE-INDUCED VIBRATIONS OF FLOOD GATES

MODELLING, EXPERIMENTATION AND DESIGN

An aerial photograph of a coastal area, showing a mix of dark, rocky terrain and lighter, sandy or silty areas. The water is a deep blue, and the overall scene is captured from a high angle, providing a clear view of the coastline and surrounding land.

O.C. TIELEMAN

WAVE-INDUCED VIBRATIONS OF FLOOD GATES

MODELLING, EXPERIMENTATION AND DESIGN

Orson Cosmo TIELEMAN

WAVE-INDUCED VIBRATIONS OF FLOOD GATES

MODELLING, EXPERIMENTATION AND DESIGN

Proefschrift

ter verkrijging van de graad van doctor
aan de Technische Universiteit Delft,
op gezag van de Rector Magnificus prof. dr. ir. T.H.J.J. van der Hagen,
voorzitter van het College voor Promoties,
in het openbaar te verdedigen op dinsdag 28 juni 2022 om 15:00 uur

door

Orson Cosmo TIELEMAN

civiel ingenieur, Technische Universiteit Delft, Nederland
geboren te Amsterdam, Nederland.

Dit proefschrift is goedgekeurd door de

promotor: prof. dr. ir. S.N. Jonkman

promotor: dr. ir. B. Hofland

copromotor: dr. ir. A. Tsouvalas

Samenstelling promotiecommissie:

Rector Magnificus,

Prof. dr. ir. S.N. Jonkman,

Dr. ir. B. Hofland,

Dr. ir. A. Tsouvalas,

voorzitter

Technische Universiteit Delft

Technische Universiteit Delft

Technische Universiteit Delft

Onafhankelijke leden:

Prof. dr. ir. O. Doaré,

Prof. dr. ir. R.D.J.M. Steenbergen,

Prof. dr. A.V. Metrikine,

Prof. dr. ir. M.R.A. van Gent,

Prof. dr. ir. A.J.H.M. Reniers

ENSTA Paris

Universiteit Ghent / TNO

Technische Universiteit Delft

Technische Universiteit Delft

Technische Universiteit Delft, reservelid



Rijkswaterstaat
Ministerie van Infrastructuur en Milieu

Cover by: A.C. Becker

Printed by: Ridderprint

Keywords: Dynamics, Fluid-structure interaction, Wave impacts, Flood gates, Modelling, Experimentation, Design, Vibrations, Semi-analytical, Mode matching, Fatigue, Overhang

Copyright © 2020 by O.C. Tieleman

ISBN 978-94-6384-349-2

An electronic version of this dissertation is available at

<https://repository.tudelft.nl/>.

SUMMARY

Flood gates form an essential part of many flood defence systems in coastal areas. During storm events, flood gates may be subjected to a number of extreme loads from various sources, such as waves, water flow, earthquakes, wind and tides. Such time-varying loads lead to a dynamic response of the gate structure. This results in structural stresses that may ultimately cause failure. This research addresses wave-induced dynamic behaviour of flood gates. Wave impacts on flood gates may occur as a consequence of wave breaking due to shoaling or due to wave overtopping. Furthermore, confined wave impacts may occur due to the presence of an overhanging structure. The incoming waves in those cases hit the overhang during their upward motion when reaching the structure and lead to high impact loads on the overhang and the flood gate. A key example where such wave impacts are relevant is the Afsluitdijk in the Netherlands. The discharge sluices of this dam contain over fifty large scale vertical lifting flood gates. As part of an ongoing renovation project, these gates will be replaced and additional discharge sluices will be realised.

Wave impacts lead to high peak pressures of short duration that can yield a dynamic response of the flood gate. This dynamic response is governed by a complex interaction between the structure and fluid. Due to the complexity involved in solving fluid-structure interaction problems, it is common engineering practice to design and assess these gates based on a simplified quasi-static approach. A dynamic amplification factor is then applied to account for the effect of the vibrations, which is derived from a single degree of freedom representation of the structure. Such an approach lacks the precision to capture the three-dimensional vibration behaviour of a gate-fluid system and can lead to overdimensioned but possibly also unsafe designs. Advanced finite element methods able to deal with the coupled fluid-structure interaction problem in complex three-dimensional geometries do exist. However, these models are computationally expensive and therefore do not allow for the large number of simulations necessary to test various parameters and boundary conditions or to perform probabilistic evaluations and fatigue assessments. This study aims to develop a method to predict the dynamic behaviour of flood gates under wave impact loading for design and safety assessments, that overcomes both the lack of accuracy involved with existing engineering methods and the high computational costs of numerical finite element models. This aim is addressed in three main parts: (i) modelling of the dynamic behaviour of the immersed flood gates, (ii) experiments of wave impacts on flood gates and (iii) improved design methods for flood gates subjected to wave impacts.

In the first part, it is shown that the fluid-structure interaction involved with vertical flood gate vibrations can be modelled successfully and efficiently by a semi-analytical mode matching approach. Within this mode matching method, the gate vibrations are first expressed in terms of in-vacuo modes while the liquid motion is described as a superposition of linear potentials. A semi-analytical solution is then derived for

the response of the coupled system to any time-varying force. The fluid-structure interaction model is made suitable for situations of increasing levels of complexity in several development steps. In the most basic form, the gate is modelled as a thin plate and assumed to be situated in an infinitely long discharge sluice. It is then shown that also composite fluid domains can be represented accurately by extending the analytical fluid-structure interaction solution, such that situations can be represented in which the gate is situated in a sluice of limited length or in which an overhanging structure is present that causes confined wave impacts. Finally, the semi-analytical method is coupled to a finite element model to enable a detailed prediction of the structural stresses for more realistic gate designs consisting of a front plate supported by horizontal and vertical stiffeners. The final version of the developed fluid-structure interaction model is available on the 4TU research repository (Tieleman, 2022, [link](#)).

The model improves the existing quasi-static design method with amplification factor on several aspects. The model predicts the two-way fluid-structure interaction taking into account both the effect of surface waves and compressibility on the hydrodynamic response. Moreover, the fluid-structure interaction model includes higher mode behaviour of the structure. By means of a design optimization case study, it is demonstrated that the model can be effectively applied in the design of flood gates under wave impact loading and may lead to substantially different designs than existing quasi-static methods, better adjusted to the dynamic behaviour of the structure. The main benefit of the developed model approach compared to existing finite element methods is its computational efficiency in solving the two way fluid-structure interaction. A comparison of the model with conventional finite element software proves to give similar results at only a fraction of the computational time of the latter.

In the second part of the thesis, scale experiments of confined wave impacts on flexible gate structures with an overhang are presented. These experiments entailed regular and irregular test conditions for various water levels and supporting static loading and hammer impact tests. The experimental approach is an extension of previous experiments of wave impacts on a rigid wall (De Almeida and Hofland, 2020b, 2021). This allows a direct comparison with the results of those studies, isolating the effect of the flexibility of the structure. A first validation of the developed fluid-structure interaction model is carried out by comparison to the measurements, with the aim to investigate whether most of the relevant physical phenomena that govern the response of flood gates to wave impacts are covered. Main assumptions of the developed modelling framework are amongst others that the wave impact may be modelled as an external load and the the presence of air can be accounted for in the prediction of this external load. Some differences between the model predictions of the dynamic response of the gates and the measurements are found, mainly regarding the dominant response frequencies of the gates and the magnitude and damping of the higher mode vibrations. However, overall the predictions show good agreement with the measurements providing a first verification that the main assumptions of the developed framework are acceptable. The experiments also provide an indication of the amount of damping for these type of problems, although more research is needed to predict the amount of damping from various sources for practical applications. The experiments additionally result in a valuable dataset, made publicly available for research on the 4TU repository (Tieleman et al., 2022a, [link](#)). The

regular wave impact tests may for instance be utilized to further study the effect of phenomena such as air entrapment and air entrainment on the response of the fluid-structure system. The irregular wave tests closely match realistic conditions and can for example be used to further validate the probabilistic design approaches presented in this thesis.

The third part of the thesis focuses on the design and assessment of flood gates. First, the effect of both compressibility and surface waves on the hydrodynamic pressures during gate vibrations is studied. Results show that for typical flood gate dimensions and excitation frequencies both surface waves and compressibility are important. Dimensionless values for the added mass and damping including the effect of compressibility and surface waves are presented for gates of various boundary conditions. These coefficients can be used in existing preliminary design methods when the problem under consideration allows for such a simplified representation of the interaction between the structure and fluid. Two methods are then presented for the design or assessment of flood gates subjected to wave impacts. The first method regards the safety of the flood gate based on the failure criterion of exceeding the maximum yield stress in the structure, while the second method is aimed at predicting the fatigue lifetime of the flood gate. Within these methods, a large number of simulations is performed either for a single design storm or for every combination of water level and wind conditions expected over the lifetime of the structure. Recently validated pressure-impulse theory is employed to predict the wave impact loads on the gate. The free surface elevation, wave impact duration and impact impulse are all considered stochastically. Predicting the dynamic response to every single wave during a governing design storm or over the lifetime of the structure is a novelty within the field of hydraulic engineering. At least when no concessions are made on the accuracy of the physical modelling of the involved fluid-structure interaction processes. The computational efficiency of the developed semi-analytical model enables such analyses.

The developed design methods and underlying fluid-structure interaction model are applied to several case studies inspired by the situation at the Afsluitdijk. It is shown that several aspects not captured in common existing design methods are crucial in the design of flood gates under wave impact loading. First, higher modes show to have a significant impact on the maximum stress occurring for typical flood gates subjected wave impacts. For fatigue damage, the higher modes even turned out to be governing in the case study. Second, the wave impact with the highest peak pressure is often assumed to be governing in present design practice. However, the governing response of the flood gate proves to be dominated mainly by the magnitude of the pressure impulse of the wave impact. Third, gate vibrations may not fully damp out between wave impacts depending on the time between impacts and the amount of damping in the system. The sequence and exact moment of wave impacts therefore influence the maximum response of the flood gate. Above effects are captured well within the presented design methods. Consequently, implementation of these design methods will lead to safer design and assessment of flood gates.

SAMENVATTING

Waterkerende schuiven maken een essentieel onderdeel uit van de kustverdediging. Tijdens stormen zijn deze schuiven onderhevig aan extreme krachten afkomstig van golven, stroming, aardbevingen, wind en getijden. Zulke krachten variëren in de tijd en kunnen daarmee een dynamische reactie van de schuif veroorzaken. Dat resulteert in spanningen en in het uiterste geval in falen van de constructie. Dit onderzoek is gericht op het dynamisch gedrag van waterkerende schuiven als gevolg van golfklapbelastingen. Zulke golfklappen kunnen bijvoorbeeld optreden door brekende of overslaande golven. Daarnaast kunnen golfklappen ontstaan wanneer deze in de loop van hun opwaartse beweging tegen overhangende constructiedelen aanslaan. Dat leidt tot grote krachten op het betreffende constructieonderdeel, maar ook op de aangrenzende waterkerende schuif. De Afsluitdijk in Nederland is een voorbeeld van een project waarin dit type golfklappen een belangrijke rol speelt. De spuisluizen van de Afsluitdijk bevatten meer dan vijftig verticale hefschuiven. In een lopend renovatieproject zullen deze schuiven worden vervangen en zullen er een nieuwe spuisluizen met schuiven worden gerealiseerd.

De kortdurende piekdrukken gemoeid met golfklappen leiden tot een dynamische reactie van de schuif. Daarbij treedt een complex interactieproces op tussen de constructie en de vloeistof. Vanwege deze complexiteit worden in de praktijk vaak vereenvoudigde quasi-statische methoden toegepast voor het ontwerpen en beoordelen van waterkerende schuiven. Het effect van trillingen wordt daarin meegenomen aan de hand van een dynamische amplificatiefactor, afgeleid van een model waarin de constructie is vereenvoudigd tot een enkelvoudig massa-veersysteem. Deze aanpak heeft niet de nauwkeurigheid benodigd om het driedimensionale gedrag van het systeem te vatten en kan daardoor leiden tot suboptimale maar ook onveilige ontwerpen. Geavanceerde eindige-elementenmethoden die in staat om driedimensionale gekoppelde vloeistof-constructie interactieproblemen op te lossen, bestaan wel, maar vragen veel numerieke rekenkracht. Uitvoeren van een groot aantal simulaties, nodig voor het toetsen van een brede set ontwerpparameters en randvoorwaarden, probabilistische veiligheidsbeoordelingen en vermoeiingsanalyses, is daardoor niet mogelijk. De doelstelling van dit onderzoek is het ontwikkelen van een in ontwerp en waterveiligheidsbeoordelingen toepasbare methode om het dynamisch gedrag van waterkerende schuif onder golfklapbelasting te voorspellen, die de beperkingen overkomt in zowel de nauwkeurigheid van bestaande praktische methoden als in de benodigde rekenkracht van eindige-elementenmethoden. Het onderzoek bestaat daartoe uit drie delen: (i) modelleren van het dynamisch gedrag van schuiven in water, (ii) experimenten van golfklappen op elastische schuiven en (iii) ontwerpmethoden voor schuiven onder golfklapbelastingen.

Het eerste deel toont aan dat het mogelijk is om de vloeistof-constructie-interactie gemoeid met trillingen van verticale waterkerende schuiven nauwkeurig en efficiënt te modelleren op basis van een semi-analytische aanpak. Binnen deze aanpak worden

de trillingen van de schuif eerst uitgedrukt in termen van de droge eigenmodes van de constructie en de vloeistofstroming als een superpositie van lineaire potentialen. Vervolgens wordt op basis daarvan een semi-analytische oplossing afgeleid voor de reactie van het gekoppelde systeem op een in de tijd variërende kracht. Het semi-analytische model is in een aantal ontwikkelingsstappen geschikt gemaakt voor situaties met toenemende complexiteit. De schuif is eerst gemodelleerd als een dunne plaat in een oneindig lang veronderstelde spuisluis. Vervolgens is aangetoond dat de semi-analytische aanpak ook toepasbaar is op situaties met samengestelde vloeistofdomeneinen, zoals schuiven in een spuisluis met beperkte lengte of een overhang die golfklappen veroorzaakt. Ten slotte is het semi-analytische model gekoppeld aan een eindige-elementenmodel om een gedetailleerde voorspelling van de spanningen mogelijk te maken voor realistischere schuifontwerpen bestaande uit een voorplaat en verstijvers. Het model is beschikbaar op de 4TU repository (Tieleman, 2022, [link](#)).

Het model verbetert de bestaande quasi-statische ontwerpmethodode met amplificatiefactor op een aantal punten. Ten eerste houdt het rekening met de volledige gekoppelde vloeistof-constructie-interactie inclusief het effect van oppervlaktegolven en compressibiliteit op de hydrodynamische respons. Daarnaast neemt het model trillingen van hogere eigenmodes van de constructie mee. Uit een optimalisatiestudie blijkt dat het model effectief kan worden toegepast voor het ontwerp van waterkerende schuiven onder golfklapbelastingen en tot substantieel andere optimale ontwerpen leidt dan de bestaande methoden, meer afgestemd op het dynamische gedrag van de constructie. Het voornaamste voordeel van de ontwikkelde aanpak in vergelijking met eindige-elementenmethoden is de numerieke efficiëntie waarmee de vloeistof-constructie interactie wordt voorspeld. Een vergelijking met een conventioneel eindige-elementenprogramma toont aan dat het model soortgelijke resultaten oplevert in een fractie van de rekentijd.

Het tweede deel van dit proefschrift presenteert de resultaten van schaalexperimenten van golfklappen op elastische schuiven met een overhangende constructie. Deze experimenten bestonden uit proeven met regelmatige en onregelmatige golven bij verschillende waterstanden en ondersteunende proeven met een statische belasting en hamerklappen. De aanpak voor de experimenten lag in het verlengde van voorgaande experimenten met golfklappen op een inelastische muur door (De Almeida and Hofland, 2020b, 2021). Dat maakt een directe vergelijking met de resultaten van die studies mogelijk om zo het effect van het dynamisch gedrag van de constructie expliciet te maken. Op basis van de resultaten van de experimenten is er een eerste validatiestudie uitgevoerd voor de ontwikkelde modelaanpak om te onderzoeken of deze de meest bepalende fysische processen voldoende afdekt. De voornaamste aannames van de ontwikkelde modelaanpak zijn dat het mogelijk is om de golfklapbelasting te modelleren als externe kracht en om het effect van eventuele luchtinsluitingen mee te nemen in de voorspelling van die kracht. De modelvoorspellingen voor de dynamische reactie van de schuiven verschillen op een aantal punten van de metingen, vooral wat betreft de reactiefrequenties van de schuiven en de omvang en demping van hogere trillingsmodes. Voor een groot deel komen de voorspellingen en metingen echter goed overeen. Dat biedt een eerste verificatie van de geldigheid van de genoemde aannames van de modelaanpak. De experimenten geven verder een indicatie van de omvang van de demping voor dit type probleem, al is er meer onderzoek nodig om de demping afkomstig van verschillende

bronnen te kunnen voorspellen voor praktische toepassingen. Ten slotte leveren de experimenten een waardevolle dataset op voor verder onderzoek, beschikbaar op de 4TU repository (Tieleman et al., 2022a, [link](#)). Zo kunnen de proeven met regelmatige golfklappen worden benut voor verder onderzoek naar de effecten van luchtinsluitingen en luchtbellen. De proeven met onregelmatige golven sluiten beter aan bij werkelijke ontwerpcondities en kunnen bijvoorbeeld gebruikt worden om de probabilistische ontwerpmethoden in dit proefschrift verder te valideren.

Het derde deel van dit proefschrift richt zich op het ontwerp en de beoordeling van waterkerende schuiven. Eerst wordt het effect van zowel oppervlaktegolven als compressibiliteit op de hydrodynamische drukken onderzocht. De resultaten tonen aan dat voor typische schuifafmetingen en excitatiefrequenties beide effecten van belang zijn. Voor schuiven met verschillende opleggingen zijn er dimensieloze coëfficiënten afgeleid voor de toegevoegde massa en demping, te gebruiken in bestaande ontwerpmethoden wanneer deze toepasbaar zijn. Vervolgens worden er twee geavanceerdere methodes gepresenteerd voor het ontwerp en de beoordeling van waterkerende schuiven onder golfklapbelastingen. De eerste methode gaat in op de betrouwbaarheid van schuiven met als faalmechanisme het overschrijden van de vloeispanning. De tweede methode richt zich op de vermoeiingslevensduur van schuiven. Binnen deze methoden wordt een groot aantal simulaties uitgevoerd van de ontwerpstorm of zelfs van elke verwachte combinatie van waterstanden en windcondities gedurende de levensduur van de schuif. Een recent gevalideerde theorie gericht op de stootkracht van de golfklappen is benut om de golfklapbelastingen op de schuif theoretisch te voorspellen. De ontwerpmethoden beschouwen de inkomende golven, kladduren en stootkracht stochastisch. Het voorspellen van de dynamische reactie van een waterkerende schuif voor iedere golf gedurende een ontwerpstorm of zelfs over de levensduur van de constructie is nieuw binnen de waterbouwkunde, in ieder geval zonder concessies te doen aan de nauwkeurigheid in het voorspellen van het vloeistof-constructie-interactieproces. De numerieke efficiëntie van het ontwikkelde semi-analytische model maakt zulke analyses mogelijk.

De ontwikkelde ontwerpmethoden en het onderliggende semi-analytische model zijn toegepast op verschillende casestudies geïnspireerd door de situatie van de Afsluitdijk. Deze laten zien dat een aantal aspecten, cruciaal voor het ontwerpen van waterkerende schuiven onder golfklapbelastingen, ontbreken in de bestaande ontwerpmethoden. Ten eerste blijken hogere modes een significante invloed te hebben op de optredende spanningen voor typische schuiven onder golfklapbelastingen. Voor vermoeiingsschade waren de hogere modes zelfs maatgevend in de casestudie. Ten tweede wordt in de huidige ontwerppraktijk vaak aangenomen dat de golfklap met de hoogste piekdruk maatgevend is. Het maatgevende dynamische gedrag van de schuiven bleek echter met name te worden bepaald door de golfklappen met de grootste stoot. Ten derde dempen trillingen niet in alle gevallen volledig uit tussen golfklappen, afhankelijk van de tijd daartussen en de mate van demping in het systeem. Als gevolg daarvan zijn de volgorde en de precieze momenten van opeenvolgende golfklappen van belang voor de uitkomst van de analyses. De ontwikkelde methoden nemen de genoemde effecten wel mee. Implementatie daarvan zal daarom leiden tot veiligere ontwerpen en beoordelingen van waterkerende schuiven.

CONTENTS

Summary	i
Samenvatting	v
1 Introduction	1
1.1 Background	2
1.2 Problem description	3
1.3 Research aim and scope.	6
1.4 Methodology and outline	7
1.5 DynaHicS research program	9
2 A semi-analytical approach to predict flood gate vibrations	11
2.1 Introduction	12
2.2 Description of the fluid-structure interaction problem	15
2.3 Theoretical formulation of the problem.	16
2.4 Solution to the fluid-structure interaction problem	18
2.5 Quantitative analysis of a wave impact on a flood gate	25
2.6 Performance of the model	34
2.7 Conclusion	35
3 Extending the semi-analytical approach for composite fluid domains	37
3.1 Introduction	38
3.2 Description of the fluid-structure response problem	39
3.3 Theoretical formulation of the problem.	41
3.4 Solution to the fluid-structure interaction problem	42
3.5 Performance of the solution.	45
3.6 Conclusion	50
4 Coupling the semi-analytical approach to a finite element model	51
4.1 Introduction	52
4.2 Description of the gate and fluid model.	54
4.3 Theoretical formulation of the problem.	56
4.4 Solution to the fluid-structure interaction problem	58
4.5 Numerical evaluation of the solution	60
4.6 Performance of the model	61
4.7 Parametric optimization of a flood gate design	67
4.8 Discussion	76
4.9 Conclusion	77

5	An experimental study of wave impacts on a flood gate	79
5.1	Introduction	80
5.2	Experimental set-up	81
5.3	Experimental test series.	88
5.4	Preliminary validation of the semi-analytical model	92
5.5	Discussion	100
5.6	Conclusion	103
6	Effect of compressibility and surface waves	105
6.1	Introduction	106
6.2	Model geometry and theoretical description	107
6.3	Hydrodynamic pressures for a horizontally vibrating gate	109
6.4	Added mass for various flexible gates	113
6.5	Conclusion	116
7	Assessing the safety of flood gates subjected to wave impacts	117
7.1	Introduction	118
7.2	Modelling framework for a probabilistic approach	119
7.3	Statistical approach for wave impact loads	121
7.4	Predicting the failure probability of the gate	125
7.5	Case study of wave impacts at the Afsluitdijk	127
7.6	Conclusion	135
8	Assessing fatigue of flood gates due to wave impacts	137
8.1	Introduction	138
8.2	System description	140
8.3	Predicting the dynamic response for a single load event	142
8.4	Probabilistic lifetime analysis	149
8.5	Case study of wave-induced fatigue of a flood gate	154
8.6	Discussion	166
8.7	Conclusions.	168
9	Discussion	171
9.1	Validity of the developed methods	172
9.2	Other applications and implementation	177
10	Conclusions and recommendations	181
10.1	Conclusions.	182
10.2	Recommendations	186
	References	189
	List of publications	199
	Curriculum vitae	201
	Acknowledgements	203



1

INTRODUCTION

1.1 BACKGROUND

A significant proportion of the world population lives in coastal and delta areas. Flood defence systems are critical in protecting many of these areas against catastrophic events. Flood gates form an essential part of many flood defence systems in coastal areas as they regulate the discharge between water bodies and prevent the hinterland from flooding during storm events (Erdbrink, 2014). These gates are in open position during regular conditions and close in case of high tide or storm conditions. Various types of flood gates exist such as lifting, mitre, sliding, radial flap, sector and visor gates. Figure 1.1 shows several examples of storm surge barriers with flood gates. Many existing flood defence structures worldwide are close to reaching the end of their lifetime and will need to be renovated in the near future. These structures must also be adapted to the more severe climate conditions expected due to climate change. Moreover, sea level rise and land subsidence are expected to increase the worldwide need for these type of flood protection systems. This poses a great design task for hydraulic engineers in the coming decades.



(a) Haringvlietsluisen, NL (ref: Rijkswaterstaat)



(b) Thames Barrier, UK (ref: istockphoto)



(c) Emssperrwerk, DE (ref: Frank Vincentz)



(d) Eidersperrwerk, DE

Figure 1.1: Several examples of flood defences with gates

During storm events, flood gates may be subjected to a number of extreme loads from various sources, such as waves, water flow, earthquakes, wind and tides. Such time-varying loads lead to a dynamic response of the gate structure. Especially flow-induced and wave-induced dynamic responses of flood gates have shown to be relevant for design and safety assessment purposes (Naudascher and Rockwell, 1994; Kolkman and Jongeling, 2007a,b). This research focuses on wave-induced dynamic behaviour of flood gates. Wave impacts on flood gates may occur as a consequence of wave breaking due to shoaling or

due to wave overtopping. Furthermore, confined wave impacts may occur due to presence of an overhanging structure (De Almeida and Hofland, 2020b). The incoming waves in those cases hit the overhang during their upward motion when reaching the structure, for some situations after being reflected at the vertical gate, and lead to high impact loads on the overhang and the adjacent flood gate. Examples of coastal structures where an overhang is present in front of the gate are culverts or dewatering sluices with a bridge deck on top. De Almeida et al. (2022) showed that a large number of hydraulic structures worldwide may be subjected to confined wave impacts. Examples include flood barriers at Lake Borgne in the United States, Bay of Bourgneuf in France and Fudai in Japan.

Wave impacts lead to high peak pressures of short duration (Ramkema, 1978; Hofland et al., 2011; Bagnold, 1939), which in turn can yield a dynamic response of the gate structure. This response differs substantially from what would be expected based on a quasi-static design approach. An accurate prediction of the dynamic response of flood gates subjected to wave impacts is therefore essential to safely and economically design and assess them. Also the trend to realise gates of increasing scale, contributes to the relevance of taking their dynamic behaviour into consideration from early design stages. Figure 1.2 and 1.3 show two examples of flood gate barriers in the Netherlands where wave impacts have proven to be critical in the design.

The discharge sluices of the Afsluitdijk dam contain fifty large scale flood gates (about 12.5 m in width and 7.25 m in height). As part of an ongoing renovation project, the existing flood gates will be renovated and additional discharge sluices and flood gates will be realised. Both at the existing and the new discharge sluices, waves impacts may occur due to overhanging construction elements in front of the gate. Figure 1.4 shows an impression of the cross section of the existing discharge sluices where wave impacts occur due to the presence of overhanging structures.

Wave impacts have also had a significant influence on the design of the flood gates in the Eastern Scheldt barrier. A gate design with a front plate supported by horizontal beams was first considered. Experiments showed, however, that wave impacts on the horizontal beams could lead to extremely high loads. The decision was therefore made to implement a gate design consisting of a front plate supported by a tubular truss structure (Kolkman and Jongeling, 2007a). Later, the dynamic behaviour of the gates was measured in practice and specifically modelled. More recently, a temporary maintenance structure was implemented at the gates of the Eastern Scheldt barrier as shown in Figure 1.2. The platform of this structure could also be subjected to wave impacts.

1.2 PROBLEM DESCRIPTION

Flood gates are by definition in contact with water when being subjected to wave impact loading during storm events. Apart from its structural characteristics, also the interaction with the fluid determines the dynamic response of a gate (Lamb, 1921). This interaction between the gate and fluid adds complexity to the prediction of the motion of the gate.

Due to the complexity involved in solving fluid-structure interaction problems, it is common engineering practice to design and assess these gates based on a simplified quasi-static approach. A dynamic amplification is applied to the maximum quasi-static force to account for the effect of vibrations of the gate on the maximum response.



Figure 1.2: The Eastern Scheldt barrier in the Netherlands (ref: Rijkswaterstaat). Wave impacts have played a major role in the design of the gates. Also the recently implemented temporary maintenance structure at the backside of the gates can be subjected to wave impacts.



Figure 1.3: The design for the Afsluitdijk renovation (ref: Levvel) and one of the gates in the existing discharge sluices. Both the existing and newly designed gates may be subjected to confined wave impacts due to overhanging elements.

Although the term amplification implies otherwise, the dynamic response may either be lower or higher than what would be expected based on a quasi-static representation. The dynamic amplification factor is derived from a single degree of freedom representation of the structure (Kolkman and Jongeling, 2007b; Cuomo, 2007). The fluid-structure interaction is not explicitly considered in such design approaches but included by using hydrodynamic coefficients. Neglecting higher mode vibrations may lead to overestimations of the response at some parts of the gate while underestimating the response at other parts. The locality of the wave peak pressures accompanied with wave impacts further complicates the problem. Although this approach yields some insight, it lacks the precision to capture the three-dimensional vibration behaviour of a gate-fluid system. This significantly limits its applicability as a design instrument as it is not guaranteed that this approach is conservative in all cases. Application of this method in design may therefore lead to overdimensioned but possibly also unsafe designs.

Advanced finite element methods able to deal with the coupled fluid-structure interaction problem in complex three-dimensional geometries do exist, for instance as part of the common software packages ANSYS or COMSOL. However, although

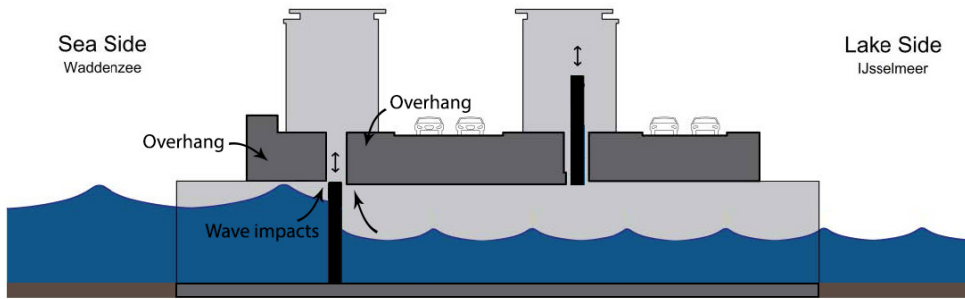


Figure 1.4: Impression of an existing flood gate complex in the Afsluitdijk where wave impacts may occur due to the presence of overhanging structures (De Almeida et al., 2019). The concrete structures are shown in dark grey and the movable vertical gates in black.

developments occur continuously, these models are still computationally expensive, which limits their effectiveness in the design phase of a project for several reasons. First, the computational limits do not allow for the large number of simulations necessary to test various parameters and boundary conditions during design (Erdbrink, 2014). Second, probabilistic assessments require many simulations. Bagnold (1939) observed that peak pressures accompanied with wave impacts show large variations for waves with very similar characteristics, and are therefore difficult to predict theoretically. A probabilistic approach could deal with this uncertainty. Moreover, several flood gates are part of the primary flood defence system in the Netherlands. This means that these gates must be assessed and designed based on a probability of failure requirement. A probabilistic method is therefore required to explicitly quantify this probability of failure. Whereas these methods are available for regular earthen flood defences and other failure modes of hydraulic structures (Schweckendiek et al., 2014; Jongejan and Maaskant, 2015), a suitable method lacks for failure of flood gates due to wave impact loads. Third, fatigue assessments are not feasible when explicitly regarding the dynamic response of a flood gate due to the millions of waves that impact the structure under different conditions during its lifetime.

Within the field of offshore engineering a semi-analytical mode matching method has been developed to predict the dynamic behaviour of for example wind turbine foundations and liquid storage tanks (Tsouvalas and Metrikine, 2014; Tsouvalas et al., 2020). This technique first describes the motion of the gate and fluid separately based on a modal decomposition in the frequency domain. A semi-analytical solution is then derived for the coupled motion of the system based on the interface conditions between the structure and fluid. The term semi-analytical is designated as although an exact analytical solution is derived for the theoretical formulation of the motion of the system based that includes an infinite number of mode shapes of both the structure and fluid, this solution is evaluated numerically truncating the number of modes to a finite number. This method has proven to solve the interaction between the structure and fluid accurately yet computationally efficient for these applications and could possibly be effective as well for the situation of a flood gate subjected to wave impacts. However, up until now this

technique has not yet been applied within the field of hydraulic engineering.

For the prediction of the wave impacts loads, experimental studies are usually employed in practice. Practical limits allow for a limited number of waves and different wave conditions in such experiments. A difficulty in predicting the impact pressures theoretically is that these pressures exhibit large variation for waves with very similar characteristics, as already known since the pioneering work of Bagnold (1939). It has been recognized however that the impulse of the entire wave impact is more predictable (Hofland et al., 2011; Cuomo et al., 2010). Pressure impulse theory by Cooker and Peregrine (1995) and Wood and Peregrine (1997) may therefore provide an opportunity to predict wave impact loads theoretically over the lifetime of the flood gate.

1.3 RESEARCH AIM AND SCOPE

The aim of this thesis is to develop a method to predict the dynamic behaviour of flood gates due to wave impacts that can be applied in design and safety assessments. This novel method should overcome both the lack of accuracy involved with existing engineering methods and the high computational costs of numerical finite element models. Moreover, it should include all essential physical phenomena that govern the response of flood gates under wave impact loading. This would allow for the explicit consideration of the dynamic behaviour of flood gates and open up the possibility to perform probabilistic safety assessments and fatigue lifetime evaluations. These analyses are expected to yield new insights on the most relevant factors governing the assessment and design of flood gates under wave impact loading. This research aim is translated to the following three main research questions and underlying questions:

1. How can a model be developed to predict bending vibrations of a flood gate and the involved fluid-structure interaction?
 - (a) How can a semi-analytical solution be formulated for the motion of a plain flood gate in a discharge sluice? (*Chapter 2*)
 - (b) How can one include a protruding element in this semi-analytical solution to represent situations with confined wave impacts? (*Chapter 3*)
 - (c) To what extent can the developed model predict the dynamic behaviour of more realistic gate designs? (*Chapter 4*)
2. Does the developed model cover the most relevant physical phenomena that govern the response of flood gates to wave impacts? (*Chapter 5*)
3. How can the safety and fatigue lifetime of flood gates under wave impact loading be assessed?
 - (a) Is the effect of compressibility and surface waves on the hydrodynamic pressures, often neglected in existing design methods, relevant for the dynamic behaviour of typical flood gates? If so, for which system parameters? (*Chapter 6*)
 - (b) How can the developed model be employed to assess the reliability of flood gates under wave impact loading? (*Chapter 7*)
 - (c) How can the developed model be employed to evaluate the fatigue lifetime of flood gates under wave impact loading? (*Chapter 8*)

The focus of this thesis lies on vertical lifting flood gates situated in a discharge sluice. Confined wave impacts on a overhang in front of the flood gate are the main source of excitation in this study. However, also an example of excitation due to breaking wave impacts is considered. The case studies that are performed throughout the thesis are inspired by the situation of the Afsluitdijk. Focusing on this one practical case provides the opportunity to study in depth the usability of the developed methods.

1.4 METHODOLOGY AND OUTLINE

This thesis consists of three main parts related to each of the main research questions presented in the previous section. The methodology applied in this thesis is discussed in more detail for each of these parts. Figure 1.5 shows an overview of the thesis outline including these three parts.

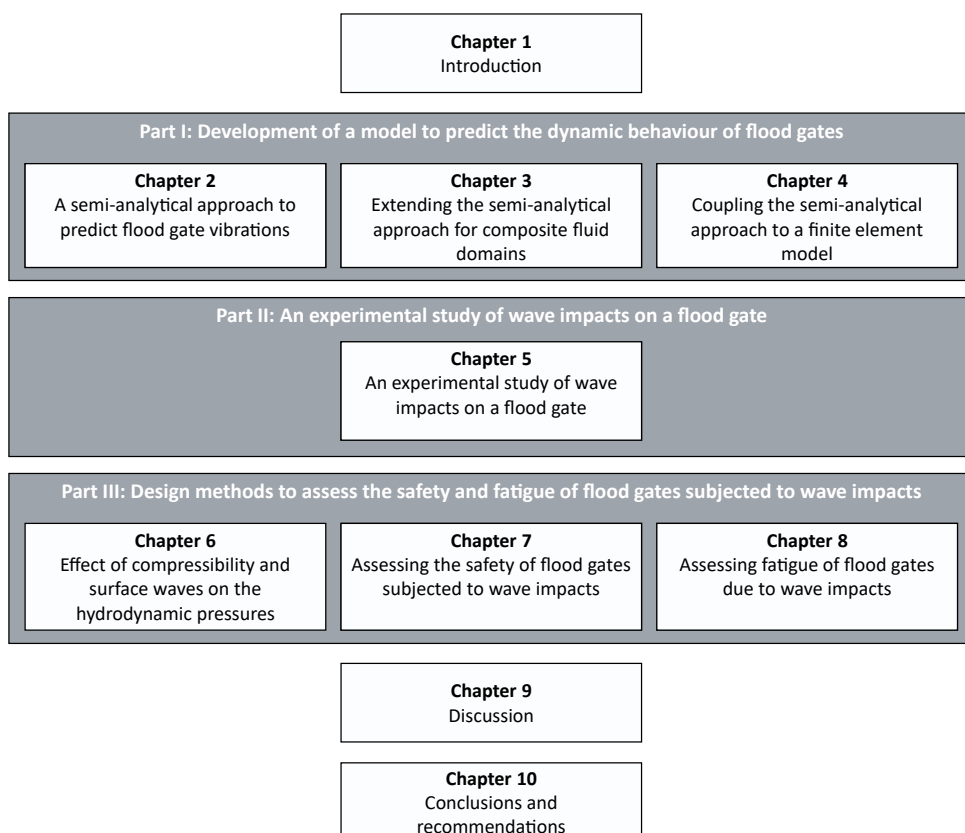


Figure 1.5: Overview of the thesis outline

I) DEVELOPMENT OF A MODEL TO PREDICT THE DYNAMIC BEHAVIOUR OF FLOOD GATES

Part I treats the first main research question: *how can a model be developed to predict bending vibrations of a flood gate and the involved fluid-structure interaction?*

A novel semi-analytical model to predict the dynamic behaviour of a flood gate is developed in this part based on a mode matching approach. This is the more mathematical part of this thesis that involves the derivation of a semi-analytical solution. Chapter 2 presents the basis of the semi-analytical model approach. The situation of a flood gate in a uniform discharge sluice is considered with a single infinite fluid domain at each side of the gate. The gate is represented as a thin plate. The model is suitable for any time-varying force. The case study in this chapter includes a breaking wave impact. The impact pressure signal is obtained from large scale experiments of breaking wave impacts on a rigid vertical wall by Hofland et al. (2011).

Chapter 3 extends this model by including composite fluid domains. This allows to accurately represent the situation of a gate with an overhang in front that can cause confined wave impacts. Chapter 4 then couples the semi-analytical approach to a finite element model. In this way, it is possible to predict the dynamic response in terms of structural stresses for more complex gate designs. This completes the development of a novel model to predict the dynamic behaviour of flood gates. A case study is performed to demonstrate the benefits of the developed model. In this case study, an optimal gate design is found parametrically for a design storm with several hundred confined wave impacts.

Throughout Chapters 2-4 each version of the model is validated by comparison to an existing time-domain coupled finite element model. The software package COMSOL is employed for this purpose. Both models in this comparison are based on a similar theoretical representation of the practical problem. This validation therefore mainly addresses the ability of the developed method of solution to solve the fluid-structure interaction problem. Furthermore, the numerical performance of both methods is compared for the validation cases.

II) AN EXPERIMENTAL STUDY OF WAVE IMPACTS ON A FLOOD GATE

Part II treats the second main research question: *does the developed model cover the physical phenomena that govern the response of flood gates to wave impacts?*

Scale experiments have been performed in order to answer this research question. Chapter 5 provides a description of these scale experiments. The semi-analytical model was validated in the first chapters by comparison to existing standard finite element software. This chapter provides a preliminary validation of the modelling framework regarding its ability to represent the considered physical problem. Furthermore, a broader dataset is generated that allows further studying of the fluid-structure interaction of wave impacts on flexible structures.

III) DESIGN METHODS TO ASSESS THE SAFETY AND FATIGUE OF FLOOD GATES SUBJECTED TO WAVE IMPACTS

This part treats the third main research question: *how can the safety and fatigue lifetime of flood gates under wave impact loading be assessed?*

This part presents design methods that make use of the abilities of the developed model. First, Chapter 7 develops a model approach that can be applied within reliability analyses to explicitly predict the failure probability of a flood gate under wave impact loading. Exceedance of the yielding stress is the considered failure mechanism in this approach. Then, Chapter 8 presents a design method to predict fatigue of flood gates over the lifetime of the structure. A case study is performed in both chapters to demonstrate how these methods can be applied in practice. For the latter chapters, a comparison with existing design methods is made for the case study.

1.5 DYNAHICS RESEARCH PROGRAM

The research in this thesis has been carried out as part of the Dynamics of Hydraulic Structures (DynaHicS) research program, which consists of two main tracks: i) the prediction of confined wave impact loads and ii) the resulting dynamic response of the structure. This thesis concerns the second track in the DynaHicS program and thus focuses on the dynamic response of the flood gate to wave impacts. Ermano de Almeida has performed the research on the first track. Pressure impulse theory to predict wave impact loads has been validated and developed further within this track (De Almeida et al., 2019; De Almeida and Hofland, 2020b,a, 2021; De Almeida et al., 2022). Also the research by Chen et al. (2019) was performed within the DynaHicS program and has contributed to this development. This knowledge has been applied extensively in the developed design methods presented in the latter chapters of this thesis. The flood gates and general situation of the Afsluitdijk in the Netherlands have been used as a central case study in the Dynahics research program.

2

**A SEMI-ANALYTICAL
APPROACH TO PREDICT
FLOOD GATE VIBRATIONS**

To safely and optimally design flood gates subjected to wave impacts an accurate prediction of their dynamic response is required. As discussed in the previous chapter, methods presently used in engineering practice lack the precision to capture the three-dimensional vibration behaviour of a gate-fluid system. On the other hand, more advanced finite element methods can accurately predict this behaviour but are too computationally costly to effectively apply in design studies.

This chapter therefore sets out to establish the basis of a semi-analytical model to predict bending vibrations of flood gates with fluid on both sides accurately yet in a computational efficient manner. This study is focused on predicting the response to a wave impact. However, the presented model is suitable for any time-varying excitation force. In the next two chapters, the semi-analytical model presented here is expanded for composite fluid domains and more realistic gate designs.

The structure of this chapter is as follows. Section 2.1 gives an introduction on the various methods that exist to solve fluid-structure interaction problems. The geometry of the studied problem is then described in Section 2.2. Section 2.3 provides the theoretical description of the fluid-structure interaction problem, for which a semi-analytical solution is then derived in Section 2.4. In Section 2.5 the semi-analytical model is applied to a typical case of an impulsive wave impact on a flood gate. The model is validated by comparison with a standard software package in Section 2.6. Finally, Section 2.7 discusses the conclusions of this chapter.

2.1 INTRODUCTION

Wave impacts on coastal flood gates may lead a dynamic response of the structure. The magnitude of this dynamic response does not only depend on the structural characteristics, but is also affected by the interaction with the surrounding fluid (Lamb, 1921). Due to the complexity involved in solving fluid-structure interaction problems, it is common engineering practice to design these gates based on a quasi-static approach in which the effect of the vibrations is accounted for by applying a dynamic amplification factor. The structure is simplified to a single degree of freedom (SDOF) system to derive this dynamic amplification factor (Kolkman and Jongeling, 2007b; Cuomo, 2007). Hattori and Tsujioka (1997) have performed a series of experiments on the response of elastic plates to wave impacts, and compared the measured response to the theoretical response based on a SDOF system. The dynamic properties of the plate in fluid were experimentally determined. The results show a relatively high discrepancy between measurements of the wall deflection and the prediction by the single degree-of-freedom model. Although SDOF models yield theoretical insight, they lack the precision to capture the three dimensional vibration behaviour of a gate-fluid system, which significantly limits their applicability as a design instrument. The locality of the peak pressures accompanied with wave impacts complicates the problem further.

The dynamic behaviour of submerged plates and the involved fluid-structure interaction have been continuously investigated in the past century. Advanced methods

This chapter is based on the publication "A three dimensional semi-analytical model for the prediction of gate vibrations immersed in fluid" in *Marine Structures* (Tieleman et al., 2019b). Some minor changes have been introduced to make the text consistent with the other chapters of the thesis.

to study vibrations influenced by fluid-structure interaction can be divided into three main categories: finite element methods (FEM), boundary element methods (BEM), and (semi)analytical solutions (Tsouvalas and Metrikine, 2013). Lamb (1921) was the first to calculate the change in resonance frequency of a thin flexible circular plate extended by an infinite rigid baffle due the presence of incompressible fluid. Many analytical solutions, developed later on, depend on the assumption that the structural modes in the submerged system are approximately the same as the in vacuo modes, which is subscribed to Lamb's work. This will be referred to as the assumed-modes approach. In this case the effect of the surrounding fluid on the respective resonance frequencies can be determined by applying hydrodynamic coefficients (Kolkman and Jongeling, 2007a) or the nondimensionalized added virtual mass incremental (NAVMI) factors (Kwak and Kim, 1991). Kolkman (1988) presents a simple numerical scheme to obtain the added mass coefficient for a given geometry based on incompressible fluid and a null potential at the free surface. Westergaard (1933) derived an analytical expression for the hydrodynamic pressures for the situation of a two-dimensional vertical rigid dam adjacent to an infinitely long and wide reservoir with compressible fluid, which is still used in engineering practice. Fu and Price (1987) studied the vibration behaviour of partially and totally immersed plates, solving the fluid pressure by employing the Green's function. The vibrational mode shapes of the plate in fluid were considered the same as the in vacuo modes. The effect of the free surface was investigated and shown to have a significant effect on the resonance frequencies. A similar problem was considered by Ergin and Ugurlu (2003) in which the in-vacuo dynamic properties of the plate were obtained using standard finite-element software. The fluid response was determined by the use of a boundary integral equation method together with the method of images.

Kwak (1996), Amabili and Kwak (1996); Amabili et al. (1996) compared resonance frequencies obtained by the NAVMI factor solution and the more accurate Rayleigh-Ritz method for rectangular, circular, and annular plates respectively for a situation similar to the Lamb problem. It was found that the fundamental mode and frequency were well estimated by the assumed-modes approach, while higher modes were computed with less accuracy. Tubaldi and Amabili (2013) investigated the stability of an infinitely long and wide plate subjected to a pulsating potential flow based on linear dynamics. Tubaldi et al. (2015) considered the non-linear dynamic behaviour of the same problem. The flow-induced vibrations of radial and other shell type gates were studied analytically and experimentally in Anami et al. (2004, 2012) and Ishii and Knisely (1992). The coupled hydrodynamic mass and damping were considered for two structural modes, being the streamwise bending of the skin plate and the rotation of the entire gate. Kvalsvold and Faltinsen (1993) studied the vibrations of wave slamming against wetdecks of catamaran-type vessels. The wetdeck is modelled as a simply supported bending beam, interacting with the fluid in a two-dimensional domain. The fluid response is determined both analytically and numerically by using the Green's function. The fully coupled gate-fluid problem is subsequently solved by using a fourth order Runge-Kutta integrator. Korobkin and Khabakhpasheva (2006) studied a similar problem into more detail including the wetting process and penetration stage based on a modified method of normal modes.

In Tsouvalas and Metrikine (2013, 2014, 2016) a semi-analytical model is presented to investigate the vibro-acoustic behaviour in offshore pile driving. A mode matching

approach was employed based on linear dynamics. Due to the high frequencies and water depths involved in this application, the effect of surface waves was omitted. Contrary to many other studies, the fluid problem is solved based on the separation of variables technique. A coupled modal analysis is performed in which the fluid and soil responses are described in terms of in vacuo structural modes. The fluid response therewith becomes an implicit part of the model. The interaction problem between structure and fluid is solved efficiently in this way. Leblond et al. (2009) apply a similar approach for the bending of an elastic cylinder, represented as a beam. Three fluid models are considered, namely potential, viscous and acoustic. The modal time dependent displacement coefficients are obtained by matrix inversion in the Laplace domain and fast numerical inversion of the Laplace transform.

Finally, most finite element (FE) packages are able to solve fluid-structure interaction problems for complex geometries. Although developments occur continuously, numerical models including fluid-structure interaction are still computationally expensive and therefore not applied in common engineering practice to test various design parameters and boundary conditions for three dimensional problems (Erdbrink, 2014).

In the present study, a model is developed to predict the bending vibrations of a flood gate immersed in fluid. Both fluid compressibility and free surface waves are considered so that the hydrodynamic fluid pressure exerted on the gate is predicted accurately in both low- and high-frequency regimes; this is expected to be relevant for typical flood gates subjected to wave impacts. The mode matching method by Tsouvalas and Metrikine (2013) is employed. This method has been applied to the field of offshore engineering, but is yet unknown within the field of engineering. A solution is now derived specifically for the situation of flood gate in a discharge sluice. Also, the effect of free surface waves is added, which is important for the study under consideration. This is the first novel contribution of this chapter.

The structural and fluid responses are expressed in the frequency domain as a superposition of modes. A semi-analytical solution of the fluid-interaction problem is derived by describing the complete system in terms of in vacuo gate modes. This requires to solve the structure and fluid eigenvalue problems only once for a given geometry and the information can be stored and used subsequently to calculate the response of the system to various load cases. This is a fundamental benefit compared to existing numerical methods. The gate-fluid system is three dimensional, allowing one to study the response to local peak pressures accompanied with wave impacts. In this study, the mode shapes of the gate are based on thin plate theory. However, the method allows for the use of any set of structural mode shapes, which could be obtained by standard FE software for more realistic gate designs.

The obtained model is able to solve the fluid-interaction for flood gate vibrations computationally efficient and accurately, and is therefore suitable as a preliminary design tool and a large number of simulations. The case study in this chapter indicates that this may lead to more optimal gate designs. Additionally, the model approach allows one to perform fatigue calculations and probabilistic evaluations. The latter is especially interesting as it allows one to study the structural response taking into account the uncertainty associated with wave impacts. This complies to the highly variable nature of wave impacts, as discussed in Hofland et al. (2011), in which waves with very similar

characteristics lead to significantly different peak pressures. The failure probability of the gate can be quantified explicitly by applying a probabilistic approach based on the developed model, which is valuable for flood safety assessments.

2.2 DESCRIPTION OF THE FLUID-STRUCTURE INTERACTION PROBLEM

The typical situation of a closed flood gate in a discharge sluice is represented by the model geometry shown in Figure 2.1. The sluice has impermeable vertical walls and a horizontal bottom, so that the cross-section of the water body is rectangular. To simplify the analytical derivations, the sluice is assumed to be infinitely long in y -direction. However, cases in which the sluice is of finite dimensions can be treated as well with the adopted modelling approach. The water depths h_l and h_r at the left and right side of the gate respectively, may vary between zero and up to the height of the gate.

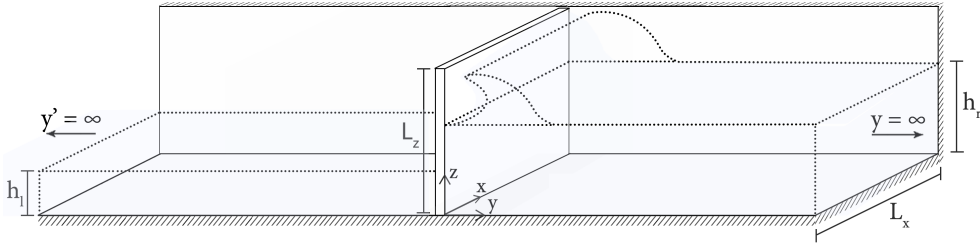


Figure 2.1: Three dimensional overview of the plate model space

The gate structure is represented by a thin plate, that is considered to be homogeneous and isotropic. It is assumed that the contact surface between the structure and fluid is a continuous vertical plane on both sides of the gate. The accuracy of the prediction for more complex gate designs can be improved relatively easily by determining the structural mode shapes with existing FE packages. The developed approach and solution remain identical, as long as the contact surfaces between the gate and fluid are vertical. The aim is to improve suitability of this method for more complex gate geometries and structure-fluid interfaces in further studies.

The gate has a width L_x (equal to that of the sluice), height L_z , distributed mass per unit surface ρ_s , and uniform bending rigidity $D = \tilde{E}t^3/(12(1 - \nu^2))$, in which E is the modulus of elasticity, t is the thickness of the gate, and ν is the Poisson's ratio. An isotropic material damping factor η is applied to the modulus of elasticity in the frequency domain by $\tilde{E} = (1 + \eta i)E$. Chapter 5 shows that including the total amount of damping in this manner can lead to good results and provides an indication of what amount of damping could potentially be expected for this type of problem.

The gate is simply supported at its vertical boundaries ($x = 0$, $x = L_x$) and bottom ($z = 0$) while its top edge ($z = L_z$) is stress-free. It is possible to incorporate more complex boundary conditions such as partially clamped in this model as well. In order to keep derivations in this study clear, these relatively simple boundary conditions are chosen without loss of generality.

The fluid system is assumed stationary at both sides with its free surface at h_l and h_r . In the present study a measured breaking wave impact is applied as the excitation force on the gate. The impact pressure is considered to be independent from the gate-fluid system, i.e. the still standing water level is not changed. This assumption is expected to be reasonable for wave impacts, as these are typically of much shorter duration (10 to 100 ms) than the period of the corresponding free surface wave (≈ 10 s) Hofland et al. (2011). Furthermore, Cooker and Peregrine (1995) developed a mathematical model to predict the wave impact pressure impulse and found it to be only weakly dependent on the shape of the free surface boundary for a similar model geometry. The validity of this assumption is planned to be tested further in experiments in ongoing studies.

2.3 THEORETICAL FORMULATION OF THE PROBLEM

The governing equations describing the motion of the gate structure and fluid, as defined in the previous section, are first introduced. Equations of motions and boundary conditions are presented in the time domain, and subsequently transformed to the frequency domain.

2.3.1 STRUCTURAL PROBLEM

The linear bending vibrations of a homogeneous isotropic rectangular thin plate are described by the following equation of motion (Clausen et al., 1969):

$$\rho_s \frac{\partial^2 w(x, z, t)}{\partial t^2} + D \left[\frac{\partial^4 w(x, z, t)}{\partial x^4} + 2 \frac{\partial^4 w(x, z, t)}{\partial x^2 \partial z^2} + \frac{\partial^4 w(x, z, t)}{\partial z^4} \right] = -p_l(x, y = 0, z, t) + p_r(x, y = 0, z, t) + f_e(x, z, t) \quad (2.1)$$

in which w denotes the displacement of the mid-surface of the plate, ρ_s is the distributed mass per unit of area, f_e the time signal of the external force distribution on the plate (e.g. the wave impact), and p_l and p_r define the dynamic fluid pressures at either sides acting on the gate in response to its motion. As the plate is considered geometrically thin, rotational inertia and shear deformation are neglected in Eq.(2.1). For the cases considered, the wavelengths excited in the structure are large compared to the thickness of the plate which further justifies the choice of the low-order plate theory neglecting high-order effects.

At the simply supported edges the displacement and bending moment in the respective direction are zero. The stress-free top edge of the plate states zero moment and effective Kelvin-Kirchoff shear force in z -direction (Leissa, 1969). The boundary conditions are therefore as follows:

$$w(x = 0, z) = m_{xx}(x = 0, z) = w(x = L_x, z) = m_{xx}(x = L_x, z) = 0 \quad (2.2)$$

$$w(x, z = 0) = m_{zz}(x, z = 0) = m_{zz}(x, z = L_z) = v_{zy}(x, z = L_z) = 0 \quad (2.3)$$

in which m_{xx} and m_{zz} are the bending moments in x - and z -direction respectively, and v_{zy} is the effective Kelvin-Kirchoff shear force in z -direction.

It is assumed that the spatial distribution of the force does not change in time, i.e. the force is separable in a space-dependent part $\hat{f}_{\text{amp}}(x, z)$ and time dependent part $f_t(t)$.

Using the Fourier transform pair as stated in Eqs.(2.4) and (2.5), transformation to the frequency domain is possible, i.e.:

$$\tilde{G}(\omega) = \int_{-\infty}^{\infty} g(t) e^{-i\omega t} dt \quad (2.4)$$

$$g(t) = \frac{1}{2\pi} \int_{-\infty}^{\infty} \tilde{G}(\omega) e^{i\omega t} d\omega \quad (2.5)$$

in which $g(t)$ is the examined quantity and $\tilde{G}(\omega)$ its amplitude in the frequency domain, being in this case the displacement of the gate or the fluid pressure. Applying Eqs.(2.4) and (2.5) in Eq.(2.1) yields:

$$-\rho_s \omega^2 \tilde{w}(x, z, \omega) + D \left[\frac{\partial^4 \tilde{w}(x, z, \omega)}{\partial x^4} + 2 \frac{\partial^4 \tilde{w}(x, z, \omega)}{\partial x^2 \partial y^2} + \frac{\partial^4 \tilde{w}(x, z, \omega)}{\partial z^4} \right] = \quad (2.6)$$

$$-\tilde{p}_l(x, y = 0, z, \omega) + \tilde{p}_r(x, y = 0, z, \omega) + \tilde{f}_e(x, z, \omega)$$

in which \tilde{w} denotes the complex vibration amplitude of the gate in the frequency domain.

2.3.2 FLUID PROBLEM

The fluid domains at both sides of the plate are mirrored in y-direction. For brevity, the fluid pressure equations are elaborated for a single side of the gate, i.e. $y > 0$, in this and the following section, and the subscripts l or r are omitted.

The fluid is considered irrotational and inviscid. It is to be expected that viscosity plays a negligible role in the dynamic response of the fluid for flood gates. In the wave impact case studied in Section 2.5 the maximum fluid velocity amplitude is approximately 2 m/s. With a hydraulic radius of the sluice channel of about 4 m this leads to a Reynolds number in the order of 10^6 , which is well within the regime where viscous forces are negligible compared to inertial forces.

Based on above consideration the motion of the compressible fluid can be described in terms of the velocity potential ϕ by: The motion of the compressible fluid is described by:

$$\nabla^2 \phi(x, y, z, t) - \frac{1}{c_p^2} \frac{\partial^2 \phi(x, y, z, t)}{\partial t^2} = 0 \quad (2.7)$$

in which ∇ is the Nabla operator, and c_p is the sound velocity in water. The fluid motion is thus described based on an Eulerian approach, where a Lagrangian approach was employed for the structural motion. From the dynamic part of the linearised Bernoulli equation for unsteady flow follows the fluid pressure relates to the velocity potential as follows:

$$p(x, y, z, t) = -\rho_f \frac{\partial \phi(x, y, z, t)}{\partial t} \quad (2.8)$$

The velocity vector of the fluid is given as:

$$v(x, y, z, t) = \nabla \phi(x, y, z, t) \quad (2.9)$$

The boundary conditions at the impermeable sluice walls and bottom simply state zero velocity. At the still water level of the fluid the free surface condition is applied as known

from linear wave theory. At the structure-fluid interface velocity compatibility is enforced. This yields the following set of boundary conditions:

$$\frac{\partial \phi(x, y, z, t)}{\partial x} \Big|_{x=0} = \frac{\partial \phi(x, y, z, t)}{\partial x} \Big|_{x=L_x} = \frac{\partial \phi(x, y, z, t)}{\partial z} \Big|_{z=0} = 0 \quad (2.10)$$

$$\frac{\partial^2 \phi(x, y, z, t)}{\partial t^2} \Big|_{z=h} + g \frac{\partial \phi(x, y, z, t)}{\partial z} \Big|_{z=h} = 0 \quad (2.11)$$

$$\frac{\partial \phi(x, y, z, t)}{\partial y} \Big|_{y=0} = \frac{\partial w(x, z, t)}{\partial t} \quad (2.12)$$

Finally, at $y \rightarrow \infty$ the radiation conditions should be satisfied at all times, which completes the statement of the problem.

After transformation to the frequency domain Eqs.(2.7) to (2.12) become:

$$\nabla^2 \tilde{\phi}(x, y, z, \omega) + k_f^2 \tilde{\phi}(x, y, z, \omega) = 0 \quad (2.13)$$

$$\tilde{p}(x, y, z, \omega) = -\rho_f i\omega \tilde{\phi}(x, y, z, \omega) \quad (2.14)$$

$$\tilde{v}(x, y, z, \omega) = \nabla \tilde{\phi}(x, y, z, \omega) \quad (2.15)$$

$$\frac{\partial \tilde{\phi}(x, y, z, \omega)}{\partial x} \Big|_{x=0} = \frac{\partial \tilde{\phi}(x, y, z, \omega)}{\partial x} \Big|_{x=L_x} = \frac{\partial \tilde{\phi}(x, y, z, \omega)}{\partial z} \Big|_{z=0} = 0 \quad (2.16)$$

$$\frac{\partial \tilde{\phi}(x, y, z, \omega)}{\partial z} \Big|_{z=h} = \frac{\omega^2}{g} \tilde{\phi}(x, y, z, \omega) \Big|_{z=h} \quad (2.17)$$

$$\frac{\partial \tilde{\phi}(x, y, z, \omega)}{\partial y} \Big|_{y=0} = i\omega \tilde{w}(x, z, \omega) \quad (2.18)$$

with $k_f^2 = \omega^2 / c_p^2$.

2.4 SOLUTION TO THE FLUID-STRUCTURE INTERACTION PROBLEM

An analytical solution to the system of equations introduced in the previous section is derived by performing a coupled modal analysis. The structural and fluid response are expressed first in terms of modes of vibration. Subsequently, the kinematic condition is satisfied at the structure-fluid interface and the final system of equations of the forced system is solved.

This method is aimed at efficiently solving the interaction between structure and fluid. It however remains possible (and in most cases favourable) to evaluate the separate structural and fluid modes and corresponding resonance frequencies numerically. In this way, the advantages of existing FE models can be exploited. The fluid equations will be solved completely analytically, since the relatively simple model geometry and separable fluid equation of motion allows for such a treatment in this case. Secondly, from a structural design perspective this is favourable, as it makes possible to quickly evaluate the behaviour of a gate in fluid based on an eigenvalue analysis of the in vacuo gate model in a standard FE package. The mode shapes and resonance frequencies of the plate structure are partially found numerically.

2.4.1 STRUCTURAL MODAL EXPANSION

The plate response can be described as the summation of in vacuo modes multiplied by unknown modal amplification:

$$\tilde{w}(x, z) = \sum_{m=1}^{\infty} \sum_{k=1}^{\infty} A_{km} W_{km}(x, z) \quad (2.19)$$

in which A_{km} are the yet unknown modal amplitudes of each structural mode W_{km} . The mode shapes and corresponding resonance frequencies ω_{km} can be found by solving the homogeneous part of Eq.(2.6) either analytically or numerically. Given the simply-supported boundary conditions along the x-direction in the examined case, a solution can be searched for by applying the separation of variables technique, i.e.:

$$W_{km}(x, z) = W_{x,k}(x) W_{z,m}(z) \quad (2.20)$$

The mode shapes are orthogonal so that the following holds:

$$\iint W_{km} W_{ln} = 0 \quad \text{for } km \neq ln \quad (2.21)$$

2.4.2 FLUID MODAL EXPANSION

The solution to the equation of motion of the fluid, i.e. Eq.(2.13), can be searched for by applying the separation of variables technique assuming a solution in the following form:

$$\tilde{\phi}(x, y, z) = X(x) Y(y) Z(z) \quad (2.22)$$

Substitution into the equation of motion yields three ordinary differential equations including unknown wave numbers k_x , k_y , and k_z for each direction that should fulfill the following condition:

$$k_x^2 + k_y^2 + k_z^2 - k_f^2 = 0 \quad (2.23)$$

For the considered boundary conditions the following infinite number of modes is found for the x - and z -directions:

$$X_p(x) = \cos(k_{x,p} x) \quad (2.24)$$

$$Z_r(z) = \cos(k_{z,r} z) \quad (2.25)$$

with $p = 1, 2, \dots, \infty$ and $r = 1, 2, \dots, \infty$. The constants are defined by:

$$k_{x,p} = \frac{(p-1)\pi}{L_x} \quad (2.26)$$

$$\omega^2 = -g k_{z,r} \tan(k_{z,r} h) \quad (2.27)$$

with h being the water depth at the considered side of the gate. Eq.(2.27) is known as the surface wave dispersion equation. Solving this equation for a given frequency, yields two imaginary eigenvalues for $k_{z,r}$ (one positive and one negative), and an infinite number of real valued roots.

The solution in y -direction states:

$$Y_p(y) = B_{pr} e^{-ik_{y,pr}y} \quad (2.28)$$

in which B_{pr} are unknown fluid modal coefficients. The separation constants $k_{y,pr}$ are known from Eq.(2.23):

$$k_{y,pr} = \pm \sqrt{k_f^2 - k_{x,p}^2 - k_{z,r}^2} \quad (2.29)$$

For $y > 0$, a decaying field representing the evanescent waves along the y -direction holds for $\text{Im}(k_{y,pr}) \leq 0$ while the radiation condition at infinity requires $\text{Re}(k_{y,pr}) \geq 0$. In the ideal case examined here, in which the damping in the fluid region is completely neglected, the latter condition for the propagating modes should always be confirmed by verifying that the group velocity of the waves propagating along the y -direction is positive. This condition is associated with the proper definition of energy propagation towards the positive y -direction carried by the propagating modes in the medium. It can be shown that for the ideal fluid waveguide it is indeed sufficient to consider the poles located on the positive real axis (for $y > 0$). In more complex waveguides, however, i.e. acousto-elastic layered media, this is not always the case as discussed in van Dalen et al. (2015). Naturally, the inclusion of a small amount of damping will shift the poles to the right half of the complex wavenumber plane making the selection of the proper poles quite straightforward and the need to check the group velocity altogether unnecessary. Thus for the domain $y > 0$ we impose $\text{Re}(k_{y,pr}) \geq 0$ and $\text{Im}(k_{y,pr}) \leq 0$ as shown in Figure 2.2.

The representation of the response of the fluid domain in the form of a modal sum over an infinite set of eigenfunctions is exact provided that all poles can be accurately determined in the complex wavenumber plane. Based on complex contour integration and residue theorem it can be shown that for the considered problem this is indeed the case (Tsouvalas, 2015).

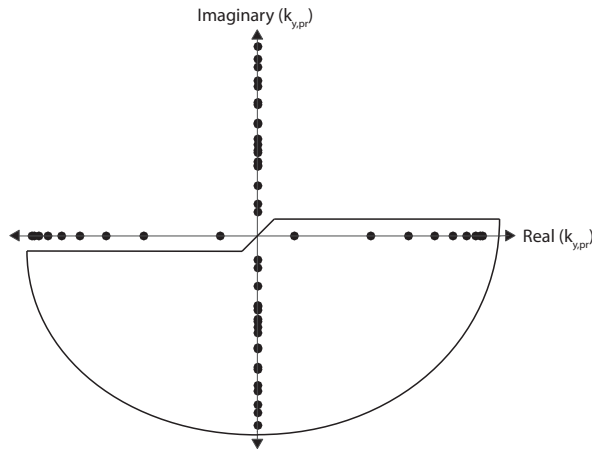


Figure 2.2: Contour integration plot for the domain $y > 0$ together with the roots of the dispersion relation for a range of arbitrary parameters

Combining the modal expansions for the fluid in each direction yields the following expression for $\tilde{\phi}$:

$$\tilde{\phi}(x, y, z) = \sum_{p=1}^{\infty} \sum_{r=1}^{\infty} B_{pr} \cos(k_{z,p} z) \cos(k_{x,r} x) e^{-ik_{y,pr} y} = \sum_{p=1}^{\infty} \sum_{r=1}^{\infty} B_{pr} \Phi_{pr}(x, z) e^{-ik_{y,pr} y} \quad (2.30)$$

in which $\Phi_{pr}(x, z)$ are the two-dimensional modal fluid shapes in the plane parallel to the surface of the gate. A similar expression holds for $y < 0$ in which the roots located in the upper half-plane of Figure 2.2 need to be considered.

2.4.3 KINEMATIC INTERFACE CONDITION BETWEEN THE STRUCTURE AND THE FLUID

To describe the fluid pressures, excited by the movement of the gate, the solutions for \tilde{w} and ϕ , shown in Eqs.(2.19) and (2.30), are substituted into the interface condition of Eq.(2.18). This yields the following expression:

$$\sum_{p=1}^{\infty} \sum_{r=1}^{\infty} B_{pr} \Phi_{pr}(x, z) \frac{d(e^{-ik_{y,pr} y})}{dy} \Big|_{y=0} = i\omega \sum_{m=1}^{\infty} \sum_{k=1}^{\infty} A_{km} W_{km}(x, z) \quad (2.31)$$

and after evaluating the derivative in the first term:

$$-i \sum_{p=1}^{\infty} \sum_{r=1}^{\infty} k_{pr} B_{pr} \Phi_{pr}(x, z) = i\omega \sum_{k=1}^{\infty} \sum_{m=1}^{\infty} A_{km} W_{mk}(x, z) \quad (2.32)$$

The orthogonality property of the fluid modes yields the following mathematical result:

$$\iint_{S_w} \Phi_{pr}(x, z) \Phi_{qs} dx dz = \delta_{pq} \delta_{rs} \Delta_{pr} \quad \delta_{pq} \delta_{rs} = \begin{cases} 1, & \text{if } p = q \text{ and } r = s \\ 0, & \text{if } p \neq q \text{ or } r \neq s \end{cases} \quad (2.33)$$

in which S is the surface occupied by the stationary fluid at $y = 0$, δ_{pq} and δ_{rs} are Kronecker deltas and Δ_{pr} is the result of the surface integration. Eq.(2.32) is multiplied by another fluid mode Φ_{qs} , and integrated over the water depth and sluice width to obtain:

$$- \sum_{p=1}^{\infty} \sum_{r=1}^{\infty} k_{pr} B_{pr} \delta_{pq} \delta_{rs} \Delta_{pr} = \omega \sum_{m=1}^{\infty} \sum_{k=1}^{\infty} A_{km} \iint_{S_w} W_{mk}(x, z) \Phi_{pr}(x, z) dx dz \quad (2.34)$$

The left-hand side of above equation is non-zero only when $p = q$ and $r = s$. This yields the following expression for B_{pr} :

$$B_{pr} = - \frac{\omega}{k_{pr} \Delta_{pr}} \sum_{k=1}^{\infty} \sum_{m=1}^{\infty} A_{km} Q_{km,pr} \quad (2.35)$$

with the variable $Q_{km,pr}$ introduced for convenience of notation:

$$Q_{km,pr} = \iint_{S_w} W_{mk}(x, z) \Phi_{pr}(x, z) dx dz \quad (2.36)$$

The fluid modal coefficients B_{pr} are now fully described in terms of the structural modal coefficients in a manner similar to Tsouvalas and Metrikine (2013). The coefficients are substituted in the solution for $\tilde{\phi}$ and subsequently in Bernoulli's pressure equation (2.14). This way the fluid pressure throughout the sluice has been obtained:

$$p(x, y, z) = i\omega^2 \rho_f \sum_{m=1}^{\infty} \sum_{k=1}^{\infty} A_{mk} \sum_{p=1}^{\infty} \sum_{r=1}^{\infty} \frac{Q_{km,pr}}{k_{y,pr} \Delta_{pr}} \Phi_{pr}(x, z) e^{-ik_{y,pr}y} \quad (2.37)$$

At the surface of the gate ($y = 0$) the exponential term drops.

From Eq.(2.37) it can be seen that the real values of $k_{y,pr}$ correspond to the propagating modes and yield an imaginary value of the hydrodynamic pressure in the frequency domain, which is equivalent to radiation damping. The imaginary values of $k_{y,pr}$ correspond to the evanescent modes, i.e. yield real valued hydrodynamic pressures, which either act as a hydrodynamic mass or stiffness depending on the sign. From a physical point of view it is indeed expected that the propagative modes take energy away from the structure.

2.4.4 FINAL SYSTEM OF EQUATIONS

The solutions for the fluid pressure and structural deflection are now described uniquely in terms of structural modal coefficients. First, the solution of $\tilde{w}(x, z, \omega)$ is substituted in the forced equation (2.6). For brevity, the function variables are emitted in the remainder of this section with the understanding that all quantities depend naturally on (x, z, ω) at $y = 0$.

$$\sum_{k=1}^{\infty} \sum_{m=1}^{\infty} A_{km} \left[-\rho_s \omega^2 W_{km} + D \left[\frac{\partial^4 W_{km}}{\partial x^4} + 2 \frac{\partial^4 W_{km}}{\partial x^2 \partial z^2} + \frac{\partial^4 W_{km}}{\partial z^4} \right] \right] = -\tilde{p}_l + \tilde{p}_r + \tilde{f}_e \quad (2.38)$$

The structural modes per definition satisfy the homogeneous structural equation of motion. This property is used to eliminate the derivative terms from Eq.(2.38). Furthermore, the expression in Eq.(2.37) for the fluid pressure is substituted. This yields the following expression:

$$\sum_{k=1}^{\infty} \sum_{m=1}^{\infty} A_{km} \rho_s (\omega_{km}^2 - \omega^2) W_{km} = - \left[i\omega^2 \rho_f \sum_{k=1}^{\infty} \sum_{m=1}^{\infty} A_{km} \sum_{p=1}^{\infty} \sum_{r=1}^{\infty} \frac{Q_{km,pr}}{k_{y,pr} \Delta_{pr}} \Phi_{pr} \right]_{\sum l+r} + \tilde{f}_e \quad (2.39)$$

in which the subscript $\sum l + r$ denotes the summation of the fluid pressure of left and right side of the gate. Note that, although the analytical expression is identical for both sides, the magnitude of Q_{pr} , k_{pr} , and Φ_{pr} depends on the water depth, and will be different at each side. Due to the orthogonality property of the structural modes the following expression is valid:

$$\iint_{S_s} W_{km}(x, z) W_{ln}(x, z) dx dz = \delta_{kl} \delta_{mn} \Gamma_{ln} \quad (2.40)$$

in which S_s denotes the gate surface and Γ_{ln} the solution of the integration. Multiplying Eq.(2.39) with another structural mode W_{ln} and integrating over the plate surface, yields:

$$\sum_{k=1}^{\infty} \sum_{m=1}^{\infty} A_{km} \rho_s (\omega_{km}^2 - \omega^2) \delta_{kl} \delta_{mn} \Gamma_{ln} = - \left[i \omega^2 \rho_f \sum_{k=1}^{\infty} \sum_{m=1}^{\infty} A_{km} \sum_{p=1}^{\infty} \sum_{r=1}^{\infty} \frac{Q_{km,pr} Q_{ln,pr}}{k_{y,pr} \Delta_{pr}} \right]_{\Sigma^{l+r}} - \iint_S \tilde{f}_e W_{ln} dx dz \quad (2.41)$$

in which $Q_{ln,pr}$ is defined similar to $Q_{km,pr}$:

$$Q_{ln,pr} = \iint_{S_w} \Phi_{pr}(x, z) W_{ln}(x, z) dx dz \quad (2.42)$$

2.4.5 SOLUTION OF THE GATE-FLUID MOTION

An infinite system of analytical equations is now obtained:

$$\sum_{k=1}^{\infty} \sum_{m=1}^{\infty} [\rho_s (\omega_{km}^2 - \omega^2) \delta_{kl} \delta_{mn} \Gamma_{ln} - L_{km,ln} + R_{km,ln}] A_{ln} = F_{ln} \quad (2.43)$$

with the fluid pressures given by:

$$L_{km,ln} = i \omega^2 \rho_f \sum_{p=1}^{\infty} \sum_{r=1}^{\infty} \frac{Q_{km,pr} Q_{ln,pr}}{k_{y,pr} \Delta_{pr}} \Big|_{h=h_l} \quad (2.44)$$

$$R_{km,ln} = i \omega^2 \rho_f \sum_{p=1}^{\infty} \sum_{r=1}^{\infty} \frac{Q_{km,pr} Q_{ln,pr}}{k_{y,pr} \Delta_{pr}} \Big|_{h=h_r} \quad (2.45)$$

and the modal force given by:

$$F_{ln} = \iint_S \tilde{f}_e(x, z, \omega) W_{ln}(x, z) dx dz \quad (2.46)$$

Due to the presence of damping, the solutions for \tilde{u} and \tilde{v} from equation (2.43) will be complex valued. The amplitudes are determined by $|w| = \sqrt{\text{Re}(\tilde{w})^2 + \text{Im}(\tilde{w})^2}$ and $|\nu| = \sqrt{\text{Re}(\tilde{\nu})^2 + \text{Im}(\tilde{\nu})^2}$.

2.4.6 STRESSES IN THE PLATE

When the structural deflection field is known, the stress in the isotropic homogeneous plate follows from:

$$\begin{bmatrix} \sigma_{xx} \\ \sigma_{zz} \\ \tau_{zx} \end{bmatrix} = - \frac{D t_y}{I} \begin{bmatrix} 1 & \nu & 0 \\ \nu & 1 & 0 \\ 0 & 0 & (1 - \nu) \end{bmatrix} \begin{bmatrix} \kappa_{xx} \\ \kappa_{zz} \\ \kappa_{zx} \end{bmatrix} \quad (2.47)$$

with κ_{xx} , κ_{zz} and κ_{zx} being the curvature of the plate in the respective direction.

As a stress criterion Von Mises could be used, which for general plane stress states:

$$\sigma_v = \sqrt{\sigma_{xx}^2 - \sigma_{xx} \sigma_{zz} + \sigma_{zz}^2 + 3 \sigma_{zx}^2} \leq f_y \quad (2.48)$$

with f_y being the yield strength of the steel material.

2.4.7 NUMERICAL EVALUATION OF THE SOLUTION

For evaluation of the system of equations (2.43), the infinite summations must be truncated to a finite number of structural and fluid modes. The necessary number of modes to provide sufficient accuracy, depends on the excitation frequency in relation to the resonance frequencies of the system. A displacement convergence criterion was presented in Tsouvalas et al. (2015), which was shown to give a good indication of internal bending moment and shear force convergence as well.

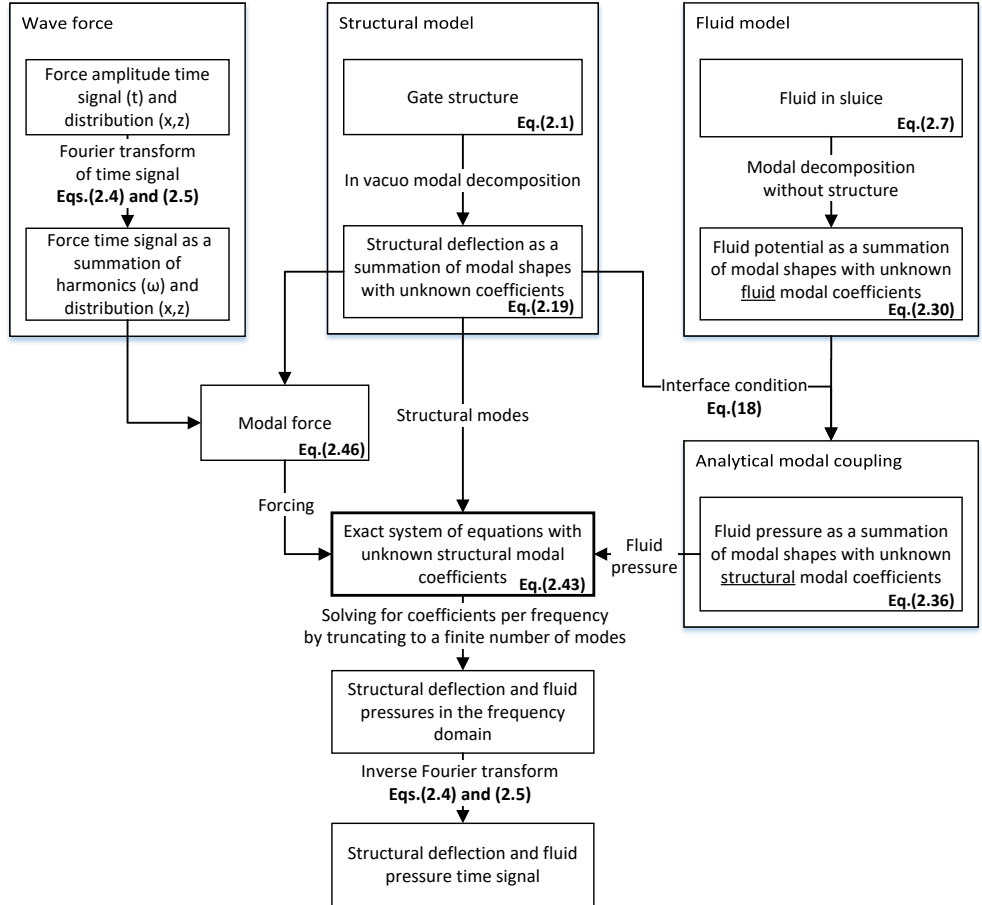


Figure 2.3: Overview of the semi-analytical method. The result of the derivations in this chapter is the system of equations in Eq.(2.43).

Part of the strength of this semi-analytical method, is that the mode shapes of the structure in vacuo are evaluated only once. Subsequently these mode shapes can be used to evaluate the response at the different excitation frequencies and force amplitude shapes. Due to the inclusion of surface waves in the model, the implicit dispersion equation must be solved for each excitation frequency, which leads to a higher numerical

effort compared to the case without surface waves. When evaluating the response for a large number of force frequencies such as is done after a Fourier transformation, in general only a part of the spectrum will result in significant contribution of surface waves.

Any spatial distribution of external forcing can be input to the calculations, as long as only the amplitude and not the distribution is time-dependent. The time-amplitude signal can then be transformed to the frequency domain. An overview of the developed model is shown in Figure 2.3. If the force distribution is in fact time-dependent, measures such as a discretization of the external force become necessary. The modal force F_{ln} can be numerically evaluated for each structural mode. Since this part is frequency-independent, a single evaluation suffices.

2.5 QUANTITATIVE ANALYSIS OF A WAVE IMPACT ON A FLOOD GATE

The developed model is used to determine the dynamic behaviour of a vertical steel flood gate subjected to a typical wave impact. For this wave impact force full scale pressure measurements are used (Hofland et al., 2011). The case study is explained in section 2.5.1 while in section 2.5.2, the modal expansion of the structure-fluid system is elaborated. Subsequently, in section 2.5.3 the quasi-static deflection of the gate is determined, and compared to the dynamic time domain response with and without the effect of the surrounding fluid in section 2.5.4.

2.5.1 CASE STUDY

The system parameters for the case study considered, are shown in Table 2.1. The gate is maintaining a water level difference of 3.0 m. The wave impact occurs towards the gate in the $y > 0$ fluid domain, where the lower water level is present. Only the linear dynamic response of the gate as a consequence of the impulsive wave impact force is considered in this study, which needs to be superimposed to the static response due to the presence of the hydrostatic loads at either side of the gate.

Table 2.1: Case parameters and their value

Structural parameters	Symbol	Value	Unit	Fluid parameters	Symbol	Value	Unit
Width	L_x	12	m	Width	L_x	12	m
Height	L_z	7.5	m	Water level left	h_l	7	m
Gate thickness	t	0.243	m	Water level right	h_r	4	m
Bending rigidity	D	$2.63 \cdot 10^8$	Nm	Fluid density	ρ_f	1025	kg/m ³
Distributed mass	ρ_s	95	kg/m ²	Fluid sound velocity	c_p	1500	m/s
Modulus of elasticity (steel)	E	$200 \cdot 10^9$	Nm ²	Gravitational constant	g	9.81	m/s ²
Moment of inertia	I	0.0012	m ³				
Poisson's ratio (steel)	ν	0.3	-				
Yield strength (steel)	f_y	$255 \cdot 10^6$	N/m ²				
Material damping (steel)	η	0.01	-				

The applied wave impact (Hofland et al., 2011, measurement s110) is of the flip through type, which is characterised by almost no entrapped air at the time of impact. This type of impact generally involves a large impact force and high peak pressures over short duration, in this case a vertically-integrated maximum force of 707 kN m⁻¹ and a maximum pressure of 827 kN m⁻². The wave pressure, measured at 19 distinct locations

over the vertical coordinate, is depicted for several moments in time during impact in Figure 2.4. It can be seen the pressure peak moves upwards during impact. The course of the total impact force per meter (gate) width in time is shown in Figure 2.5 (top).

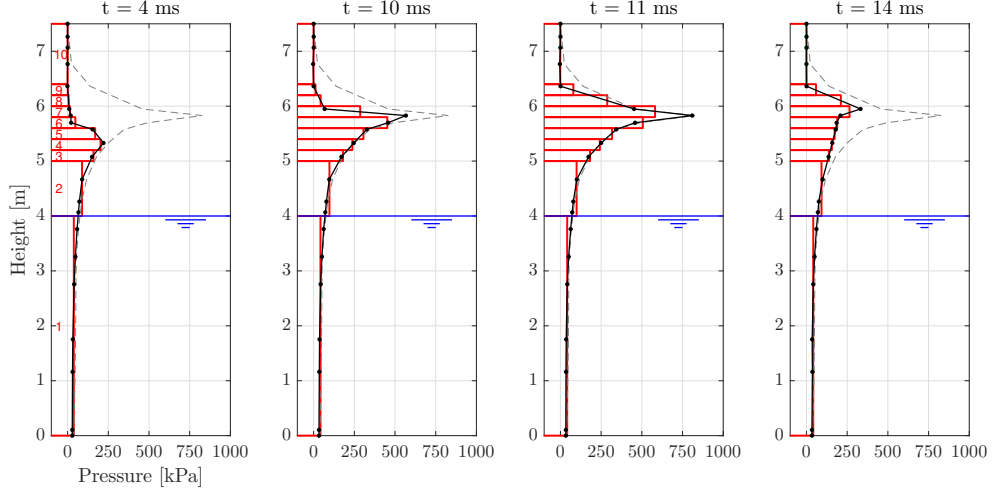


Figure 2.4: Wave pressure over the vertical at four moments during impact. The dashed line denotes the envelope of the extreme pressures per location. For the dynamic assessment, the pressures are averaged within discrete intervals over the height of gate. The resulting pressures, input to the model predictions, have been indicated in red.

As the force distribution changes over time, it cannot be separated into a space and time dependent part directly, as required for a direct one-dimensional Fourier transform with respect to time. For this reason, the wave force is divided into ten intervals over the vertical coordinate, which are shown in red in Figure 2.4. For every time step, it holds that the vertically-integrated value of the applied pressure is equal to that of the original signal. Each interval will now have its own amplitude-time signal, as shown in Figure 2.5 (bottom). The total external force is a summation of the signals in each interval:

$$f_e(x, z, t) = \sum_{n=1}^{10} [H(z - z_n) - H(z - z_{n+1})] f_{n,t}(t) \quad (2.49)$$

with f_e being the external wave force, z_n the vertical coordinates that denote the divisions between the intervals, and $f_{n,t}(t)$ the amplitude-time signal for each interval. The error resulting from dividing the force into a certain number of intervals depends mainly on the spatial distribution of the system resonance modes and impact force over the height. For the considered case, the error made by the division of the force into ten intervals was found to be small.

Each signal is Fourier transformed to the frequency domain, and subsequently the plate response is determined. As the model is linear, these responses may be summed. The summed response is transformed back to the time domain, which results in the prediction of the gate response.

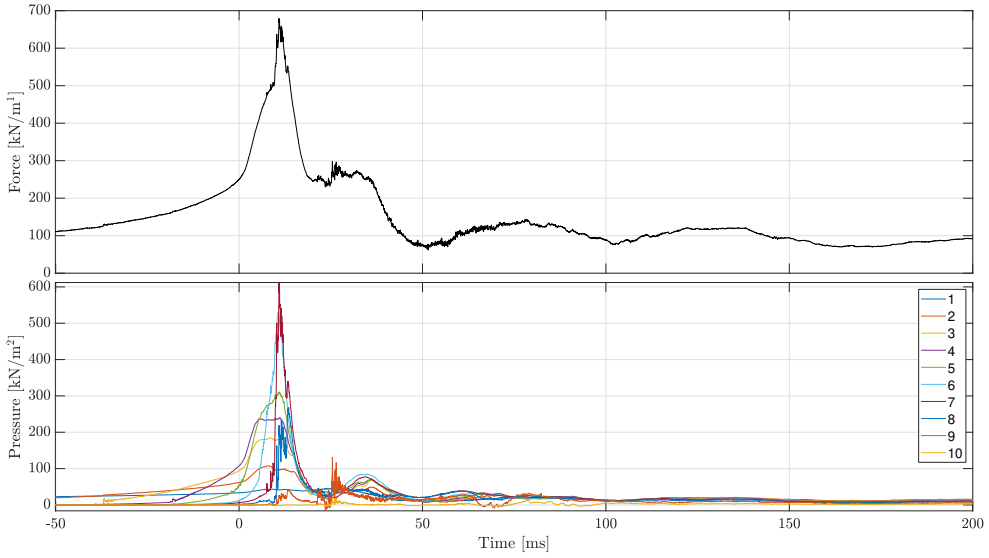


Figure 2.5: Vertically integrated wave force and the wave pressure amplitudes for each of the 10 intervals over the vertical of the gate as defined in Figure 2.4 over time. The maximum of the integrated wave pressure occurs at $t = 10.88$ ms.

2.5.2 MODAL EXPANSION OF THE SYSTEM

First, the modal expansion of the gate and fluid will be elaborated for the given system. For simplicity, the material damping η is neglected in the presentation of these results. In Figure 2.6 the in vacuo mode shapes of the plate and the corresponding resonance frequencies are shown. These have been validated by comparison with the analytical results by Leissa (1969). Since in the studied case the wave impact force has a constant magnitude over the width of the gate, and is therewith symmetric, there will be no response of purely antisymmetric modes to this force. This directly follows from the definition of the modal force in Eq.(2.46). In the present analysis, the structural and fluid modal expansion are both truncated to the first one hundred mode shapes. For the considered case this was proven to be more than sufficient based on the convergence of the deflection and stresses in the plate as discussed further in Section 2.5.4.

In Figure 2.7 for the fluid domain at $y < 0$ the first 25 roots of the dispersion equation Eq.(2.29) are depicted for two excitation frequencies. $\text{Re}(k_{y,pr}) \leq 0$ and $\text{Im}(k_{y,pr}) \geq 0$ are imposed for the fluid domain at $y < 0$ to satisfy the radiation conditions as was discussed in section 2.4.2. The real valued roots $k_{y,pr}$ correspond to propagative fluid modes resulting in hydrodynamic damping, while the imaginary valued roots $k_{y,pr}$ correspond to evanescent modes resulting in hydrodynamic mass and stiffness.

The first six shapes of the submerged structure are shown in Figure 2.8. The shape of the submerged gate at the first resonance mode is reasonably similar to the first natural mode of the in vacuo structure as shown in Figure 2.6. The vibration shapes at higher resonance frequencies alter substantially. Secondly, the resonance frequencies reduce

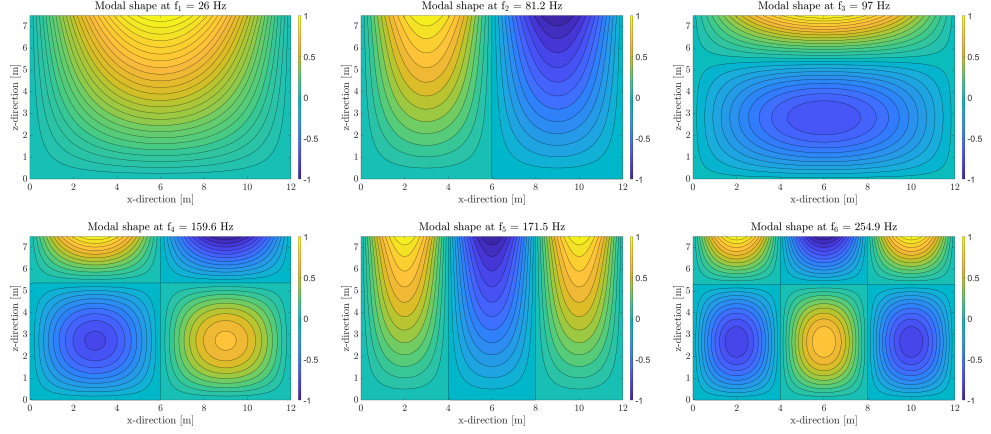


Figure 2.6: The in vacuo mode shapes of the gate at the first six resonance frequencies

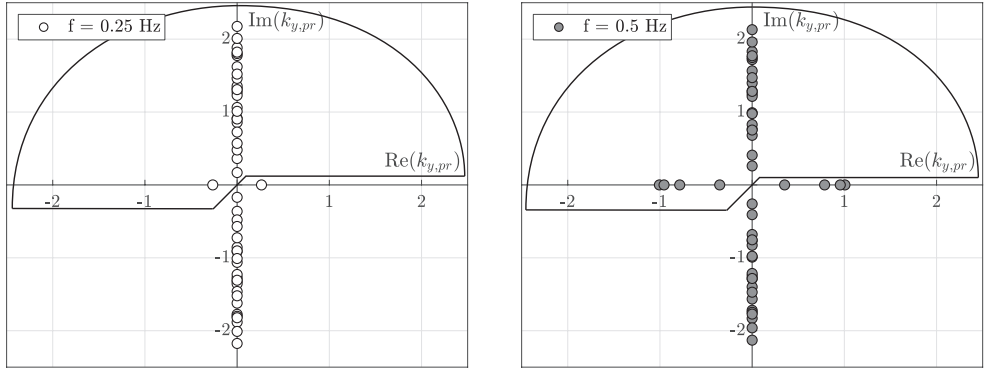


Figure 2.7: The first 25 roots $k_{y,pr}$ of the dispersion relation for the fluid domain at $y < 0$ ($h_l = 7$ m) at frequencies 0.25 and 0.5 Hz

significantly compared to those of the in vacuo gate, as can be seen in Table 2.2. Surface waves have a negligible effect on the resonance frequencies as the resonance frequencies are relatively high compared to typical frequencies of surface waves at the considered water depths. The effect of surface waves is expected to be greater in the case of a gate-fluid system with lower resonance frequencies. The effect of compressibility increases for higher frequencies. The error of considering the fluid as incompressible is limited to approximately 5% for the first 10 resonance frequencies as can be seen from Table 2.2.

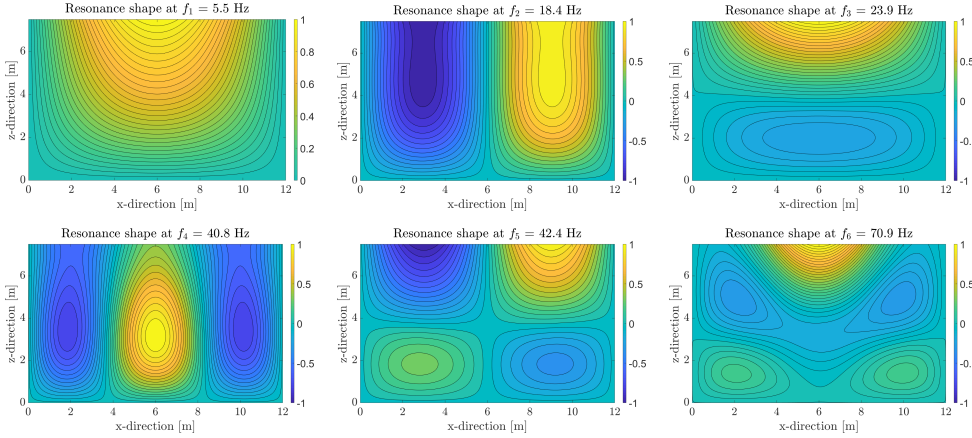


Figure 2.8: The amplitude of the complex valued response of gate $\sqrt{\text{Re}^2(w) + \text{Im}^2(w)}$ for the first six resonance frequencies including the effect of the fluid pressure

Table 2.2: First ten resonance frequencies of the gate in vacuo and submerged. The resonance frequencies are shown as well for the cases when surfaces waves are excluded or the fluid is considered incompressible.

Condition	f_1	f_2	f_3	f_4	f_5	f_6	f_7	f_8	f_9	f_{10}
In vacuo [Hz]	26.0	81.2	97.0	159.6	171.5	254.9	257.5	297.8	321.1	384.0
Submerged [Hz]	5.5	18.4	23.9	40.8	42.4	70.9	74.6	95.1	114.5	130.6
- Excluding surface waves	5.5	18.4	23.9	40.8	42.4	70.9	74.6	95.1	114.5	130.6
- Incompressible fluid	5.5	18.5	24.1	41.7	43.2	73.8	76.9	100.5	121.1	125.9

Figure 2.9 shows the normalised absolute fluid pressure (in the fluid domain at $y > 0$) corresponding to the structural motion for two resonance frequencies of the submerged structure. For the fourth resonance frequency, the vibration shape of the gate is clearly recognised. The fluid pressure decays quickly in the direction normal to the surface of the gate. The tenth resonance frequency of the gate-fluid system is close to theoretical resonance frequency of the compressible fluid. At the resonance frequencies of the fluid, the separation constant $k_{y,pr}$ tends to zero. From Eq.(2.37), it can be seen that the fluid pressure will then tend to infinity, as $k_{y,pr}$ is in the denominator of the fraction. Secondly, the decay in y-direction tends to diminish as the exponential term $e^{-ik_{y,pr}y} \rightarrow 1$. The shape of the fluid pressure is in this case almost entirely determined by the sluice geometry. For

both frequencies shown in Figure 2.9, the effect of surface waves on the fluid response has diminished, as the pressure at the still water level is approximately zero.

2.5.3 QUASI-STATIC RESPONSE

The quasi-static response of the gate to the wave impact is evaluated with the developed model. The maximum occurring total wave impact force during the recorded time interval is applied for this purpose. The wave force is divided into ten intervals with equal pressure as defined in Figure 2.4 to obtain a valid comparison with the dynamic response. The static behaviour to this force is obtained by setting $\omega = 0$ in Eq.(2.43). For the quasi-static consideration, the fluid pressure as a consequence of the movement of the gate due to the impact load does not play a role as follows from applying a zero frequency in the expressions for the fluid impedance in Eqs.(2.44) and (2.45).

The static response of the gate to the wave impact is depicted in Figure 2.10. The maximum deflection of 80.6 mm is found at the middle of the top edge of the gate. This prediction has been validated by a FE model of the plate and results are in good agreement. Stresses and the structural safety are assessed according to the Von Mises yielding stress criterion as presented in Eq.(2.48). The maximum stress at the surface of the gate is 129 N/mm².

2.5.4 DYNAMIC RESPONSE

The dynamic response is determined by Fourier transforming each force interval (over the height of the gate) from the time domain to the frequency domain, as was discussed in Section 2.5.1. These frequency domain signals are input to the model and the total deflection is found by the summation of the responses to each of the force intervals. To obtain a stable time signal after application of the inverse Fourier transform, a small amount of material damping of $\eta = 0.01$ is introduced at this point (Kvalsvold and Faltinsen, 1993). The experiments in Chapter 5 indicate that a higher amount of damping may possibly be expected for this type of problem. However, further substantiation is required to deviate from this more conservative value and apply a higher amount of damping. Introducing this type of material damping has a minor effect on the resonance frequencies of the gate, which herewith become complex.

The displacement of several locations of the gate immersed in fluid during and after impact is shown in Figure 2.11. These locations are chosen such that the first three non-asymmetric resonance frequencies could be distinguished well. The maximum deflection occurs at the top middle of the gate, and is 45.7 mm. This is significantly lower than the previously determined quasi-static response, which can be explained by the fact that the peak pressure duration (≈ 20 ms) is substantially lower than the first resonance period of the submerged gate ($T_1 = 1/5.5 \approx 182$ ms). Considering the first resonance frequency, the system is in fact slow so that the response is not amplified. This is characterised by the deflection of the plate reaching its maximum at $t = 60.0$ ms, while the wave peak pressure occurs at $t = 10.9$ ms. The maximum internal stress is 75.8 N/mm².

In the design of hydraulic engineering, analyses have been applied before in which the effect of the hydrodynamic response has been neglected altogether. For comparison, Figure 2.11 therefore also shows the response of the in vacuo gate, thus without the effect

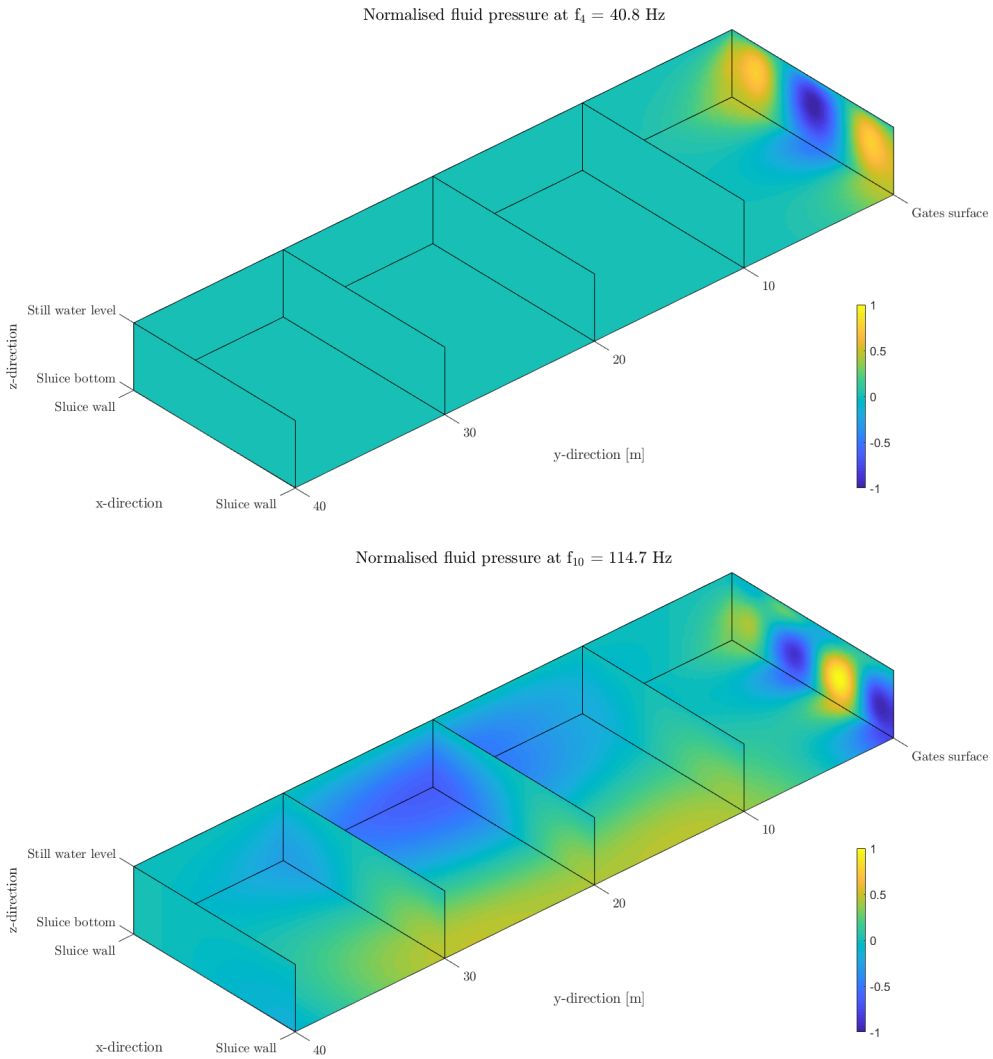


Figure 2.9: Normalised absolute fluid pressure (for $0 \leq y \leq 40$ m) corresponding to the structural motion for two resonance frequencies of the submerged gate.

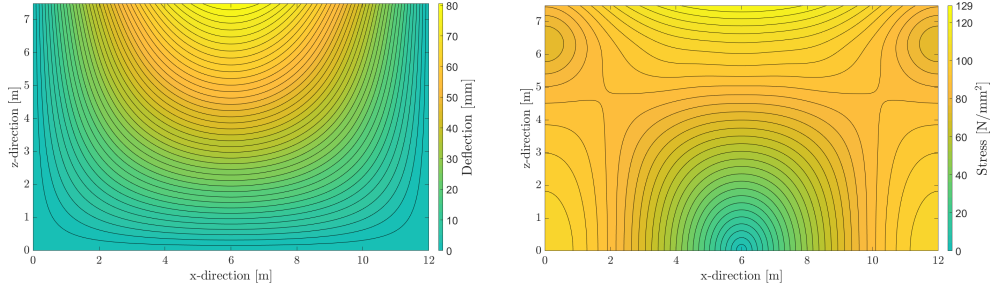


Figure 2.10: Quasi-static deflection and stress at the plate's surface due to the maximum wave impact force

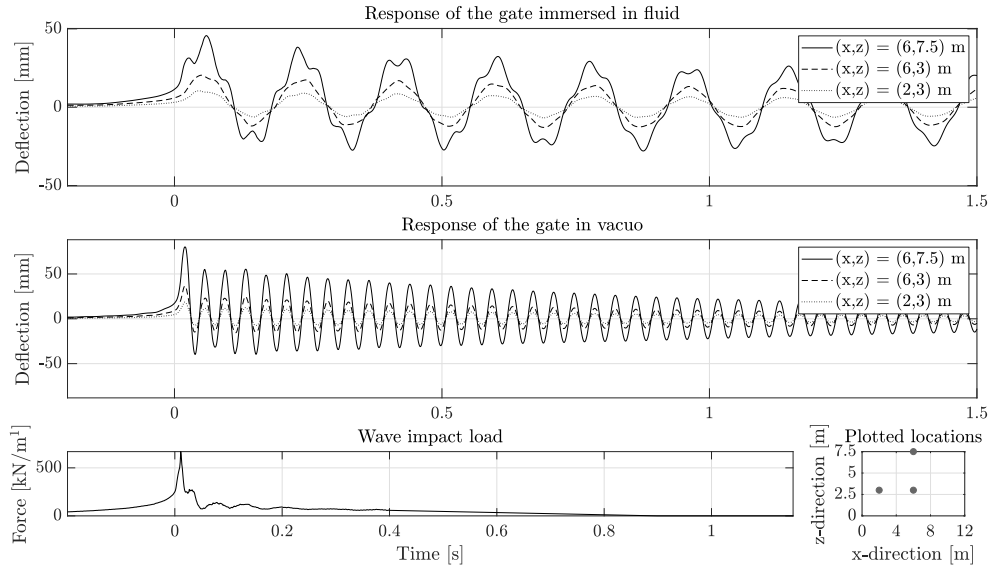


Figure 2.11: The dynamic deflection response to the wave impact of several locations of the gate immersed in fluid and in vacuo

of the hydrodynamic response. The maximum deflection would be 80.2 mm, which is in this case substantially higher than the response including the hydrodynamic pressures.

In common engineering practice when a quasi-static modelling approach is used, an amplification factor is generally applied to the force to account for possibly unfavourable dynamic behaviour of the structure. Depending on the characteristics of the structure and the type of wave impact, the applied factor varies between 1.0 and 1.5. For the considered case, regarding the dynamic behaviour of the gate immersed in fluid actually lead to a reduction of the maximum stress by almost half of the one obtained with the quasi-static calculation described in Section 2.5.3.

The maximum deflection and internal stress occur at the same time. It is also possible that the maximum internal stress occurs at a different moment in time than the maximum deflection, which can amongst others be a consequence of the excitation of higher structural modes. This is explained by the increase in curvature for higher mode shapes, which leads to larger internal stresses for a given maximum deflection. In Figure 2.11 the excitation of higher natural modes can be distinguished as well by the multi-peaked vibration. The deflection at the top middle of the gate, where the maximum occurs, is governed by the first two resonance frequencies.

The results show to be sufficiently converged for the hundred plate and hundred fluid modes taken into account to determine the dynamic response. In Figure 2.12 the relative error in the found maximum plate stress is shown in relation to the amount of modes taken into account. When considering higher excitation frequencies a higher number of modes is required to obtain the same level of accuracy. However, this dependence is relatively weak.

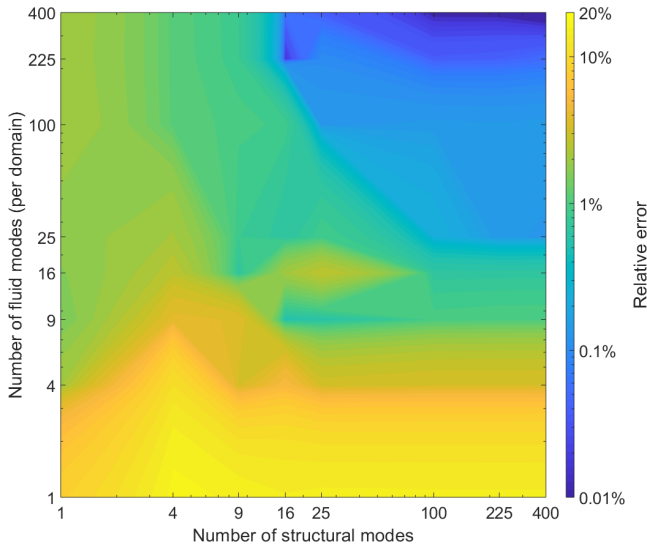


Figure 2.12: The error in maximum plate stress found as a function of the number of structural and fluid modes taken into account relative to the result for both four hundred structural and fluid modes.

2.6 PERFORMANCE OF THE MODEL

The performance of the developed semi-analytical model is investigated by comparing its results with the software package COMSOL (COMSOL, 2018). The same gate-fluid system as described in the previous section is investigated. The gate is represented by shell elements (3D) in COMSOL. The material of the gate is considered to be isotropic and linear elastic. The fluid is compressible and modelled with the transient pressure acoustics module of COMSOL. To simplify the COMSOL model surface waves are excluded from the analysis. Instead, a zero pressure boundary condition is applied at the free surface. It has been shown in the previous section that this may be assumed for the presented case. The infinite sluice length in y-direction is represented by a standard wave radiation condition at a distance of 100 m from the gate in both fluid domains. For a detailed overview of the shell and transient pressure acoustics theory used in COMSOL is referred to COMSOL (2018). As it is not possible to include material damping in the COMSOL time-domain model, a distributed viscous damping of $c_d = 10 \text{ kNs/m/m}^2$ is introduced, which acts on the entire surface of the plate. A variable triangular mesh is used for the shell and a variable tetrahedral mesh for the fluid domain. Both have a maximum element size of 1 m. The time-domain results converge for this element size.

The results of the wave impact case are not directly compared with the FE model as it is difficult to apply a large number of time-varying force signals at various locations of the gate in the software package COMSOL. Instead, an idealized triangular impact force with a duration of 10 ms is applied on the left upper part of the gate. Such an impact force of short duration is especially suitable for the purpose of validation, as it ensures a wideband frequency spectrum that excites multiple system modes. The same numerical routine is used to obtain the results for the validation study as for the wave impact case.

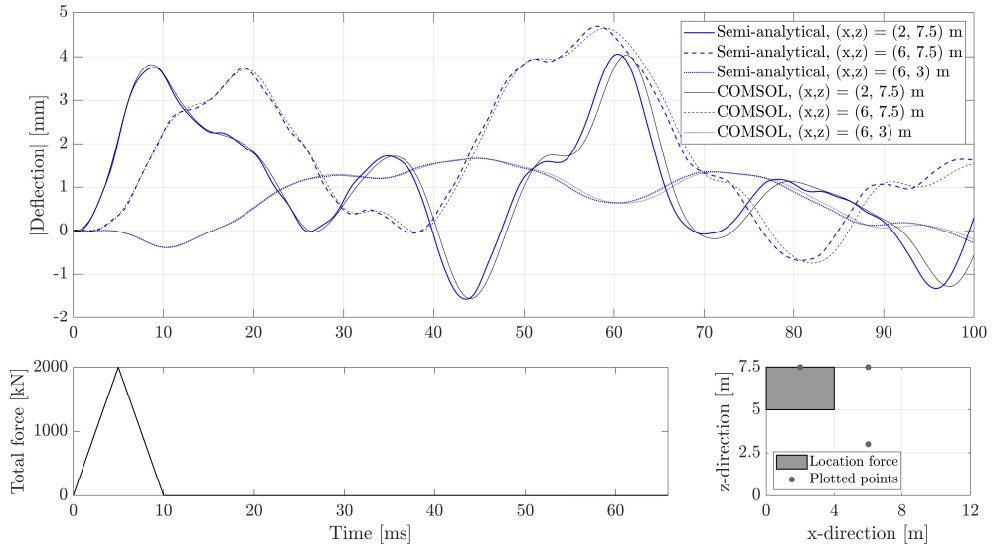


Figure 2.13: The time-domain response of the gate immersed in fluid to a triangular peak load predicted by the semi-analytical model and COMSOL

The time domain results of both models are shown for multiple locations on the gate in Figure 2.13. As can be seen, the results match closely even though minor differences in predicted frequencies of the response cumulate over time. A comparison of the resonance frequencies predicted by both models is shown in Table 2.3. The relatively small differences in the resonance frequencies for the in vacuo plate are expected to be caused by the omission of rotational inertia and shear deformation in the semi-analytical model. As expected, this error increases for higher modes. The difference between predicted resonance frequencies for the immersed condition is in the same order. This is expected to partially originate from the COMSOL model as results showed some dependency on mesh size and sluice length for eigenfrequency analysis, which did not converge within the range that could be investigated with reasonable computation times.

Table 2.3: Comparison of the first five predicted resonance frequency between the semi-analytical and COMSOL model for the in vacuo and immersed system.

Condition	Model	f_1	f_2	f_3	f_4	f_5
In vacuo	Semi-analytical [Hz]	26.05	81.15	96.97	159.61	171.49
	COMSOL [Hz]	25.93	80.43	95.78	156.60	168.69
	Relative difference [-]	0.46%	0.90%	1.24%	1.92%	1.66%
Immersed	Semi-analytical [Hz]	5.51	18.36	23.89	40.81	42.39
	COMSOL [Hz]	5.49	18.14	23.52	40.39	41.50
	Relative difference [-]	0.36%	1.21%	1.57%	1.04%	2.14%

The computation time of the semi-analytical model for the presented time-domain analysis took 12 minutes on a 3.60 GHz quad core processor, while computation with the COMSOL model lasted approximately 19.5 hours. The computational efficiency of the semi-analytical code has not been fully optimised yet and can still be improved. Furthermore, the response of the same system can be investigated for a range of loads with relatively little additional computation time.

It must be noted that the superposition of modal responses is valid only for a linear system. Any non-linearities are therefore omitted. For highly non-linear interaction problems, it therefore remains necessary to resort to the more computationally intensive coupled numerical time domain methods. For many hydraulic engineering cases however, the presented method is expected to represent the behaviour with sufficient accuracy at least for preliminary design stages. For flood defence structures in the Netherlands especially the linear elastic behaviour of the material is relevant, as these structures must be designed based on a non-plastic stress criterion.

2.7 CONCLUSION

A semi-analytical model has been developed that allows to study the bending vibrations of a gate immersed in fluid subjected to any time varying force. The developed method accounts for the three dimensional behaviour of both the structure and fluid, and solves the involved interaction efficiently. It is important to mention that one needs to solve the structure and fluid eigenvalue problems only once for a given geometry and water heights.

The values can be stored and used to calculate the response to any given impact load. This is a fundamental difference compared to standard numerical methods. The adopted method does not depend on the assumed-modes approach. Furthermore, surface waves and compressibility were taken into account so that the hydrodynamic fluid pressure exerted on the gate is predicted accurately in both low and high frequency regimes. Due to the method's computational efficiency and accurate representation of the problem, it can be applied efficiently as a preliminary design tool. This is a step forward from the single or two degree of freedom models used often in present design practice, which give no continuous information on the deflection and internal stresses along the gate or in the fluid domain. Additionally, the model allows to perform fatigue calculations and probabilistic assessments. Results of the developed model were compared against the ones obtained with FEM simulations for the case of an idealized triangular pressure pulse applied on the gate. It is demonstrated that the computational method adopted in the former is capable of providing results similar to those of a detailed FE model within a fraction of the computation time of the latter.

A measured wave impact signal was applied to a flood gate design as a case study. As expected, the prediction of the dynamic response, including the interaction between the gate and the surrounding fluid system, lead to a significantly different assessment of the safety than based on the static response only. For the case, the consideration of the dynamic behaviour and the fluid-structure interaction resulted in a less costly design. This illustrates that considering the dynamic behaviour in gate design, rather than using a quasi-static approach with a conservative amplification factor (usually a 50% increase of the maximum force), can also have advantages in terms of design optimization and therewith costs next to the more accurate determination of the expected dynamic behaviour.

Surface waves did not significantly influence the hydrodynamic response of the gate for the excitation and resonance frequencies that were involved in the breaking wave impact case study. Compressibility mainly had an effect on the higher resonance frequencies of the gate-fluid system. For the studied gate, which was considered homogeneous and isotropic, the first two system resonance frequencies governed its response. Considering more realistic and detailed gate designs consisting of beams and plates, and varying design impacts for certain parts of these gates, is expected to further increase the importance of taking higher vibration modes into account. This is investigated further after extending the model for composite fluid domains and coupling it to a finite element model to represent more complex gate designs in the next chapters.

3

**EXTENDING THE
SEMI-ANALYTICAL
APPROACH FOR
COMPOSITE FLUID
DOMAINS**

In the previous chapter, the basis of a semi-analytical fluid-structure interaction model was presented that is able to predict flood gate vibrations in a long dewatering sluice. A single infinitely long fluid domain was accounted for at each side of the gate. Practical situations also exist where such a representation may not always be sufficient. A relevant example is that of a flood gate with an overhanging structure in front that causes violent reflecting wave impacts. Moreover, a sea or lake is often present at the end of the dewatering sluice which must be accounted for depending on its length. These aspects affect the dynamic behaviour of the gate. In this chapter, the semi-analytical model is therefore extended to represent these type of problems. The following chapter then combines the here presented semi-analytical solution with a finite element model to predict gate vibrations for a wider range of flood gate designs.

Section 3.1 further introduces the topic of this chapter and the model techniques that are applied. Section 3.2 gives a description of the geometry of the gate and fluid model. Section 3.3 presents the theoretical formulation of the problem. In Section 3.4 a semi-analytical solution is derived for this problem. Section 3.5 then again validates this solution by comparison to a standard finite element package. Finally, Section 3.6 presents the conclusions of this chapter.

3.1 INTRODUCTION

Many examples of coastal structures exist where an overhang is present in front of the gate, such as culverts, dewatering sluices with a bridge deck on top and vertical breakwaters with a return crown wall or overhanging slab to reduce overtopping (De Almeida and Hofland, 2020b; Kisacik et al., 2014). Violent wave impacts can occur in these situations when reflected standing waves hit the bottom of the overhang in front of the gate. This has for instance been an important design consideration for the renovation of the Afsluitdijk (Figure 1.4). The presence of an overhang is not only the cause of wave impacts, but also affects the hydrodynamic pressures that result from the motion of the gate and therewith the response of the gate-fluid system.

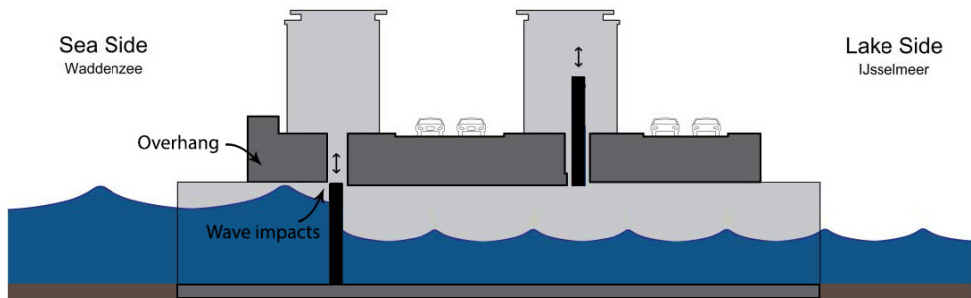


Figure 3.1: Impression of an existing flood gate complex in the Afsluitdijk where wave impacts may occur due to the presence of an overhanging structure (De Almeida et al., 2019)

This chapter is based on parts of the publication "A fluid–structure interaction model for assessing the safety of flood gate vibrations due to wave impacts" in Coastal Engineering (Tieleman et al., 2021). Some minor changes have been introduced to make the text consistent with the other chapters of the thesis.

This chapter therefore establishes a linear semi-analytical model to predict the dynamic behaviour of a flood gate with an overhang. The presented method solves the involved fluid-structure interaction in a computationally efficient manner. This makes it possible to perform probabilistic evaluations, which is not feasible when applying time-domain finite element methods. Based on the developed model here, a probabilistic design approach is presented in Chapter 7 that deals with the uncertainty accompanied with wave impacts.

The method of solution is based on a substructuring mode matching technique as used in the previous chapter and by Tsouvalas and Metrikine (2014). To represent the considered situation with overhang, a solution is derived for composite fluid domains, which was not yet included in the previous version of the model. The main computational advantage of the mode matching technique lies in the ability to store and reuse partial results in contrast to the stepwise calculation in finite element (FE) methods. For instance, when regarding a large number of loads, the frequency response function of the gate fluid system has to be computed only once. Tsouvalas et al. (2020) have applied this technique to predict the seismic response of liquid storage tanks. Leblond et al. (2009) apply a similar approach for the bending of an elastic cylinder. Three fluid models are considered, namely potential, viscous and acoustic. The modal time dependent displacement coefficients are obtained by matrix inversion in the Laplace domain and fast numerical inversion of the Laplace transform. In Tsouvalas and Metrikine (2016), the mode matching method was successfully employed to predict the noise reduction by the application of an air-bubble curtain in offshore pile driving, showing that a solution can be derived for composite fluid domains with varying boundary conditions. In this study, the specific solution for the situation of a flood gate with overhang is presented. The resulting model is validated by comparison to an existing time-domain finite element model.

3.2 DESCRIPTION OF THE FLUID-STRUCTURE RESPONSE PROBLEM

Figure 3.2 shows the geometry of the model. The gate is represented by a thin flexible plate, which is homogeneous and isotropic and is in full contact with the fluid at the vertical plane. Generally, flood gate designs consist of a front plate and several supporting back beams. More complex gate configurations such as these can be considered by determining the structural mode shapes with existing FE package. This is the subject of the following chapter. This study focuses on correctly representing the hydrodynamic pressures for the presence of an overhanging structure. The relatively straightforward representation of the gate as a thin plate is deemed sufficient without loss of generality.

The gate has a width L_x , height L_z , distributed mass per unit surface ρ_s , and uniform bending rigidity $D = \tilde{E}t^3/(12(1 - \nu^2))$, in which \tilde{E} is the modulus of elasticity, t is the thickness of the gate, and ν is the Poisson's ratio. An isotropic material damping factor η is applied to the modulus of elasticity in the frequency domain by $\tilde{E} = (1 + \eta i)E$. The gate is simply supported at its vertical boundaries ($x = 0$, $x = L_x$) and bottom ($z = 0$) while its top edge ($z = L_z$) is stress-free.

Fluid is present in a sluice structure at both sides of the gate, for which three fluid regions can be distinguished. On one side of the gate the sluice has a limited length and an overhang is present. On the other side of the gate the sluice extends to infinity, which is

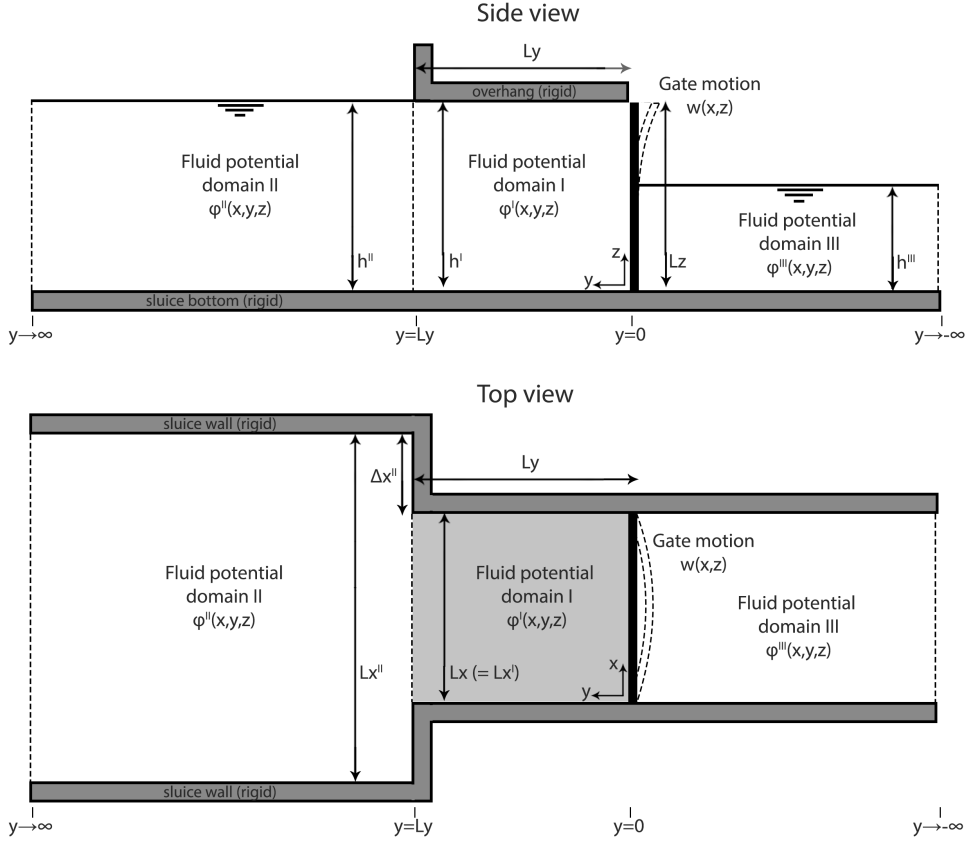


Figure 3.2: Side and top view of the model domain consisting of a flexible gate and three fluid regions

a valid representation of situations with long sluice lengths compared to the water depth. Based on the same method of solution, the model can be extended to include additional fluid domains accounting for a finite sluice length on both sides of the gate.

All regions have impermeable walls and a horizontal bottom. Region I occupies the domain $0 \leq y \leq L_y$ and $0 \leq x \leq L_x^I (= L_x)$. An impermeable overhang is present at $z = L_z$ restricting the fluid flow in the vertical direction. At the moment of a wave impact, the water height h_I in this region is equal to the height of bottom of the overhang. Region II occupies the domain $L_y \leq y \leq \infty$ and $-\Delta x^{II} \leq x \leq L_x^{II} - \Delta x^{II}$. No overhang is present so that the fluid has a free surface. The water level can be equal or higher than in region I. However, a water level close to the bottom of the overhang generally leads to the highest impact pressures and is thus of most interest De Almeida and Hofland (2020b). The width of this domain can be chosen much larger than that of region I to represent the presence of a lake or sea at the end of a sluice or culvert. Finally, Region III occupies the domain $y < 0$ and $0 \leq x \leq L_x^{III} (= L_x)$. This region has similar boundary conditions as region II. A free surface boundary condition is applied at the free surface. Tieleman et al. (2019a) have presented

in which regimes of water depths and excitation frequencies surface waves influence the hydrodynamic response of the structure. Furthermore, the fluid is considered to be compressible, irrotational and inviscid.

3.3 THEORETICAL FORMULATION OF THE PROBLEM

The governing equations describing the dynamic response of the system are presented. The equation of motion of the gate includes the fluid pressure acting on both sides as well as the external force:

$$\rho_s \frac{\partial^2 w(x, z, t)}{\partial t^2} + D \nabla^2 \nabla^2 w(x, z, t) = p^I(x, y = 0, z, t) - p^{III}(x, y = 0, z, t) + f_e(x, z, t) \quad (3.1)$$

in which w denotes the displacement of the mid-surface of the plate, $\nabla^2 = \frac{\partial^2(\cdot)}{\partial x^2} + \frac{\partial^2(\cdot)}{\partial z^2}$, ρ_s is the distributed mass per unit of area, f_e is the external force, and p_I and p_{III} are the pressures exerted by the fluid on either side as a consequence of the motion of the gate. The external force in Eq.(3.1), being the wave impact force in this study, is predefined. Since the model includes the responsive fluid pressures resulting from the motion of the gate, the external force needs to be based on the situation of a rigid structure. Chapter 7 presents a theoretical model to predict the wave impact force for a given design spectrum.

The boundary conditions at $x = 0; L_x$ and at $z = 0; L_z$ read (Leissa, 1969):

$$w(x = 0, z) = m_{xx}(x = 0, z) = w(x = L_x, z) = m_{xx}(x = L_x, z) = 0 \quad (3.2)$$

$$w(x, z = 0) = m_{zz}(x, z = 0) = m_{zz}(x, z = L_z) = v_{zy}(x, z = L_z) = 0 \quad (3.3)$$

in which m_{xx} and m_{zz} are the bending moments in x- and z-direction, and v_{zy} is the effective Kelvin-Kirchoff shear force in z-direction.

For the description of the fluid motion, the velocity potential function $\phi^j(x, y, z, t)$ is introduced with $j = I, II, III$ denoting the respective fluid region in accordance with Figure 3.2. The equation of motion of each fluid region reads:

$$\nabla^2 \phi^j(x, y, z, t) - \frac{1}{c_p^{j^2}} \frac{\partial^2 \phi^j(x, y, z, t)}{\partial t^2} = 0 \quad (3.4)$$

in which c_p^j is the sound velocity in water in each region. The velocity vector and pressure are given by:

$$\nabla \phi^j(x, y, z, t) = -\mathbf{v}^j(x, y, z, t) \quad (3.5)$$

$$p^j(x, y, z, t) = -\rho_f^j \frac{\partial \phi^j(x, y, z, t)}{\partial t} \quad (3.6)$$

in which ρ_f^j is the fluid density per region. Fluid regions I and II will generally have the same fluid density. The fluid density at both sides of the flood gate might differ however, for example when the flood gate separates sea and fresh water.

Between fluid regions I and II kinematic and dynamic continuity are enforced and at the structure-fluid interfaces velocity compatibility is enforced. This leads to the following

interface conditions:

$$\left. \frac{\partial \phi^j(x, y, z, t)}{\partial y} \right|_{y=0} = -v_y^j(x, y, z, t) \Big|_{y=0} = -\frac{\partial w(x, z, t)}{\partial t} \quad (\text{for } j = I, III) \quad (3.7)$$

$$\rho_f^I \frac{\partial \phi^I(x, y, z, t)}{\partial t} \Big|_{y=L_y} = \rho_f^I \frac{\partial \phi^{II}(x, y, z, t)}{\partial t} \Big|_{y=L_y} \quad (\text{for } \Delta x^{II} \leq x \leq L_x^{II} - \Delta x^{II}) \quad (3.8)$$

$$\left. \frac{\partial \phi^I(x, y, z, t)}{\partial y} \right|_{y=L_y} = \left. \frac{\partial \phi^{II}(x, y, z, t)}{\partial y} \right|_{y=L_y} \quad (\text{for } \Delta x^{II} \leq x \leq L_x^{II} - \Delta x^{II}) \quad (3.9)$$

Furthermore, at $y \rightarrow \infty$ and $y \rightarrow -\infty$ the radiation conditions should be satisfied at all times in both regions II and III. This results in conditions for the wave numbers in y -direction as discussed further at the end of this section.

The boundary conditions at the impermeable sluice walls and bottom simply state zero fluid velocity. At the still water level of the fluid in regions II and III a pressure release boundary condition is applied, while the overhang poses a zero velocity condition in domain I. This leads to the following boundary conditions:

$$\left. \frac{\partial \phi^j(x, y, z, t)}{\partial x} \right|_{x=0} = \left. \frac{\partial \phi^j(x, y, z, t)}{\partial x} \right|_{x=L_x^j} = 0 \quad (\text{for } j = I, III) \quad (3.10)$$

$$\left. \frac{\partial \phi^{II}(x, y, z, t)}{\partial x} \right|_{x=-\Delta x^{II}} = \left. \frac{\partial \phi^{II}(x, y, z, t)}{\partial x} \right|_{x=L_x^{II}-\Delta x^{II}} = 0 \quad (3.11)$$

$$\left. \frac{\partial \phi^I(x, y, z, t)}{\partial z} \right|_{z=0} = \left. \frac{\partial \phi^I(x, y, z, t)}{\partial z} \right|_{z=h^I} = 0 \quad (3.12)$$

$$\left. \frac{\partial \phi^j(x, y, z, t)}{\partial z} \right|_{z=0} = 0 \quad (\text{for } j = II, III) \quad (3.13)$$

$$\left. \frac{\partial^2 \phi^j(x, y, z, t)}{\partial t^2} \right|_{z=h_j} + g \left. \frac{\partial \phi^j}{\partial z} \right|_{z=h_j} = 0 \quad (\text{for } j = II, III) \quad (3.14)$$

Eqs.(3.1)-(3.14) complete the mathematical statement of the problem in the time domain.

3.4 SOLUTION TO THE FLUID-STRUCTURE INTERACTION PROBLEM

By applying the Fourier transform pair as stated below, equations (3.1)-(3.14) are transformed to the frequency domain.

$$\tilde{G}(\omega) = \int_{-\infty}^{\infty} g(t) e^{-i\omega t} dt \quad (3.15)$$

$$g(t) = \frac{1}{2\pi} \int_{-\infty}^{\infty} \tilde{G}(\omega) e^{i\omega t} d\omega \quad (3.16)$$

in which ω is the angular frequency, $g(t)$ is the examined quantity and $\tilde{G}(\omega)$ its amplitude in the frequency domain, i.e. the displacement of the gate or the fluid pressure. A model decomposition scheme is introduced as in Tieleman et al. (2019b) yielding the following

modal expansions:

$$\tilde{w}(x, z, \omega) = \sum_{k=1}^{\infty} A_k(\omega) W_k(x, z) \quad (3.17)$$

$$\tilde{\phi}^I(x, y, z, \omega) = \sum_{p=1}^{\infty} \left(B_p^-(\omega) e^{-ik_{y,p}^I(L_y-y)} + B_p^+(\omega) e^{-ik_{y,p}^I y} \right) \Phi_p^I(x, z) \quad (3.18)$$

$$\tilde{\phi}^{II}(x, y, z, \omega) = \sum_{r=1}^{\infty} C_r^+(\omega) e^{-ik_{y,r}^{II}(y-L_y)} \Phi_r^{II}(x, z) \quad (3.19)$$

$$\tilde{\phi}^{III}(x, y, z, \omega) = \sum_{t=1}^{\infty} D_t^+(\omega) e^{-ik_{y,t}^{III}(-y)} \Phi_t^{III}(x, z) \quad (3.20)$$

In Eqs.(3.17)-(3.20) local axis systems are introduced for the exponential terms in accordance with Schmidt and Tango (1986) and Jensen et al. (2011) to ensure unconditional numerical stability of the global matrix of equations that will form the solution to the presented problem. The coefficient A_k , B_p^- , B_p^+ , C_r^+ and D_t^+ denote the amplitudes (at $y = 0$) of the corresponding plate modes W_k and fluid modes Φ_p^I , Φ_r^{II} and Φ_t^{III} in the vertical plane. In region II and III only outgoing waves are permitted to satisfy the conditions at $y = \pm' \infty$.

The wave numbers $k_{y,p}^I$, $k_{y,r}^{II}$ and $k_{y,t}^{III}$ can be found by solving the eigenvalue problem for each region separately Tieleman et al. (2019b):

$$k_x^{j^2} + k_y^{j^2} + k_z^{j^2} - k_f^2 = 0 \quad (3.21)$$

A decaying field representing the evanescent waves along the y-direction in region II and III hold for $\text{Im}(k_y^j) \leq 0$ while the radiation condition at infinity requires $\text{Re}(k_y^j) \geq 0$ (Tieleman et al., 2019b).

To satisfy Eqs.(3.10)-(3.14), the eigenshapes of the fluid in the vertical plane Φ_p^I , Φ_r^{II} and Φ_t^{III} are:

$$\Phi_p^I(x, z) = \cos(k_{z,p_1}^I z) \cos(k_{x,p_2}^I x) \quad \text{with: } k_{x,p_1}^I = \frac{(p_1-1)\pi}{L_x^I} \quad (3.22)$$

$$\text{and: } k_{z,p_2}^I = \frac{(p_2-1)\pi}{h^I}$$

$$\Phi_r^{II}(x, z) = \cos(k_{z,r_1}^{II} z) \cos(k_{x,r_2}^{II} x) \quad \text{with: } k_{x,r_1}^{II} = \frac{(r_1-1)\pi}{L_x^{II}} \quad (3.23)$$

$$\text{and: } \omega^2 = -g k_{z,r_2}^{II} \tan(k_{z,r_2}^{II} h^{II})$$

$$\Phi_t^{III}(x, z) = \cos(k_{z,t_1}^{III} z) \cos(k_{x,t_2}^{III} x) \quad \text{with: } k_{x,t_1}^{III} = \frac{(t_1-1)\pi}{L_x^{III}} \quad (3.24)$$

$$\text{and: } \omega^2 = -g k_{z,t_2}^{III} \tan(k_{z,t_2}^{III} h^{III})$$

The structural mode shapes W_k and corresponding resonance frequencies ω_k , which satisfy Eqs.(3.2)-(3.3) as well as the unforced equation of motion of the plate, i.e. with zero right-hand side, can be found either analytically or numerically for the presented

boundary conditions. Leissa (1969) presents a solution for the boundary conditions used in this study. The only unknowns remaining in Eqs.(3.17)-(3.20) are therefore the modal coefficients A_k , B_p^- , B_p^+ , C_r^+ and D_t^+ .

To solve the coupled problem Eqs.(3.1)-(3.14) are transformed to the frequency domain and expanded in terms of Eqs.(3.17)-(3.20). By introducing additional sets of structural and fluid modes (e.g. W_l and Φ_q^I) and making use of their orthogonality property in a similar matter as in the previous chapter, the following solvable set of three equations can be derived:

$$\sum_{k=1}^{\infty} A_k \left(I_k \delta_{kl} + \sum_{t=1}^{\infty} \frac{\rho_f i \omega^2 T_{k,t} T_{l,t}}{k_{y,t} \Delta_t} \right) + \sum_{p=1}^{\infty} B_p^- \left(\rho_f i \omega Q_{l,p} e^{-ik_{y,p}^I L_y} \right) + \sum_{p=1}^{\infty} B_p^+ \left(\rho_f i \omega Q_{l,p} \right) = F_l \quad (3.25)$$

$$\sum_{k=1}^{\infty} A_k (\omega Q_{k,q}) + \sum_{p=1}^{\infty} B_p^- \left(k_{y,p}^I e^{-ik_{y,p}^I L_y} \Delta_q \delta_{pq} \right) - \sum_{p=1}^{\infty} B_p^+ \left(k_{y,p}^I \Delta_q \delta_{pq} \right) = 0 \quad (3.26)$$

$$\sum_{p=1}^{\infty} B_p^- \left(\frac{\rho_f^I}{\rho_f^{II}} \Delta_p \delta_{pq} + k_{y,p}^I \sum_{r=1}^{\infty} \frac{R_{r,q} R_{r,p}}{k_{y,r}^{II} \epsilon_r} \right) + \sum_{p=1}^{\infty} B_p^+ e^{-ik_{y,p}^I L_y} \left(\frac{\rho_f^I}{\rho_f^{II}} \Delta_p \delta_{pq} - k_{y,p}^I \sum_{r=1}^{\infty} \frac{R_{r,q} R_{r,p}}{k_{y,r}^{II} \epsilon_r} \right) = 0 \quad (3.27)$$

In above, the modal force is defined as:

$$F_l = \iint_{S_s} \tilde{f}_e(x, z) W_l(x, z) dx dz \quad (3.28)$$

and the impedance coefficients at the two structure-fluid interfaces and the fluid-fluid interface are given by:

$$Q_{l,p} = \iint_{S_{s-I}} \Phi_p^I(x, z) W_l(x, z) dx dz \quad (3.29)$$

$$Q_{k,q} = \iint_{S_{s-I}} \Phi_q^I(x, z) W_k(x, z) dx dz \quad (3.30)$$

$$T_{k,t} = \iint_{S_{s-III}} \Phi_t^{III}(x, z) W_k(x, z) dx dz \quad (3.31)$$

$$R_{r,q} = \iint_{S_{I-II}} \Phi_q^I(x, z) \Phi_r^{II}(x, z) dx dz \quad (3.32)$$

$$R_{r,p} = \iint_{S_{I-II}} \Phi_p^I(x, z) \Phi_r^{II}(x, z) dx dz \quad (3.33)$$

in which S_{s-I} and S_{s-III} denote the surface area of the plate in contact with fluid domain I and III respectively and S_{I-II} the surface area of the interface between fluid domain I and

II. The coefficient I_l is defined as:

$$I_l = \rho_s (\omega_l^2 - \omega^2) \Gamma_l \quad (3.34)$$

Finally, Γ_l , Δ_q , Δ_r and Δ_t are the result of the surface integrations of the modes:

$$\Gamma_l = \iint_{S_s} W_l^2(x, z) dx dz \quad (3.35)$$

$$\Delta_q = \iint_{S_I} (\Phi_q^I)^2(x, z) dx dz \quad (3.36)$$

$$\Delta_r = \iint_{S_{II}} (\Phi_r^{II})^2(x, z) dx dz \quad (3.37)$$

$$\Delta_t = \iint_{S_{III}} (\Phi_t^{III})^2(x, z) dx dz \quad (3.38)$$

in which S_j denotes the surface area of the modes in the respective domains. By solving this system of equations simultaneously, the unknown sets of coefficients A_k , B_p^- and B_p^+ can be obtained. Subsequently, the coefficients C_r^+ and D_t^+ follow from:

$$C_r = \frac{1}{ik_{y,r}^{II} \epsilon_r} \sum_{p=1}^{\infty} \left(-B_p^- ik_{y,p}^I + B_p^+ ik_{y,p}^I e^{-ik_{y,p}^I L_y} \right) R_{r,p} \quad (3.39)$$

$$D_t^+ = -\frac{\omega}{k_{y,t}^{III} \Delta_t} \sum_{k=1}^{\infty} A_k T_{k,t} \quad (3.40)$$

To solve the system of equations, the infinite summations need to be truncated. The amplitude fields of the velocity and pressure at the interfaces between the gate and different fluid domains that result from the solution can be used as a measure of convergence for the number of modes, as discussed in Tsouvalas et al. (2015). In this study, the number of modes is chosen in accordance the standard rules mentioned in Tsouvalas and Metrikine (2016), which means amongst others taking into account all propagating fluid modes. Convergence is subsequently checked by trial and error. Tieleman et al. (2019b) show the convergence for the number of structural modes for a similar problem. Alternatively, one could apply convergence criteria that are based on the satisfaction of the interface conditions between structure and fluid as discussed in Tsouvalas et al. (2015).

The system contains structural damping due to application of a complex modulus of elasticity and fluid damping as a consequence of wave radiation. As a consequence, the solutions for \tilde{w} and v^j will be complex valued. The amplitudes follow from $|w| = \sqrt{\text{Re}(\tilde{w})^2 + \text{Im}(\tilde{w})^2}$ and $|v^j| = \sqrt{\text{Re}(\tilde{v}^j)^2 + \text{Im}(\tilde{v}^j)^2}$. The stresses in the gate follow from the standard strain-stress relations for isotropic homogeneous plates Leissa (1969). As a stress criterion Von Mises can be used.

3.5 PERFORMANCE OF THE SOLUTION

The developed semi-analytical model is validated by comparison with a finite element model using the standard software package COMSOL (COMSOL, 2018). A similar

validation case is chosen as in the previous chapter, in which a model was developed for the situation without overhang. The model results were validated by comparison with a time-domain finite element model using the standard software package COMSOL (COMSOL, 2018). To validate the solution derived in this study, a comparison is made using the same validation case, but with the addition of an overhang. Both a short and longer overhang or considered. Table 3.1 gives an overview of the system parameters for this validation case.

The finite element model in COMSOL is set-up for the same geometry. The fluid domains are required to have a finite length in this model. The results show convergence for a domain length of 50 m for both sides of the gate. At the end of the fluid domains a plane wave radiation condition is applied. The model is discretized by a tetrahedral mesh of flexible size between 0.02 and 1 m is applied.

Table 3.1: Case parameters and their value

Structural parameters	Symbol	Value	Unit	Fluid parameters	Symbol	Value	Unit
Width	L_x	12	m	Width	$L_x^{I,II,III}$	12	m
Height	L_z	7.5	m	Water level left	$h^{I,II}$	7	m
Gate thickness	t	0.243	m	Water level right	h^{III}	4	m
Bending rigidity	D	$2.63 \cdot 10^8$	Nm	Overhang length	L_y	0.5-5	m
Distributed mass	ρ_s	95	kg/m ²	Horizontal offset I-II	Δx^{II}	0	m
Poisson's ratio (steel)	ν	0.3	-	Fluid density	$\rho_f^{I,II,III}$	1025	kg/m ³
				Fluid sound velocity	c_p	1500	m/s
				Gravitational constant	g	9.81	m/s ²

Table 3.2 shows the resonance frequencies predicted by both the semi-analytical and frequency-domain solver the COMSOL model. The case with the longer overhang results in lower resonance frequencies, as the presence of an overhang leads to an increase in the hydrodynamic mass. The results match closely for both the in vacuo and immersed gate. The in vacuo resonance frequencies and mode shapes of the gate are based on Leissa (1969) and in fact input to the model. The relative difference between this solution and COMSOL is in the order of 1-2%. The fluid-structure interaction is then solved by the semi-analytical response model to obtain the resonance frequencies of the immersed gate. The predicted resonance frequencies of the immersed gate match even more closely to the outcome of the COMSOL model than for the in vacuo gate. It can therefore be concluded that the developed response model solves the involved fluid-structure interaction with a very minor additional error for this validation case.

An idealized impact force with a triangular temporal variation and a duration of 10^{-2} s is now applied to the gate. Such an impact force of short duration is especially suitable for the purpose of validation, as it ensures a wideband frequency spectrum that excites multiple modes of the system. The response of the case with a long overhang is investigated, as the differences in resonance frequencies predicted by the semi-analytical model and COMSOL were slightly larger for that situation. The time-varying numerical solver of COMSOL is applied to predict the response to the considered impact load. The COMSOL model does not allow for a structural damping coefficient. A distributed

3.5. PERFORMANCE OF THE SOLUTION

Table 3.2: Comparison of the first five predicted resonance frequency predicted by the semi-analytical and COMSOL model for the in vacuo and immersed gate for overhang lengths of 0.5 and 5 m

Condition	Model	f_1	f_2	f_3	f_4	f_5
In vacuo	Semi-analytical [Hz]	26.1	81.2	97.0	159.6	171.5
	COMSOL [Hz]	25.9	80.6	96.0	157.1	169.1
	Relative difference [-]	0.44%	0.75%	1.04%	1.62%	1.39%
Immersed ($L_y = 0.5$ m)	Semi-analytical [Hz]	5.24	17.8	22.0	39.2	40.2
	COMSOL [Hz]	5.26	17.8	22.0	39.1	39.8
	Relative difference [-]	0.47 %	0.04 %	0.02 %	0.26 %	1.01 %
Immersed ($L_y = 5$ m)	Semi-analytical [Hz]	3.54	15.0	19.8	34.8	36.8
	COMSOL [Hz]	3.53	15.1	20.0	35.4	37.3
	Relative difference [-]	0.23%	0.6%	1.06%	1.51%	1.34%

damping force of 10^4 Ns/m/m² is therefore introduced on the surface of the gate in both models.

Figure 3.3 shows the time-domain results of the developed semi-analytical model match closely to the FE model in COMSOL. Minor differences in predicted frequencies of the response do cumulate over time. This has no impact on the magnitude of the response after a single impact, but may have some effect when consecutive impacts within a storm are considered, since ongoing vibrations due to the previous impact can then affect the response to the following impact. However, due to damping this cumulation of frequency differences in the predicted response is limited. Figure 3.4 demonstrates this for the case of two consecutive peak loads. The predicted responses by both models match just as closely after the first peak load as after the second peak load. At the end of the considered time window, the difference between the predictions of the semi-analytical and the finite-element model even seem to be smaller than for the single peak load of Figure 3.3. Minor phase differences may lead to a higher response after the one wave impact and a lower response after another. However, this effect will average out over the thousands of storms and waves that occur within each storm. This effect is therefore expected to have a negligible impact on the outcome of the design approach presented in later chapters of this thesis.

Overall, it can be concluded that the semi-analytical is in very good agreement with the prediction of the time-domain finite element model. However, further validation of the developed model is planned to be performed by comparison with experiments in ongoing studies to investigate effects that are possibly omitted in both models. For the studied validation case, the computation time of the semi-analytical model for the presented time-domain analysis was 36 min on a 3.60 GHz quad core processor, while computation with the COMSOL model lasted approximately 58 h. The computational efficiency of the semi-analytical algorithm has not been fully optimised yet and can still be improved.

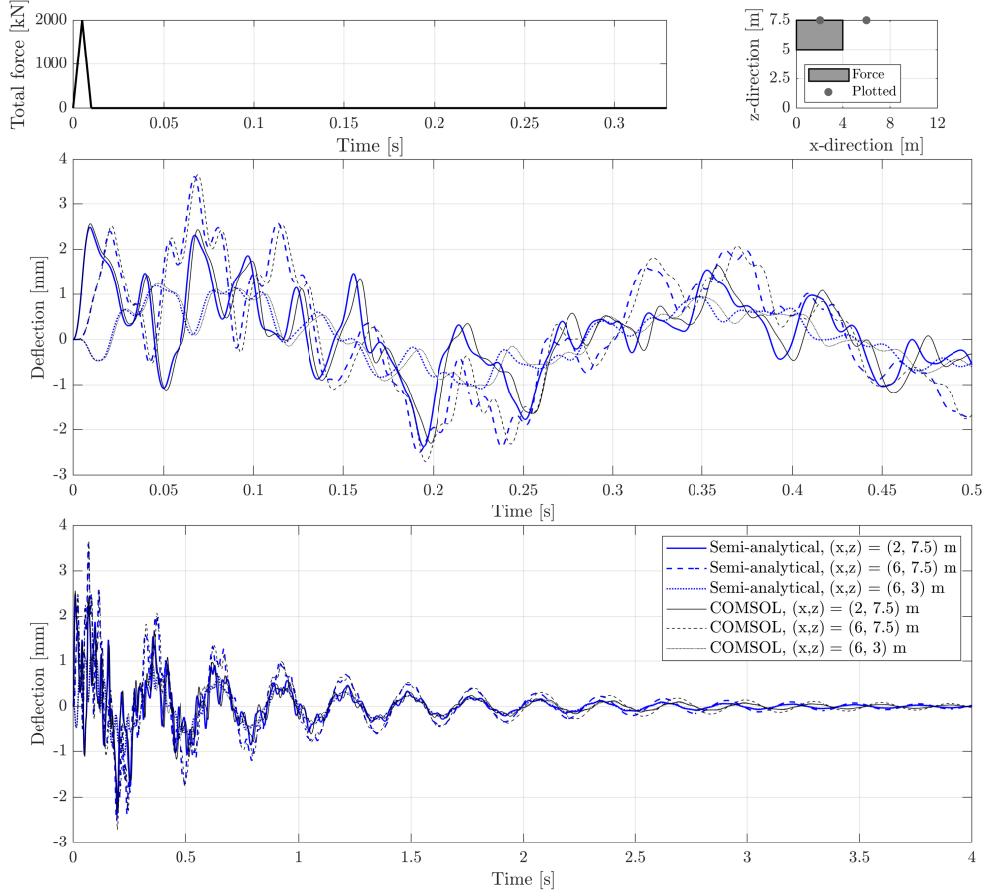


Figure 3.3: The time-domain response of the gate immersed in fluid for a triangular peak load predicted by the developed semi-analytical model compared to the FE COMSOL model on two different time scales. The upper right graph shows an overview of where on the surface of the gate the force is applied and of the locations for which the response has been shown.

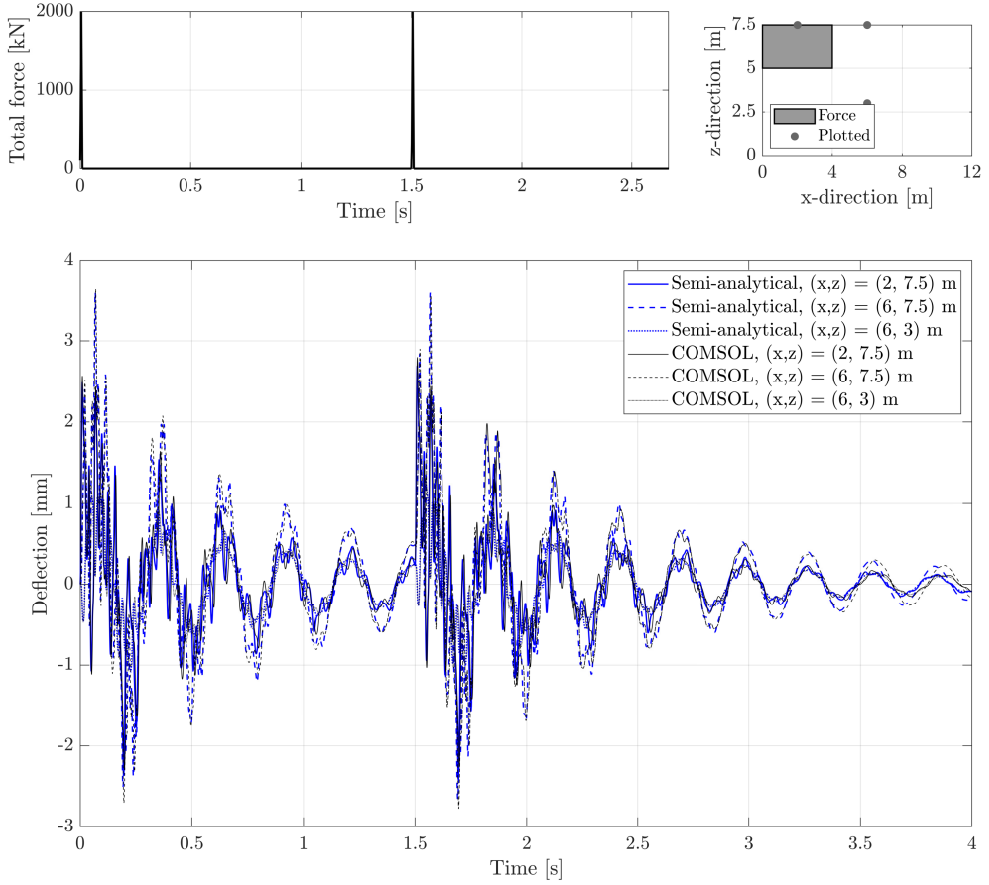


Figure 3.4: The time-domain response of the gate immersed in fluid for two consecutive peak triangular loads predicted by the developed semi-analytical model compared to the FE COMSOL model.

3.6 CONCLUSION

A semi-analytical fluid-structure interaction (FSI) model has been developed to accurately predict the dynamic behaviour of flood gates in composite fluid domains. This model is an extension to the one presented in the previous chapter. It is aimed at the situation of a gate with an overhanging structure in front that may cause confined wave impacts. This situation might for example occur when culverts or bridge decks are situated on top of discharge sluices. Also a wide fluid domain can now be included at the end of the discharge channel to represent a sea or lake. The method of solution is based on a mode matching technique of the structure and fluid. The effect of surface waves compressibility of the fluid on both sides of the gate is included in the model.

The results of the developed fluid-structure interaction model showed to be accurate based on a comparison with a conventional finite element package. The main benefit of the developed model is the computation efficiency in solving the two way fluid-structure interaction. For a simulation period of several seconds, the semi-analytical model proves to be almost a hundred times faster. Moreover, only a single computation is needed to obtain the response amplitude operator for a certain frequency range, regardless of the number of loads that is subsequently considered. In contrast, a time-domain FE model needs to compute the response to each different load in order. The semi-analytical model therefore has especially great benefits regarding computational efficiency when a large number of loads is considered. This benefit is employed in the design approaches presented in later chapters of this thesis.

4

**COUPLING THE
SEMI-ANALYTICAL
APPROACH TO A
FINITE ELEMENT
MODEL**

A semi-analytical model has been developed in the previous chapters to predict flood gate vibrations. The gate was represented by a thin plate. The mode shapes of both the structure and fluid were found completely analytically. The developed semi-analytical model is now coupled to a finite element model of the structure. The strong points of both methods, the computational efficiency of the semi-analytical method and the versatility of a finite element method to model complex geometries, are combined. This allows to predict the structural stresses during vibrations of a wider range of realistic flood gate designs.

This chapter is structured as follows. Section 4.1 further discusses the motivation for this chapter and provides background on the topic. The geometry of the studied problem is described in Section 4.2. Section 4.3 provides the theoretical description of the fluid-structure interaction problem, for which a semi-analytical solution is then derived in Section 4.4. Section 4.5 discusses how this numerical evaluation should be numerically evaluated. The developed model is validated in Section 4.6 by comparison to a conventional finite element package. In Section 4.7 the developed model is applied to a design optimization study. Section 4.8 discusses the key assumptions of the presented model and identifies several possibilities for further research. Section 4.9 discusses the conclusions of this chapter.

4.1 INTRODUCTION

Many studies have been performed into the coupled motion of plates and fluid based on a FE approach (Horáček et al., 1995; Wang et al., 2016). However, numerical models including fluid-structure interaction are computationally expensive for three dimensional problems Erdbrink (2014). For a finite element model the time-domain simulations required for the fatigue evaluation of a flood gate are very challenging given the long computation times (Zheng et al., 2020). If one includes, additionally, the need for parametric studies during the design stage of new flood gates, the computational task above becomes impossible with current FE software packages and established procedures to include fluid-structure interaction (FSI).

A semi-analytical method was developed in the previous chapters (Tieleman et al., 2019b, 2021) to accurately predict the dynamic behaviour of flood gates in a computationally efficient manner. The method of solution is based on a substructuring mode matching technique similar to Tsouvalas and Metrikine (2014, 2016) and Leblond et al. (2009). The main computational advantage of the mode matching technique lies in the ability to store and reuse partial results in contrast to the stepwise calculation in FE methods. For instance, when regarding a large number of loads, the frequency response function of the gate fluid system has to be computed only once. In the previous chapters, the flood gate is represented by a homogeneous thin flexible plate which allows to for an analytical solution of the in vacuo mode shapes.

Many other studies have focused on predicting the vibrations of plates in fluid. Lamb (1921) was the first to calculate the change in resonance frequency of a thin flexible

Parts of this chapter are based on the article "A hybrid semi-analytical and finite element parametric model to predict flood gate vibrations" submitted to Engineering Structures. Some minor changes have been introduced to make the text consistent with the other chapters of the thesis.

circular plate due the presence of incompressible fluid, later verified experimentally by Powell and Roberts (1922). Fu and Price (1987) studied the vibration responses of cantilevered vertical and horizontal plates partially or totally immersed in water. These studies assumed the mode shapes of the plates in vacuo and in contact with fluid to be the same. Kwak and Kim (1991); Kwak (1996); Kwak and Yang (2013); Amabili and Kwak (1996); Kwak and Yang (2013) have performed a series of studies into the vibrations of circular and cantilever plates presenting the nondimensionalized added virtual mass incremental (NAVMI) factors for these problems. Gorman and Horáček (2007) have studied the vibration behaviour of a circular plate in interaction with a cylindrical fluid cavity. The motion of the plate and fluid are coupled through a Galerkin technique. In many engineering applications however, the gate structure is more complex and cannot be represented by a plate when the aim is to obtain accurate stress predictions. Most commonly, a vertical flood gate consists of a continuous front plate with stiffening beams at one side. For such designs, existing analytical models do not allow for an accurate and detailed prediction of the structural stresses necessary for fatigue evaluations.

This chapter presents a model for engineering purposes that is able to predict vibrations and resulting structural stresses for realistic flood gate structures while maintaining the advantage of a high computational efficiency. Figure 4.1 gives an overview of the model approach. The existing semi-analytical mode matching method by Tieleman et al. (2021) for a thin plate structure is extended. A hybrid method is developed that exploits the benefits of both the semi-analytical mode matching technique and conventional FE methods. The semi-analytical part of the model solves the dynamic response of the gate including the involved fluid-structure interaction based on a mode matching technique. The fluid mode shapes and wave numbers are found analytically. A finite element model is employed to obtain the modal displacement shapes and resonance frequencies of the in vacuo gate. This allows to for a detailed prediction of the structural stresses for more realistic gate designs for any given time-varying load. Chapter 8 employs the model developed in a design method to perform fatigue evaluations of flood gates under wave impact loading.

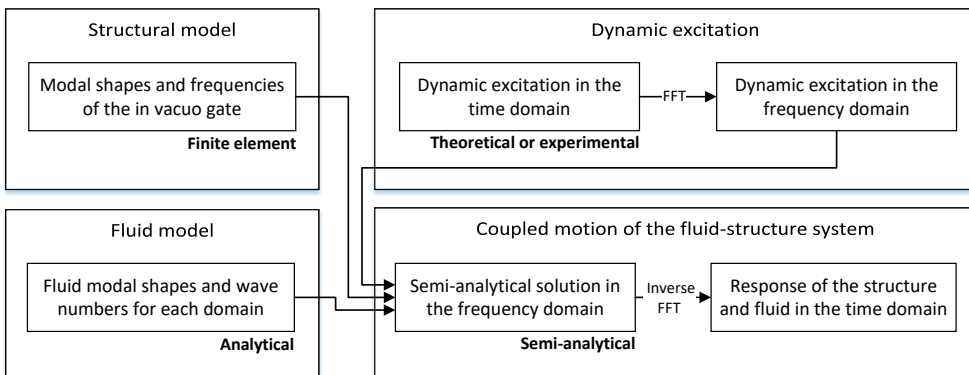


Figure 4.1: Main components of the developed model

Previous studies (Kerboua et al., 2008; Ergin and Ugurlu, 2003) have applied combinations of analytical and finite element methods for plates but not for this type of more realistic gate structures. The performance of the developed model is investigated by comparison to a numerical time-domain finite element model highlighting the accuracy and computational efficiency of the proposed method.

The gate design is described parametrically in this chapter. A numerical algorithm has been developed that is able to obtain the in vacuo mode shapes and frequencies of this parametric design from a standard finite element method. This algorithm then evaluates the semi-analytical solution to the fluid-structure interaction problem to determine the response of the gate over time for any excitation force. This enables the possibility of performing a parametric design study. This purpose is demonstrated in a case study of a flood gate with overhang on which wave impacts occur during a certain design storm event.

4.2 DESCRIPTION OF THE GATE AND FLUID MODEL

The geometry of the model is shown in Figure 4.2. A flood gate is situated in a discharge sluice with water present on both sides. During storm events the gate is in closed position to retain the sea water and prevent flooding of the hinterland. On one side of the gate, the sluice has a limited length and an overhang is present. On the other side of the gate the sluice extends to infinity. During storm events waves from the sea side lead to wave impacts when hitting the bottom of the overhang and cause (additional) peak loads on the flood gate.

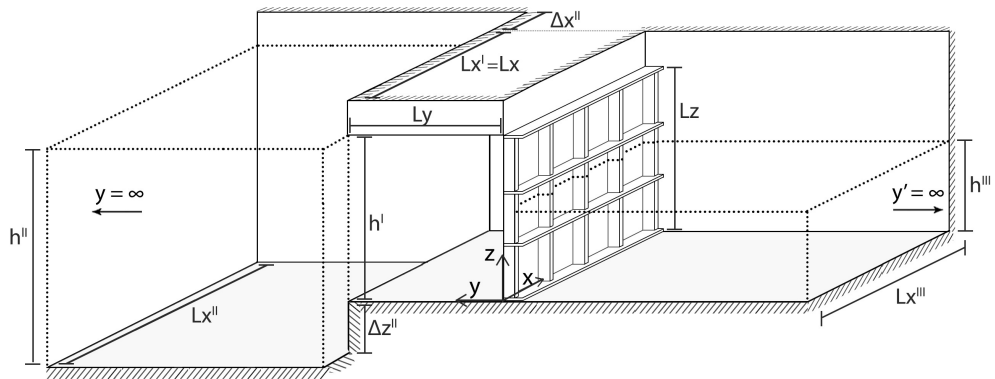


Figure 4.2: Overview of the gate-fluid coupled system

4.2.1 GATE DESIGN

A typical vertical steel flood gate design is considered with a continuous front plate supported by horizontal and vertical stiffeners. Different types of vertical gate designs could also be included in the developed model approach, such as a front plate with a truss structure as supporting elements. However, a key assumption of the semi-analytical

approach is that the interface between the gate and structure can be considered as a continuous flat surface. On the high water side, flood gate designs usually indeed have a flat surface to prevent direct wave impacts on structural elements. On the low water side, the assumption of a flat surface is expected to be valid for designs where the length of elements that protrude into the fluid is limited and the frequency spectrum of the excitation is such that the wavelengths excited in the structure are not very short. This assumption will be tested in Section 4.6 by comparison to a fully coupled gate-fluid FE model.

The gate is described parametrically such that it can be optimised for a given dynamic excitation in a parametric design approach. An overview of the gate design and parameters is shown in Figure 4.3. The gate has a width L_x and height L_z . The front plate has a thickness of t_{plate} . The stiffeners can have any distribution over the width and height of the gate. The validation study in this chapter considered a design with evenly distributed stiffeners, while the optimization study considers multiple variants. We distinguish horizontal and vertical stiffeners at the edges from those in the middle of the gate, as in practice the edge stiffeners often have different dimensions. The horizontal stiffeners have a length (in y-direction) of L_{hm} in the middle and L_{he} at the edges and corresponding thicknesses of t_{hm} and t_{he} . The same notation applies to the vertical stiffeners (L_{vm} , L_{ve} , t_{vm} , t_{ve}). The steel material has a mass density ρ_s and linear modulus of elasticity E_s .

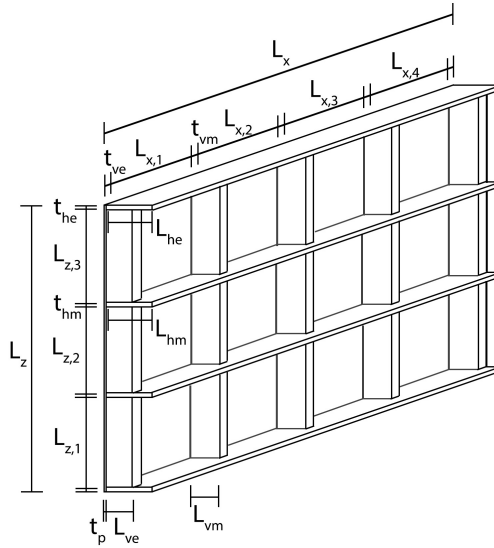


Figure 4.3: Parametrically defined gate design with front plate and stiffeners

Any time-independent boundary conditions can be set for the gate. Generally, the bottom and top ($z = 0$ and $z = L_z$) of the flood gate are free. The vertical front edges ($x = 0$ and $x = L_x$ at $y = 0$) are considered to have a certain rotation stiffness varying from zero

(simply supported) to infinite (clamped). Finally, an isotropic material damping factor is implemented representing energy losses due to straining of the gate material.

4.2.2 FLUID DOMAINS

Three fluid regions can be distinguished. All fluid regions have impermeable walls and a horizontal bottom. Region I occupies the domain $0 \leq y \leq L_y$ and $0 \leq x \leq L_x^I (= L_x)$. An impermeable overhang is present at $z = L_z$ restricting the fluid flow in the vertical direction. At the moment of a wave impact, the water height h_I in this region is equal to the height of bottom of the overhang. Region II occupies the domain $L_y \leq y \leq \infty$ and $-\Delta x^{II} \leq x \leq L_x^{II} - \Delta x^{II}$. No overhang is present so that the fluid has a free surface. The water level can be equal or higher than in region I. However, a water level close to the bottom of the overhang generally leads to the highest impact pressures and is thus of most interest De Almeida and Hofland (2020b). The bottom of region II may be lower than region I at $z = -\Delta z^{II}$. The width of this domain can be chosen much larger than that of region I to represent the presence of a lake or open sea at the end of a sluice or culvert. Finally, Region III occupies the domain $y < 0$ and $0 \leq x \leq L_x^{III} (= L_x)$. This region has similar boundary conditions as region II.

A free surface boundary condition is applied at the free surface. Tieleman et al. (2019a) have presented the regimes of water depths and excitation frequencies within which surface waves become relevant to the hydrodynamic response of the structure. Furthermore, the fluid is considered to be compressible, irrotational and inviscid.

4.2.3 WAVE IMPACT LOADING

Any time-varying load can be considered in the model approach. This study focuses on wave impacts that occur when incoming waves during storm events reach the gate and hit the bottom of the overhang. The wave impact force is modelled as an external force on the surface of the gate. The force is therefore assumed independent of the structural response. Also, the impact force does not affect the still water level. In Tieleman et al. (2019b) this was discussed to be a reasonable assumption for the time scales involved in impulsive wave impacts. The validity of these assumptions is being tested further in experiments in ongoing studies. The external wave impact pressures must then be predicted based on a model schematisation or experimental study with rigid gate. The optimization case study in Section 4.7 predicts the wave impact based on pressure-impulse theory (Cooker and Peregrine, 1995; Wood and Peregrine, 1997). Also the static hydrodynamic loading due to the water level difference over the gate is accounted for.

4.3 THEORETICAL FORMULATION OF THE PROBLEM

This section presents the governing equations describing the motion of the system presented in Section 4.2. Two parts can be distinguished making up the responsive part of this system: 1) the gate structure and 2) the fluid domains. The motion of the structure is described as a general multiple degree of freedom system upon discretization in a FE model. The fluid velocities and pressures are described analytically within an unknown set of complex modal amplitudes in the frequency domain. The wave impact is modelled

as an external force. The case study in Section 4.7 provides an example of how this force can be predicted.

The equation of motion still includes the fluid pressure acting on both sides as well as the external force. In contrast to previous chapters, the equation of motion of the gate is now presented in a discretized form:

$$\mathbf{M}\ddot{\mathbf{u}}(t) + \mathbf{C}\dot{\mathbf{u}}(t) + \mathbf{K}\mathbf{u}(t) = \mathbf{f}_e(t) - \mathbf{p}^I(t) + \mathbf{p}^{III}(t) \quad (4.1)$$

in which \mathbf{u} denotes the displacement of the gate structure in y-direction at a certain discretized point, \mathbf{M} , \mathbf{C} and \mathbf{K} are the mass, damping and stiffness matrices respectively, \mathbf{f}_e is the external force and \mathbf{p}^I and \mathbf{p}^{III} are the pressure fields exerted by the fluid on either side as a consequence of the motion of the gate. The structural boundary conditions are implicitly included in the discretization of the structural system.

For the description of the fluid motion, the velocity potential function $\phi^j(x, y, z, t)$ is introduced with $j = I, II, III$ denoting the respective fluid region in accordance with Figure 4.2. The equation of motion of each fluid region reads:

$$\nabla^2 \phi^j(x, y, z, t) - \frac{1}{c_p^2} \frac{\partial^2 \phi^j(x, y, z, t)}{\partial t^2} = 0 \quad (4.2)$$

in which c_{p^j} is the sound velocity in water in each region. The fluid velocity vector \mathbf{v}^j and pressure p^j are given by:

$$\nabla \phi^j(x, y, z, t) = -\mathbf{v}^j(x, y, z, t) \quad (4.3)$$

$$p^j(x, y, z, t) = -\rho_f^j \frac{\partial \phi^j(x, y, z, t)}{\partial t} \quad (4.4)$$

In above, ρ_f^j is the fluid density per region, which will be equal for fluid regions I and II in most cases.

The mathematical description of the fluid boundary conditions imposed by the impermeable gate bottom and walls and the free surface is straightforward. Between region I and II a continuous velocity and pressure is imposed at the interface. At $y \rightarrow \infty$ and $y' \rightarrow \infty$ the radiation conditions should be satisfied at all times in both region II and III. Tieleman et al. (2021) gives a full overview of the mathematical descriptions of these conditions.

The interface conditions in this case differ from Tieleman et al. (2021), where the gate was described as a continuous plate rather than the more realistic structure with front plate and stiffeners. Also other studies such as Tsouvalas and Metrikine (2014, 2016) and Tieleman et al. (2019b), considering monopiles and flood gates respectively, considered a continuous interface between structure and fluid. To derive a straightforward semi-analytical solution for the fluid response within this fluid-structure interaction problem, the interface between the structure and fluid is also assumed to be a continuous plane at both sides in this study. At the front of the gate, where the high water level is usually present, the interface surface is indeed flat. At the back of the gate stiffeners are present. The possible effect of the more complex interaction surface between these stiffeners and

the fluid is neglected. This is expected to lead to reasonable results when the stresses in the gate are dominated by the global rather than local vibrations of the gate. Generally, the first few global modes do tend to be most relevant for this type of problem Tieleman et al. (2019a, 2021). Section 4.6 tests the validity of this assumption.

This requires choosing a representative plane for the motion of the gate for the purpose of evaluating the interface conditions. A single plane is chosen for both interfaces in this study. The surface of the front plate ($y=0$), which is indeed a continuous plane, is expected to give good results and is deemed most practical for the presented problem. This results in the following conditions stating equal velocity of the structure and fluid at the two interfaces:

$$\dot{\mathbf{u}}_y(t)|_{y=0} = \mathbf{v}_y^I(t)|_{y=0} \quad (4.5)$$

$$\dot{\mathbf{u}}_y(t)|_{y=0} = \mathbf{v}_y^{III}(t)|_{y'=0} \quad (4.6)$$

in which $\dot{\mathbf{u}}_y$ is the velocity of the gate at the representative plane at discretized points and \mathbf{v}_y^I and \mathbf{v}_y^{III} the velocity of the fluid in y -direction at those coordinates (x, z) at the front and back surface of the gate respectively. However, within the method of solution presented in this study it is also possible to choose different planes at the front and back side of the structure to evaluate the two interface conditions.

4.4 SOLUTION TO THE FLUID-STRUCTURE INTERACTION PROBLEM

The coupled problem is solved in the same manner as in the previous chapter. Equations (4.1)-(4.6) are transformed to the frequency domain by applying the Fourier transform pair in equations (3.15) and (3.16). A modal decomposition scheme is introduced to describe the motion of the fluid potential in the various regions according in the frequency domain. This schema is identical to the one in Eqs. (3.17)-(3.20) with the exception that the motion of the gate is now described in terms of discretized mode shapes (U_k):

$$\tilde{u}(x, y, z, \omega) = \sum_{k=1}^{\infty} A_k(\omega) U_k(x, y, z) \quad (4.7)$$

The structural mode shapes U_k and corresponding resonance frequencies ω_k are found by solving the unforced equation of motion of the gate, i.e. Eq. (4.1) with zero right-hand side. A finite element model of the in vacuo gate will be employed for this purpose.

The solution for the fluid modes in the previous chapter is based on a flat interface between the gate and the fluid. In the problem considered here, stiffening beams are present at the backside of the gate. The interface between the gate and the fluid in domain III is therefore more complex. However, also here this interface is assumed to be flat to be able to derive the solution in a similar way. This validity of this assumption is tested in the next sections. With this assumption, the fluid modes of Eqs. (3.22)-(3.24) can be employed directly. Note that in the model geometry considered here, the water level in fluid domain III can be higher than the water level in fluid domain II due to a varying bottom level.

By introducing additional sets of structural and fluid modes (e.g. U_l and Φ_q^I) and making use of their orthogonality property a solution can be then derived for the motion of the gate and the fluid potential in the frequency domain. This yields the following solvable

set of three equations:

$$\sum_{k=1}^{\infty} A_k \left(I_k \delta_{kl} + \sum_{t=1}^{\infty} \frac{\rho_f i \omega^2 T_{k,t} T_{l,t}}{k_{y,t} \Delta_t} \right) + \sum_{p=1}^{\infty} B_p^- \left(\rho_f i \omega Q_{l,p} e^{-i k_{y,p}^I L_y} \right) + \sum_{p=1}^{\infty} B_p^+ \left(\rho_f i \omega Q_{l,p} \right) = F_l \quad (4.8)$$

$$\sum_{k=1}^{\infty} A_k (\omega Q_{k,q}) + \sum_{p=1}^{\infty} B_p^- \left(k_{y,p}^I e^{-i k_{y,p}^I L_y} \Delta_q \delta_{pq} \right) - \sum_{p=1}^{\infty} B_p^+ \left(k_{y,p}^I \Delta_q \delta_{pq} \right) = 0 \quad (4.9)$$

$$\sum_{p=1}^{\infty} B_p^- \left(\frac{\rho_f^I}{\rho_f^{II}} \Delta_p \delta_{pq} + k_{y,p}^I \sum_{r=1}^{\infty} \frac{R_{r,q} R_{r,p}}{k_{y,r}^{II} \epsilon_r} \right) + \sum_{p=1}^{\infty} B_p^+ e^{-i k_{y,p}^I L_y} \left(\frac{\rho_f^I}{\rho_f^{II}} \Delta_p \delta_{pq} - k_{y,p}^I \sum_{r=1}^{\infty} \frac{R_{r,q} R_{r,p}}{k_{y,r}^{II} \epsilon_r} \right) = 0 \quad (4.10)$$

The modal force is defined as:

$$F_l = \iint_{S_s} \tilde{f}_e(x, z) U_l(x, y=0, z) dx dz \quad (4.11)$$

and the impedance coefficients at the two structure-fluid interfaces and the fluid-fluid interface are given by:

$$Q_{l,p} = \iint_{S_{s-I}} \Phi_p^I(x, z) U_l(x, y=0, z) dx dz \quad (4.12)$$

$$Q_{k,q} = \iint_{S_{s-I}} \Phi_q^I(x, z) U_k(x, y=0, z) dx dz \quad (4.13)$$

$$T_{k,t} = \iint_{S_{s-III}} \Phi_t^{III}(x, z) U_k(x, y=0, z) dx dz \quad (4.14)$$

$$R_{r,q} = \iint_{S_{I-II}} \Phi_q^I(x, z) \Phi_r^{II}(x, z) dx dz \quad (4.15)$$

$$R_{r,p} = \iint_{S_{I-II}} \Phi_p^I(x, z) \Phi_r^{II}(x, z) dx dz \quad (4.16)$$

in which S_{s-I} and S_{s-III} denote the surface area of the plate in contact with fluid domain I and III respectively and S_{I-II} the surface area of the interface between fluid domain I and II. The coefficient I_k is defined as:

$$I_k = \left[((1 + \eta i) \omega_k)^2 - \omega^2 \right] \Gamma_k \quad (4.17)$$

in which η is the isotropic material damping factor. The variables Γ_k , Δ_q , Δ_r and Δ_t are the result of the surface integrations of the modes:

$$\Gamma_k = \iint_{S_s} \rho_s(x, z) U_k^2(x, y=0, z) dx dz \quad (4.18)$$

$$\Delta_q = \iint_{S_I} (\Phi_q^I(x, z))^2 dx dz \quad (4.19)$$

$$\Delta_r = \iint_{S_{II}} (\Phi_r^{II}(x, z))^2 dx dz \quad (4.20)$$

$$\Delta_t = \iint_{S_{III}} (\Phi_t^{III}(x, z))^2 dx dz \quad (4.21)$$

in which ρ_s is the mass of the gate at each location over its surface area. Generally, finite element packages produce mass-normalized mode shapes such that $\Gamma_k = 1$ for each mode shape. This is practically convenient, as that avoids the need to define a mass field for a given structure in the semi-analytical model. Finally, δ_{kl} and δ_{pq} represent Kronecker deltas.

By solving this system of equations simultaneously, the sets of modal coefficients A_k , B_p^- and B_p^+ can be found. Subsequently, the coefficients C_r^+ and D_t^+ follow from:

$$C_r = \frac{1}{ik_{y,r}^{II} \epsilon_r} \sum_{p=1}^{\infty} \left(-B_p^- ik_{y,p}^I + B_p^+ ik_{y,p}^I e^{-ik_{y,p}^I L_y} \right) R_{r,p} \quad (4.22)$$

$$D_t^+ = -\frac{\omega}{k_{y,t}^{III} \Delta_t} \sum_{k=1}^{\infty} A_k T_{k,t} \quad (4.23)$$

The displacement of the gate now follows from Eq.(4.7). A finite element package can be employed to not only evaluate the modal displacement shapes U_k but also the modal stress shapes $S_{k,x}$, $S_{k,y}$, $S_{k,z}$, $S_{k,xy}$, $S_{k,xz}$, $S_{k,yz}$ that correspond to each of these modes. The frequency domain stresses in the plate then follow from:

$$\tilde{\sigma}_{ij}(x, y, z, \omega) = \sum_{k=1}^{\infty} A_k(\omega) S_{k,ij}(x, y, z) \quad (4.24)$$

with $\tilde{ij} = x, y, z, xy, xz, yz$. These directional stresses can then be translated to Von Mises stress or principal stresses. It must be noted that it is not possible to directly use the Von Mises or principal stresses corresponding to the modes in the above equation, as these stresses can not be added linearly. Finally, an inverse Fourier transform can then be applied to obtain the displacements and stresses at the time domain.

4.5 NUMERICAL EVALUATION OF THE SOLUTION

To solve the system of equations (4.8)-(4.10), the infinite summations need to be truncated. Tsouvalas et al. (2015) has presented a convergence criterion for the number of modes based on the difference in predicted displacements at the interface between the

structure and fluid. It must be noted however that the predicted stresses convergence less rapidly than displacements as higher modes have increasing curvatures. Tsouvalas and Metrikine (2016) provides general standard rules for the number of modes to be taken into account that can be applied to the problem considered here. Convergence of the predicted structural stresses must then subsequently be checked by trial and error. For the validation case in Section 4.6 convergence of the solution is investigated both in terms of displacements and stresses.

The set of mode shapes of the in vacuo gate in terms of displacement $U_k(x, y, z)$ and stresses $S_{k,ij}(x, y, z)$, and corresponding resonance frequencies ω_k , can be found using any standard finite element packages, such as ANSYS (Kidger, 2012), COMSOL (COMSOL, 2018) and SCIA Engineer. The numerical algorithm applied in the case study in Section 4.7 employs SCIA Engineering as it is commonly used to design flood gates and allows for external control of a parametric geometry. The integrals in Eqs.(4.12)-(4.16) for the various interfaces between structure and fluid domains or between fluid domains can be evaluated numerically. As discussed earlier, in this study the surface of the front plate $U_k(x, y = 0, z)$ is chosen as a reference plane for both structure-fluid interfaces. The analytical solutions for the vertical fluid modes in Eqs.(3.22)-(3.24) can be discretized matching the mesh of the structural modes in the reference plane, the front of the gate, for the purpose of evaluating these integrals.

An interesting characteristic of the presented method of solution is that two different meshes can be used to solve the system of equations and to evaluate the displacement or stresses of the gate. The first mesh dictates the accuracy of the numerical integration of the integrals and evaluation of the semi-analytical solution for the motion of the gate and fluid. The mesh chosen is a trade-off between accuracy and computational speed as is usually the case with any finite element model. The solution is fully captured in terms of modal coefficients provided that enough modes are chosen in the modal scheme. When translating these modal coefficients to the motion and stress by applying those to the displacement and stress modes according to Eqs.(4.7) and (4.24), these quantities of interest can then be evaluated at any point of the gate or fluid (possibly as part of a second mesh) even when it was not part of the mesh used to find the solution. This is a fundamental difference with time-domain finite element fluid-structure interaction models.

4.6 PERFORMANCE OF THE MODEL

Tieleman et al. (2018, 2021) have shown that the presented method of solution is able to accurately predict the dynamic behaviour of a thin plate immersed in fluid. This chapter considers a more realistic gate structure with front plate and stiffening beams. This introduces several new uncertainties.

First of all, the mode shapes and frequencies of the in vacuo plate were found analytically in previous studies. Here, a finite element model is employed to obtain the model shapes and the eigenfrequencies of the gate structure. The numerical routine obtaining this data from a finite element model must be verified. Moreover, previous studies focused on the performance of this method of solution predicting displacements. The presented hybrid model aims to also predict structural stresses within the flood

gate. This validation therefore focuses on the performance of the model regarding the prediction of structural stresses. Furthermore, in the case of a plate, the interface with fluid is continuous on both sides. For the gate design with front plate and stiffening beams the interface between the gate and fluid is more complex. To derive the semi-analytical solution for the more realistic gate structure, the interface interface was assumed to be a vertical plane however. The displacement of the gate at the front plate is considered to be representative. The validity of this assumption is investigated in this section.

4.6.1 DESCRIPTION OF THE VALIDATION CASE

The presented semi-analytical model is compared to a time-domain finite element model in COMSOL. Two geometries are considered, a continuous plate and a realistic gate structure with stiffening beams. The mode shapes and frequencies could be found analytically for the continuous plate. However, for the comparison the mode shapes and frequencies are for both cases obtained from the COMSOL model. By comparing the results for the continuous plate and realistic gate structure errors introduced by the assumption of a continuous interface surface between structure and fluid become apparent.

As a validation case, typical dimensions are chosen for the gate and fluid domains, such as found in the Afsluitdijk in the Netherlands. Table 4.1 gives an overview of the relevant system parameters and their values. For both the continuous plate and realistic gate a zero displacement condition is imposed over the full vertical sides of each the structure.

Table 4.1: Parameters and their values for the realistic gate structure

Structural parameters	Symbol	Value	Unit	Fluid parameters	Symbol	Value	Unit
<i>General</i>				<i>General</i>			
Width	L_x	12.5	m	Width	$L_x^{I,II,III}$	12.5	m
Height	L_z	7.6	m	Water level left	$h^{I,II}$	7	m
Elasticity modulus (steel)	E	$200 \cdot 10^9$	Nm ²	Water level right	h^{III}	3	m
Material density (steel)	ρ_m	7850	kg/m ³	Overhang length	L_y	1	m
Poisson's ratio (steel)	ν	0.3	-	Horizontal offset I-II	Δx^{II}	0	m
Boundary condition sides	-	hinged	-	Bottom offset I-II	Δz^{II}	0	m
<i>Realistic gate</i>				Fluid density	$\rho_f^{I,II,III}$	1025	kg/m ³
Front plate thickness	t_{plate}	0.05	m	Fluid sound velocity	c_p	1500	m/s
Vertical stiff. spacing	$L_{x1,x2,x3,x4}$	3	m				
Vertical stiff. width	L_{vm}, L_{ve}	0.25	m				
Vertical stiff. thickness	t_{vm}, t_{ve}	0.1	m				
Horizontal stiff. spacing	$L_{z1,z2,z3}$	2.4	m				
Horizontal stiff. width	L_{hm}, L_{he}	0.5	m				
Horizontal stiff. thickness	t_{hm}, t_{he}	0.1	m				
<i>Continuous plate</i>							
Plate thickness	t_{plate}	0.1	m				

The structure is represented by three-dimensional solid elements in COMSOL. The material of the gate is isotropic and linearly elastic. At both sides of the gate the fluid domains have a length of 50 m, after which a wave radiation condition is applied. The fluid

is compressible and modelled with the transient pressure acoustics module of COMSOL. To simplify the COMSOL model, surface waves are excluded from the analysis. Instead, a zero pressure boundary condition is applied at the free surface. Based on previous studies (Tieleman et al., 2019b,a) surface waves have a negligible effect on the behaviour of the gate for the considered dimensions and frequencies. A tetrahedral mesh is applied with a flexible element size of 0.1-1 m.

4.6.2 PREDICTING THE RESONANCE FREQUENCIES IN WATER

Table 4.2 shows the resonance frequencies predicted for the immersed structures by both the semi-analytical and frequency-domain solver the COMSOL model for the undamped system. The resonance frequencies predicted by the semi-analytical model are obtained by a peak picking method. The number of structural and fluid modes required to obtain this solution is discussed in Section 4.6.4. COMSOL finds the resonance frequency by solving the eigenvalue problem of the system. For the continuous plate the differences in the predicted resonance frequencies between both models are in the order of 0.4–0.8%. In Tieleman et al. (2021), the mode shapes were found analytically for the in vacuo gate. The differences in prediction resonance frequencies between the finite element model and the semi-analytical method were in the same order (0.2–1.4%) for both the in vacuo and immersed gate. Due to the large computation time of the COMSOL model, it is not possible to fully check convergence for the mesh size and the length of the fluid domains at both sides of the gate. This considered, the differences between both models are very minor.

For the gate structure with front plate and stiffeners the differences in prediction increase from 0.4–0.8% to about 1.2–1.5%. The additional error could be the result of the assumption in the semi-analytical model of a continuous interface between the structure and fluid. For higher more local modes, the error will likely increase as a consequence of this assumption. At least for the first few modes considered here the total error can still be considered very minor. Especially when compared to other design methods applied in practice that do not require much computational effort, such as one degree of freedom representations of the structure.

Table 4.2: Comparison of the first five predicted resonance frequency predicted of the immersed continuous plate and realistic gate by the semi-analytical and COMSOL model

Gate	Model	f_1	f_2	f_3	f_4	f_5
Continuous plate	Semi-analytical [Hz]	3.32	6.33	10.70	15.89	17.73
	COMSOL [Hz]	3.29	6.31	10.61	15.85	17.62
	Relative difference [-]	0.8%	0.4%	0.8%	0.3%	0.6%
Realistic gate	Semi-analytical [Hz]	3.87	6.73	10.90	12.59	15.69
	COMSOL [Hz]	3.82	6.66	10.75	12.43	15.48
	Relative difference [-]	1.2%	1.1%	1.5%	1.3%	1.4%

For gates with stiffening beams that extend further into the fluid the accuracy of the presented method will likely decrease. When applying this method to such designs,

it is therefore recommended to validate the model specifically for those situations. If proven necessary, extension of this method of solution could be investigated to increase its applicability.

4.6.3 PREDICTING THE DYNAMIC RESPONSE TO AN IMPACT LOAD

An idealized impact force with a triangular temporal variation and a duration of 10^{-2} s is now applied. This force acts over part of the front surface of the gate. Such an impact force of short duration is especially suitable for the purpose of validation, as it ensures a wideband frequency spectrum that excites multiple modes of the system. The time-varying numerical solver of COMSOL is used to predict the response to the considered impact load. The COMSOL model does not allow for a structural damping coefficient. A distributed damping force of $5 \cdot 10^3$ Ns/m/m² is therefore introduced on the surface of the gate in both models. Figure 4.4 and Figure 4.5 show the response of the continuous plate and realistic gate structure predicted by both models. The results are presented in terms of displacements and two stress components σ_x and σ_{xz} at several locations at the front and back of the structures. The points at the top and middle of the gate are chosen as these are likely to capture most relevant excited global modes, and the point in the field between stiffeners as it might be influenced by more local modes.

Similar to previous studies (Tieleman et al., 2019b, 2021), the results of both models do deviate over time due to the minor differences in predicted frequencies of the response. As expected based on the previous section, this effect is larger for the realistic gate structure than for the continuous plate. In Tieleman et al. (2021), it has been reasoned that the effect of this phenomenon on the maximum response over the course of a storm with consecutive impacts is expected to be limited. Moreover, it is also possible that this difference originates from the time-domain solver of COMSOL. The maximum displacement and stress predicted by both models match quite well for both types of structures. The relative difference in predicted maximum displacement is 1.2% for the plate and 5.7% for the gate, while the difference in the predicted maximum dominant principal stress σ_x is 1.1% and 6.7% respectively. The predictions for the principal stress components with low maximums show larger differences, but are less relevant to the safety assessment. Fatigue assessments based on the predictions of the two models are also expected to lead to similar outcomes as the most relevant stress variations occur right after the impact. Overall, it can be concluded that the semi-analytical model is in good agreement with the prediction of the time-domain finite element model for both types of structures.

4.6.4 CONVERGENCE OF THE SOLUTION FOR THE NUMBER OF MODES

The convergence of the solution for a number of structural and fluid modes is checked by simulating the response for increasing numbers of structural and fluid modes. A maximum of 65 structural modes is included. For the fluid, a maximum of 225 modes is taken into account for each domain. This is the number of modes that was included in the previous analyses. Figure 4.6 shows the relative error in the maximum displacement and stress (σ_x) predicted compared to this number of maximum modes. As expected from the discussion in Section 4.5, the predicted displacement convergences more rapidly than the

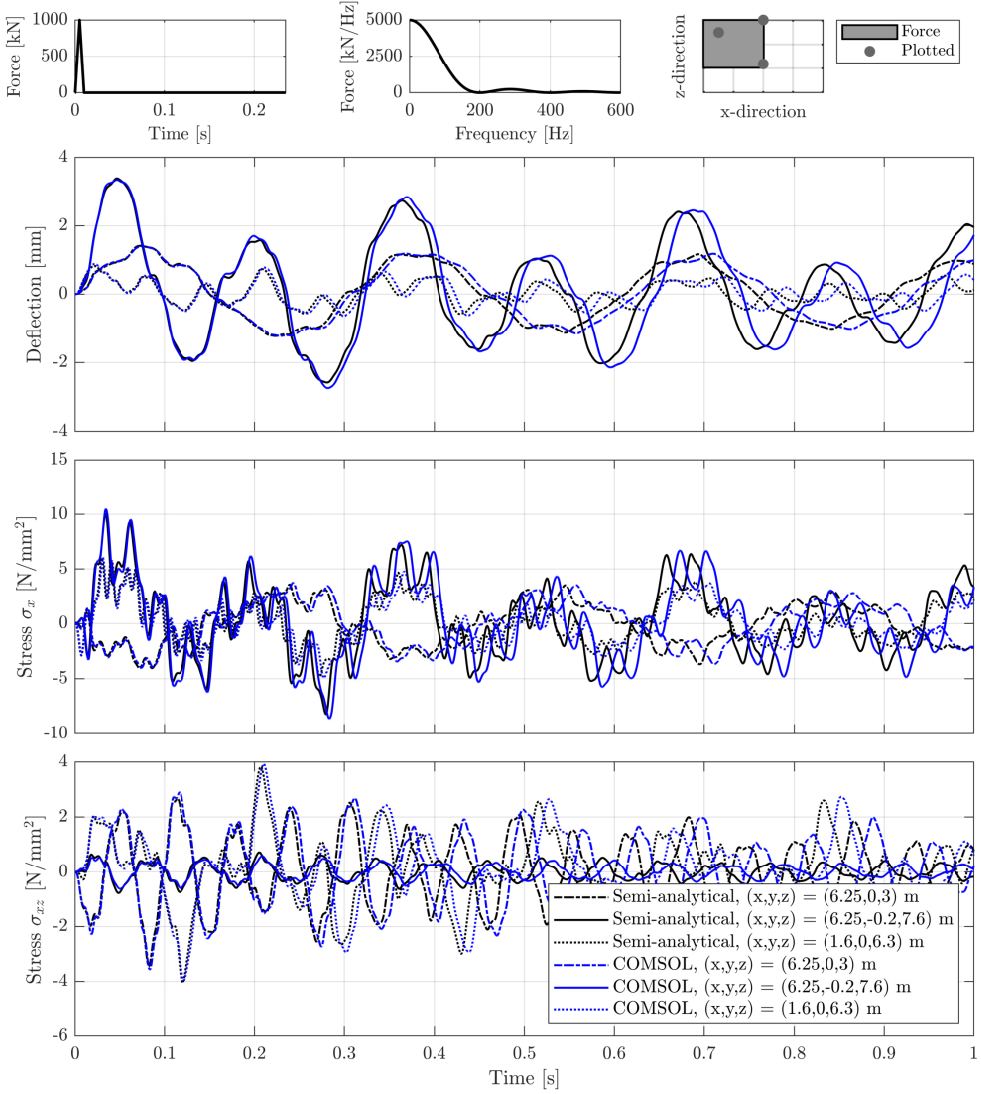


Figure 4.4: The time-domain response of the plate immersed in fluid for a triangular peak load predicted by the developed semi-analytical model compared to the FE COMSOL. The upper right graph shows an overview of where on the surface of the gate the force is applied and of the locations (x,z) for which the response has been shown.

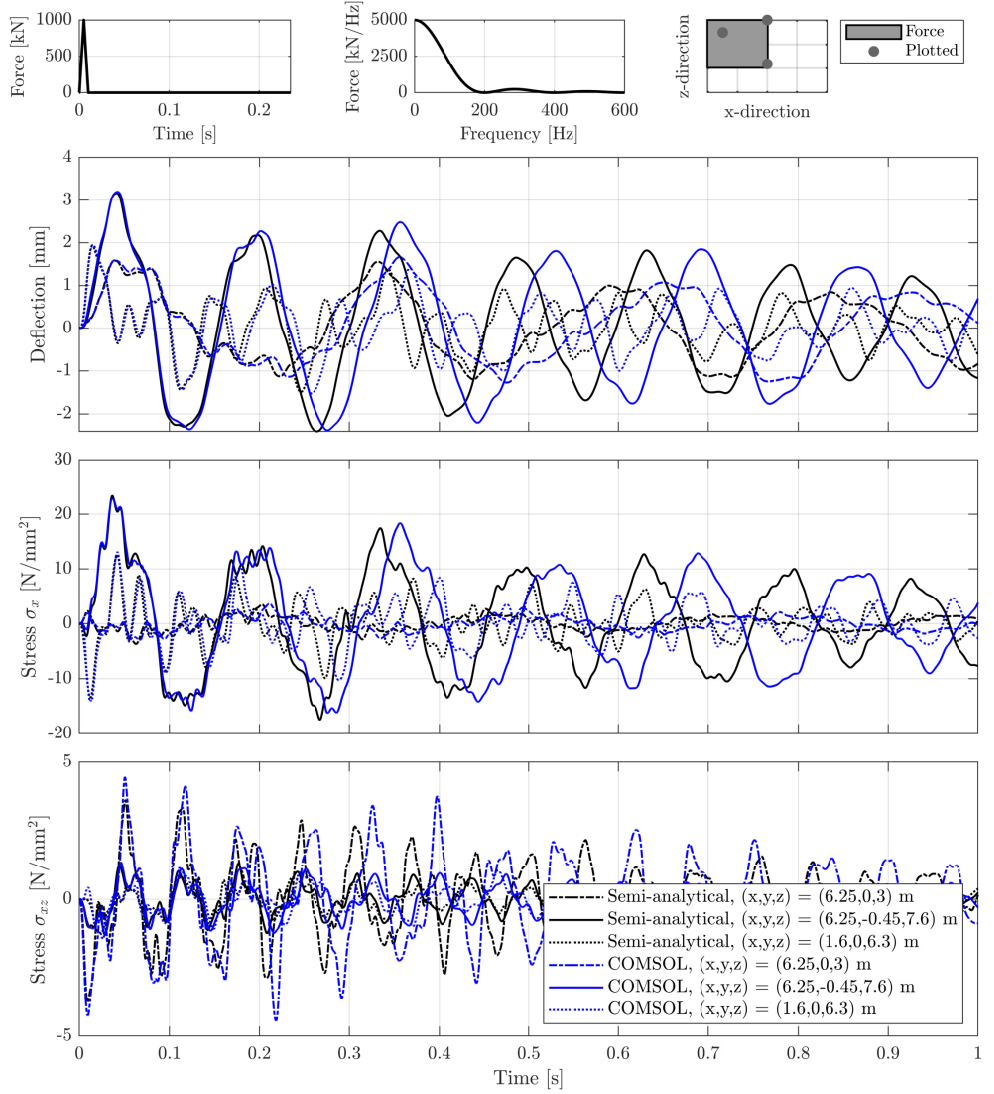


Figure 4.5: The time-domain response of the gate immersed in fluid for a triangular peak load predicted by the developed semi-analytical model compared to the FE COMSOL. The upper right graph shows an overview of where on the surface of the gate the force is applied and of the locations (x,z) for which the response has been shown.

stress. Both the displacements and stresses are deemed to be sufficiently converged for the maximum number of modes considered in the previous analyses. Further increasing the number of modes is expected to lead to an additional reduction of the computational error of the predicted stress of less than 1%.

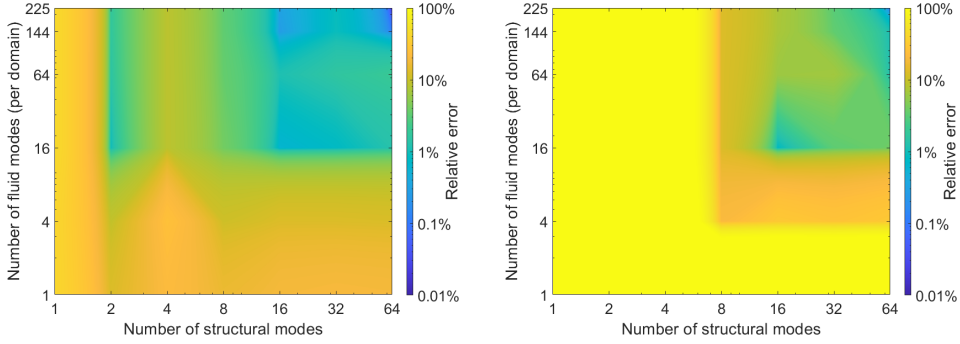


Figure 4.6: Convergence of the predicted maximum displacement(left) and stress σ_x (right) for increasing number of structural and fluid modes included in the numerical evaluation of the solution. The data points of the simulation correspond to the labels on both axes.

4.6.5 COMPUTATIONAL PERFORMANCE

For the case with realistic gate structure, the computation time of the semi-analytical model was 23 min on a 3.60 GHz quad core processor, whilst the computation time for the COMSOL model was about 38 hours. The computational efficiency of the semi-analytical algorithm was programmed in Matlab, a slow non-compiled scripting language, and has not been fully optimised yet. Furthermore, the computation time increases approximately linearly with the simulation period for finite element models. The semi-analytical model needs only a single computation to obtain the response amplitude operation for a certain frequency range, regardless of the number of loads that is subsequently considered. The semi-analytical model therefore has especially great benefits regarding computational efficiency when a large number of loads is considered, such as in a probabilistic analysis or fatigue assessment.

4.7 PARAMETRIC OPTIMIZATION OF A FLOOD GATE DESIGN

A design case study is performed of a flood gate in a discharge sluice subjected to wave impacts roughly inspired by the situation of the Afsluitdijk dam in the Netherlands. The response of a large number of preliminary design alternatives is simulated for a series of wave impact loads. This leads to an optimal design for the given conditions.

The aim of this case study is to demonstrate the benefits of the developed method and to investigate potential differences in outcome of this and existing methods. The intention of the case study is not to draw conclusions on the reliability of flood gates under wave impact loading in general. Safety factors are therefore for example omitted in this study.

Section 4.7.1 presents the basic parameters of the gate fluid system and the various gate designs that are considered in this optimization study. Section 4.7.2 then discusses

the wave impact design conditions. The parametric finite element model of the gate is elaborated in Section 4.7.3. Section 4.7.4 presents the optimal flood gate design that was found and its response to the governing design storm. Finally, 4.7.5 discusses further possible applications of the presented model in design studies.

4.7.1 GATE FLUID SYSTEM

Table 4.3 presents the basic parameters of the system considered in this case study. The gate has a width of 12 m and a height of 7.5 m. The design conditions correspond to a constant still water level at sea of 7.5 m up to the height of the overhang and of 3 m at the inner lake, resulting in a head difference of 4.5 m.

Table 4.3: Parameters and their values of the gate and fluid geometry applicable to all design variants considered in the case study

Structural parameters	Symbol	Value	Unit	Fluid parameters	Symbol	Value	Unit
Width	L_x	12	m	Width	$L_x^{I,II,III}$	12	m
Height	L_z	7.5	m	Water level left	$h^{I,II}$	7.5	m
Front plate thickness	t_{plate}	0.05	m	Water level right	h^{III}	3	m
Horizontal stiff. thickness	t_{vm}, t_{ve}	0.15	m	Overhang length	L_y	2	m
Vertical stiff. spacing	$L_{x1,x2,x3,x4}$	2.8125	m	Horizontal offset I-II	Δx^{II}	0	m
Vertical stiff. thickness	t_{vm}, t_{ve}	0.15	m	Bottom offset I-II	Δz^{II}	0	m
Elasticity modulus (steel)	E	$200 \cdot 10^9$	Nm ²	Fluid density	$\rho_f^{I,II,III}$	1025	kg/m ³
Material density (steel)	ρ_m	7850	kg/m ³	Fluid sound velocity	c_p	1500	m/s
Poisson's ratio (steel)	ν	0.3	-				
Material damping factor	η	0.01	-				
Yield strength (steel)	f_y	690	N/mm ²				
Boundary condition sides	-	hinged	-				

A relatively large number of preliminary design variants is considered in this optimization study, which is possible due to the high computational efficiency of the developed model. As discussed in the next section, wave impacts are considered that have constant pressures over the width of the gate. In contrast, the distributed of wave impacts pressures substantially vary over the height of the gate. Therefore, the design variations for the flood gate are aimed at the vibration modes over the vertical of the gate, which are in turn mostly influenced by the location and width of the horizontal stiffeners.

Figure 4.7 shows all design variants that are considered in this optimization study. The gate has four horizontal stiffeners. Generally, two stiffeners are located at the top and bottom of the gate. For the location of the two other horizontal stiffeners several designs are considered. In the base configuration (A), the horizontal stiffeners are distributed evenly over the height of the gate. Two alternatives are considered in which the two stiffeners are shifted more towards to bottom of the gate (B) and the top of the gate (C). The former would especially makes sense when the hydrostatic load is dominant while the latter is more aimed at the wave impact load, which has its maximum at the top of the gate. Finally, two designs are considered where the horizontal stiffeners are shifted towards the bottom and top (D) or the middle of the gate (E). These designs are aimed at providing stiffness at the critical locations of higher vibration modes.

Furthermore, the width of the two stiffeners (normal to the front plate) at the gate edges ($L_{h,e}$) and the two inner stiffeners ($L_{h,i}$) is varied. Three lengths (y-direction) are considered for each of the two types of stiffeners: 0.25 m, 0.35 m and 0.45 m. This amounts to nine different variants (1-9) for each of the above mentioned designs for the stiffener locations (A-E). This means that in total 45 design variants are considered in this optimization study. The optimal design variant is considered to be the one that is sufficiently safe, i.e. for which the yield stress is not exceeded for the design conditions, with the least use of material.

4.7.2 DESIGN STORM

The design event is described in terms of a set of hydraulic conditions with a certain design return period (e.g. 10.000 years). The governing storm event is considered to have a total duration of one hour. The water level at the sea side is at the overhang level for the entire storm duration. This is generally the governing water level in terms of wave impact pressures. The wave field is incoming from the sea side of the gate where the high water level is present. The storm conditions correspond to a JONSWAP spectrum with a peak period of 9 s and a significant wave height of 1.2 m. Besides the wave loading, the water level difference results in a constant hydrostatic load on the gate.

The aim of this design optimization study is to demonstrate the purpose of the developed method and compare its outcome to existing more conventional methods. Given this aim, some reliability aspects are omitted here that would in practice be relevant for design. For instance, safety factors (European committee for Standardization, 2006) are not included and uncertainties on the resistance side are not accounted for. The model routine presented in Chapters 7 and 8 is employed to translate the design wave spectrum to a realistic time series of the wave impact loading. This model routine employs different theories to predict the quasi-steady pulsating and the impulsive part of the wave load. The total wave pressure is the summation of both (Chen et al., 2019; De Almeida and Hofland, 2020b). Figure 4.8 shows a part of the resulting hour long time series of the depth-integrated wave force on the gate.¹

The quasi-steady oscillatory part of the load and the sharp peaked impulsive part can be clearly distinguished. Also the distribution of the dimensionless pressure impulse of the wave impact, according to the definition in De Almeida et al. (2019), is shown. The impulsive wave pressures are much higher at the top of the gate at the level of the overhang than at the bottom. The quasi-steady wave pressure has a different distribution, but also has its maximum at the top of the gate. The wave pressures are constant over the width of the gate.

An overview of the force, duration and impulse of the impulsive part of each wave impact is given in Figure 4.9. The five highest peak force and the five highest impulses are

¹Within the model routine of Chapters 7 and 8, several wave impact parameters are described stochastically. The random phase/amplitude model is used to translate the spectrum to a surface elevation realisation. And subsequently per wave impact, a Gaussian distributed correction factor β_{im} ($\mu = 1.17$ and $\sigma = 0.11$ (De Almeida and Hofland, 2020b)) and a triangularly distributed impact duration τ ($a = 0.010$ s, $b = 0.100$ s, $c = 0.200$ s (Tieleman et al., 2021)) are applied. Given these stochastic parameters, a large number of simulations is performed to find the wave load conditions that lead to the governing response of the flood gate. Here, only a single realisation of the wave loads is performed for the given storm conditions however and assumed to be governing. This approach is deemed sufficiently accurate for the purpose of this design study.

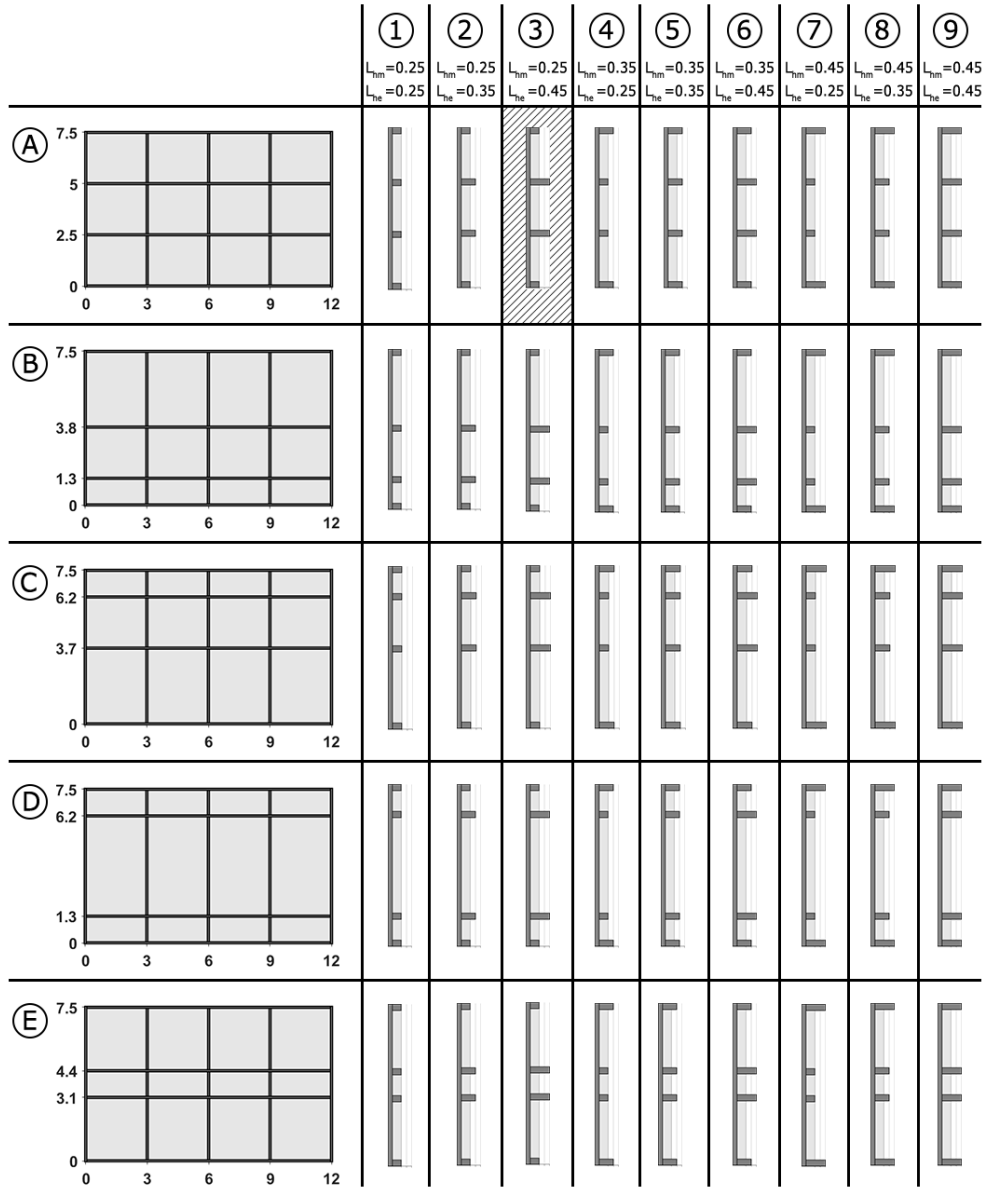


Figure 4.7: Gate design variants (45 in total) that are considered in the optimisation study. The light grey vertical lines in the side views are drawn for reference (at 0.25, 0.35 and 0.45 m). The resulting optimal design is indicated.

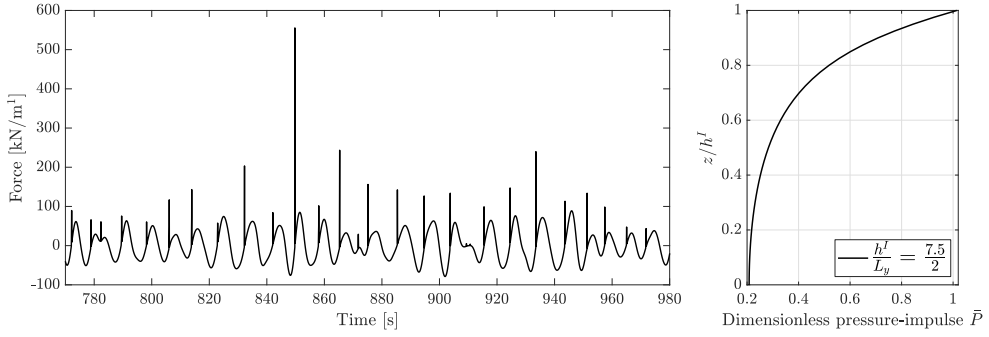


Figure 4.8: A time history of the wave force on the gate during part of the hour long design storm (left) and the distribution of the dimension pressure impulse over the height at the surface ($y = 0$) of the gate (right)

indicated. As can be seen, the highest peak loads correspond to short impact durations, but are not necessarily the wave impacts with the largest impulse. The dynamic response of each gate design is dependent on the impulse of a wave impact, the ratio between its resonance frequencies and the wave impact duration, but also the time between consecutive impacts. It therefore usually is hard to say in advance which wave impact will be governing for the response of each of the gate designs. This further endorses the need to simulate a large number of wave impact series in the design of flood gates as done in Tieleman et al. (2021).

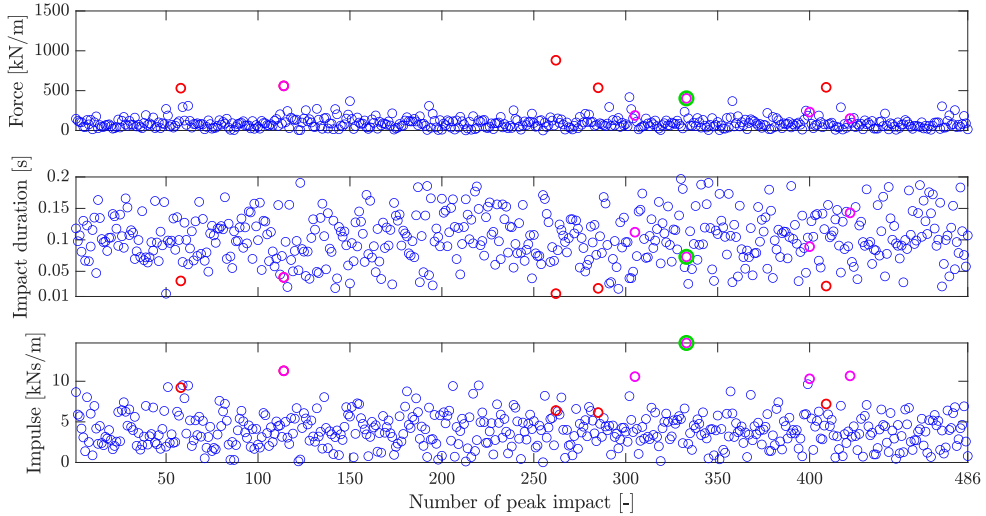


Figure 4.9: Peak force, impact duration, and impulse for each wave impact during the design storm. The five impacts with the highest force and impulse are shown in red and purple respectively. The wave impact that leads to the governing response for the optimal design is highlighted in green.

4.7.3 FINITE ELEMENT MODEL OF THE IN VACUO FLOOD GATE

The finite element software package SCIA Engineer is applied to perform the modal analysis of the in vacuo design variants. This software package is chosen as it is widely used in the field of engineering for the design of flood gates. Moreover, the software packages allows for parametric input. This is especially useful when evaluating multiple design variants as done in this optimization study. A numerical algorithm is written that makes use of this feature by setting the parametric geometry input for each design variant and executing the eigenmode analysis in SCIA Engineer. The algorithm obtains the resulting three-dimensional mode shapes in terms of displacements and stresses and the corresponding modal frequencies. The same algorithm then evaluates the semi-analytical fluid-structure interaction solution.

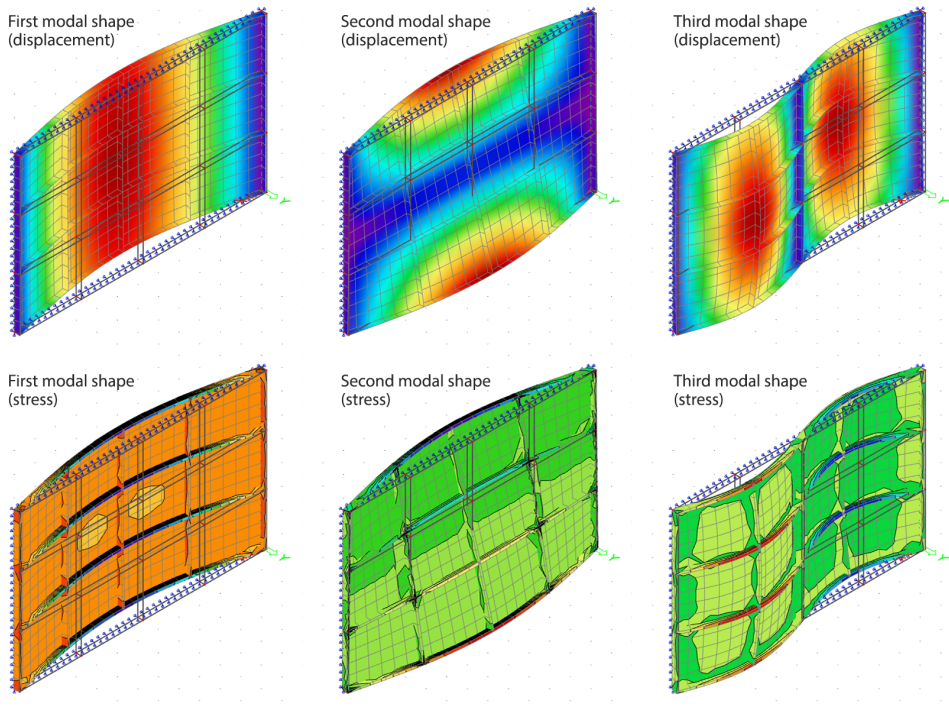


Figure 4.10: Modal shapes in terms of displacements and stresses of the first design variant (A1)

The structural model in SCIA Engineer applies isotropic shell elements for the front plate and the stiffeners of the gate designs according to Mindlin-Reissner plate theory (Reissner, 1945; Mindlin, 1951). Adjustable spring boundary conditions are applied along the edge of the front plate, which are parametrically set to relevant boundary conditions for this optimization study. For the free boundary conditions, this for example means a stiffness of zero. Figure 4.10 shows the mode shapes of the first design variant (A1) as an example.

SCIA Engineer is able to return the mode shapes mass normalized (such that $\Gamma_l = 1$). This avoids the necessity to define a mass field for the structure, as was discussed in Section 4.4. The displacement output is generated at the center line of each element in the finite element model, while the stress output is generated on the two outer edges of each element. The modal displacements at the center of the front plate are applied in the semi-analytical model to evaluate the surface integrals on the interfaces with the fluid, as was discussed in Sections 4.3 and 4.4.

4.7.4 OPTIMAL DESIGN

The response of each of the design variant to the design storm is now simulated with the presented model. Figure 4.11 shows the maximum stress and maximum displacement of each design during the design storm. The maximum stress in the gate turns out to be more sensitive to the length than the location of the stiffeners. As expected, the variants with stiffeners of minimum length (1) and maximum length (9) show the highest and lowest maximum structural stresses respectively. Even so, the maximum stress still varies quite significantly over the various designs (A-E). For example, design variant C1 with stiffeners shifted to the top edge of the gate results in a maximum stress of around 1400 MPa, while design B1 with stiffeners shifted towards the bottom results in a maximum stress of 950 MPa. Both these design variants have a minimal stiffener size.

For most variants, the design (C) with stiffeners shifted to the top edge of the gate results in the highest stress and thus is the most inadequate. A quasi-static design method would actually yield this as the optimal design as the wave impact leads to much higher pressures at the top than at the bottom of the gate (De Almeida and Hofland, 2020b; Tieleman et al., 2021). The hydrostatic pressure does have its maximum at the bottom of the gate, but is much lower than the peak force of the maximum wave impacts, as can be seen in the example in Figure 4.8. The dynamic response of the structure to these forces however leads to a response that is more balanced at the top and bottom of the gate, as could be expected from the first two mode shapes shown in Figure 4.10. For most variants (1-9) either the design with evenly distributed stiffeners (A) or even with stiffeners shifted to the bottom (B) is therefore optimal.

Fifteen design variants turn out to be sufficiently safe, as the yield stress is not exceeded for these variants. Design variants A3, B3 and E3 equally have the lowest material use of the safe variants. Of these, design variant A3 has the lowest maximum stress and would therefore be considered the optimal design. However, the difference in maximum stress for each of these design variants is limited. In practice, other criteria for instance regarding the ease of manufacturing will likely determine which of these design variants would be optimal.

Design variant A3 has evenly distributed horizontal stiffeners over the height of the gate. The two middle stiffeners are large (0.45 m) while the edge stiffeners are smaller (0.25 m). This seems remarkable as the highest fluid pressures occur at the top and bottom of the gate. This can be explained by the fact that although an increase in stiffener length adds to the overall stiffness of the gate, it also attracts higher stresses due to the increased centroidal distance to the outer edge of the stiffener. The two large middle stiffeners target the first mode of vibration as effectively as the edge stiffeners, and will also add some stiffness to the second mode. This reduces stresses in the edge stiffeners without

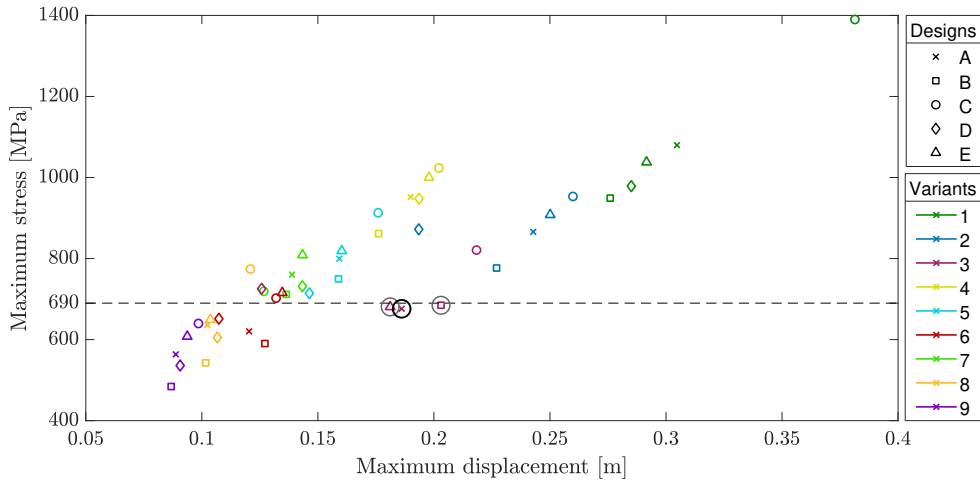


Figure 4.11: Maximum stress and displacement response for all design variants. The optimal design variants are encircled. Design variant A3 is encircled with a thick line

increasing their length. This effect does not play a role in the displacements. The variants with large edge stiffeners (7) therefore do show lower maximum displacements than the variants with large middle stiffeners (3).

Figure 4.12 shows the response over time in the middle of the the bottom and top stiffeners of the gate to the hydrostatic and wave loads for the governing part of the design storm. Figure 4.13 shows the displacement and stress fields at the moment the maximum stress is reached in the gate. The stress in middle of the bottom stiffeners turns out to be governing. Also in the middle stiffeners high stress peaks occur. Based on a quasi-static design approach, the location of the maximum stress would have been predicted in the top stiffener as the maximum peak impact force is a few times larger than the hydrostatic load and the impact pressures at maximum at the top of the gate.

In Figure 4.9, showing the peak force, impulse and duration of the wave impacts during the design storm, the governing wave impact (no. 333) for this design variant was indicated. This wave impact is the one with the highest impulse during the storm. It has an average impact duration and therefore not an extraordinarily high peak force. Present quasi-static design methods often assume the wave impact with the highest peak force to be governing. This may therefore lead to an underestimation of the predicted maximum stress response of the structure.

The governing wave impact differs for the various design variants. For design variant E3, one of the other safe designs with the lowest use of material, the governing response occurs after several high impulse wave impacts shortly follow one another (impact no. 399 and 400). Since the motion of the gate is not fully damped out between wave impacts, a compound effect arises for this gate that results in a larger maximum response. The last wave impact does have a high impulse but not the highest one during the storm. This underlines the importance of taking consecutive wave impacts into account in design methods as was discussed in Tieleman et al. (2021) and Kleiberg et al. (2022).

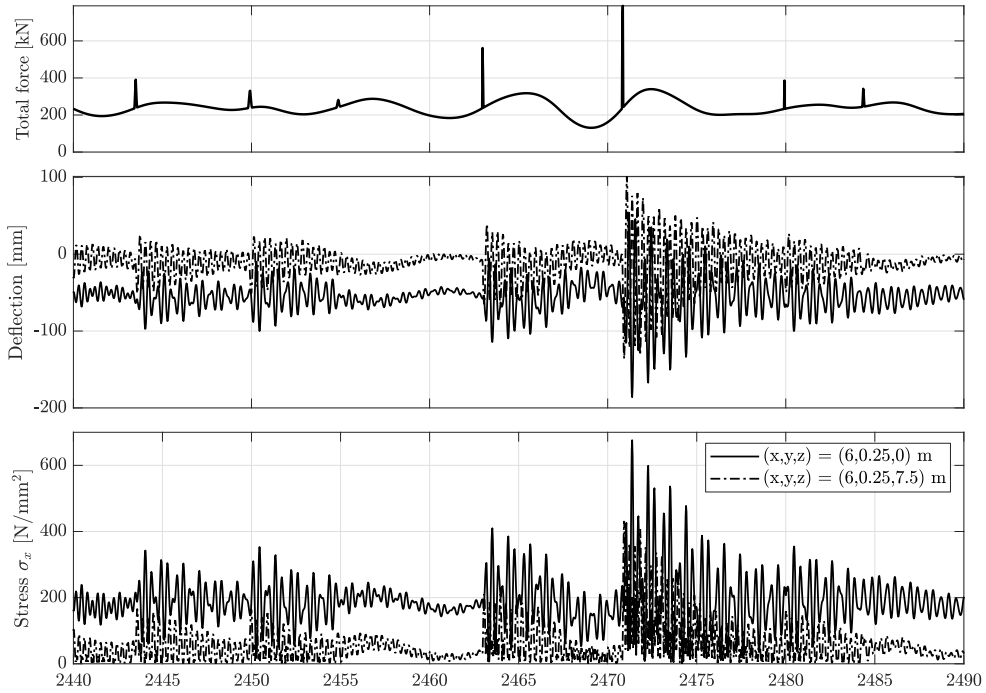


Figure 4.12: Response of the optimal gate design (A3) to the governing part of the wave impact series

4.7.5 LIMITATIONS AND FURTHER POSSIBILITIES FOR DESIGN STUDIES

As was shown in this optimization study, the computational efficiency of the model allows for the simulation of the dynamic response of the structure including the involved dynamic FSI for multiple design alternatives and a relatively long load duration. The frequency response function of the gate fluid system only has to be evaluated once for a given design. The additional computational effort required for a longer load duration is limited. Fatigue analyses in which the response to each load over the lifetime over the gate structure could be simulated, are therefore also within the range of possibilities and provide another interesting application of the presented model (Kleiberg et al., 2022).

The frequency response function obviously does have to be evaluated for each individual design alternative. This includes employing the finite element model to obtain the mode shapes and frequencies of the in vacuo gate. This optimization study considered a reasonable number of design alternatives. However, the number of possible design alternatives increases rapidly when more parameters are varied and more values per parameter are considered. Simulating the dynamic response for each of such a number of design alternatives definitely does exceed practical computational limits. Methods such as generative algorithms do provide possibilities to limit the number of design alternatives that has to be simulated to find an optimal design.

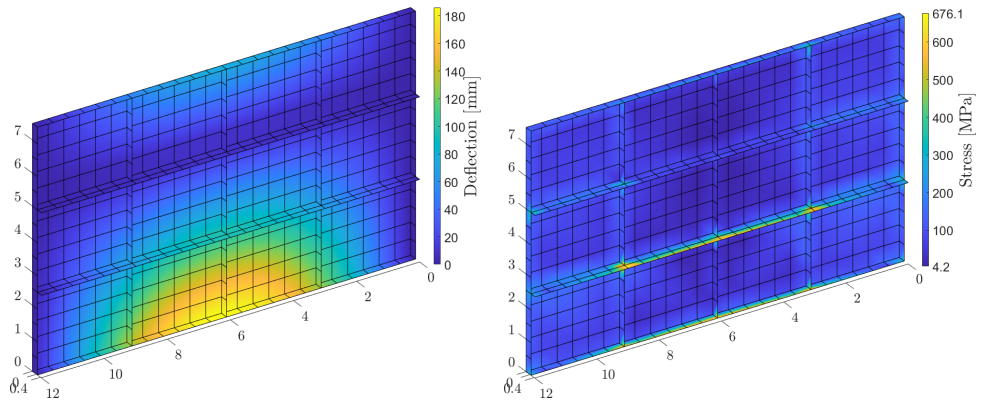


Figure 4.13: Displacement and stresses of the gate at the moment of maximum stress response during the design storm

4.8 DISCUSSION

A hybrid semi-analytical and finite element model was presented to predict the dynamic behaviour of flood gates immersed in water. The employed method of solution was shown to solve the fluid-structure interaction much more efficiently than coupled finite element models. On the other hand, finite element models have a wide applicability range, while the analytical solution of the developed fluid-structure interaction model is aimed specifically at the design of flood gates under wave impact loading. Several key assumptions of the developed model and considerations for the application to design are therefore discussed.

One of the main assumption in deriving the semi-analytical solution concerns the continuous interface between the structure and fluid on both sides of the gate. The effect of the stiffeners at the backside of the gate on the fluid-structure interaction is neglected. Second, the semi-analytical solution was derived in the frequency domain and based on linear dynamics of the structure and fluid. Non-linear effects were thus neglected. Results showed to be in good agreement with a conventional finite element model that both incorporates the full interaction with the stiffeners and non-linear dynamics. Nevertheless, it is recommended to extend this comparison for different gate designs or fluid domain geometries and water levels to gain more insight in the applicability limits posed by these assumptions. Also if one is interested in the plastic deformation of the gate, non-linear behaviour must be considered. At least regarding the effect of non-linearity, there are possibilities to incorporate this in frequency domain methods to extend the applicability of the developed model.

Furthermore, this study focused on flood gates with common boundary conditions. The developed fluid-structure interaction model is suitable for any time-independent boundary condition. Supports of vertical lifting gates such as guiding wheels and sliding supports can in principle be incorporated in the finite element model that is employed to obtain the modal information of the in vacuo gate. However, in some practical cases slack can be present between the gate and the supports. The gate can then be pushed off the

supports by the wave impact and hit the supports at the other side, either directly or after a bounce back from the initial response to the wave impact. Due to this behaviour, the boundary conditions for the gate become time-dependent. This situation can therefore not be predicted straightforwardly with the developed fluid-structure interaction model. It is recommended to study the behaviour of the flood gate with this type of supports first with a time domain model. The results can give an indication to what extent it might be feasible to represent this situation with an adjusted version of the developed fluid-structure interaction model.

Finally, wave impact loads may cause entrainment of air bubbles in the water column. These air bubbles can significantly decrease the sound velocity in the water in front of the gate (Bullock et al., 2007). The sound velocity of water is around $c_p = 1500$ m/s, but could drop as low as 150 m/s for a water-air mixture with 1% air (Gibson, 1970). This may lead to lower resonance frequencies of the fluid due to compressibility and therefore alter the fluid response. Acoustic damping may become more significant as well. As a first step for further research, a sensitivity analysis could be performed for various levels of air bubbles, and thus sound velocities, extending over various distances from the gate. Also experiments by De Almeida et al. (2019) and De Almeida and Hofland (2021), and ongoing laboratory experiments of wave impacts on a flexible gate, provide data to further investigate the relevance of this effect.

4.9 CONCLUSION

A novel hybrid semi-analytical and finite element model has been developed to predict the dynamic response of a flood gate. It is aimed at the situation of a gate located in a discharge sluice with an overhanging structure in front that may cause confined wave impacts. A typical gate design is considered with a front plate supported by horizontal and vertical stiffeners. The semi-analytical part of the model solves the dynamic response of the gate including the involved fluid-structure interaction based on a mode matching technique. In earlier studies, the gate was represented by a thin plate and the mode shapes and frequencies of the in vacuo structure were obtained analytically. The semi-analytical method has now been coupled to a finite element model to obtain this modal information. This allows for a detailed prediction of the structural stresses for more realistic gate designs. The developed model gives similar results as conventional FE software at only a fraction of the computational time of the latter. This makes the model especially suitable to perform design optimization studies with various parameters or fatigue calculations and probabilistic assessments in which many load cases over long periods must be considered. The numerical algorithm of the developed fluid-structure interaction model has been made available on the 4TU research repository (Tieleman, 2022, [link](#)).

The developed model has been applied to a design optimization study. The response of large number of design variants was simulated for an hour long design storm that includes several hundred wave impacts. The results of the study differed from what would have been expected based on a quasi-static design approach often applied in practice. An optimal design was found with the most stiffness in the field of the gate while the excitation load had its maximum at the top of the gate. Furthermore, the maximum stress

occurred at a different location than what would be expected quasi-statically. Generally, in practice the wave impact with the highest impact peak pressure rather than impact impulse is chosen as the governing design load, while the impulse is more strongly correlated to the maximum response. Moreover, a compound effect of vibrations due to consecutive wave impacts is not taken into account. In this study, the governing part of the storm turned out to be either the impact with the highest impulse or several consecutive wave impacts with high impulse depending on the design variant. This underlines the need to investigate a large number of possible wave combinations in design without doing concessions to the physical modelling of the dynamics of the fluid-structure system. This becomes a possibility with the model presented in this study.

Given its benefits it is recommended to apply the developed hybrid fluid-structure interaction in the design of flood gates under wave impact loading. The later chapters of this thesis present design methods regarding the safety and fatigue lifetime of flood gates under wave impacts utilizing the developed model.

5

**AN EXPERIMENTAL STUDY
OF WAVE IMPACTS ON A
FLOOD GATE**

Previous chapters have presented a novel semi-analytical approach to predict vibrations of flood gates including the involved fluid-structure interaction. This model has been validated throughout these chapters by comparison to a conventional time-domain finite element model. This chapter answers the question whether the developed modelling framework covers the most relevant physical phenomena that govern the response of flood gates to wave impacts. For this purpose, an experimental study of wave impacts on flexible gates has been performed. A first experimental validation of the developed model is carried out by comparing predictions to the measurements. Furthermore, a valuable dataset is presented that allows to further study physical phenomena that are not yet described by the existing models.

Section 5.1 introduces the topic and provides some relevant background literature. Section 5.2 presents the experimental set-up and Section 5.3 the various test series that have been performed. In Section 5.4, the preliminary validation of the developed semi-analytical model is performed. Section 5.5 discusses possibilities for further research and potential improvements of the applied methods. Section 5.6 presents the conclusions of this chapter.

5.1 INTRODUCTION

De Almeida et al. (2019); De Almeida and Hofland (2020b,a) have performed extensive experimental studies on the hydrodynamics of confined wave impacts on vertical structures with an overhang. It was shown that pressure-impulse theory is effective in predicting the wave impact loads for these situations. The structure considered in these experiments was a rigid¹ vertical wall. Huang and Chen (2022) have recently performed experiments for a similar situation with confined wave impacts on a cantilever slab. The experiments did not contain structural response measurements as the setup was rigid, but a structural response analysis of a flexible plate was performed based on the impact pressures. The previous chapters Tieleman et al. (2019b, 2021) have shown that for the design of flood gates their dynamic behaviour and interaction with the surrounding fluid is key. The structure may thus not be considered as rigid in that type of problem.

Chen et al. (2019) have presented a first modelling framework to predict the response of flexible structures to wave impact loads based on a one degree of freedom representation of the structure. Tieleman et al. (2022b) have presented a novel computationally efficient hybrid semi-analytical and finite element model that can be applied in the design of flood gates, which includes multiple mode behaviour and the two-way fluid-structure interaction. Both the effect compressibility and surface waves on the fluid response to the movement of the gate were considered. This model was validated by comparison to existing numerical finite element software. However, wave impacts are accompanied with uncertainties that are not yet included in existing models. Although the interaction with the still standing surrounding fluid is considered in the model by Tieleman et al. (2022b), the wave impact is modelled as an external load. This load can for instance be based on measurements on a rigid structure such as in De Almeida et al. (2019) or pressure-impulse theory (Cooker and Peregrine, 1995; Wood and Peregrine, 1997; De

¹The stiffness of the structure is here regarded in relation to the excitation frequencies involved with these type of confined wave impact loading on overhangs.

Almeida and Hofland, 2020b). The flexibility of the structure will, however, influence the wave impact process to some extent. Furthermore, according to De Almeida and Hofland (2020a), entrapped air pockets under the overhang are strongly related to the way the impact pressures vary over time and thus also the impact duration. These air pockets may also influence the response of the flexible structure. Finally, Bullock et al. (2001, 2007) and Gibson (1970) have shown that air bubbles can significantly decrease the sound velocity in fluid surrounding the gate. Kleiberg et al. (2022) discussed that this could potentially impact the response of the flood gate and recommended further study on this topic.

Suitable experimental data is needed to study these phenomena and validate the fluid-structure interaction model by Tieleman et al. (2022b) for wave impacts on flood gates. However, as discussed by De Almeida and Hofland (2020b), previous research has mainly focused on the study of wave impacts caused by breaking waves (Bagnold, 1939; Minikin, 1950; Takashi, 1994; Oumeraci et al., 2001; Cuomo et al., 2010) and overtopping waves (Chen et al., 2015, 2016, 2017). Moreover, these experiments focused on wave impacts on rigid structures. A few experimental studies of breaking wave impacts on flexible vertical walls do exist. Hattori and Tsujioka (1997) performed experiments of breaking wave impacts on a partially rigid and partially flexible wall. Pressure transducers were placed in a rigid part of the wall to measure the wave impact pressures. It was assumed that the impact pressures are constant over the width over the wave and equal for both the rigid and flexible part of the wall. A one degree of freedom model was used to predict motion of the wall. Kirkgöz (1990) performed experiments on breaking wave impacts on a completely flexible wall. The pressure transducers were placed in the elastic wall. Tanrikulu et al. (2002) compared the experimental results of this study with theoretical predictions. The motion of the gate was predicted numerically based on elastic shell theory (Timoshenko and Woinowsky-krieger, 1959). The fluid pressure, both due to the wave impacts and the motion of the wall, is modelled as an external load based on measurements during the impact. Experimental data of wave impacts on a flexible vertical wall or gate with overhang is lacking altogether.

Laboratory experiments have therefore been performed for the situation of a flexible gate subjected to wave impacts on an overhang. The approach is an extension of the one applied in the experiments on a rigid vertical wall by De Almeida and Hofland (2020b,a). The rigid wall is replaced by a flexible gate. A relatively large number of accelerometers and strain gauges is introduced to identify multiple modal vibrations of the gates. The measurement results are compared to the predictions by the theoretical model developed in the previous chapter (Tieleman et al., 2022b) with the aim of providing a first validation of this model. Moreover, a valuable dataset is presented that can be used to further study the mentioned phenomena such as the effect of air bubbles in the fluid on the response of the structure. This dataset has been made publicly available for research on the 4TU repository (Tieleman et al., 2022a, [link](#)).

5.2 EXPERIMENTAL SET-UP

The laboratory experiments in this study were performed in the wave flume of the Hydraulic Engineering Laboratory at Delft University of Technology. Figures 5.1 and 5.2 show a schematic overview and several impressions of the experimental facility and

setup. The wave flume is 42 m long, 1 m high and 0.8 m wide. The wave generation equipment consists of a piston-type wave maker able to generate regular and irregular waves and is equipped with active reflection compensation (ARC) and second order wave steering. Similar to De Almeida and Hofland (2020b,a), a heavy concrete block of 920 kg with aluminium frame is situated in the wave flume. An aluminium overhang and a stainless steel gate are mounted on this aluminium frame. Water is present only at one side of the gate. The gate is designed such that a dynamic response is expected, while the overhang is rigid. The bottom and front plates that form the overhang are relatively thick and supported by the aluminium frame at several points over their width to ensure sufficient stiffness in regard to the wave impact loading. For more information on the design of the concrete block and aluminium supporting frame is referred to De Almeida and Hofland (2020b). The next two sections discuss in more detail the gate designs and the measurement instrumentation applied in the experiments.

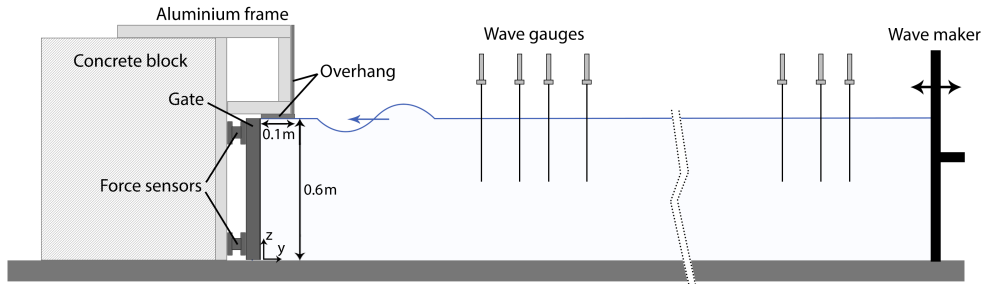


Figure 5.1: A schematic side view of the experimental setup



Figure 5.2: Impressions of the experimental facility and setup. The concrete block is placed in the wave flume. On the photo on the right, the front steel plate of the overhang and tapes on the sides of the gate to ensure water tightness have not yet been installed.

5.2.1 GATE DESIGNS

Two gate designs are tested in the experiments: a plain gate and a reinforced gate. These gates consist of a rigid U-shaped frame and a flexible front plate. For the reinforced gate, the flexible front plate is additionally supported by two flexible horizontal stiffeners. The rigid U-frame is mounted on four load sensors which are mounted on the aluminium frame attached to the concrete block. The plain gate is expected to have the most straightforward response. The developed fluid-structure interaction model in the previous chapters is expected to give the best results for this type of gate. However, the reinforced gate more closely matches the realistic flood gate designs applied in practice. For a design with stiffeners the higher, more local, modes are also expected to be more relevant than for a solid plate.

Figure 5.3 shows the two gate designs in the flume detached from the supports (with instrumentation explained in the following section). The front plate of the overhang is not installed yet in these pictures. The gates are made of stainless steel (type 304) with a density of 7950 kg/m^3 and an elasticity modulus of 193 GPa. The U-shaped frame is designed such that no significant deformations are expected under the wave impact loading. The flexible parts of the gates are glued to this frame to create a straightforward single solid structure. Gluing was preferred over welding, as the latter may result in remnant strains in the structure. For the reinforced gate, recesses were made in the rigid frame to house the two horizontal beams. Furthermore, in the bottom part three circular holes were drilled in which fluid pressure sensors were mounted. The rigid frame effectively results in clamped supports at the bottom and both sides of the flexible part of the gate. The top of the gate is free.

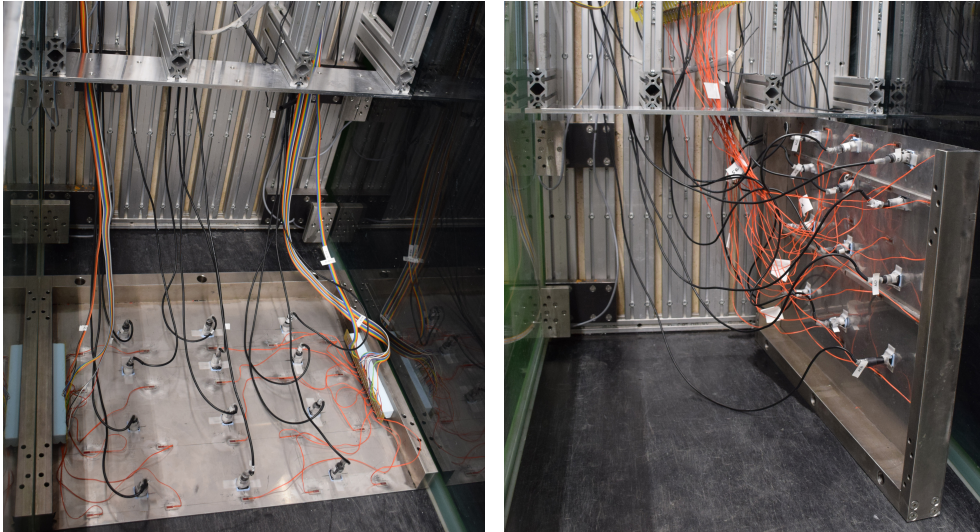


Figure 5.3: The plain (left) and reinforced (right) gates in the flume with the accelerometers and strain gauges installed. The gates are detached from the four load cell supports. The front plate of the overhang has not yet been installed on the aluminium support frame in these picture.

A thin gap is present between the top of the gate and the overhang to allow it to freely vibrate. This gap has been minimized (to ≈ 1 mm). Also between the U-frame of the gate and the bottom and walls of the wave flume gaps are left (≈ 5 mm) to avoid friction at these points. This allows the four load sensors on which the gate is mounted to measure the total force transferred onto the supports of the gate. Water tightness of the gate is then realised by placing flexible tapes between the gate and walls and overhang. These tapes are applied with sufficient slack to avoid the transfer of forces at these locations as much as possible and prevent disturbance of the load sensor measurements or the vibrations of the flexible part of the gate.

The hybrid semi-analytical and finite element fluid-structure interaction model presented in the Chapter 4 has been employed to obtain a detailed design of the gates. The finite element software ANSYS (Kidger, 2012) was used in this case to obtain the in vacuo mode shapes and frequencies of the gate. The detailed design mainly concerned the thickness of the front plates and, in case of the reinforced gate, the locations and dimensions of the reinforced beams. Two criteria design criteria were applied. First, plastic deformation due to the exceedance of the material yield strength is avoided. Second, a dynamic response to the wave impact loading is aimed for. When possible, the excitation of multiple modes is preferred. A time domain analysis was performed based on a theoretical prediction of the impact loads tested in the experiments to evaluate these criteria. Given the clamped supports and the geometric constraints imposed by the flume, there were limited possibilities to design the plain gate such that vibrations of multiple modes are relevant. The first resonance mode of the immersed gate is expected to dominate the response of the plain gate. The reinforced gate has more design possibilities. The ratio between the stiffness of the front plate and the reinforcement beams and also the distribution of those beams over the height of the gate were varied to maximize the excitation of higher vibration modes. Figure 5.4 shows the finite element model geometries of the resulting gate designs.

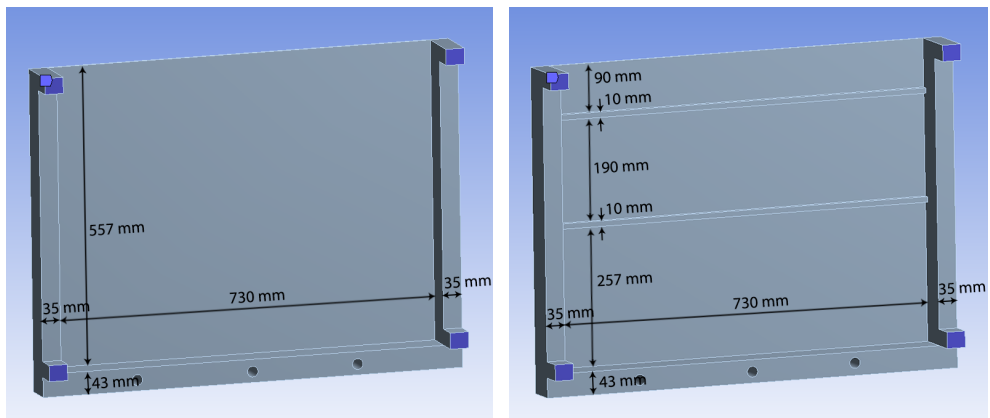


Figure 5.4: Overview of the finite element models including key dimensions of both the plain gate (left) and the reinforced gate (right). The four fixed supports of the gate in the finite element model, representing the attachments to the load sensors, are shown in blue.

The gates in the finite element model have a width of 0.8 m and a height of 0.6 m. The realized gates for the experimental setup are slightly smaller, as on the bottom 3 mm and on each side 5 mm of space is covered by the water retaining tapes instead of the steel frame. The plain gate has a front plate with a thickness of 3 mm, while the reinforced gate has a thinner front plate of 2 mm supported by two horizontal stiffeners with a height and thickness of 10 mm. The holes in the bottom beam have been included in the finite element model to verify that these do not significantly impact the stiffness of the frame.

Table 5.1 shows the predicted resonance frequencies of both the in vacuo gate (predicted by the finite element model) and the immersed gate (predicted by the hybrid fluid-structure interaction model). The peak impact duration of the wave impacts is expected to lie within the range of 10-60 ms (De Almeida and Hofland, 2021), which is within the range of several resonance frequencies of the immersed gates.

Table 5.1: The first six resonance frequencies predicted for the in vacuo gate (by ANSYS) and the immersed gate at a water depth of $h = 0.6$ m (by the hybrid semi-analytical model)

Gate	Condition	f_1 [Hz]	f_2 [Hz]	f_3 [Hz]	f_4 [Hz]	f_5 [Hz]	f_6 [Hz]
Plain gate	In vacuo	33.7	72.3	85.6	126.4	158.4	163.6
	Immersed ($h = 0.60$ m)	10.8	28.3	31.4	54.5	69.1	75.7
Reinforced gate	In vacuo	82.3	93	133.3	167.4	179.8	204.1
	Immersed ($h = 0.60$ m)	26.4	39.7	64.3	72.1	103.7	111.2

Figure 5.5 and 5.6 show the predicted mode shapes of the in vacuo plain and reinforced gate respectively. The mode shapes of the immersed gate are relatively similar, although the presence of the fluid does alter the mode shapes to some extent. As can be seen, the reinforcement beams considerably influence the mode shapes of the gate. More local modes in the 'fields' between stiffeners occur. Moreover, mode shapes in the vertical direction have lower resonance frequencies compared to those in the horizontal direction. It is further noted that the wave loads are expected to be uniform along the horizontal direction. These loads therefore do not excite anti-symmetric modes of the system. This involves the third and fourth mode of the plain gate and the fourth and fifth of the reinforced gate.

An issue was encountered with the glue connections during the experiments. The connections between reinforcement beams and the front plate failed in the wave impact tests on the reinforced gate. This also revealed that the glue was not applied over the full interface surface between the front plate and the solid U-frame. This may have lead to a more flexible gate than accounted for in the design, which impacts the resonance frequencies and response of the gate. For the plain gate, the glue connections were redone and improved for this reason before executing the tests. The expectation is that the issue was therewith solved for that design. This topic is further discussed in Section 5.4 based on the comparison between the model predictions and the experimental results.

5.2.2 INSTRUMENTATION

Figure 5.7 shows the location of all measurement devices that were applied for both the plain gate and reinforced gate experiments with the exception of the wave gauges.

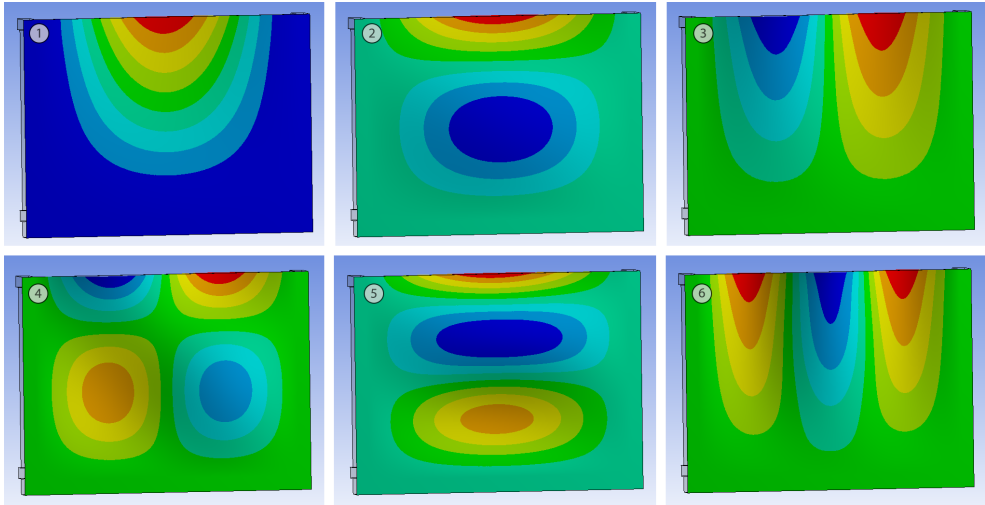


Figure 5.5: Modal shapes of the in vacuo plain gate as determined by the finite element software (ANSYS). The mode shapes correspond to the frequencies (in vacuo) from Table 5.1.

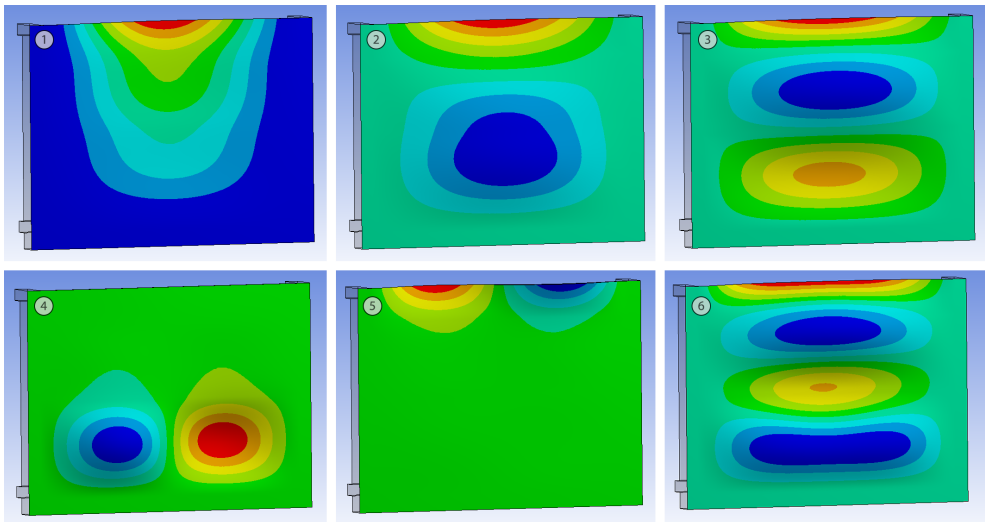


Figure 5.6: Modal shapes of the in vacuo reinforced gate as determined by the finite element software (ANSYS). The mode shapes correspond to the frequencies (in vacuo) from Table 5.1.

The coordinates of each of the measurement devices has also been included in the experimental data (Tieleman et al., 2022a, [link](#)). The experiments are aimed at investigating the interaction between the gate structure and fluid. Measurement devices were therefore applied both to measure the wave load and the structural response. All measurement devices have been calibrated and the measurements have been translated to the relevant physical quantities in the presented data set.

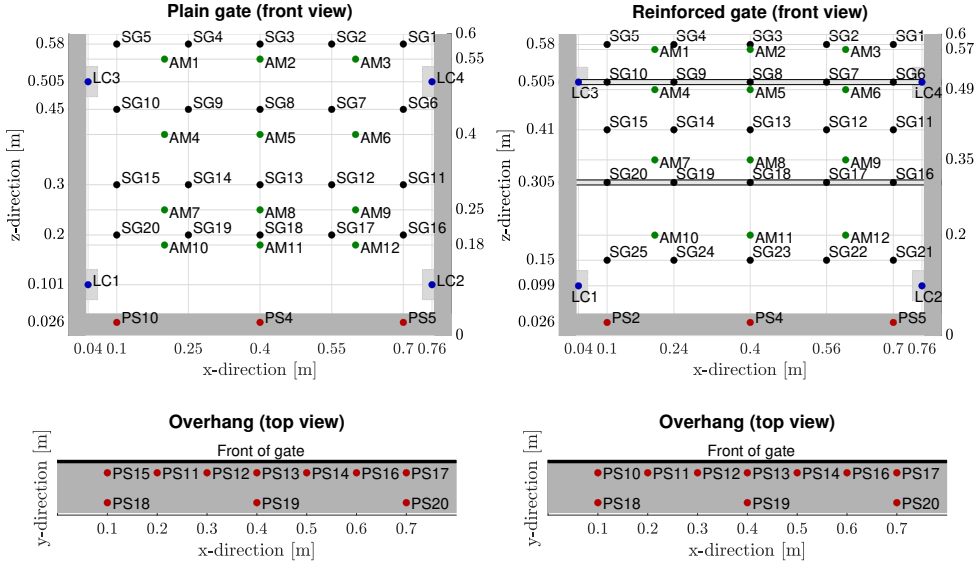


Figure 5.7: Locations of the load sensors (LC1-4), pressure sensors (PS2, PS4, PS5, PS10-PS20), strain gauges (SG1-25) and accelerometers (AM1-12) applied during the tests for both the plain and reinforced gate. A front view is shown of the gates. However, the measurement devices are located at the dry backside of the gate.

The incoming waves were measured by seven wave gauges (WG1-7), of which four are placed near the gate ($y_{WG7-WG4} = 1.495, 1.895, 2.19, 2.59$ m) and three near the wave maker ($y_{WG3-WG1} = 23.50, 23.90, 24.20$ m). All wave gauges were equipped with temperature compensation systems in order to ensure the accuracy of the water level measurements in all conditions during the tests. The rigid frame of the gate is mounted on four load cells (LC1-4) from HBM model U3. These loads cells measure the total force on the supports of the gate, which will be a combination of the wave load acting on the surface of the gate and the inertia forces due to the movement of the gate. The fluid pressure was measured by Kulite HKM-375M-SG pressure sensors (PS2, PS4, PS5, PS10-PS20) with a 1 bar measurement range and sealed gauge. Thirteen sensors were used simultaneously in each test setup, of which three in the bottom of the gate frame and ten in the overhang. The locations of the pressure sensors were matched with those in the rigid wall experiments by De Almeida and Hofland (2021) as much as possible to make a comparison possible. The arrangement of the specific pressure sensor devices differs slightly for the plain gate and the reinforced gate although the locations of the measurements are identical. No pressure sensors were located in the flexible part of the gate however. This makes it difficult to

interpolate the measurements to obtain an accurate estimate of the full pressure field on the gate at any time. However, the rigid wall experiments by De Almeida and Hofland (2021) in principle provide measurements of the wave loads on the gate. The combination of the load cell and pressure measurements, together with theoretical predictions, are expected to sufficiently provide the data required to investigate differences due to the flexibility of the gate.

The motion of the gate was measured by both strain gauges and accelerometers. One-dimensional strain gauges were placed horizontally (in the x-direction). A relatively large number was used with the aim of being able to interpolate the results to obtain a complete strain shape of each gate during the vibrations. Twenty strain gauges were used for the plain gate (SG1-20). Because of the discontinuities in the reinforced gate design, a slightly higher number of twenty-five gauges (SG1-25) was used for those tests. The strain gauges were glued to the back of the front plate and, in case of the reinforced gate, the reinforcement beams. The strain gauges were thus not reusable between gate designs. The sensors SG1-20 are therefore different physical devices for the plain and reinforced gate tests. Finally, twelve ADXL335 accelerometers were attached to the back of the gates by means of a sticky clay, which did allow to reuse these sensors for the two gate designs. These accelerometers are able to measure accelerations in three directions. However, only the accelerations perpendicular to the surface of the gate (in y-direction) are of interest for this problem and were thus measured in these experiments. The accelerometer data was adjusted for any misalignment of the angle of the devices in the vertical direction by making use of the measured gravitational acceleration before application of the loading. These adjustments were limited to several percent at most.

5.3 EXPERIMENTAL TEST SERIES

The experiments are aimed at the situation of wave impacts on a gate with overhang. The key part of the experimental test series therefore consists of regular and irregular waves of various conditions. However, also several supporting test series were performed with other types of loading: static loading, aimed hammer impacts and random hammer impacts. Table 5.2 gives a complete overview of the performed test series including the load conditions of each tests and the test data code. Each of these tests has been performed for both the plain gate (PG) and reinforced gate (RG). The folder structure of the experimental data made available at the 4TU repository (Tieleman et al., 2022a, [link](#)) matches these test series names and data codes together with a reference to either the plain gate (PG) or reinforced gate (RG). The test data codes for the wave impact tests match those introduced in the study by De Almeida and Hofland (2020b).

Each of the test series and load conditions are explained further in the following paragraphs. Section 5.4 utilizes the measurements of the random hammer and regular wave impact tests to validate the fluid-structure interaction model.

5.3.1 STATIC LOAD TESTS

The response of the dry gates was measured for a static load. The fluid-structure interaction model developed by Tieleman et al. (2022b) obtains the mode shapes of the in vacuo gate through a finite element model and then uses this modal information to

5.3. EXPERIMENTAL TEST SERIES

Table 5.2: Overview of the test series in the experiments. PG indicates the plain gate and RG indicates the reinforced gate. Tests are referred to be a combination of the gate abbreviation and the test data code (for example: RG_SLH).

Test series	Water depth	Loading conditions	Gates tested	Test data code
Static load	Dry	Locations 1-9, high weight	RG	SLH
	Dry	Locations 1-9, low weight	RG	SLL
Aimed hammer impacts	Dry	Locations 1-9	PG/RG	AHI1-AHI9
Random hammer impacts	Dry	Random locations	PG/RG	RHI00
	$h = 0.30$ m	Random locations	PG/RG	RHI30
	$h = 0.40$ m	Random locations	PG/RG	RHI40
	$h = 0.50$ m	Random locations	PG/RG	RHI50
	$h = 0.56$ m	Random locations	PG/RG	RHI56
	$h = 0.60$ m	Random locations	PG/RG	RHI60
	$h = 0.63$ m	Random locations	PG/RG	RHI63
Regular wave impacts	$h = 0.56$ m	Wave condition A-E	PG/RG	AS56R-ES56R
	$h = 0.60$ m	Wave condition A-E	PG/RG	AS56R-ES56R
	$h = 0.63$ m	Wave condition B-E	PG/RG	BS56R-ES56R
Irregular wave impacts	$h = 0.56$ m	Wave condition A	PG/RG	AS56I
	$h = 0.60$ m	Wave condition A-E	PG/RG	AS56I-ES56I
	$h = 0.63$ m	Wave condition A	PG/RG	AS56I

predict the dynamic response of the gate. Static load tests allow to investigate possible differences between the outcome of such a finite element model of the in vacuo gate and the actual response of the gates in the experimental setup without the uncertainty involved with the fluid-structure interaction process.

For this purpose, the gate and load cells were not mounted on the concrete block but situated on a flat ground surface. Both a low and high weight (16.5 N and 83.4 N) were placed on nine different locations of the gate. During each test, the weight was placed on the first location for about 15-20 seconds, removed from the gate for about 10 seconds, and then placed on the next location. Figure 5.8 (left) shows an overview of the locations on the gate on which the centre of the weight was placed. Both weights had a square footprint of approximately $4 \cdot 10^{-4} \text{ m}^2$.

The instrumentation for these tests was limited to strain gauges, as there is no fluid involved and the accelerometers are not relevant for static loading. The data acquisition turned out to have failed for the tests on the plain gate. Only the test results for the reinforced gate are therefore available. Figure 5.8 (right) shows an example of the static strain gauge response of the reinforced gate.

5.3.2 HAMMER IMPACT TESTS

Both gates were hit by an hammer in two different test series: aimed hammer impacts and random hammer impacts. The part of the hammer that hits the gate is relatively sharp and stiff. The hammer impact therefore results in an impulse load on the gate of short duration, which is expected to lead to the excitation of a wide range of resonance frequencies of the gate.

For the aimed hammer impact tests the gates are excited with single hammer hits at specific locations on the front of the gate. These locations match the ones of the static load

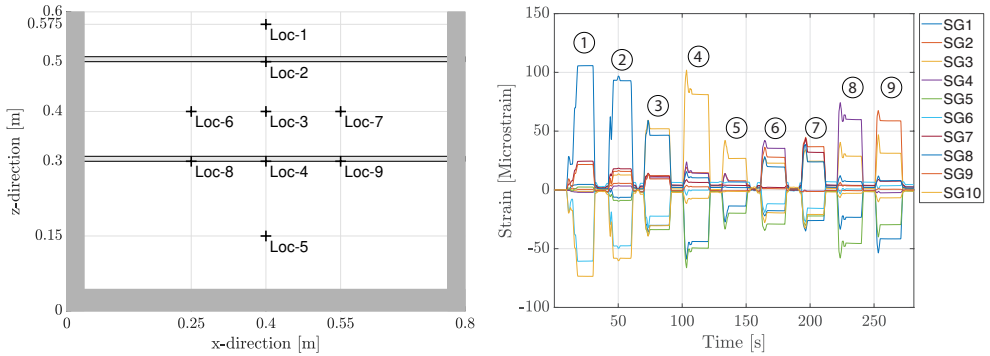


Figure 5.8: Locations of the applied load in the static tests (left) and the strain response of the reinforced gate for the high static loading (right). A moving average filter (of 1.5 s) has been applied to the strain response data. The numbers (1-9) indicating the response peaks correspond to the load locations (Loc1-9).

tests as indicated in Figure 5.8. Each test consists of a few consecutive hits in which the motion of the structure is allowed to full damp in between impacts. These tests have only been performed in the situation without water in the flume. These tests allow to analyse the response of the gate to a dynamic load in the dry situation. Especially the amount of damping in the dry situation is an important parameter that may be deduced from these tests.

For the random hammer impact tests the gate is hit for a period of approximately 40 seconds at random locations over the entire gate. The idea of these tests is to mimic a 'raindrop' type loading, which is the most convenient input for an experimental analysis of the mode shapes and resonance frequencies of the gate. These experiments are executed for the dry situation and for several water levels in the flume. For each situation the random impact test has been repeated about three to five times. There was no space available to hammer the gate from the back. Also in these tests, the gate was therefore hammered from the front through the fluid, accepting some interference of the hammering on the surrounding fluid. In the tests with lower water levels, the gate was also hit above the water line. Section 5.4.1 uses the data of the random hammer impact tests to determine the resonance frequencies of the gates in the experimental setup and compare these to the predictions by the fluid-structure interaction model.

The response of the gate was measured by both strain gauges and accelerometers in both types of hammer tests. The load cells are employed to measure the force on the supports, which may be utilized mainly in the aimed hammer impact tests (together with the response measurements of the gate) to deduce the impulse of the impacts.

5.3.3 WAVE IMPACT TESTS

Both regular and irregular wave conditions have been tested in the wave impact experiments. For these tests all the instrumentation described in Section 5.2.2 was employed. An overview of the regular and irregular wave impact tests is shown in Table 5.2. The wave impacts tests have been carried out at three different water depths: slightly below the overhang ($h = 0.56$ m), at the overhang level ($h = 0.6$ m) and above

the overhang level. Five different wave conditions were tested. Table 5.3 shows the wave height and period for the regular wave tests. The irregular wave tests entailed a standard JONSWAP spectrum ($\gamma = 3.3$) with a peak wave height and peak period corresponding to the conditions of the regular tests. In the regular wave test series wave condition A was not tested at the highest water level as wave impacts do not occur for that combination. For the irregular tests all wave conditions were tested for the water level at the overhang level ($h = 0.6$ m). For the lower and higher water level only wave condition A was tested. Due to the irregular behaviour of the surface elevation in that case wave impacts do occur also for the higher water level.

The regular wave tests have a duration of about 2 to 4 minutes depending on the wave conditions tested, such that test contains approximately 50 waves. This enables to obtain a first indication of the variability of the quantities of interest for regular wave loading. The irregular wave tests more closely match the conditions in design applications. These measurements may be valuable to compare the outcome of probabilistic design approaches. These tests have a longer duration of approximately 20 to 40 minutes. This results in a relatively higher number of wave impacts and therewith facilitates statistical analyses.

Table 5.3: Various target wave conditions of the regular and irregular wave test series. For the irregular test series, the wave height and period refer to the significant wave height and peak period of the JONSWAP spectrum. The type of impact is based on the tests with regular wave impacts on a rigid wall by De Almeida and Hofland (2021) for the situation with the water level at the overhang.

Condition	H or H_{m0}	T or T_p	Impact type (for regular waves and $h = 0.6$ m)
A	0.06 m	1.30 s	Medium peak, intermediate air vibrations
B	0.08 m	1.60 s	Medium peak, reduced air vibrations
C	0.10 m	1.30 s	Medium peak, intermediate air vibrations
D	0.10 m	1.60 s	Medium peak, reduced air vibrations
E	0.10 m	2.00 s	High short peak, reduced air vibrations

The wave conditions tested match the rigid wall experiments performed by De Almeida and Hofland (2021). That study indicates what type of wave impact may be expected for the various conditions in the case of regular waves with water at the overhang level. For the regular wave conditions AS60R and CS60R the fluid pressure measurements showed vibrations after the initial peak as a consequence of an entrapped air pocket, while conditions B, D and E showed this behaviour to a lesser extent. Furthermore, wave condition E showed the sharpest impulsive peak load with a peak duration (τ) of approximately 10 ms. The impact peak duration varied between approximately 35 to 50 ms for the other wave conditions. The irregular wave tests will naturally lead to a mix of wave impacts of various types for each condition, thus some with air entrapment and other without. Section 5.4.2 utilizes the data of the regular wave impact tests to perform a preliminary validation of the fluid-structure interaction model for flexible gates under wave impact loading.

5.4 PRELIMINARY VALIDATION OF THE SEMI-ANALYTICAL MODEL

A preliminary validation of the semi-analytical fluid-structure interaction model developed in the Chapters 2–4 is carried out. Section 5.2.1 presented gate geometries and material properties applied in the finite element model of the in vacuo gates and the resulting mode shapes and frequencies. This modal information is input to the fluid-structure interaction model. The fluid-structure interaction model then determines the dynamic response of the gate immersed in fluid to an excitation force. A (material) damping factor of $\eta = 0.035$ has been used in the time domain analyses, which is discussed further in the following sections. A fluid density (ρ_f) of 1000 kg/m^3 and a fluid sound velocity (c_p) of 1500 m/s were applied in the model.

Two comparisons are made in this section for the preliminary validation. First, the resonance frequencies of the plain gate predicted by the model are compared to an experimental modal analysis of the random hammer impact measurements for various water levels (PG_RHI00, PG_RHI30, PG_RHI40, PG_RHI50 and PG_RHI60). Then, the predicted time response of both the plain gate and reinforced gate to impact loading is compared to the measurements for several regular wave conditions (PG_CS60R, PG_ES60R and RG_ES60R).

5.4.1 PREDICTION OF THE RESONANCE FREQUENCIES OF THE IMMERSED GATE

Helsdingen (2021) performed an experimental modal analysis of the gate designs based on the results of the random hammer impacts and compared these to the prediction by the fluid-structure interaction. The frequency domain decomposition method by Brincker et al. (2001) was applied to find the resonance frequencies of the system. The frequency peaks were manually selected. The modal assurance criterion (MAC)² (Pastor et al., 2012) was then employed to match the mode shapes found experimentally and predicted by the fluid-structure interaction model developed in this thesis. Helsdingen (2021) interpolated the point measurements to mode shapes over the entire gate surface for that purpose. This approach proved to be most reliable for the plain gate and more challenging for the reinforced gate due to the discontinuities in the geometry. As discussed, also some issues were encountered with the glue connections in the reinforced gate. These issues will be discussed based on the results of the wave impact tests. This section therefore focuses on the plain gate.

Figure 5.9 shows the outcome of the comparison for the plain gate. The resonance frequencies predicted by the fluid-structure interaction model have been updated here for some minor adjustments in the material properties and finite element model geometry to exactly match the model employed to predict the other results in this study. These may therefore differ slightly from the ones reported in Helsdingen (2021). Only the resonance frequencies predicted by the fluid-structure interaction model of which the mode shapes match the ones found experimentally ($\text{MAC} \leq 0.75$) are shown in the comparison.

The resonance frequencies of the in vacuo gate are predicted by a finite element model as discussed in Section 5.2.1. The predictions tend to overestimate the resonance frequencies, with differences between the predictions and results from the experimental analysis varying approximately between 4.5% and 7.5% for the first four modes and is

²The MAC value varies from 0 to 1, in which 0 corresponds to the worst possible match and 1 to the best match.

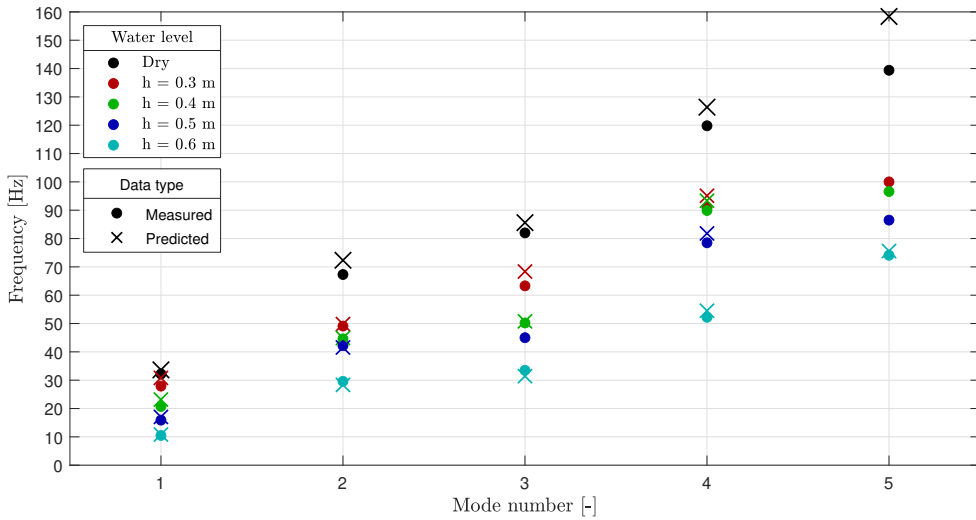


Figure 5.9: Resonance frequencies of the plain gate in the dry situation and for various water levels predicted by the model versus results of the experimental modal analysis by Helsdingen (2021). Only the resonance frequencies predicted by the fluid-structure interaction model of which the mode shapes match to the outcome of the experimental analysis ($MAC \leq 0.75$) are included in the comparison.

about 14% for the fifth mode. For the water levels below the overhang the differences are in the same order varying from 0 to 13%. For the water level at the overhang the relative differences are only 3–6% for the first five modes. This water level is usually most relevant for design as it goes accompanied with the highest wave impact loads. The semi-analytical fluid-structure model can thus predict the resonance frequencies of the plain gate immersed in fluid quite well. This is in line with the comparisons made with finite element models in the previous chapters.

5.4.2 PREDICTION OF THE RESPONSE TO WAVE IMPACT LOADING

The gate response predicted by the fluid-structure interaction model is now compared to the measurements for wave impact loading on the flood gates. In the model predictions, the wave impact is considered as an external excitation force. The model then predicts the change in fluid pressure as a consequence of the motion of the structure.

The wave pressures for the situation with a rigid structure measured in the experiments by De Almeida and Hofland (2021) are employed to predict the response of the gate. Regular wave conditions are considered, such that the wave conditions in these experiments can be matched to those in the rigid wall experiments. Of the most recent experiments by De Almeida and Hofland (2021), only the wave pressure data of the tests with the water level at the overhang ($h = 0.6$ m) is available at this point. The fluid pressure was measured at five locations over the height in the middle of the gate ($x = 0.4$ m) in the rigid wall experiments. A polynomial fit of the fourth order is applied to this data to obtain a continuous pressure distribution over the entire height of the gate. Over the width of the gate this pressure is assumed to be constant. The tests by De Almeida and Hofland (2021)

additionally included several sensors near the edges of the gate ($x = 0.1$ m and $x = 0.7$ m) and in the overhang. This information is not utilized in this analysis but could be used in future analyses to further refine the force input signal.

The predicted response for the wave load measured in the rigid wall experiments (De Almeida and Hofland, 2021) is compared to the response of the elastic gate measured in the present experiments in comparable conditions. This is referred to as the predicted versus the measured response in the remainder of this chapter.

PLAIN GATE RESPONSE TO A WAVE IMPACT WITHOUT AIR ENTRAPMENT

Results are first compared for regular wave test ES60R on the plain gate (PG_ES60R). The model is expected to give the best prediction for this test condition as this particular wave condition goes accompanied with the least amount of entrapped air. The following section will investigate the performance of the model for a wave condition with more air involved. The dynamic response of the gate is predicted for all waves from the start till the end of the test series. The comparison between the predicted response and measurements is made for the waves at approximately 50 s after the start of the tests. At this point, a constant wave load and response pattern has surely settled in. On the other hand, reflecting waves due to possible imperfections in the active reflection compensation by the wave maker, which might alter incoming wave conditions, will not yet have made it back to the gate.

Figure 5.10 shows the comparison of the the strain response in the middle of the gate for multiple consecutive waves. The predicted and measured response are relatively constant over the different waves, on first sight more than the wave impact force (measured in the rigid wall experiments).

Figure 5.11 and Figure 5.12 show the response to a single wave in the same time window in more detail both in terms of strains and accelerations. The depicted locations are expected to capture all relevant modes of the immersed gate. Figure 5.13 shows the acceleration response to the same wave in the frequency domain.

In these analyses, the material damping factor (as defined in Eq.(4.17) in Chapter 4) was set to 0.035 to best match the measurements. For steel the material damping factor generally varies between 0.0001 and 0.01 (Harris, 1991). In the case studies in this thesis a relatively high material damping factor of 0.01 has been applied. This amount of damping is therefore much higher than what could be expected for steel and must originate from other sources. This may include friction in the supports, the presence of air, and energy leaving the system through the wave flume structure. Also the water retaining tapes at the edges of the gate may transfer some energy. Including these sources in the material damping factor in the model is a simplification.

The measurements shows a very similar response at the left and right side of the gate especially in terms of strains (SG15 and SG11). This substantiates the expectation that the wave impact force is uniform over the width of the gate. The developed fluid-structure interaction model somewhat overestimates the strain and accelerations in the gate at some locations. This seems especially be the case for the higher mode vibrations, which is most apparent from the comparison of the measured accelerations. These higher modes also seem to damp more quickly than predicted. This is likely a consequence of the simplified manner of modelling the damping in these predictions. More in depth analyses

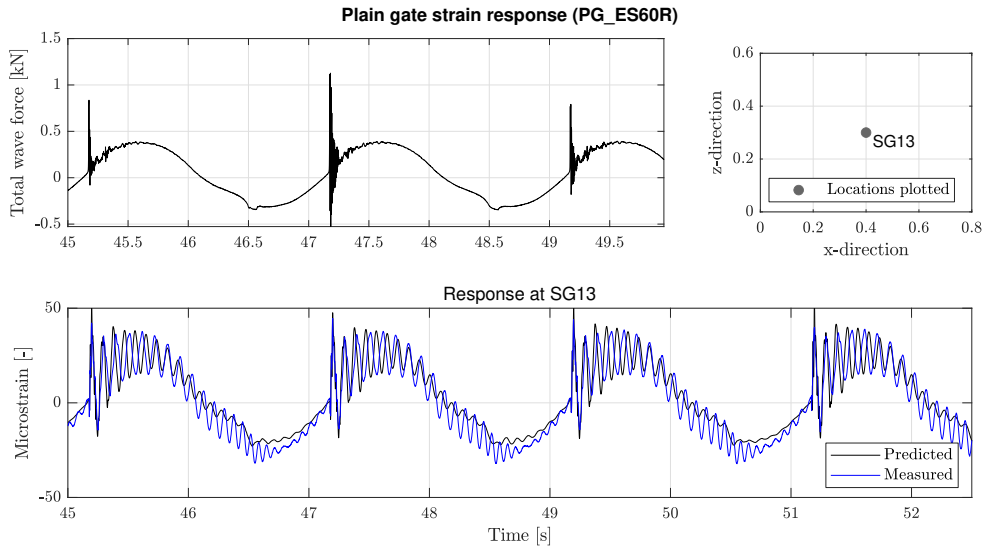


Figure 5.10: Predicted versus measured strain response of the plain gate for multiple consecutive waves of the regular wave test PG_ES60R with a wave height of 0.1 m and wave period of 2 s. The total wave force shown is measured for a rigid wall setup in previous experiments and has been applied as input to the fluid-structure interaction model.

of the measurements are necessary to determine the various types of damping. The aimed hammer impact experiments of the dry gate provide the necessary data to isolate the amount of damping originating from the structure.

Furthermore, from the frequency domain acceleration response shown in Figure 5.13, it is apparent that the first resonance frequency is slightly overestimated and the second underestimated. This may have several explanations. First, the connections are likely not as stiff in every direction as assumed in the finite element model. As discussed, some issues were encountered with the glue connections. The experimental modal analysis in Section 5.4.1 did indicate an overestimation of the resonance frequencies of the in vacuo gate by the finite element model. Also here, the in vacuo aimed hammer tests may provide data to study errors in the modelling of the dynamics of the structure separately from the uncertainties introduced by the fluid-structure interaction the wave impact loading. Second, the wave pressure has been measured by a limited number of pressure sensors in the rigid wall experiments. Some errors will originate from extrapolating these pressures over the entire height of the gate. Third, the fluid-structure interaction model may not capture all phenomena involved in the problem. This may entail detailed interaction processes between the wave impact and the gate or entrained air bubbles in the water column. Also the limited amount of entrapped air under the overhang could be a cause. However, the analysis in the next section suggests that this effect is limited. The pressure sensor data may be analysed to also compare the fluid pressures predicted by the fluid-structure interaction model with the measurements. Further analysis is required to obtain more insight in which of these sources may be dominant. Section 5.5 discusses possible

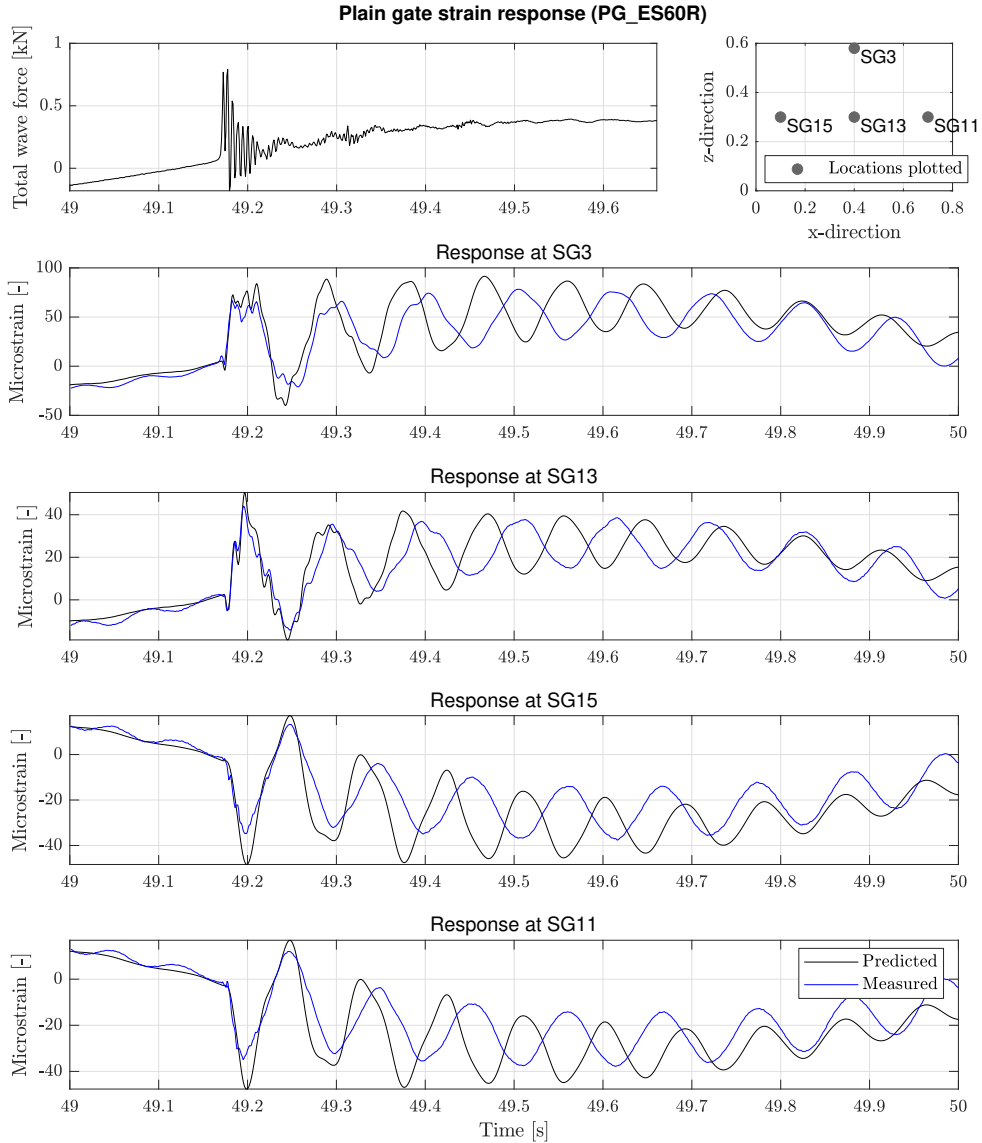


Figure 5.11: Predicted versus measured strain response of the plain gate for a single wave of the regular wave test PG_ES60R.

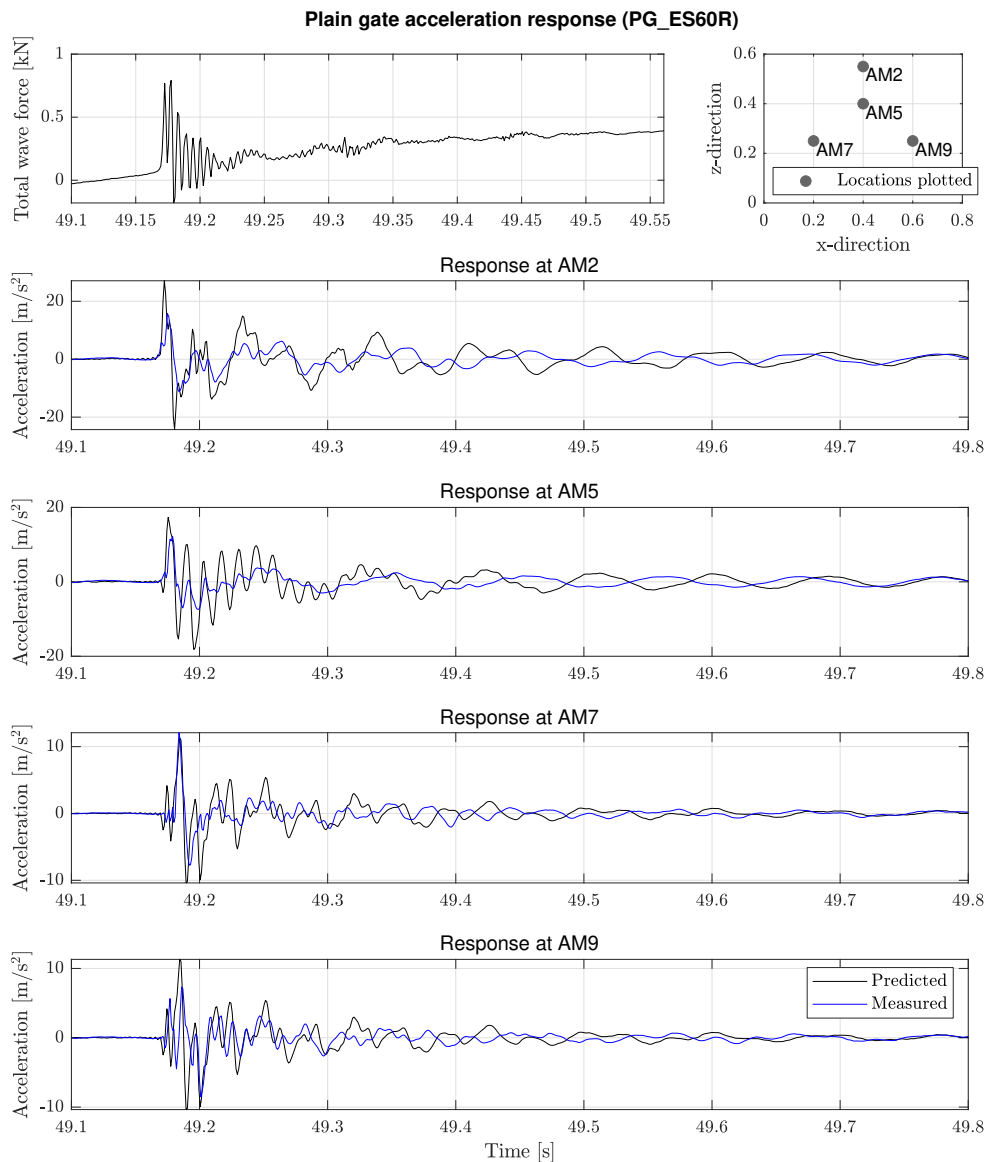


Figure 5.12: Predicted versus measured acceleration response of the plain gate for a single wave of the regular wave test PG_ES60R.

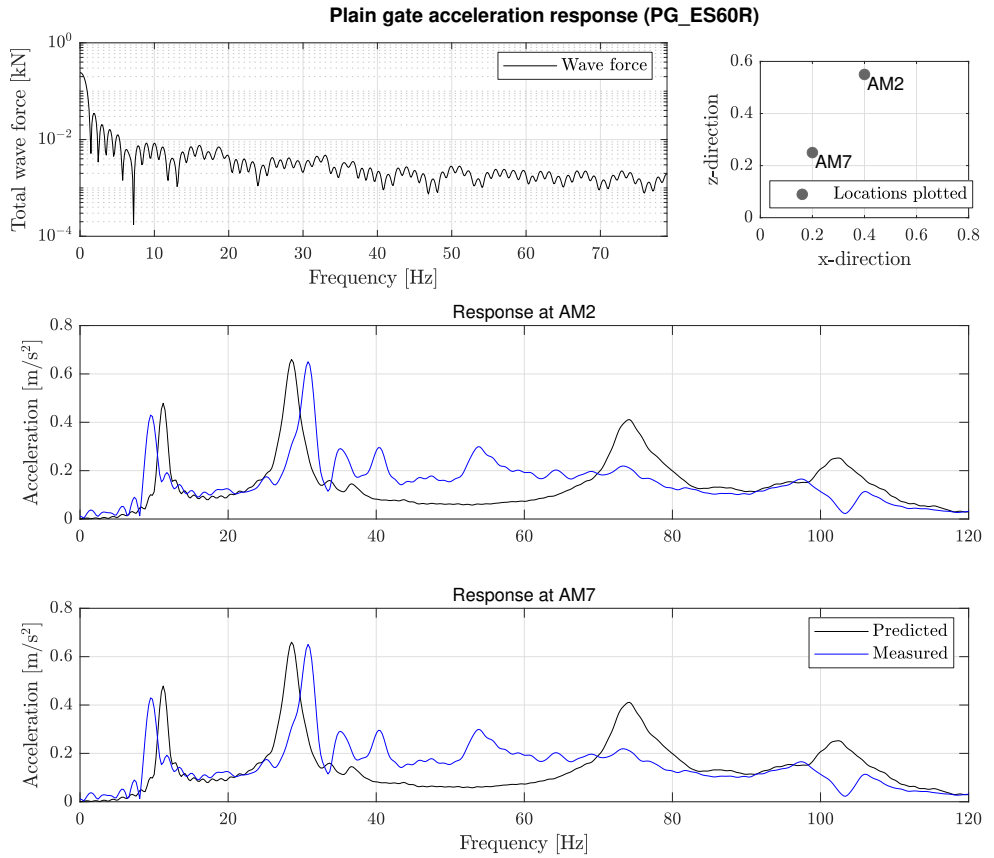


Figure 5.13: Predicted versus measured acceleration response of the plain gate during the time window $t = 49.1$ – 49.8 shown in the frequency domain for regular wave test PG_ES60R

measurement errors and the possibilities for further more detailed analyses.

Overall, even though there are some differences with the measurements, the predictions by the fluid-structure interaction model match the measurements quite well for this wave impact without (much) air entrapment. Within the proposed modelling framework the wave impact is modelled as an external load. For the comparison in this study, the wave pressure measurements from the rigid structure by De Almeida and Hofland (2021) were applied. The results indicate that such an approach can be effective in predicting the dynamic response of flood gates to wave impact loading.

PLAIN GATE RESPONSE TO A WAVE IMPACT WITH AIR ENTRAPMENT

The semi-analytical response model does not specifically include the dynamic response of air. It is assumed implicitly that the effect of entrapped air is sufficiently accounted for in the wave impact force. As was shown by De Almeida and Hofland (2020b,a), the entrapment of air may lead to fluctuations in the wave impact pressures even for the rigid wall setup. To obtain an indication whether this assumption is acceptable, a comparison is made between the model predictions and the measurements for the regular wave conditions CS60R on the plain gate (PG_CS60). For these conditions, a relatively high amount of entrapped air under the overhang is expected based on the rigid wall experiments. Figure 5.14 shows this comparison for the middle point of the gate.

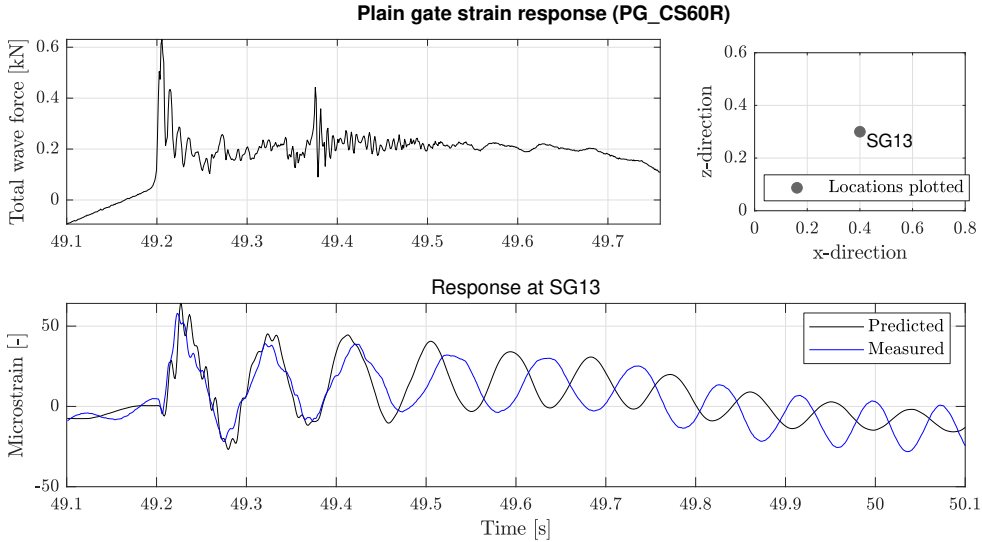


Figure 5.14: Predicted versus measured response of the plain gate for the regular wave conditions PG_CS60R with a wave height of 0.1 and a wave period of 1.3 s.

Also for this type of wave impact the prediction matches the measurements quite well with differences similar to the case of a wave impact without much air entrapment. The entrapment of air under the overhang thus does not seem to have a significant impact on the performance of the model. This indicates that it may indeed be sufficient to capture

this phenomenon in a wave load prediction model based on a rigid schematisation of the structure.

REINFORCED GATE RESPONSE

Figure 5.15 compares the predicted and measured strain response for the reinforced gate for the regular wave condition PG_ES60R. For some locations of the gate the predicted maximum response is in the same order of the measurements, while for others it is much lower. In contrast to the plain gate, the dominant response frequency predicted is much lower than the measured response. Further remarkable is that especially the prediction of the quasi-static strain response to the more slowly varying wave pressures differs strongly from the measurements. Those differences are not caused by errors in the modelling of the fluid-structure interaction, as at those moments the response is not governed by dynamic effects. The differences are most likely the consequence of the failing glue connections between front plate, the reinforced beams and rigid frame. The finite element model then does not accurately represent the behaviour of the reinforced gate. Unfortunately, these measurements therefore do not seem suitable to validate the fluid-structure interaction model. Section 5.5 discusses this topic further.

5.5 DISCUSSION

This section elaborates on the validity of the presented experimental data and the preliminary validation of the semi-analytical fluid-structure interaction model that has been carried out. Several possibilities for further research are discussed.

The approach taken is an extension of the experiments of wave impact on rigid structures by De Almeida et al. (2019); De Almeida and Hofland (2020b, 2021). This allowed for a direct comparison of the wave pressures with the results of that study. Moreover, by applying a proven measurement method the uncertainties in the water level and wave pressure measurements could be minimized. Most encountered issues and possible inaccuracies in the measurements therefore relate to the additional aspects of the flexible gate measurements.

Most importantly, the glue connections of the reinforced gate failed at some point during the wave impact tests. As discussed in Section 5.4.2, the response of the measured reinforced gate to wave impact loading was much more flexible than expected based on the model predictions, also during periods of quasi-static loading. This indicates that the glue connections had already failed during these tests. These measurements therefore do not seem suitable to validate the fluid-structure interaction model. This could be further confirmed by analysing the response of the in vacuo gate in the static load and the aimed hammer tests. Possibly, the glue failure only occurred after a certain point during the wave impact tests, making some of the tests still useful. An analysis of the frequency response of the reinforced gate in the various tests may reveal the point of failure by a sudden change in response. For the plain gate, the glue connections were redone and improved. Even so, also these connections likely involve more flexibility than intended.

The strain gauge and accelerometer measurements of the dynamic gate response are another addition compared to the previous rigid wall experiments. One issue has been the proper alignment of the accelerometers in the direction perpendicular to the surface of the gate. Figure 5.3 showed the accelerometers installed on the gates. As discussed before,

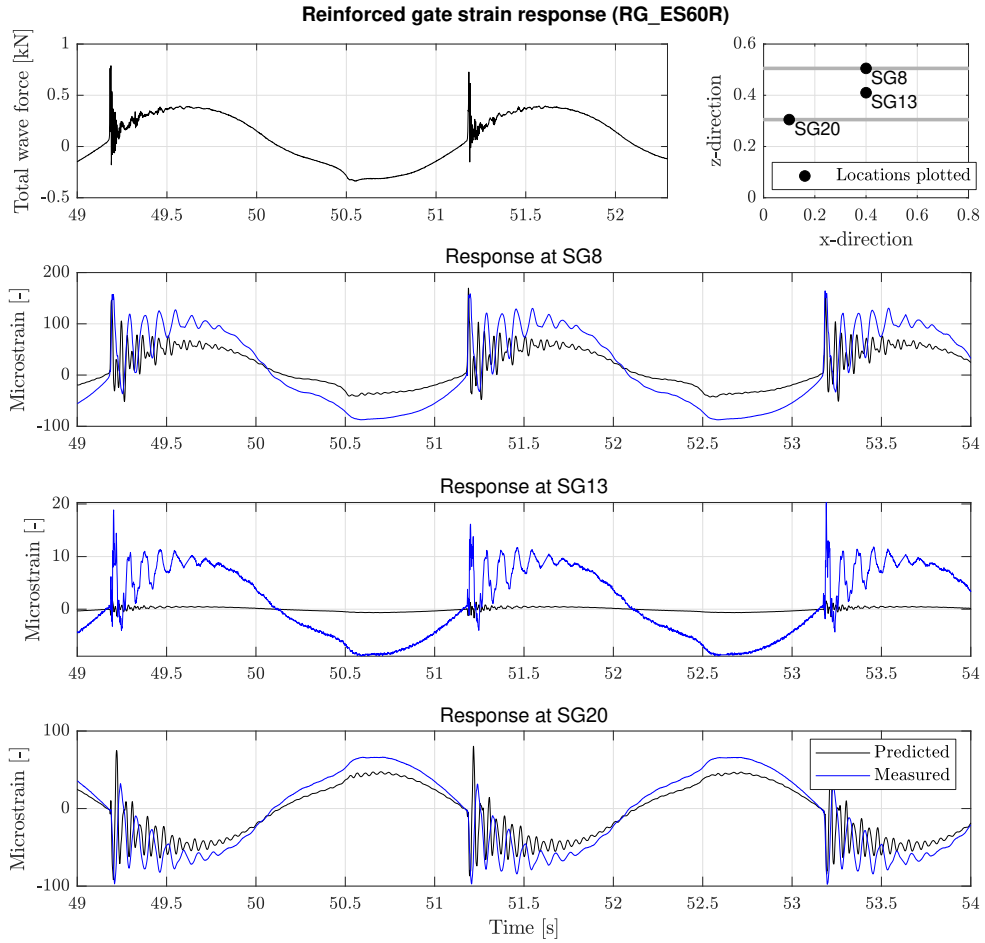


Figure 5.15: Predicted versus measured response for the regular wave conditions RG_ES60R with a wave height of 0.1 m and wave period of 2 s. The total wave force shown is measured for a rigid wall setup in previous experiments and has been applied as input to the fluid-structure interaction model.

a skewness was measured in the vertical direction. Correction factors were applied which were in the order of a few percent. Any possible skewness in the horizontal direction may be in the same order, but was not be measured and could thus not be corrected for. This may lead to some inaccuracy in these measurements.

Also the water retaining tapes may have had some influence on measurements. Most importantly, the slight gap and tape on the top of the gate. This setup may lead to some pressure release at the top of the gate during wave impacts. However, based on the theory by Hofland et al. (2019) the magnitude of this pressure release is expected to be minimal given the limited height of the gap (< 1 mm). The resulting tape-water pocket behind the gate may additionally have resulted in some damping.

The regular wave impact tests were employed to carry out a first validation study of the developed fluid-structure interaction model. Several improvements and additional analyses are possible to perform a more in depth validation of the fluid-structure interaction model. The wave pressure measurements of the rigid wall experiments by De Almeida and Hofland (2021) were used as input to the model. The wave pressures in these experiments were measured by a limited number of five pressure sensors over the height. These measurements were interpolated to obtain the complete pressure field. This relatively coarse interpolation may introduce some inaccuracies in the prediction. The interpolation may be possibly improved by separating the quasi-steady and impulsive wave pressures based on the theory by Chen et al. (2019); De Almeida et al. (2019); Wood and Peregrine (1997) and applying more dedicated interpolation techniques for both of the pressure contributions that match the theoretical bases. However, performing rigid wall tests with a more dense measurement field over the height of the gate would ultimately be preferred. Over the width of the gate, the wave pressures were assumed uniform. Earlier studies (De Almeida et al., 2019; De Almeida and Hofland, 2020b) as well as the response of the gate in the regular wave impact tests indicated this assumption to be valid for the scale of the performed experiments. Furthermore, the wave gauge data may be used to verify that the incoming wave conditions match the ones in the rigid wall tests. Results may be then adjusted for deviations. Differences are expected to be minor however compared to the influence of the flexibility of the gates.

The results of the experiments were used to perform a first validation of the developed semi-analytical response model. An interesting next step would be to validate the entire model routine presented in the later chapters. The wave impact load must then be predicted theoretically based on pressure impulse theory instead of applying the pressures measured in the experiments by De Almeida and Hofland (2021).

The experiments further provide several opportunities to extent the performed validation by utilizing more measurement results. First of all, the in vacuo aimed hammer test results were not yet analysed. These tests can provide insights in the ability of the finite element model to represent the structural behaviour of the in vacuo gate designs. This allows to isolate these inaccuracies from those in the modelling of the fluid-structure interaction in response to wave impact loading. The same applies to the amount of structural damping from sources such as material strain and friction in the supports. The hammer impact tests allow to determine the damping per in vacuo mode shape. Any additional damping in the wave experiments can then be contributed to the presence of the fluid and the wave impacts (and the interface of the fluid with the surrounding

flume structure). The amount of damping is also useful knowledge for practical design problems, in which many of these types of damping will also play a role. It is important to note however, that also other types of damping may be present in practical problems that are not represented here, and vice versa. One example is the interaction with the subsoil.

Furthermore, only the structural response was investigated for the regular wave impact tests, which is of most interest for practical problems. Studying the wave pressures on the gate in combination with the load sensor measurements can give more in depth insight in the dynamic behaviour of the fluid-structure system. A first analysis could focus on comparing predictions by the fluid-structure interaction model with the pressures measured during the wave impact tests. The fluid pressure measurements may also be compared with the results of the rigid wall experiments to study the effect of the flexibility of the gate on the wave load.

Also several test series of irregular wave loading on the gates were performed. These tests more closely match the conditions in design applications. Also for the irregular wave tests, force input is available from the rigid wall experiments by De Almeida and Hofland (2021). However, even though the same spectrum was applied, the waves in those experiments may not match exactly the ones in this study due to the variable nature of the irregular waves and a difference in the distance between the gate and wave maker. A wave by wave comparison of the model predictions to the measurements will not be possible in that case. However, this input may be valuable in a study to validate probabilistic design approaches that focus on the prediction of the ultimate (strain and acceleration) response during these relatively long test series. Such probabilistic approaches are presented in Chapters 7 and 8. Also the wave impact is predicted theoretically in these approaches by employing pressure impulse theory Wood and Peregrine (1997) and De Almeida and Hofland (2020b). The effect of air entrapment is included in the distribution of the impact duration, which were shown to be dependent by Ramkema (1978) and De Almeida and Hofland (2020a,b). It is recommended to carry out an experimental validation of the complete framework in which both the wave impact loads and dynamic structural response are predicted theoretically.

Finally, it is noted that scale effects may play a role in the experiments. The flood gate size and the tested wave heights and periods were not scaled from one particular case. However, the scale is approximately 1:10–1:20 compared to common practical applications. Especially the effect of aeration of the water and air entrapment under the overhang may become more relevant for larger scales. This may also effect the amount of damping in the system. Full scale experiments are therefore necessary to further substantiate that the developed model accurately predicts the dynamic response of flood gate to wave impacts that involve air entrapment.

5.6 CONCLUSION

Experiments of confined wave impacts on flexible gate structures with an overhang have been carried out. These experiments entailed regular and irregular test conditions for various water levels. Additionally, supporting static loading and hammer impact tests were carried out. Two gate designs were tested: a plain gate of which the flexible part consists of a solid steel plate, and a reinforced gate in which reinforcement beams

additionally support the front plate. The experimental approach is an extension of previous experiments of wave impacts on a rigid wall. This allows a direct comparison with the results of those studies, isolating the effect of the flexibility of the structure. It has been shown that based on the implemented experimental approach it is possible to successfully investigate the dynamic response of a flexible gate under wave impact conditions.

A preliminary validation of the developed fluid-structure interaction model was performed. The first few resonance frequencies of the gate in fluid predicted by the model were within 3–6% of the experimental results for the generally governing water level at the overhang. Compared to the models commonly applied in design, the developed model thus is able to accurately predict the higher resonance frequencies of the immersed gate. The predicted response to wave impact loading was compared the measurements in the regular wave impact tests. The aim of this validation was to obtain an indication whether most of the relevant physical phenomena that govern the response of flood gates to wave impacts are covered in the developed model. One of the main assumptions of the developed modelling framework is that the wave impact may be applied as an external load. The design approaches presented later in this thesis apply a combination of linear wave and pressure impulse theory (Cooker and Peregrine, 1995; Wood and Peregrine, 1997; De Almeida and Hofland, 2020b) to predict these wave pressures. In the validation study, the force input was based on previous experiments of confined wave impacts on a rigid vertical wall with overhang. Some differences between the predictions and measurements were found regarding the dominant response frequencies and the magnitude and damping of the higher mode response. However, overall the predictions showed good agreement with the measurement results, providing a first verification that modelling the wave impact as an external force is acceptable.

The validation study further showed no reduction in accuracy of the predictions for wave impacts with air entrapment under the overhang. This indicates that it is possible to account for the presence of some air in the prediction of the wave load instead of explicitly modelling it as a domain in the fluid-structure interaction response model.

The model predictions best matched the measurements for a structural damping factor of $\eta = 0.035$. Although applied as structural damping in the model, this amount of damping is higher than would be expected based on material damping alone and must thus originate from other sources such as friction in the supports and the loss of energy through the surrounding flume structure. This provides some indication of the amount of damping for these type of phenomena, although more research is recommended to be able to better predict the amount of damping from various sources for practical applications.

The experiments additionally resulted in a valuable dataset, made publicly available for research on the 4TU repository (Tieleman et al., 2022a, [link](#)), that can be used to further study wave impacts on flexible structures. It is recommended to utilize this data to for instance study the effect of phenomena such as air entrapment and air entrainment on the response of the fluid-structure system in more detail. The irregular wave tests closely match realistic conditions and can for example be used to further validate the probabilistic design approaches presented in this thesis.

6

**EFFECT OF
COMPRESSIBILITY AND
SURFACE WAVES ON
THE HYDRODYNAMIC
PRESSURES**

A fluid-structure interaction model has been developed to predict vibrations of flood gates immersed in fluid. The fluid-structure interaction is implicitly solved in the developed model approach and includes both the effect of surface waves and compressibility of the fluid. Within existing design approaches, hydrodynamic coefficients are usually applied to determine the first resonance frequency of the structure in fluid. The estimation of these hydrodynamic coefficients generally does not include the effect of surface waves and compressibility. This chapter therefore investigates the relevance of these effects on the hydrodynamic response. Hydrodynamic coefficients are then presented that include these effects for several common cases.

Section 6.1 provides a further introduction into the topic. Section 6.2 gives an overview of the considered geometry and provides the basic solution for the fluid response. Section 6.3 then investigates the effect of surface waves and compressibility on the hydrodynamic response for a horizontally vibration rigid gate. Section 6.4 addresses the situation of a flexible gate. Section 6.5 discusses the conclusions of this chapter.

6.1 INTRODUCTION

In engineering practice, simplified methods are usually applied to capture the fluid-structure interaction process accompanied with the dynamic behaviour of flood gates immersed in water. Most common is to represent the structure as a system of finite number of degrees of freedom including the effect of the hydrodynamic pressure as an added mass, stiffness and damping to the system. Alternatively, one may apply the so-called non-dimensional added virtual mass incremental (NAVMI) factor to estimate the resonance frequencies of the gate immersed in fluid.

Multiple studies have analysed the effect of the hydrodynamic pressure in various situations in such a way that it becomes suitable for engineering applications. Amabili et al. (1996) have determined the change in the resonance frequencies of an annular plate due to the presence of a fluid in terms of the NAVMI factor. Amabili and Kwak (1996) have performed similar studies for circular and rectangular plates, in which the fluid is present in a half space. Furthermore, the fluid is considered incompressible and no free water surface is present. The method employed to obtain the NAVMI factors assumes that the mode shapes of the plate in fluid are the same as those of the plate in-vacuo (assumed modes approach). In Kolkman and Jongeling (2007a) the added mass is presented for a horizontally vibrating rigid gate based on the assumption of an incompressible fluid without considering the effect of surface waves. In Kolkman (1988) a general numerical scheme is presented to determine the added mass based on these assumptions.

Flood gates are often located in discharge sluices where they are in opened position during normal conditions and retain the water during storm events. This situation differs from the previously mentioned studies as the fluid is confined by the sluice structure and a free surface is present which may affect the hydrodynamic pressures. Furthermore, wave impacts are often one of the key excitation mechanisms for flood gates. For such impacts of short duration, compressibility of the fluid may be of some significance.

This chapter is based on the publication "Effect of compressibility and surface waves on the hydrodynamic pressures for a vertical flood gate" in the proceedings of the Twenty-ninth (2019) International Ocean and Polar Engineering Conference (Tieleman et al., 2019a). Some changes have been introduced to make the text consistent with the other chapters of the thesis.

In this study, the hydrodynamic pressures are investigated for the above described situation. The effect of compressibility and surface waves on the added mass is first investigated for a horizontally vibrating rigid gate and compared to the results of Kolkman and Jongeling (2007a). Ranges in terms of water depths and excitation frequencies are identified for which these effects should be considered to avoid significant errors, so that it is known in which cases simplified numerical schemes like in Kolkman (1988) can be employed. Subsequently, the hydrodynamic pressure is analysed for the case of a flexible gate of various boundary conditions. It is shown that the derived ranges are generally applicable. The obtained values for the hydrodynamic pressure are directly applicable to engineering applications, for example by including these in a finite element model of the structure in vacuo.

6.2 MODEL GEOMETRY AND THEORETICAL DESCRIPTION

The hydrodynamic pressures are studied for a vibrating flood gate situated in a discharge sluice. The discharge sluice is assumed infinitely long. Water is present at one side of the gate with a water level equal to the height of the gate. An overview of this situation is shown in Figure 6.1.

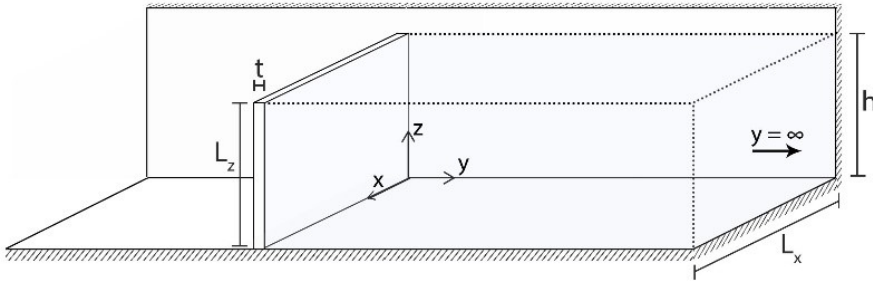


Figure 6.1: Three-dimensional overview of a flood gate situated in an infinitely long discharge sluice with water at one side

The fluid is described as a compressible potential flow with a surface boundary condition that accounts for the generation of surface waves. The equation of motion and boundary conditions for the fluid domain are:

$$\nabla^2 \phi(x, y, z, t) - \frac{1}{c_p^2} \frac{\partial^2 \phi(x, y, z, t)}{\partial t^2} = 0 \quad (6.1)$$

$$\frac{\partial^2 \phi(x, y, z, t)}{\partial t^2} + g \frac{\partial \phi(x, y, z, t)}{\partial z} = 0 \quad (\text{at } z = h) \quad (6.2)$$

$$\frac{\partial \phi(x, y, z, t)}{\partial z} = 0 \quad (\text{at } z = 0) \quad (6.3)$$

$$\frac{\partial \phi(x, y, z, t)}{\partial x} = 0 \quad (\text{at } x = 0 \text{ and } x = L_x) \quad (6.4)$$

$$\frac{\partial \phi(x, y, z, t)}{\partial y} = \frac{\partial w(x, z, t)}{\partial z} \quad (\text{at } y = 0) \quad (6.5)$$

in which ∇ is the Nabla operator, $\phi(x, y, z)$ is the velocity potential, c_p is the sound velocity in water, g is the gravitational acceleration, w is the deflection of the gate normal to the surface, h is the water level in the sluice and L_x is the sluice width. Additional to the equations above, the radiation condition at $y = \infty$ should always be satisfied. The fluid pressure p_f follows from:

$$p_f(x, y, z, t) = -\rho_f \frac{\partial \phi(x, z, y, t)}{\partial t} \quad (6.6)$$

in which ρ_f is the fluid density. In Tieleman (2016) and Tieleman et al. (2019b), it was shown that the amplitude of the fluid pressure in the frequency domain \tilde{p}_f acting on the gate can be described analytically by:

$$\tilde{p}_f = i\omega\rho_f \sum_{p=1}^{\infty} \sum_{r=1}^{\infty} \frac{Q_{pr}}{k_{y,pr}\Delta_{pr}} \Phi_{pr}(x, z) \quad (6.7)$$

with:

$$Q_{pr} = \iint_S W \Phi_{pr} dx dz \quad (6.8)$$

$$\Phi_{pr}(x, z) = \cos(k_{x,p}x) \cos(k_{z,r}z) \quad (6.9)$$

$$\Delta_{pr} = \iint_S \Phi_{pr}^2 dx dz \quad (6.10)$$

$$k_{x,p} = \frac{(p-1)\pi}{L_x} \quad (\text{with } p = 1, 2, \dots, \infty) \quad (6.11)$$

$$\omega^2 = -gk_{z,r} \tan(k_{z,r}h) \quad (\text{with } r = 1, 2, \dots, \infty) \quad (6.12)$$

$$k_{y,pr} = \pm \sqrt{k_f^2 - k_{x,p}^2 - k_{z,r}^2} \quad (6.13)$$

$$k_f^2 = \omega^2 / c_p^2 \quad (6.14)$$

in which $k_{x,p}$, $k_{y,pr}$ and $k_{z,r}$ are the wave numbers in each direction, ω is the radial vibration frequency, W is the vibration shape of the gate. Furthermore, for $y > 0$, a decaying field representing the evanescent waves along the y-direction is satisfied only when $\text{Im}(k_{y,pr}) \leq 0$ while the radiation condition at infinity requires generally that $\text{Re}(k_{y,pr}) \geq 0$.

The total added mass M_f can be deduced from the amplitude of the hydrodynamic pressure in Eq.(6.7) by:

$$M_f = \frac{\text{Re}(\iint_S \tilde{p}_f'(y=0) dx dz)}{-\omega^2} \quad (6.15)$$

The dimensionless added mass coefficient C_m is then defined as:

$$C_m = \frac{M_f}{\rho_f L_x h^2} \quad (6.16)$$

The total added damping C_f follows from:

$$C_f = \frac{\text{Im}(\iint_S \tilde{p}_f'(y=0) dx dz)}{i\omega} \quad (6.17)$$

The added damping is made dimensionless in different ways depending on the cause of damping, which will be discussed in next section.

6.3 HYDRODYNAMIC PRESSURES FOR A HORIZONTALLY VIBRATING GATE

The hydrodynamic pressures are first studied for the case of a gate being rigid and vibrating horizontally as shown in Figure 6.2. To determine the hydrodynamic pressure in this case, a rigid body motion is assumed, i.e. $W=1$ in Eq.(8).

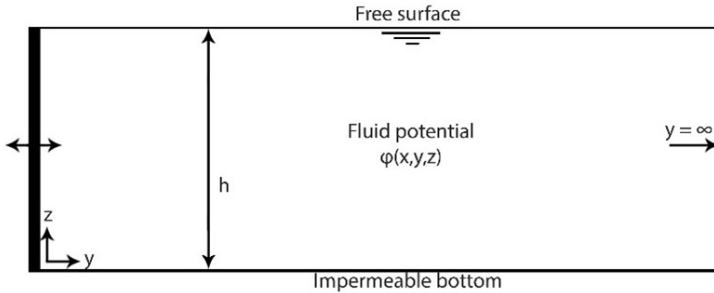


Figure 6.2: Schematic side view of a horizontally vibrating rigid gate with fluid at one side

In Kolkman and Jongeling (2007a) it is shown that for this problem in case of an incompressible fluid and without the effect of surface waves, the dimensionless added mass coefficient C_m defined in Eq.(16) is equal to 0.54. The added mass is in this case independent of the excitation frequency. Furthermore, for an incompressible fluid and excluding the effect of surface waves no added damping will be present.

Whether the solution of Kolkman and Jongeling (2007a) is applicable and thus the effect of compressibility and the generation of free surface waves may be neglected when determining the hydrodynamic pressures, is expected to depend on the involved excitation frequencies and water depths. In the following sections, the dimensionless added mass coefficient is investigated including one or both effects. Subsequently, the results are compared with the solution of Kolkman and Jongeling (2007a). Based on this comparison, ranges are defined for which the effect of compressibility and surface waves can be classified as important.

6.3.1 EFFECT OF SURFACE WAVES

For the purpose of studying independently the effect of surface waves on the hydrodynamic response, the fluid is first considered incompressible. The same solution technique applies, as summarised in Eqs.(7)-(14), by setting $k_f^2 = 0$. This practically implies an infinitely large bulk modulus K for the fluid (related by $c_p = \sqrt{K/\rho_f}$).

In Figure 6.3 the dimensionless added mass and damping is compared to the value given by Kolkman and Jongeling (2007a) as a function $\omega^2 h/g$. As can be seen, the added mass is influenced significantly by surface waves for low values $\omega^2 h/g$. Allowing an error of 5% in the estimation of the total added mass while neglecting the effect of surface waves, the following limit values are obtained for which surface waves have a significant effect and,

thus, cannot be neglected:

$$\omega < 6.7 \sqrt{g/h} \quad \text{or} \quad f < 1.1 \sqrt{g/h} \quad (6.18)$$

The presence of surface waves also leads to added damping as energy is extracted from the system when these propagate away from the structure. Approximately the same limit applies for added damping as for the effect on added mass. The dimensionless coefficient for damping resulting from surface waves C_{cs} is defined for this purpose as:

$$C_{cs} = \frac{C_f}{\rho_f L_x h \sqrt{gh}} \quad (6.19)$$

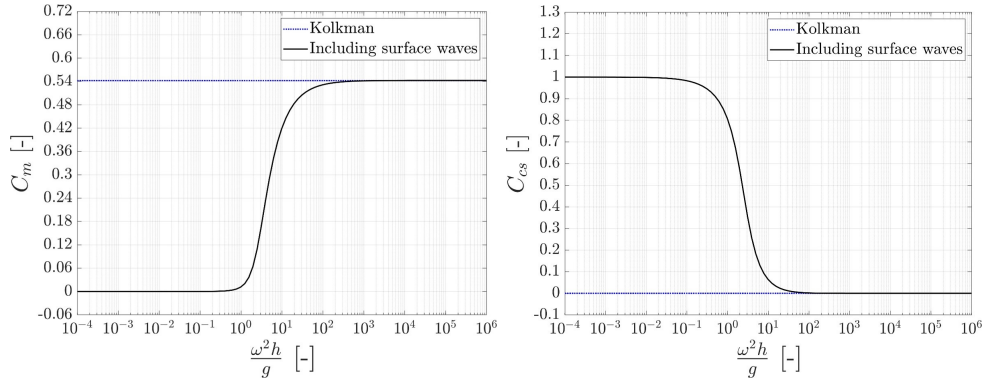


Figure 6.3: Dimensionless added mass coefficient C_m and added damping coefficient C_{cs} with and without surface waves and excluding compressibility

6.3.2 EFFECT OF COMPRESSIBILITY

To study the effect of compressibility on the hydrodynamic response independently, the fluid is now considered compressible while excluding the effect of surface waves. In this case a pressure release boundary condition applies and Eq.(6.13) changes to:

$$k_{z,r} = (2r - 1)\pi/2h \quad (\text{with } r = 1, 2, \dots, \infty) \quad (6.20)$$

while the rest of the solution given by Eqs.(6.7)-(6.14) remains unaltered. In Figure 6.4 the dimensionless added mass and damping are presented for the compressible fluid and compared to the value of Kolkman as a function of the vibration frequency, which is normalised by the fundamental compressible resonance frequency of the fluid ($\omega_1 = \pi c_p/2h$).

Allowing an error of 5% in the estimation of the total added mass while neglecting the effect of compressibility of the fluid, the following limit values can be determined for which compressibility has a significant effect and, thus, cannot be neglected:

$$\omega > 0.32 \pi c_p/2h \quad \text{or} \quad f > 0.32 c_p/4h \quad (6.21)$$

Also due to compressibility energy will propagate away from the gate leading to added damping. This effect starts to play a role when $\omega/\omega_1 > 1$. The dimensionless coefficient for damping resulting from compressibility C_{cc} is for this purpose defined as:

$$C_{cc} = \frac{C_f}{\rho_f L_x h c_p} \quad (6.22)$$

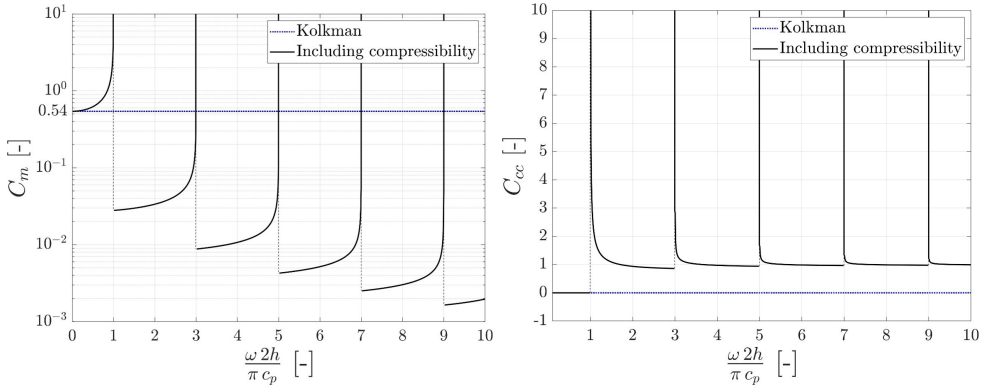


Figure 6.4: Dimensionless added mass coefficient C_m and added damping coefficient C_{cc} with and without compressibility and excluding surface waves

6.3.3 TOTAL ADDED MASS AND DAMPING

Results obtained in the previous sections are now combined. In Figure 6.5 the dimensionless added mass is shown as a function of ω/ω_1 and c_p/\sqrt{gh} for the case in which both compressibility and surface waves are taken into account. The resulting value can be directly applied to determine the added mass for a horizontally vibrating rigid gate. To determine the total added damping acting on the gate the contributions from surface waves and compressibility that follow from Figure 6.3 and Figure 6.4, may be summed as follows:

$$C_f = C_{cs} \rho_f L_x h \sqrt{gh} + C_{cc} \rho_f L_x h c_p \quad (6.23)$$

6.3.4 IMPORTANCE OF COMPRESSIBILITY AND SURFACE WAVES FOR FLOOD GATES

In previous sections the effect of surface waves and compressibility on the hydrodynamic pressures acting on a vertical flood gate was investigated. Ranges are determined for the regime in which surface waves and compressibility have a significant effect on the hydrodynamic pressures. These ranges are summarized in Table 6.1. Although the hydrodynamic pressures will differ for a flexible gate due to the change in vibration shape, the ranges themselves are expected to be representable for other situations as well. This hypothesis is verified in the next section.

Regarding $g = 9.81 \text{ m/s}^2$ and $c_p = 1500 \text{ m/s}$ as constants, the water depth and frequency are the relevant variables in these ranges. Water levels adjacent to typical flood

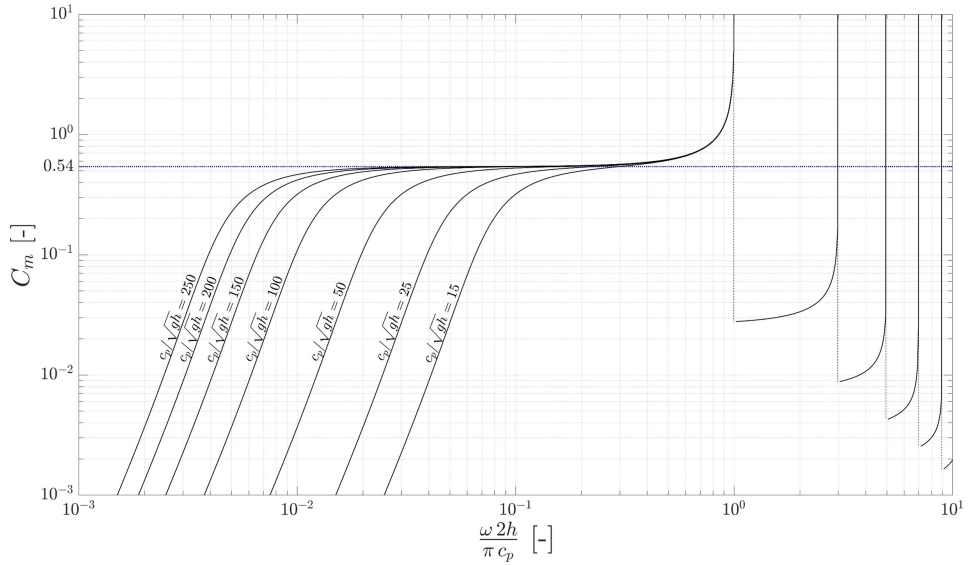


Figure 6.5: Dimensionless added mass coefficient C_m for a horizontally vibrating rigid gate in an infinitely long discharge sluice with the effect of compressibility and surface waves (black) and without (blue dotted)

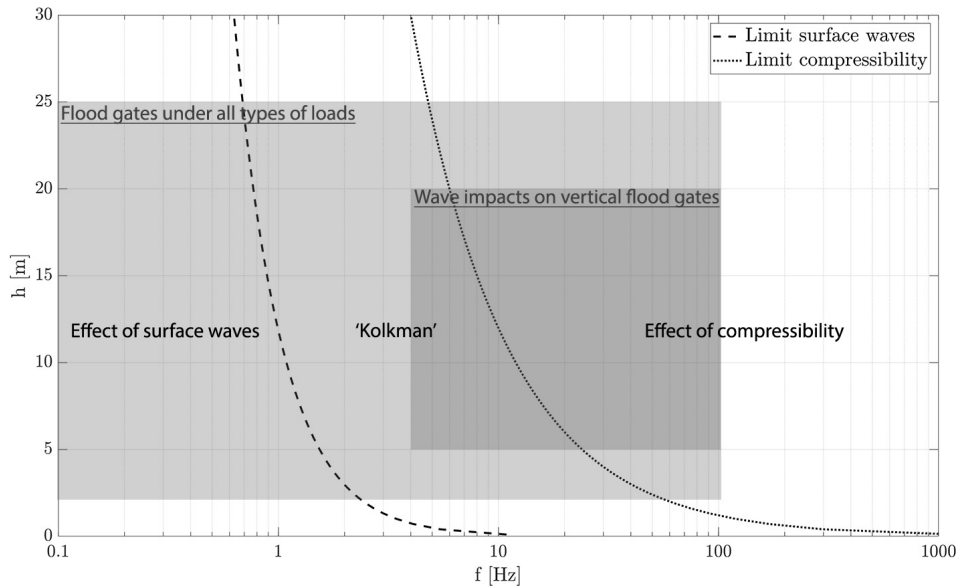


Figure 6.6: Dimensionless added mass coefficient C_m for a horizontally vibrating rigid gate in an infinitely long discharge sluice with the effect of compressibility and surface waves (black) and without (blue dotted)

Table 6.1: Frequency ranges for which the effect of surface waves and compressibility on the hydrodynamic pressures is significant. Numeric examples are based on $g = 9.81 \text{ m/s}^2$ and $c_p = 1500 \text{ m/s}$

Water level	Effect of surface waves	Effect of compressibility
h	$f < 1.1\sqrt{g/h}$	$f > 0.32c_p/4h$
2 m	$f < 2.4 \text{ Hz}$	$f > 60 \text{ Hz}$
10 m	$f < 1.1 \text{ Hz}$	$f > 12 \text{ Hz}$
20 m	$f < 0.8 \text{ Hz}$	$f > 6.0 \text{ Hz}$

gates generally vary from 2 to 25 m. Excitation frequencies relevant for the dynamic response of these gates approximately vary from 0.05 Hz resulting from regular waves to 100 Hz from wave impacts with short peak durations. In Figure 6.6 the derived applicability ranges are shown together with these typical values. It can be seen that for flood gates both surface waves and compressibility are of importance. However, for the typical vertical flood gates under wave impact loading studied in this thesis only compressibility plays a role.

6.3.5 EFFECT OF FLUID-AIR MIXTURE ON THE EFFECT OF COMPRESSIBILITY

In particular situations, the occurrence of wave impacts on a flood gate may lead to the presence of air in the surrounding fluid. Bullock et al. (2001) have investigated the compressibility of water-air mixtures and show that even minor ratios of air over water volume can lead to a significant increase in compressibility of the mixture compared to water. This will lead to a reduction of the sound velocity in the fluid and affects for which frequencies compressibility influences the hydrodynamic pressure acting on the flood gate.

Bullock et al. (2001) have determined the bulk modulus K as a function the voids ratio $\beta = V_a / (V_w + V_a)$, in which V_a is the volume of air and V_w the volume of water. The velocity of sound in the fluid follows from the bulk modulus through $c_p = \sqrt{K/\rho_f}$. Based on these relations, the frequency ranges are investigated for which compressibility changes may influence the added mass due to the presence of air-bubbles in the fluid. For this purpose, the void ratio is considered the same throughout the entire fluid domain in the case of an infinitely long sluice. Table 6.2 summarises the results of the analysis.

In practice, when air-bubbles are generated in the fluid due to wave impacts at the flood gate, those will only be present at the vicinity of the the gate. For such cases, the effect of air-water mixture on the compressibility limit may be smaller. However, based on Table 2 it can be concluded that compressibility may influence the magnitude of the hydrodynamic pressures at much lower excitation frequencies when air is present in the fluid.

6.4 ADDED MASS FOR VARIOUS FLEXIBLE GATES

The added mass is now studied for the first resonance shape of a flexible gate considering various boundary conditions. The same geometry is considered as in previous sections, shown in Figure 6.1.

Table 6.2: Numerical examples of how the frequency limit for the effect of compressibility could change due the presence of air in water. The bulk modulus is based on freshwater at a gauge pressure of 20 kPa and adiabatic compression as presented in Bullock et al. (2001)

β [%]	K [MPa]	c_p [m/s]	$h = 2$ [m]	$h = 10$ [m]	$h = 20$ [m]
0.00	2050	1432	$f > 57$ Hz	$f > 11.5$ Hz	$f > 5.7$ Hz
0.01	929	964	$f > 39$ Hz	$f > 7.7$ Hz	$f > 3.9$ Hz
0.10	157	396	$f > 16$ Hz	$f > 3.2$ Hz	$f > 1.6$ Hz
1.00	16.8	130	$f > 5.2$ Hz	$f > 1.0$ Hz	$f > 0.52$ Hz
10.00	1.70	41	$f > 1.6$ Hz	$f > 0.3$ Hz	$f > 0.16$ Hz
100.00	0.170	13	$f > 0.5$ Hz	$f > 0.1$ Hz	$f > 0.05$ Hz

6.4.1 FUNDAMENTAL MODE SHAPES OF VARIOUS FLEXIBLE GATES

The gate structure is represented by a thin plate, that is linearly elastic, homogeneous and isotropic. The effect of rotational inertia and shear deformation is neglected. The free linear bending vibrations of the in vacuo plate can then be described as follows (Leissa, 1969):

$$\rho_s w_{tt} + D[w_{xxxx} + 2w_{xxzz} + w_{zzzz}] = 0 \quad (6.24)$$

in which $w(x,z)$ denotes the displacement of the mid-surface of the plate, ρ_s is the distributed mass per unit of area and D is the flexural rigidity of the gate. Several boundary conditions of that are common for flood gates are considered: simply supported on all four sides (SSSS), simply supported on three sides and free on the top (SSSF), and simply supported at the sides and free on the top and bottom (SSFF). These boundary conditions can be formulated as follows:

$$\text{SSSS:} \quad w(0, z) = m_{xx}(0, z) = w(L_x, z) = m_{xx}(L_x, z) = 0 \quad (6.25)$$

$$w(x, 0) = m_{zz}(x, 0) = w(x, L_z) = m_{zz}(x, L_z) = 0 \quad (6.26)$$

$$\text{SSSF:} \quad w(0, z) = m_{xx}(0, z) = w(L_x, z) = m_{xx}(L_x, z) = 0 \quad (6.27)$$

$$w(x, 0) = m_{zz}(x, 0) = v_z(x, L_z) = m_{zz}(x, L_z) = 0 \quad (6.28)$$

$$\text{SSFF:} \quad w(0, z) = m_{xx}(0, z) = w(L_x, z) = m_{xx}(L_x, z) = 0 \quad (6.29)$$

$$v_{zy}(x, 0) = m_{zz}(x, 0) = v_{zy}(x, L_z) = m_{zz}(x, L_z) = 0 \quad (6.30)$$

in which m_{xx} and m_{zz} are the bending moments in x - and z -direction respectively, and v_{zy} the effective Kelvin-Kirchoff shear force in z -direction. Applying these boundary conditions together with Eq.(6.24), the first mode shape of the in vacuo plate is derived for each set of conditions. The results are shown in Figure 6.7.

6.4.2 ADDED MASS ACTING ON FLEXIBLE GATES

The hydrodynamic pressure at the gate corresponding to each of these mode shapes can be investigated by employing the derived system of equations (6.7)-(6.14). These equations were solved by the semi-analytical model of Tieleman et al. (2019b), which was verified against a FE/CFD model. The water level in the discharge sluice is chosen equal to the height of the gate. The first in vacuo mode shape W of each gate is applied in Eq.(6.9).

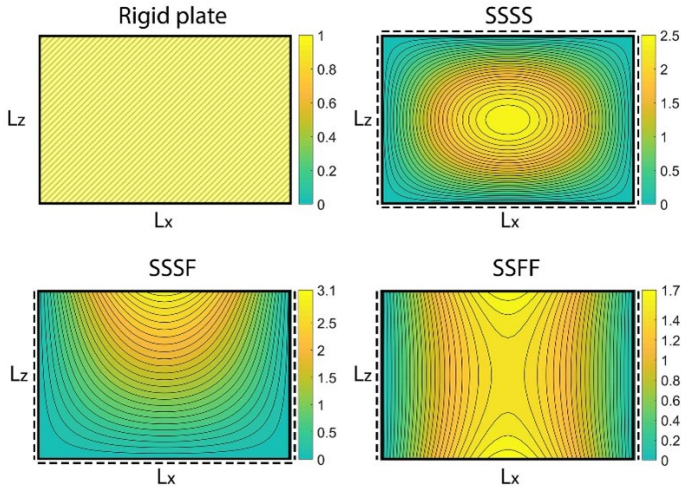


Figure 6.7: First resonance shape of the in-vacuo plate for various boundary conditions

Employing this approach to determine the hydrodynamic pressures corresponding to the first resonance frequency of the immersed plate, assumes the resonance shape of the immersed gate is equal to that of the in-vacuo gate and thus does not change due to the acting hydrodynamic pressures. Kwak (1996) showed this assumption is generally valid for the first few mode shapes of the plate. To ensure a valid comparison between the total hydrodynamic pressure acting on each mode shape, these are normalized such that the average amplitude is equal to one like the unit displacement of the rigid gate. The resulting maximum amplitude of each mode shape is shown in Figure 6.7.

In Figure 6.8 the total added mass is shown for each of the considered flexible gates as a function of the dimensionless frequency ω/ω_1 and a given value of $c_p/\sqrt{gh} = 150$. For comparison, the results of the previous section for the horizontally vibrating rigid gate are included. The added mass for the flexible gates is relatively close to the case of a rigid gate. The SSSF gate has the lowest added mass, which can be explained from the first resonance shape of this gate having the highest deflection amplitudes at the top of the gate (and adjacent water column), where hydrodynamic pressures are relatively low. In Table 6.3, the added mass coefficient for each gate configuration is presented for the case without compressibility and surface waves. These values are directly applicable to cases with governing excitation frequencies and water depths within the previously presented ranges.

Table 6.3: Added mass coefficient for the considered gate boundary conditions excluding the effect of compressibility and surface waves

Gate type:	Rigid plate	SSSS	SSSF	SSFF
C_m [-]:	0.54	0.57	0.44	0.54

The relative effect of compressibility and surface waves on the acting hydrodynamic pressures shows to be mainly dependent on the characteristics of the fluid domain and is therefore approximately the same for each of the considered gates. The ranges derived in previous section for the effect of compressibility and surface waves could therefore be considered generally applicable for the examined sluice geometry.

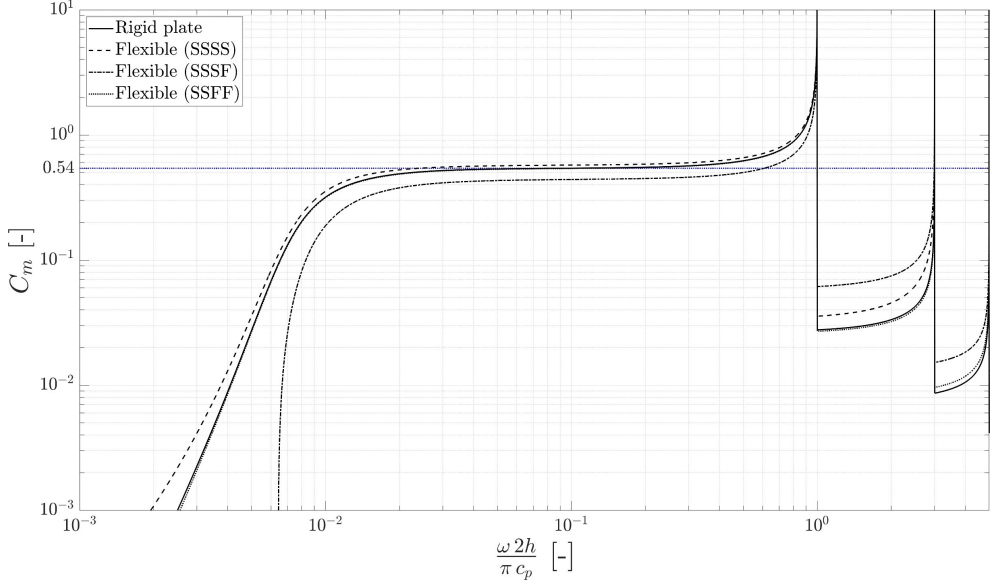


Figure 6.8: Dimensionless added mass coefficient C_m for the first mode shape of flexible gates with different boundary conditions (rigid and horizontally translating, SSSS, SSSF, SSFF) in an infinitely long discharge sluice including the effect of compressibility and surface waves for $c_p / \sqrt{gh} = 150$. The blue line shows the added mass coefficient for the rigid translating gate in case compressibility and surface waves are neglected.

6.5 CONCLUSION

The hydrodynamic pressures on a flood gate in a discharge sluice were investigated. An exact solution for the hydrodynamic pressures given a certain gate vibration shape was presented that includes the effect of surface waves and compressibility. The results of this solution were compared to existing solutions that neglect these effects in order to investigate their applicability. Ranges were derived in terms of excitation frequencies and water depths for which compressibility and surface waves have a significant effect on the magnitude of the hydrodynamic pressure. Results show that for typical flood gate dimensions and excitation frequencies both effects can be of importance. Furthermore, a first numerical study showed that a small amount air present in the surrounding fluid can result in compressibility effects already at much lower excitation frequencies. Dimensionless values for the added mass are presented including the effect of compressibility and surface waves for gates of various boundary conditions. Results are applicable to engineering applications, for example, by including these in a finite element model of the in vacuo gate.



7

ASSESSING THE SAFETY OF FLOOD GATES SUBJECTED TO WAVE IMPACTS

A computationally efficient semi-analytical model to predict the dynamic behaviour of flood gates immersed in water has been developed and validated in the first part of this thesis (Chapters 2-4). A design approach is now presented to utilize this model in reliability analyses to explicitly predict the probability of failure of a flood gate subjected to wave impact loads during an entire design storm. The failure mechanism considered in this design method is exceedance of the critical yield strength, in contrast to the next chapter that presents a design method for fatigue of flood gates.

The structure of this chapter is as follows. Section 7.1 introduces the probabilistic approach. The general model approach is discussed in Section 7.2. Subsequently, in Section 7.3 the approach to predict the wave impact loads is presented. These loads are processed in a probabilistic framework explained in Section 7.4. In Section 7.5 the developed models and probabilistic approach are applied to the case of the Afsluitdijk. Finally, results are discussed in Section 7.6.

7.1 INTRODUCTION

Flood gates can be subjected to millions of wave impacts during their lifetime. Bagnold (1939) observed that peak pressures accompanied with wave impacts show large variations for waves with very similar characteristics, and are therefore difficult to predict theoretically. A probabilistic approach allows to take into account the uncertainty accompanied with wave impacts. However, probabilistic evaluations require a large number of simulations of the wave impact loads and dynamic analyses. Within the field of hydraulic engineering, simulating the dynamic response of a structure for a large number of waves or storms is therefore not part of design practice. Within the fields of marine and offshore engineering these type of simulations are more common, for example, when evaluating fatigue damage of offshore platforms (Zheng et al., 2020) or workability of dredging or pipe laying operations (Van der Wal and de Boer, 2004). However, simulating the full dynamic behaviour of a ship or structure for a multitude of storms to analyse the reliability of the system is also rare within these fields.

The main reason for this is the large computational effort required to accurately predict the dynamic behaviour of a ship or structure including the involved fluid-structure interaction for a large number of loads. For a finite element model the time-domain computational task required for a probabilistic evaluation of the dynamic behaviour of a flood gate would be almost an impossible mission given the large number of required simulations (Zheng et al., 2020). Less computationally demanding methods are applied within engineering practice. Most common is a simplified quasi-static approach in which a dynamic amplification factor (DAF) is applied to account for the effect of vibrations. This factor is derived from a single degree of freedom representation of the structure (Kolkman and Jongeling, 2007b; Cuomo, 2007). The fluid-structure interaction is not explicitly solved but included by using hydrodynamic coefficients. Such an approach lacks the precision to capture the three-dimensional vibration behaviour of a gate-fluid system (Tieleman et al., 2018). Vertical breakwaters such as caissons subjected to wave impacts

This chapter is based on parts of the publication "A fluid-structure interaction model for assessing the safety of flood gate vibrations due to wave impacts" in *Coastal Engineering* (Tieleman et al., 2021). Some changes have been introduced to make the text consistent with the other chapters of the thesis.

are most commonly designed on the basis of guidelines developed by Goda (2000). To the authors' knowledge no similar guideline exists for the design of vertical flood gates, such as sluice and sea lock gates. Hence, the formulas of Goda are also used for hydraulic structures at the moment (Technische Adviescommissie voor de Waterkeringen, 2003; US Army Corps of Engineers, 2002).

The semi-analytical model developed in the first chapters of this thesis overcomes the above mentioned challenges. It allows to perform probabilistic evaluations regarding the dynamic response of flood gates, or most other hydraulic structures, without compromising on the accuracy of the physical modelling. A design approach is therefore presented in this chapter to employ the developed semi-analytical model in reliability analyses. The situation of a flood gate with an overhang is regarded. Violent wave impacts can occur in this situation when reflected standing waves hit the bottom of the overhang in front of the gate. This has for instance been an important design consideration for the renovation of the Afsluitdijk. A Monte Carlo type analysis is performed simulating a large number of storms. Within this approach, the dynamic response of the flood gate is predicted for the consecutive wave impact loads within each storm. In this way, the conditional failure probability of a certain flood gate design can be explicitly determined for given design storm conditions. This is valuable for flood safety assessments, since as part of flood defence systems, gates are required to withstand impact loads with a certain maximum failure probability Vrijling (2001).

The wave impact loads are predicted for a given wave spectrum by employing two separate theories for the quasi-steady and impulsive part of the wave load (De Almeida and Hofland, 2020b; Chen et al., 2019). Pressure-impulse theory by Wood and Peregrine (1997) is applied to predict the impulsive wave load. Experiments have shown that the pressure-impulse is more constant and therefore has a better predictability than the peak pressures (Hofland et al., 2011; Bagnold, 1939; De Almeida and Hofland, 2020b). Pressure-impulse theory was recently developed further and validated by Chen et al. (2019) and De Almeida and Hofland (2020b). Employing this method to determine the wave impact loads may avoid the necessity for time-consuming and costly physical experiments. This theory is applied for the first time in combination with a model to predict the dynamic response of flood gates, in which the latter model includes the responsive fluid pressures resulting from the motion of the gate. The design approach is applied to a case study inspired by the situation of the Afsluitdijk (Rijkswaterstaat, 2020a) to demonstrate its purpose.

7.2 MODELLING FRAMEWORK FOR A PROBABILISTIC APPROACH

The design approach developed in this chapter consists of several model components. The wave impact force on the gate and the gate-fluid response are predicted by separate analytical and semi-analytical models. These models are based on the same geometry, but different schematisations for the structure and fluid. In this way, the strong points of the different models can be exploited. Figure 7.1 gives an overview of the key components within this approach.

The semi-analytical gate-fluid response model developed in the first chapters of this thesis is employed to predict the response of the flood gate. The case study in this chapter

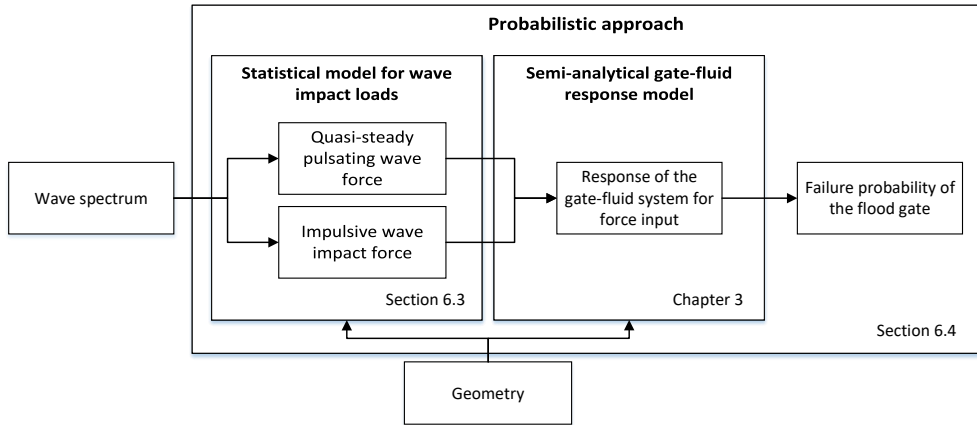


Figure 7.1: Overview of the model approach used in this study

is consistent with the representation in Chapter 3, in which the gate is represented as a thin plate. However, also the more advanced representation of a flood gate design as presented in Chapter 4 could be used within this approach. For the reader's convenience a side view of the model geometry is repeated here in Figure 7.2.

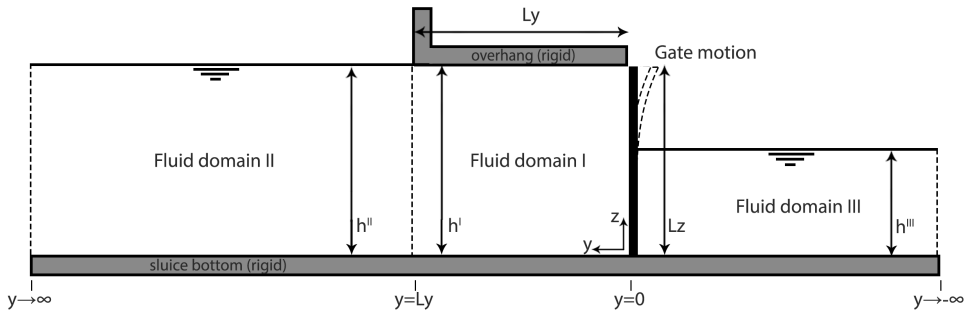


Figure 7.2: Side view of the model domain consisting of a flexible gate and three fluid regions

In the semi-analytical gate-fluid response model, the wave impact force is modelled as an external excitation force on the gate. This force is assumed not to be altered by the dynamic response of the gate-fluid system. The interaction between the movement of the gate and the pressures in the surrounding fluid is solved within this semi-analytical model using a mode matching technique. The fluid pressures caused by the flexibility of the gate are predicted as part of the response model and effectively superposed on these external wave pressures. In Tieleman et al. (2019b), this was discussed to be a reasonable assumption for the time scales involved in impulsive wave impacts. The validity of this assumption is being tested further in experiments in ongoing studies.

The external wave impact pressures must then be predicted based on a model schematisation with a rigid gate. The wave spectrum is translated to an incoming wave

field based on linear wave theory using a statistical approach and translated to wave impact loads. For this purpose, two sub-models are employed. The quasi-steady wave pressure as a result of the pulsating waves is predicted using linear wave theory. Pressure-impulse theory is then applied to predict the wave pressures resulting from the impacts on the overhang. The result is a time-series of the total wave pressure on the gate for a given storm event, which is input to the semi-analytical response model.

The wave impact and response models are both based on linear structural and fluid dynamics in this study. This approach is expected to give a reasonable accuracy for the situation of a gate subjected by wave impact on an overhanging structure, which can be described better by a linear description than for example impacts due to wave breaking. However, it is still the subject of ongoing experiments to what extent phenomena such as the presence of large air pockets under the overhang during the wave impact air entrapment may introduce non-linear behaviour. Because the wave impact pressure is input to the response model in the chosen model approach, one can apply more sophisticated non-linear wave impact models relatively straightforwardly. For the application of the response model to situations with strong non-linear behaviour, the Galerkin method could be employed to approximate the solution.

Both model components are combined within a probabilistic routine in which the response of the gate is predicted for a large number of simulated storms. It is demonstrated how this routine may be employed to determine a conditional failure probability of a flood gate for a given design storm. Section 7.4 further explains this routine after presenting the statistical approach for wave impacts loads in the coming section.

7.3 STATISTICAL APPROACH FOR WAVE IMPACT LOADS

A novel approach is employed to predict the impact load on the gate for a certain incoming wave spectrum. Within this approach different theories are applied for the quasi-steady pulsating and the impulsive impact part of the wave load resulting in a time-series of the total wave pressure on the gate. This approach was recently validated by De Almeida and Hofland (2020b) and Chen et al. (2019). Using this method to determine the wave impact loads, the necessity for time-consuming and costly physical experiments can be avoided. Section 7.3.1 explains the translation from design spectrum to surface elevation. Subsequently, Section 7.3.2 presents the method to predict the wave load.

7.3.1 DESIGN WAVE SPECTRUM

In engineering practice, the most common design spectrum for wind sea in oceanic waters is the JONSWAP spectrum Hasselmann (1973). A one-directional JONSWAP spectrum is considered with a design significant wave height H_{m0} . Linear wave theory is used to obtain the surface elevation and quasi-steady wave force from the wave spectrum. The presented approach does allow for more advanced wave theories, as the developed gate-fluid response model does not require linear force input. Although the response model is based on linear dynamics, any external force may be applied on the gate after applying a Fourier transform to translate it to the frequency-domain. However, in this study linear wave theory is deemed sufficient for the purpose of demonstrating the probabilistic

framework. De Almeida and Hofland (2020b) have also shown that linear wave theory can be used to predict wave impact loads with reasonable accuracy for a wave steepness up to 2%. Based on the random-phase/amplitude model, a random realisation is generated for the time-record of the surface elevation as the sum of a large number of statistically independent harmonic wave components for the entire duration of the design storm speak (T_{storm}) Holthuijsen (2007):

$$\eta_w(y, t) = \sum_{i=1}^N a_i \cos(\omega_{w,i} t + k_{w,i} y + \phi_i) \quad (7.1)$$

in which η_w is the surface elevation due to the incoming wave field, a_i is the amplitude of the respective harmonic, following from the energy in the spectrum at the given frequency (band) and $k_{w,i}$ is the wave number following from the dispersion equation for free surface waves $\omega_{w,i}^2 = k_{w,i} g \tanh(k_{w,i} h^I)$. The random phase shift ϕ_i is uniformly distributed between 0 and 2π .

The surface elevation at the end of the overhang follows from:

$$\eta_{\text{overhang}}(t) = (1 + c_r) \eta_w(y = L_y, t) \quad (7.2)$$

in which c_r is the reflection coefficient. For the considered geometry with vertical wall, experiments show the reflection coefficient to be close to 1.0. (De Almeida and Hofland, 2020b)

7.3.2 WAVE IMPACT LOADS

Different theories are applied to predict the quasi-steady pulsating and the impulsive part of the wave load for the obtained surface elevation field, such that the total wave pressure is the summation of both (De Almeida and Hofland, 2020b; Chen et al., 2019):

$$f_w(x, y = 0, z, t) = f_{qs}(x, y = 0, z, t) + f_{im}(x, y = 0, z, t) \quad (7.3)$$

in which f_w is the total wave pressure, f_{qs} is the quasi-steady wave pressure and f_{im} the impulsive wave impact pressure. Regarding the developed gate-fluid model, only the wave pressure at the surface of the gate (at $y = 0$) is needed. Figure 7.3 shows the separation in these two parts for a typical wave force time series and Figure 7.4 shows examples of the pressure and pressure impulse distribution on the gate at given moments in time.

As discussed in Section 7.2, the wave force is predicted for the situation with a rigid gate, as the gate fluid model includes the responsive fluid pressures resulting from the motion of the gate. For typical flood gates, the impulsive impact part of the wave load is expected to cause gate vibrations, while the quasi-steady part of the wave load gives a quasi-static structural response. However, this distinction in structural response is not necessary in the presented approach, as the total wave load can be applied in the gate-fluid model.

PULSATING WAVE FORCE

For the quasi-steady pulsating wave pressure linear wave theory is applied, which was recently validated for waves with a steepness up to 3.8% in De Almeida et al. (2019).

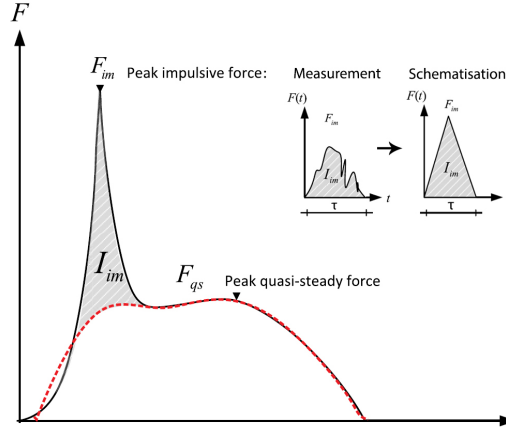


Figure 7.3: Typical time history of a wave impact on a (vertical) wall with or without a horizontal overhang split into a quasi-steady and impulsive part. The impulsive load is schematised as a triangular peak with duration τ . (Chen et al., 2019)

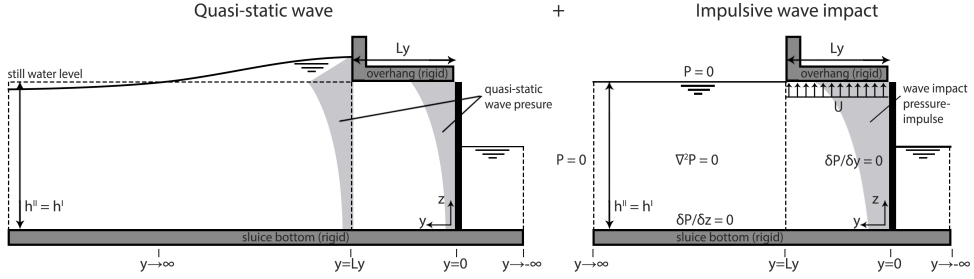


Figure 7.4: Example of the quasi-steady wave pressure (at the moment of a wave top) and the wave impact pressure impulse (at the moment of impact) acting on the gate

The pressure over the vertical up to the bottom of the overhang (i.e. over height of the gate) acting on the surface of the gate is based on the surface elevation at the end of the overhang. This premise is valid for a short overhang length (L_y) in comparison to the deep water wave length (L_0), i.e. $L_y/L_0 < 0.1$ De Almeida and Hofland (2020b). The pressure at the gate then following from the well known relation:

$$f_{qs}(z, t) = \sum_{i=1}^N \rho_f^I g \eta_{\text{overhang},i}(t) \frac{\cosh(k_{w,i}z)}{\cosh(k_{w,i}h)} \quad (7.4)$$

in which $\eta_{\text{overhang},i}$ is the surface elevation at the end of the overhang caused by each individual random harmonic wave and its reflection ($\eta_{\text{overhang},i}(t) = (1+c_r)\eta_{w,i}(y=L_y, t)$). Higher-order theories or Goda could be used for waves of higher steepness.

IMPULSIVE WAVE FORCE

At the moment the upward moving wave surface hits the bottom of the overhang a violent wave impact occurs De Almeida and Hofland (2020b). Bagnold (1939) observed that peak pressures accompanied with wave impacts show large variations for waves with very similar characteristics, and are therefore difficult to predict theoretically. However, as discussed in Hofland et al. (2011) and De Almeida and Hofland (2020b), the pressure-impulse shows to be remarkably constant and therefore has a better predictability. For this reason, pressure-impulse theory is applied in this study to predict the impulsive wave force. The pressure-impulse is defined as the area enclosed by the pressure-time curve:

$$P_{im}(x, z) = \int_{t_0}^{t_1} f_{im}(x, z, t) dt \quad (7.5)$$

in which t_0 and t_1 define the start and end of the impact peak respectively.

The theory of Wood and Peregrine (1997) is used to predict the pressure impulse field as a function of the upward wave velocity at the moment of impact. This method assumes governing equations as shown in Figure 7.4, excluding both the effect of free surface waves and compressibility on the pressure impulse. The dimensionless pressure impulse of a wave impact is defined as: (De Almeida and Hofland, 2020b):

$$\bar{P}(x, y = 0, z) = \frac{P(x, y = 0, z)}{\beta_{im} \rho_f^I U_w L_y} \quad (7.6)$$

in which P is the pressure impulse, β_{im} a correction factor for the effect of compressibility of entrapped air, U_w is the impact velocity of the considered wave impact and L_y is the overhang length. The pressure impulse is regarded at the surface of the flood gate ($y = 0$).

The dimensionless pressure impulse field (i.e. \bar{P}) is constant for a given geometry and can be solved numerically. For the situation with an overhang, Wood and Peregrine (1997) have also presented a semi-analytical solution. Figure 7.5 shows the dimensionless pressure impulse shape over the depth for several water depth over overhang length ratios. For a further description of this solution, is referred to Wood and Peregrine (1997) and De Almeida and Hofland (2020b).

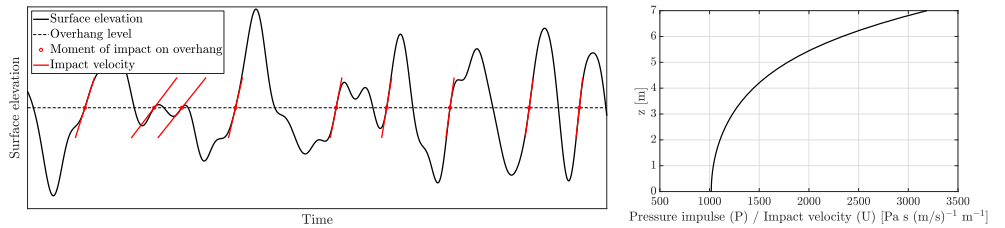


Figure 7.5: Example of surface elevation with the moments and velocities of impact (left) and the pressure impulse shape on the gate for varying overhang lengths (right)

The magnitude of the pressure impulse depends on the impact velocity of each wave impact, which is the upward velocity of the waterfront at the moment of impact. This velocity is known for each impact from the surface elevation time-series. For this purpose,

again the surface elevation at the end of the overhang is considered. The moment of impact happens at each upward crossing of the level of the overhang bottom, i.e. when $h^I + \eta_{\text{overhang}}(t) = L_z$.

In experiments De Almeida and Hofland (2020b,a) have shown that the compressibility of entrapped air between the overhang and standing wave crest may in practice lead to larger impact impulses than the analytical solution predicts. For this reason, the correction factor β_{lm} is introduced in Eq.(7.6). Based on experiments, De Almeida and Hofland (2020b) derived a value of 1.17 for this correction factor in the case of short overhang lengths ($L_y/h^I < 1$). Finally, through the impact peak duration τ the pressure impulse field is translated to a triangularly shaped peak time series of the impact pressure, as shown in Figure 7.3. This impulsive pressure is added to the quasi-static pulsating wave pressure resulting in a time-series of the total wave pressure, of which the lower part of Figure 7.11 shows an example.

7.4 PREDICTING THE FAILURE PROBABILITY OF THE GATE

The numerical efficiency of the developed gate-fluid and wave load models makes it possible to perform a large number of simulations. A model approach is presented that can be employed in reliability analyses of flood gates. Starting point of this method is a design storm corresponding to a set of hydraulic conditions with a certain return period. The conditional failure probability of the gate is then quantified explicitly for this design storm. The focus of this study lies on the model routine for the wave impact loads and the dynamic gate-fluid response. Some essential aspects of reliability analyses are therefore omitted. For instance, the uncertainties on the resistance side are not accounted for. These aspects should be included when performing a reliability analysis of a flood gate in practice.

Within the model approach, a Monte Carlo simulation is performed in which the dynamic behaviour of the gate is evaluated for a large number of storm simulations following from the statistically described design wave spectrum. Figure 7.6 shows an overview of the presented probabilistic approach.

The following parameters related to the wave loads are considered stochastically in this approach:

- The phase shift ϕ_i of each surface elevation harmonic is considered uniformly distributed between 0 and 2π in accordance with the well-known random phase/amplitude model as for instance discussed in Holthuijsen (2007).
- The correction factor β_{lm} to account for the variability of the pressure impulse due to the compressibility of entrapped air between the overhang and standing wave crest. The factor is considered normally distributed with a mean $\mu_{\beta_{\text{lm}}} = 1.17$ and standard deviation $\sigma_{\beta_{\text{lm}}} = 0.11$. This distribution has been derived by (De Almeida and Hofland, 2020b) based on experiments dedicated to the specific situation of a gate with overhang.
- The wave impact duration τ for each impulsive wave impact. Measurements (De Almeida and Hofland, 2020b) show that the impact durations of wave impacts on an overhang vary between 10 to 200 ms independent of the wave characteristics such as impact velocity. Based on those results a triangular distribution is proposed with $a = 0.010$ s, $b = 0.105$ s and $c = 0.200$ s.

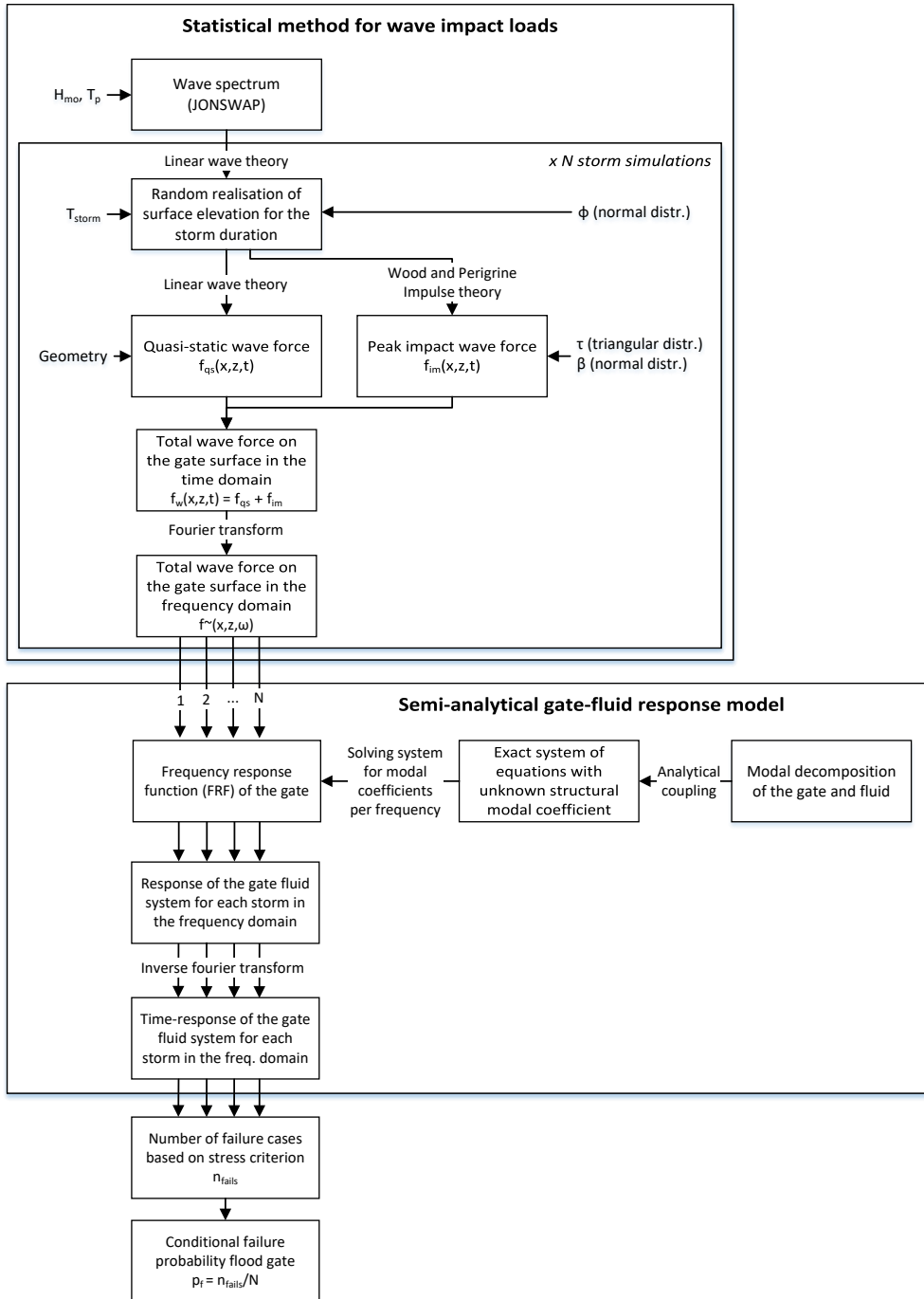


Figure 7.6: Overview of the probabilistic approach for the dynamic response of a gate with overhang to wave impact loads

The scale experiments by De Almeida and Hofland (2020a) indicated a correlation between the correction factor β and the impact duration τ , as both these effects are influenced by the amount of air present under the overhang during a wave impact. However, on larger scales the impact duration is expected to behave differently (Bagnold, 1939). More research is investigate whether there is a correlation between these parameters on realistic scales. Within this approach, these parameters are therefore considered to be independent.

The water levels at both sides of the flood gate are considered to be constant during the duration of the storm. On the sea side, a water level equal to the bottom of the overhang is considered, which leads to the highest wave impact loads. This assumption is therefore expected to lead to a conservative estimate of the failure probability of the flood gate. The distribution of water levels during the course of the design storm can be included straightforwardly within the presented method. Nevertheless, when performing a complete reliability analysis in practice, the complete set of boundary conditions are corresponding probabilities of occurrence should be accounted for.

A Monte Carlo simulation is performed in which a number of realisations N is generated for the time-series of the wave impact pressures for a given design wave spectrum $S(\omega_p)$ and storm duration T_{storm} . The gate-fluid model is employed to determine the response of the flood gate for each storm realisation. The parameters of the responsive gate and fluid model are deterministic in this study.

As a failure criterion, the Von Mises stress is used, which for general plane stress states:

$$\sigma_v = \sqrt{\sigma_{xx}^2 - \sigma_{xx}\sigma_{yy} + \sigma_{yy}^2 + 3\tau_{xy}^2} \leq f_y \quad (7.7)$$

with f_y being the yield strength of the steel material. Exceedance of this limit in any point of the gate is considered as failure, which is considered to be a (strongly) conservative approach. The conditional failure probability of the gate for the design storm and given the properties of the resistance side then follows from:

$$p_f = \frac{n_{\text{fails}}}{N} \quad (7.8)$$

in which p_f is the conditional failure probability of the gate, n_{fails} is the number of simulations in which the gate fails and N is the total number of simulations.

7.5 CASE STUDY OF WAVE IMPACTS AT THE AFSLUITDIJK

The presented semi-analytical gate-fluid model, wave load theory and probabilistic routine are applied to a case study inspired by the situation of the Afsluitdijk. The Afsluitdijk in the Netherlands separates Lake IJssel from the Waddensea. This dam contains two discharge sluice complexes in which a large number of gates regulate the water discharge and protect the hinterland from flooding during a storm event. The coming years the Afsluitdijk is being renovated, which includes the replacement of the flood gates. An impression of a set of gates in one of discharge sluices was shown in Figure 3.1. The flood gate at the Waddensea side is considered in this case.

The flood gate is required to withstand a design storm with a duration of 4 hours that correspond to a set of hydraulic conditions with a certain return period (e.g. 10.000 years).

The maximum conditional failure probability for this design storm may not be larger than 0.1. To quantify the failure probability of the gate, the wave loads and response of the gate are simulated 1000 times for the design storm according to the approach presented in the previous section. When less than 100 of the 1000 simulations lead to structural stresses exceeding the capacity, this means that the maximum failure probability requirement is met. The number of simulations in relation to the accuracy of the estimated failure probability will be discussed further on this section.

In Section 7.5.1 the parameters of the gate and fluid system are introduced and the resulting resonance frequencies are investigated. Section 7.5.2 presents the design storm and the resulting incoming wave field and impact loads. Subsequently, in Section 7.5.3 the dynamic response of the gate fluid system is investigated for a few consecutive wave impacts. Section 7.5.4 presents the probability of failure of the flood gate by means of a Monte Carlo analysis. Finally, Section 7.5.5 discusses the accuracy of this analysis in relation to the number of simulations performed.

7.5.1 GATE-FLUID SYSTEM

Table 7.1 gives an overview of the relevant case parameters regarding the gate-fluid system. The parameters are in accordance with the model description presented in Chapter 3. High water and waves are present at the Waddensea side of the flood gate. At the other side of the gate low water is present. The sluice length at the Waddensea side of the gate is limited compared to the water depth. A much wider second fluid domain is therefore considered. The sluice length at the lake side of the gate is sufficiently long to be considered infinite with respect to the hydrodynamic pressures acting on the gate.

Table 7.1: Gate-fluid system parameters and their value as applied in the case study

Structural parameters	Symbol	Value	Unit	Fluid parameters	Symbol	Value	Unit
Width	L_x	12	m	Width domain I	L_x^I	12	m
Height	L_z	7.5	m	Width domain II	L_x^{II}	60	m
Gate thickness	t	0.22	m	Width domain III	L_x^{III}	12	m
Bending rigidity	D	$1.95 \cdot 10^8$	Nm ²	Water level domain I	h^I	7	m
Distributed mass	ρ_s	345	kg/m ²	Water level domain II	h^{II}	7	m
Modulus of elasticity (steel)	E	$200 \cdot 10^9$	Nm ²	Water level domain III	h^{III}	4	m
Moment of inertia	I	0.00089	m ⁴	Overhang length	L_y	3	m
Poisson's ratio (steel)	ν	0.3	-	Fluid density domain I-III	ρ_f^j	1025	kg/m ³
Yield strength (steel)	f_y	$460 \cdot 10^6$	N/m ²	Fluid sound velocity I-III	c_p^j	1500	m/s
Material damping (steel)	η	0.01	-	Gravitational constant	g	9.81	m/s ²

The approximate resonance frequencies and responses of the gate in vacuo and immersed are obtained by exciting the system by a harmonic load with a range of frequencies. Table 7.2 shows the first ten resonance frequencies of the gate in vacuo and immersed.

These resonance frequencies are all within the range of the peak impact durations, i.e. 10 to 200 ms, and may therefore give a dynamic response. Since in the studied case, the wave impact loads have a constant magnitude over the width of the gate, there will be no response to the modes that are antisymmetric in horizontal direction. For the given

Table 7.2: First ten resonance frequencies of the gate in vacuo and immersed.

Condition	f_1	f_2	f_3	f_4	f_5	f_6	f_7	f_8	f_9	f_{10}
In vacuo [Hz]	11.8	36.7	43.8	72.1	77.5	115.2	116.4	134.6	145.2	173.6
Immersed [Hz]	3.5	13.6	16.3	29.1	32.1	50.0	53.5	64.4	66	69.9

water levels, Figure 7.7 shows the first four shapes of immersed gate resulting from the semi-analytical model that are not antisymmetric.

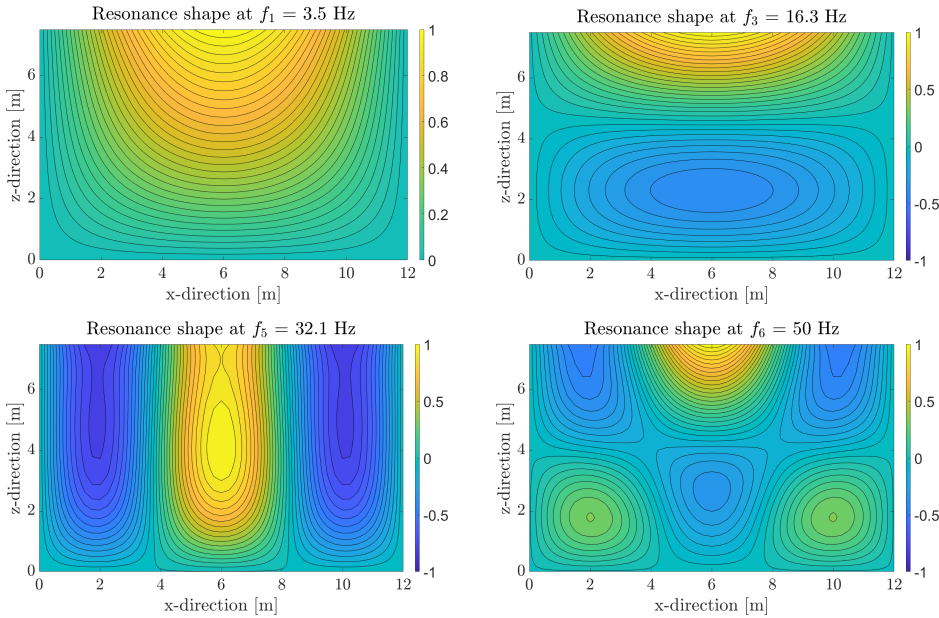


Figure 7.7: The amplitude of the complex valued response $|w|$ of the immersed gate for several resonance frequencies

Figure 7.8 shows the fluid pressure amplitudes for two of the resonance frequencies of the submerged gate. The effect of the boundary condition imposed by the presence of the overhang on the distribution of the fluid pressure can be seen clearly. Furthermore, the fluid pressure shows to be continuous over the interface between fluid domain I and II, satisfying the interface conditions between these two domains.

7.5.2 DESIGN STORM

A design storm with a total duration of four hours is considered in this case study. The water level at the sea side (Waddensea) is at the overhang level for the entire duration, which is the governing water level in terms of wave impact pressures. However, with the presented methods a multivariate probabilistic analysis including water levels and wave heights could be carried out as well. The wave field is incoming from the sea side of the

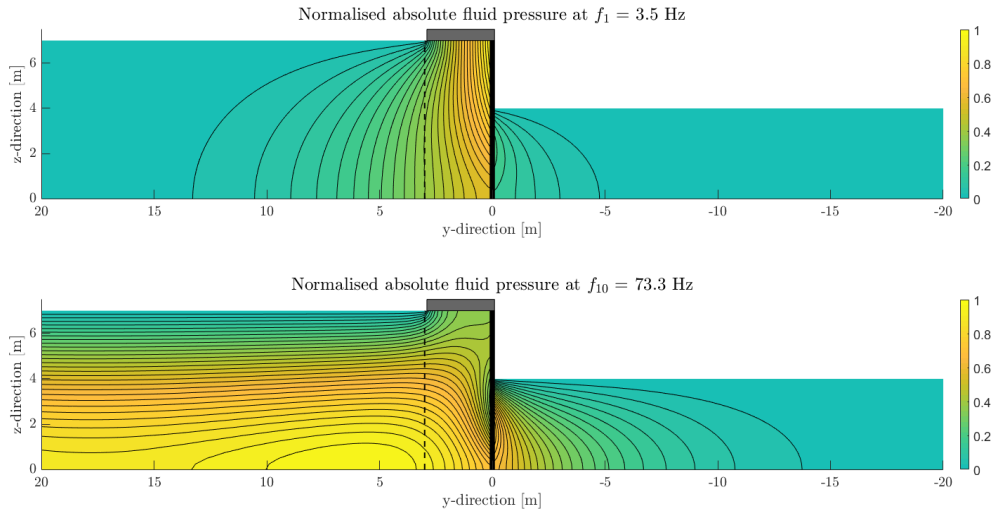


Figure 7.8: Normalised absolute fluid pressure at $x = 4$ m on both sides of the gate for two resonance frequencies of the immersed gate

gate where the high water level is present, and is described by a JONSWAP spectrum with a peak period T_p of 4.5 s and a significant wave H_{m0} of 1.5 m. Table 7.3 gives an overview of the wave impact parameters and their probabilistic distributions as discussed in Sections 7.3 and 7.4.

Table 7.3: Design storm parameters and their distribution and values as applied in the case study

Parameter	Symbol	Distribution	Value (range)	Unit
Water levels	h^I, h^{II}, h^{III}	Deterministic	(See Table 7.1)	
Storm duration	T_{storm}	Deterministic	4	h
Peak period (JONSWAP spectrum)	T_p	Deterministic	4.5	s
Significant wave height (JONSWAP spectrum)	H_{m0}	Deterministic	1.5	m
Reflection coefficient	c_r	Deterministic	0.8	-
Impact peak duration	τ	Triangular	$10 \leq \tau \leq 200$	ms
Surface elevation phase shift (per harmonic i)	ϕ_i	Uniform	$0 \leq \phi \leq 2\pi$	rad
Impulse correction factor	β_{im}	Normal	$\mu_\beta = 1.17, \sigma_\beta = 0.11$	-

The applied spectrum contains relatively steep waves above the limit of 2% for linear theory as mentioned earlier. Higher order wave theory can be applied in design to obtain a more accurate prediction. However, for the purpose of demonstrating the probabilistic framework linear wave theory is deemed sufficient. Moreover, the difference between the free surface velocity predicted by linear and higher order wave theory happens to be minor around the point of the still standing water level, which is considered to be at the overhang level for the entire storm duration in this case study (Tadjbakhsh and Keller, 1960). The impact velocity, which is the governing parameter for the impulsive impact load, is therefore expected to be predicted reasonably by linear wave theory for this case.

As an example, Figure 7.9 on the left hand side shows the wave force distributed over the gate width for a one minute time interval of a certain storm realisation using the parameters of Table 7.1 and 7.3. The impulsive impact peaks can be distinguished clearly and show quite some variability in magnitude. On the right hand side, the magnitude of all 3903 peak impacts that occur within this 4 hour storm simulation are shown.

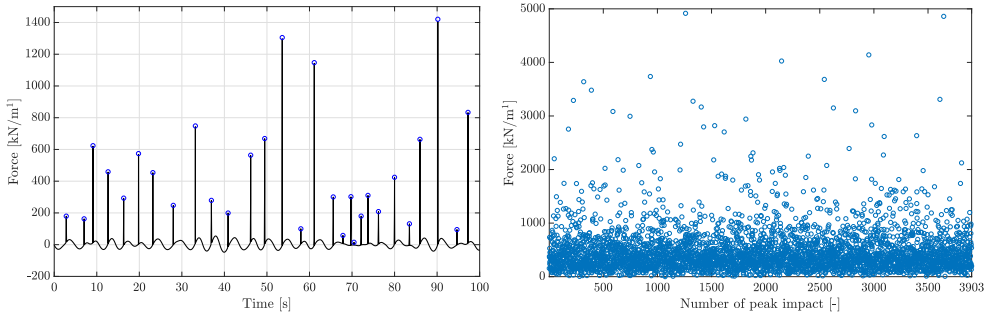


Figure 7.9: Wave force distributed over the gate width for a random one minute storm interval (left) and all peak pressures that occur within the entire 4 hour storm simulation

Figure 7.10 shows the exceedance probability of the maximum wave force distributed over the gate width in a single storm with a duration of 4 hours based on the 1000 storm simulations performed in this case study. The maximum wave force found in the performed simulations is approximately 11000 kN/m.

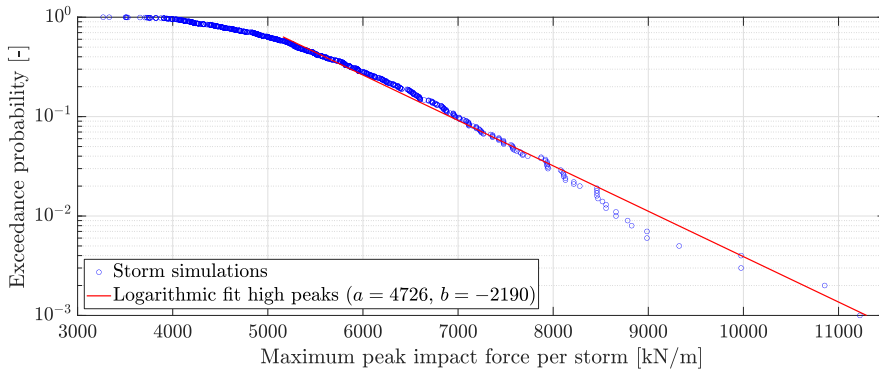


Figure 7.10: Exceedance probability of the maximum depth-integrated peak pressure in a single storm with a duration of 4 h based on the 1000 simulations. A logarithmic fit of the upper part of the maximum peak forces of the form $F_{\text{peak}} = a + b \log(p_{\text{exc}})$ with $a = 4726$ kN/m and $b = -2190$ kN/m is shown.

7.5.3 RESPONSE OF THE GATE TO SEVERAL WAVES

The developed semi-analytical model is now used to determine the response of the gate-fluid system. The continuous response of the gate is simulated for the entire 4 hour storm duration for each of the 1000 simulations. Figure 7.11 as an example shows a time series of

the deflection of the gate in response to several consecutive wave impacts. The response is governed by the first resonance mode. However, higher modes are excited by the wave peak impacts of shorter duration, which can be seen especially in the response after the third peak impact (at $t \approx 101$ s).

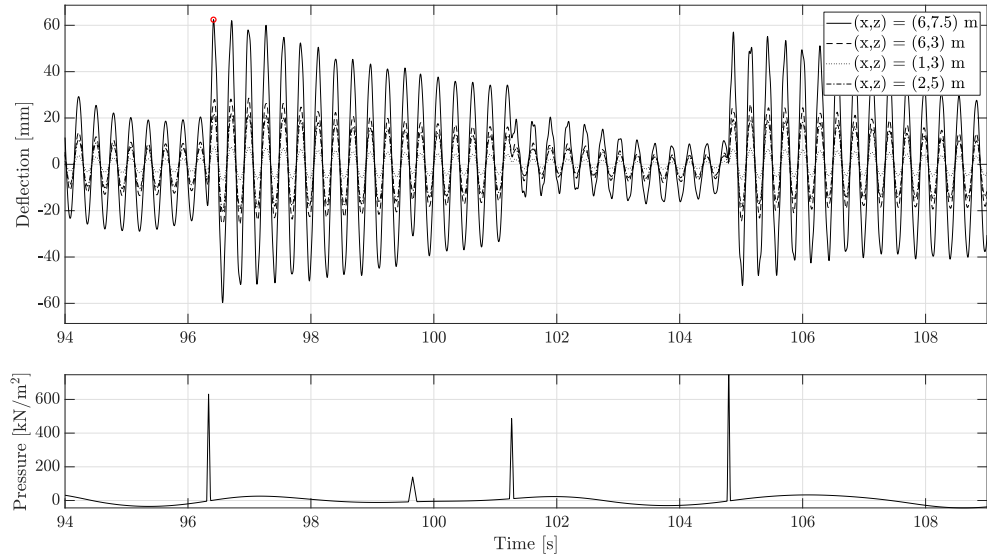


Figure 7.11: The displacement response of the gate for several wave impacts within a storm simulation

Vibrations of the gate do not fully damp out between wave impacts. In this case, vibrations from the previous wave impact quite strongly influence the maximum response after the following impact. The sequence and exact moment of wave impacts are therefore relevant when predicting the reliability of the flood gate. This effect is not included in conventional design methods using the dynamic amplification factor (Kolkman and Jongeling, 2007a), but is captured well within the presented probabilistic approach.

Moreover, the maximum peak force does not lead to the maximum response for this time interval. Figure 7.12 shows the maximum response of the gate for all wave impacts occurring with a single four hour storm for both the peak force and the pressure impulse of each wave impact. Above a certain limit, higher peak pressures no longer lead to a significant increase in response, most likely because the structural system is insensitive to the short impact durations of those wave impacts. The structural response is therefore more strongly correlated to the pressure impulse than to the peak pressure of a wave impact. This motivates the use of pressure impulse theory as the governing load parameter for wave impacts on these particular type of structures in contrast to the peak force that is often used within design practice. As discussed in Section 7.3.2, the pressure impulse of a wave impact has also shown to be better predictable in experiments (Hofland et al., 2011; De Almeida and Hofland, 2020b).

Figure 7.12 shows a large variation in the response of the gate for both the peak force and pressure impulse within one of the storm simulations. The previously described effect

of consecutive wave impacts is the main cause for this variation. Further, the distribution of the correction factor β_{lm} causes some variation.

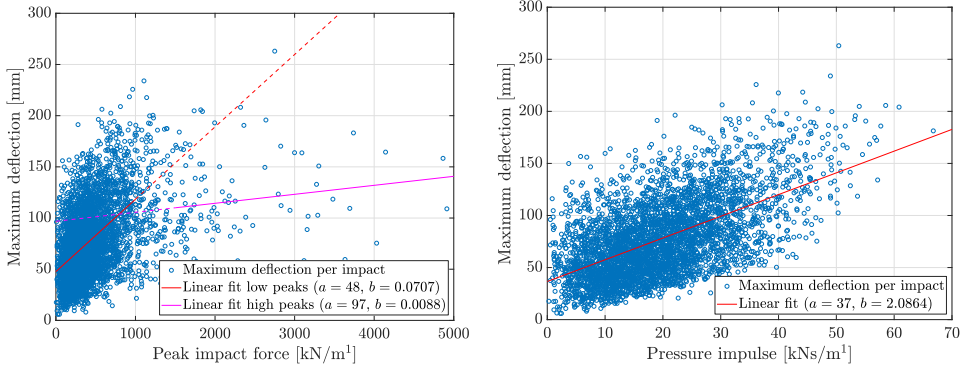


Figure 7.12: Correlation between the maximum local deflection of the gate and the peak impact force (left) and the pressure impulse (right) for all wave impacts within a single storm simulation

Figure 7.13 shows the deflection and yield stress fields over the plate for the moment of maximum deflection during the time interval shown in Figure 7.11. It can be seen clearly that the first vibration mode first mode (see Figure 7.8) is governing at that moment in time.

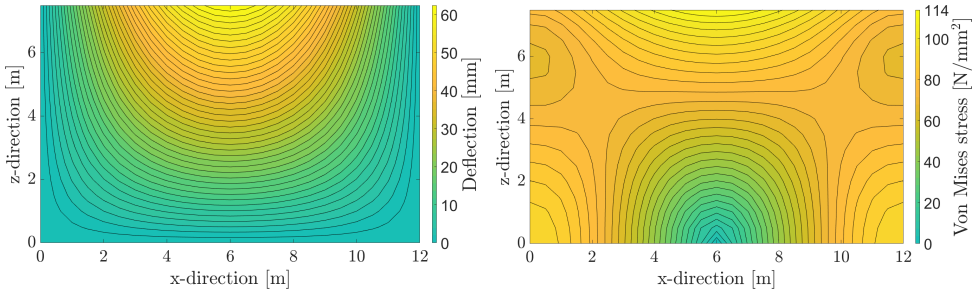


Figure 7.13: Deflection and stress at the surface of the plate at a local maximum response ($t = 96.4$ s) to a wave impact

7.5.4 PROBABILITY OF FAILURE OF THE SYSTEM

The gate response is now investigated for a thousand storms simulations, determining the maximum stress in the gate for each storm. Exceedance of the yield stress at any time during the four hour storm, is considered as failure of the gate. Figure 7.14 shows the maximum stress found in each of the storm simulations and their distribution. The yield stress is exceeded in 25 of the 1000 simulations, leading to the following conditional failure probability of the gate for the given design storm:

$$p_{f,gate} = \frac{n_{fails}}{N} = \frac{25}{1000} = 0.025 \quad (7.9)$$

The failure conditional probability is below the required maximum of 0.1, so that in this case study the gate design suffices.

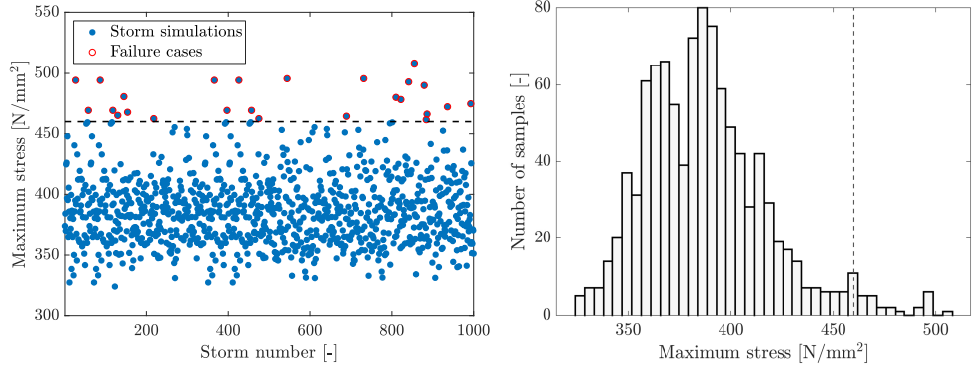


Figure 7.14: Maximum stress found in each of the 1000 storm simulations compared to the deterministic value of the yield strength (left) and the number of samples per maximum stress interval (right)

In the previous analysis, the yield strength was considered as a deterministic value. The conditional probability of failure is also investigated for the situation in which the yield strength of the steel gate is considered stochastically with a mean value 460 N/mm^2 and a standard deviation of 20 N/mm^2 . The uncertainty involved with the yield strength of the gate leads to a higher number of failures, resulting in a failure probability of 0.035.

7.5.5 ACCURACY OF THE MONTE CARLO SIMULATION

The accuracy of the performed simulation is now discussed. Generally, the coefficient of variation (relative error) ϵ of a Monte Carlo analysis resulting can be estimated by (Jonkman et al., 2016):

$$\epsilon = \frac{1}{\sqrt{N p_f}} \quad (7.10)$$

in which N is the number of simulations and p_f the required conditional failure probability for the given design storm. For the failure probability and number of simulations in our case this leads to an approximate coefficient of variation of 10%.

This estimate relies on the assumption that the outcome of the Monte Carlo simulation is binomially distributed. This is generally the case when the underlying stochastic variables are well behaved, also interpreted as slowly varying. It is argued that this is true for the stochastic variables considered in this case study. The correction factor and impulse duration are normally distributed and have a direct linear relation with the peak impact force of the wave impacts. The random-phase amplitude model is known to result in a smooth Rayleigh distribution of the wave height (Holthuijsen, 2007), which in turn is also linearly related to the impact velocity and peak impact force.

Figure 7.14 shows that the resulting distribution of the maximum stresses is indeed approximately binomial for the situation regarded in the case study. However, the distribution does show a double peak and is not entirely smooth at its tail. To obtain an additional indication of the robustness of the result, the number of simulations is

varied. As shown in Figure 7.15, the found probability of failure is relatively stable after 300 simulations at least when compared to the requirement.

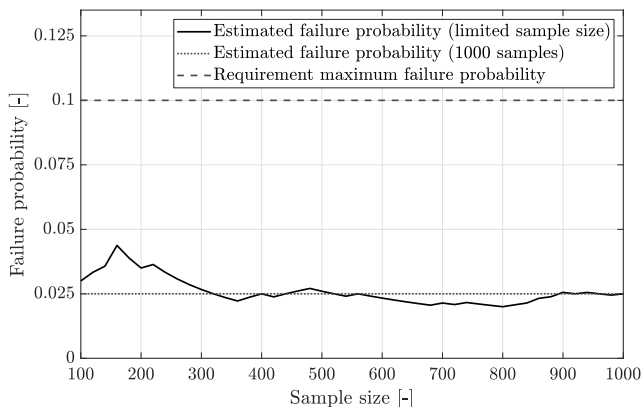


Figure 7.15: The conditional probability of failure for the given design storm found for an increasing number of simulations.

This accuracy is therefore expected to be sufficient for this case study. For design, when optimizing the design for the required failure probability, a higher number of simulations could be desirable however. Alternatively, sampling techniques exist that can improve the accuracy for a given number of simulations (Jonkman et al., 2016).

In the performed case study the water level was considered to be constant at the level of the overhang. It must be noted that a less smooth result is expected when performing a multivariate probabilistic analyse both including wave heights and water levels. Maximum wave impact forces occur when the water level is equal to the bottom of the overhang, which could possibly be just a small interval compared to the stochastic variation in water levels in some cases. Such an analysis therefore most likely requires a higher number of simulations.

7.6 CONCLUSION

A design approach has been presented for flood gates subjected to wave impacts. It was shown that this approach can be employed within a simplified reliability analysis to explicitly quantify the conditional failure probability of a flood gate for a given design storm. A large number of storms is simulated in a Monte Carlo type analysis, in which each storm could have a duration of several hours and involve thousands of wave impacts. The free surface elevation, wave impact duration and impulse correction factor are considered stochastically. The response of the flood gate is investigated for each storm simulation.

The computational efficiency of the fluid-structure interaction model developed in this thesis allows for the large number of simulations required within this approach. Predicting the response to every single wave during a governing design storm without doing concessions on the accuracy of the physical modelling of the involved fluid-structure interaction processes is a novelty within the field of hydraulic structures.

Predicting the response of the flood gate to each storm simulation using existing time-domain finite element models would be a computationally impossible mission.

A recently validated approach is employed to predict the wave impact loads on the gate, making use of different theories are applied to predict the quasi-steady pulsating and impulsive impact part of the wave load. For the impact part, pressure impulse theory is applied, which has shown a better theoretical predictability than peak pressures. Employing this method, avoids the necessity for time-consuming and costly experiments for every new situation. The combination of the relatively new fluid-structure interaction model and the analytical formulation to obtain the impulse of the confined-wave impacts was not applied before.

The approach and developed gate-fluid and wave load model were applied to a case study inspired by the situation of the Afsluitdijk, demonstrating their applicability as a design method. For the case study, vibrations of the gate did not damp out between wave impacts. The sequence and exact moment of wave impacts therefore influence the maximum response of the flood gate. This effect is not included in more conventional design methods, but is captured well within the presented approach.

Furthermore, results show that the pressure impulse is not only better predictable than the peak pressure when regarding the wave impact load, but also the response of the flood gate is more strongly correlated to the pressure impulse. This further motivates the use of pressure impulse theory as the governing load parameters for wave impacts on these particular type of structures, where now the peak pressures are generally considered in design practice.

Finally, an interesting further step in this approach would be to include the water level variation during the course of a storm within the presented probabilistic approach. This variation will be included in the design approach for fatigue presented in the following chapter.

8

ASSESSING FATIGUE OF FLOOD GATES DUE TO WAVE IMPACTS

The previous chapter presented a probabilistic approach to predict the failure probability of flood gates subjected to wave impacts. This approach focused on the ultimate limit state with exceedance of the critical yield strength as the failure mechanism. Also fatigue has in practice proven to be a relevant failure mechanism in the design of flood gates subjected to wave impacts. This chapter therefore provides a design method to predict wave-induced fatigue of flood gates over the lifetime of the structure. Again, the semi-analytical model developed in first chapters of this thesis is employed within this design method.

The structure of this chapter is as follows. Section 8.1 provides relevant background and discusses the motivation to develop a design method for wave-induced fatigue of flood gate. Section 8.2 describes the gate and fluid system that is considered in this design method. Section 8.3 elaborates a model routine to predict fatigue damage for a single storm event. Section 8.4 then presents a probabilistic approach to predict the fatigue lifetime of flood gates utilising this model routine. The benefits of the model are demonstrated by application to a case study inspired by the Afsluitdijk in Section 8.5. Section 8.6 discusses the key assumptions and potential improvements of the presented design method. Finally, Section 8.7 presents the conclusions of this chapter.

8.1 INTRODUCTION

Flood gates are commonly used in storm surge barriers and discharge sluices to regulate discharges and prevent flooding. Many of these structures are ageing and increased flood safety standards have made renovation or replacement necessary. As sea levels rise the hydraulic loads will become larger and more unpredictable. (Groeneweg et al., 2013; van den Hurk et al., 2006). Fatigue life estimation plays an essential role in the design and assessment of such gates, which are generally subjected to time-varying loads induced by a variety of sources. Especially wave impacts have the potential to lead to large fatigue damage for a number of reasons. First, they have a relatively high frequency of occurrence. During a single storm event several thousand wave impacts may occur. Second, these loads generally involve short but high pressure peaks (Ramkema, 1978; Hofland et al., 2011; Bagnold, 1939), which have the potential to cause significant gate vibrations and lead to a succession of stress cycles after each impact. Fatigue due to wave impacts has for instance proved to be a relevant failure mechanism in the design of the more than fifty flood gates at the Afsluitdijk dam in the Netherlands (Rijkswaterstaat, 2020a) (shown in Figure 1.4). The wave impacts in that situation occur due to the presence of overhanging structure, such as a bridge deck or concrete beam, in front of the flood gate. If the water level is sufficiently high, a wave collide with the bottom of the overhang and cause a pressure spike which results in a dynamic response of the gate.

Fluid-structure interaction makes the prediction of the dynamic behaviour of the gate due to wave impact pressures complex. In addition, this process is accompanied by different sources of uncertainty. Short-term wave statistics are subject to a lot of variance. The variation as well as long-term development of hydraulic boundary

This chapter is based on the article "A novel design method for wave-induced fatigue of flood gates" submitted to the Journal of Coastal and Hydraulic Structures. The conceptualization, analysis, methodology, and writing of this publication have been performed in collaboration with the first author. Some changes have been introduced to make the text consistent with the other chapters of the thesis.

conditions introduce further uncertainties. Moreover wave impacts have a highly variable nature (Hofland et al., 2011; Chen et al., 2019; Kortenhaus et al., 1999) in which waves with very similar characteristics lead to significantly different peak pressures. Another complicating issue is that the dynamic response cannot always be regarded by looking at individual wave impact loads. As shown by Tieleman et al. (2021), the response to consecutive waves should be taken into account. A probabilistic design approach for fatigue which accounts for all of these uncertainties could result in a both safer and more cost-effective design.

The key challenge for such an approach is to accurately model the gate and fluid response in a computationally efficient manner that allows a multitude of varying simulations of the entire lifetime of the structure. Existing methods used in engineering practice tend to rely on finite element simulations which fulfil the requirement of being accurate, but are not sufficiently computationally efficient. For a finite element model the time-domain simulations required for the fatigue evaluation of a flood gate are very challenging given the long computation times (Zheng et al., 2020). Within the field of hydraulic engineering, simulating the dynamic response of a structure for a large number of waves or storms is therefore rarely done in practice. When fatigue or probabilistic analyses are performed, the wave loading and structural model are strongly simplified. Within the fields of marine and offshore engineering these type of simulations are more common (e.g. when evaluating the fatigue damage of offshore platforms (Zheng et al., 2020) or the feasibility of dredging or pipe laying operations (Van der Wal and de Boer, 2004)). However, simulating the full dynamic behaviour of a ship or structure for a multitude of storms over the entire lifetime while also analysing the reliability of the system is rare within these fields as well.

This chapter presents a novel design method that evaluates fatigue damage due to confined wave impacts over the lifetime of a flood gate, without making concessions on the number of considered load cases or the accuracy of the response calculation. The methods are based on the developed model routine for the evaluation of the ultimate limit state presented in the previous chapter. However, the model routine is adapted to enable the evaluation of fatigue damage by accounting for all expected loads over the lifetime of the structure instead of a single storm event. Furthermore, complex gate geometries with stiffeners are accounted for rather than a homogeneous plate. A probabilistic description of the load cases account for the variable nature of the hydraulic boundary conditions and wave impact loads. The expected environmental conditions are derived from historical data in this study. Random wave states are derived from the environmental conditions with commonly used spectral shapes from Hasselmann (1973) and Hughes (1984). These realisations are used to derive pressures on the surface of the gate according to a combination of linear wave theory (Airy, 1845) and pressure-impulse theory (Wood and Peregrine, 1997), which dynamically excite the gate-fluid system. The response of the system is derived with the semi-analytic method from Tieleman et al. (2018) combined with a FEM-model based on Vorderegger (2019). The stress histories obtained from this model are then used to derive the fatigue by extracting the stress cycles with the Rainflow algorithm (Matsuishi and Endo, 1968) and calculating a fatigue damage factor with the linear damage summation rule from Miner (1945). The high loads involved with wave impacts make that this type of problem usually involves low cycle fatigue. In

a Monte Carlo analysis, the continuous wave loads, gate response and resulting fatigue damage are simulated for the environmental conditions over the lifetime of the flood gate a number of times. This results in an expected fatigue lifetime of the structure. Similar to the previous chapter, the focus of this chapter lies on the model approach. Not all aspects and uncertainties necessary for a practical reliability analysis are therefore included and discussed.

A case study is performed to demonstrate the benefits of the presented design method. The outcome is compared to the result of commonly applied simplified methods showing significant improvement in the prediction of the fatigue lifetime.

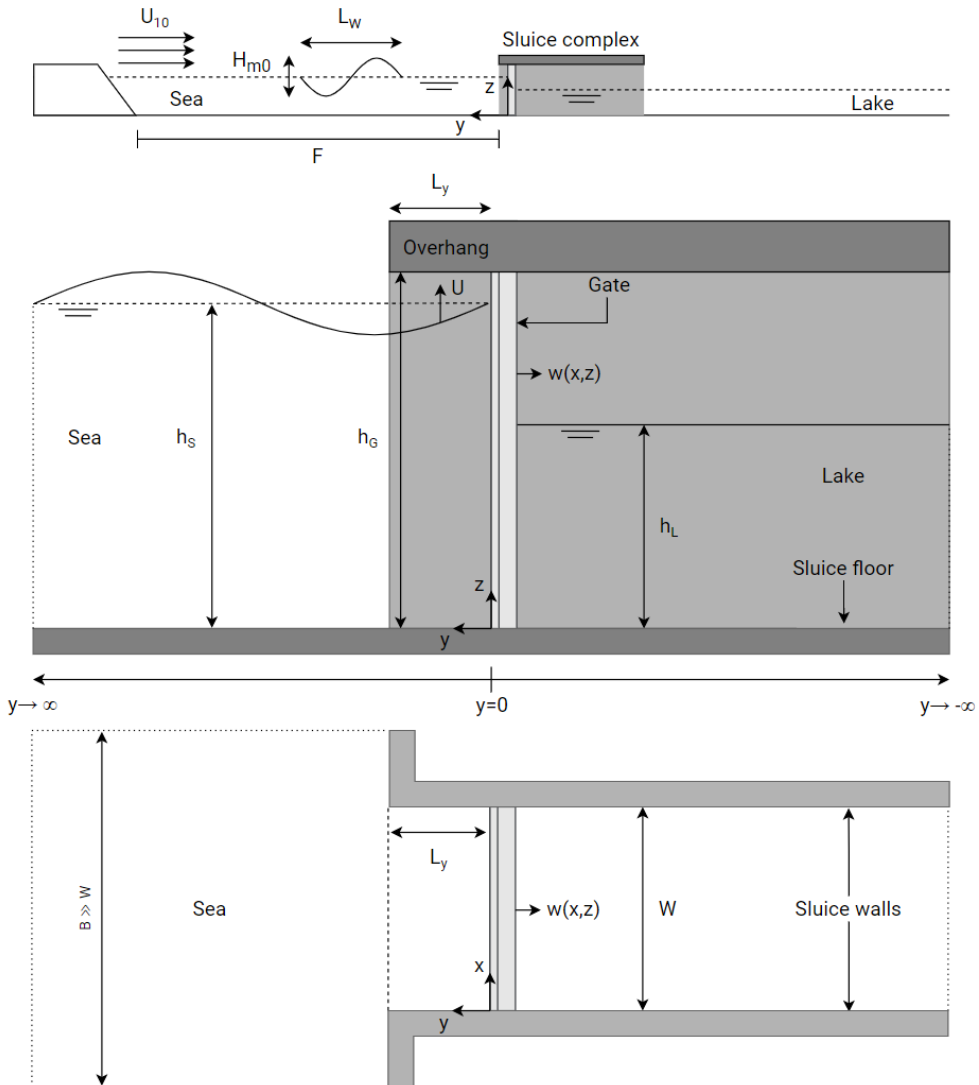
8.2 SYSTEM DESCRIPTION

A schematised overview of the system is shown in Figure 8.1. A discharge sluice is situated between a shallow sea with water level h_S and a lake with water level h_L . The water level at sea is subject to variations due to various sources such as tides and storm surge, while the water level at the lake is considered to be regulated and therefore constant in this study. Variations of the water level on this side could be considered as well within the presented method however. During a storm event, the water level at sea will be higher than the water level at the lake. A flood gate is therefore installed in the discharge sluice to stop intrusion of sea water when necessary.

The width of the gate W [m] is equal to that of the discharge sluice. The gate has a height h_G [m]. At the sea side an overhang is present over the length of the discharge sluice on this side L_y [m]. For the purpose of the hydrodynamic response the sluice extends to infinity, which means the boundaries don't influence the system. The sea is modeled as infinitely wide and long. The walls and floor of the discharge sluice are rigid and impermeable. The water has a free surface everywhere except when constrained by the overhang. The water on both sides is considered to be compressible, irrotational, and inviscid.

The gate consists of a front plate with rectangular stiffeners on the lake-facing side in both the vertical and horizontal directions. The horizontal stiffeners are reinforced with flanges. The geometry of the gate is described parametrically according to the definitions in Figure 8.2. The gate has a uniform mass density ρ_s [kg/m³] and modulus of elasticity E [MPa]. Generally, these type of vertical lift flood gates are simply supported at the sides and unsupported at the top and bottom. This study therefore considers these boundary conditions. However, the fluid structure interaction (FSI) model from Tieleman et al. (2019a) allows any combination of geometry and boundary conditions to be evaluated.

The gate is subjected to loads by waves at the sea side. These waves are either locally generated by wind over a fetch length F [m] and with a velocity u_{10} [m/s] at 10m height, or swell waves originating further out at sea. The average water depth at sea is assumed constant over the fetch. The waves are confined by the presence of an overhang in front of the gate, which causes pressure spikes and a highly dynamic response. Other loads such as wind, ice or operational loads will not be considered in this study but can be included in the presented design method.



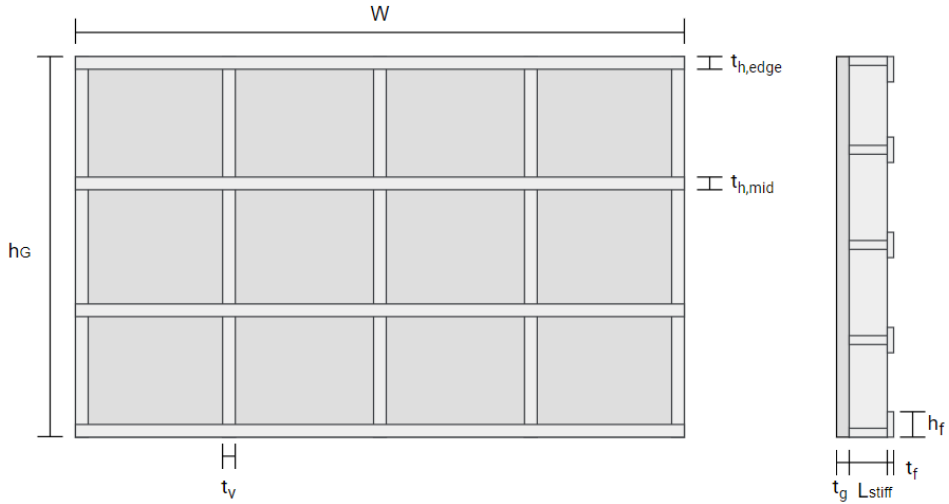


Figure 8.2: Parametric dimensions of the gate

8.3 PREDICTING THE DYNAMIC RESPONSE FOR A SINGLE LOAD EVENT

Starting point of the design method are load cases, consisting of a set of environmental conditions (the water level at sea h_S and the wind velocity u_{10} , and their associated probability of occurrence. This section presents a model routine to predict fatigue damage for a single load event. The probabilistic design method presented in the following section utilises this model routine to predict the expected fatigue lifetime of the flood gate.

This model routine combines several existing and recently developed theories. The routine comprises multiple independent modules, as shown in Figure 8.3. A random wave series is first derived from the environmental conditions. This wave field will be used to create a two-dimensional pressure field on the gate surface for the duration of the load event. The dynamic response is predicted for the entire duration of the load case by employing a hybrid semi-analytic and finite element fluid-structure interaction model. The resulting stress time series are turned into a fatigue damage factor with the Rainflow algorithm from Matsuishi and Endo (1968) and the Palmgren-Miner method (Miner, 1945). The modularity of this model approach makes it possible to apply different theories each component when preferred for a specific study, for example higher order wave theory or computational fluid dynamics instead of linear wave theory.

8.3.1 WAVE FIELD

The wave conditions are predicted in this study based on historic water level and wind data. Historic wave data can also be used directly in combination with water level data. However, for many locations other than the Dutch coast long term and high-resolution wave data is not available. The more general approach based on water level and wind data is therefore presented here.

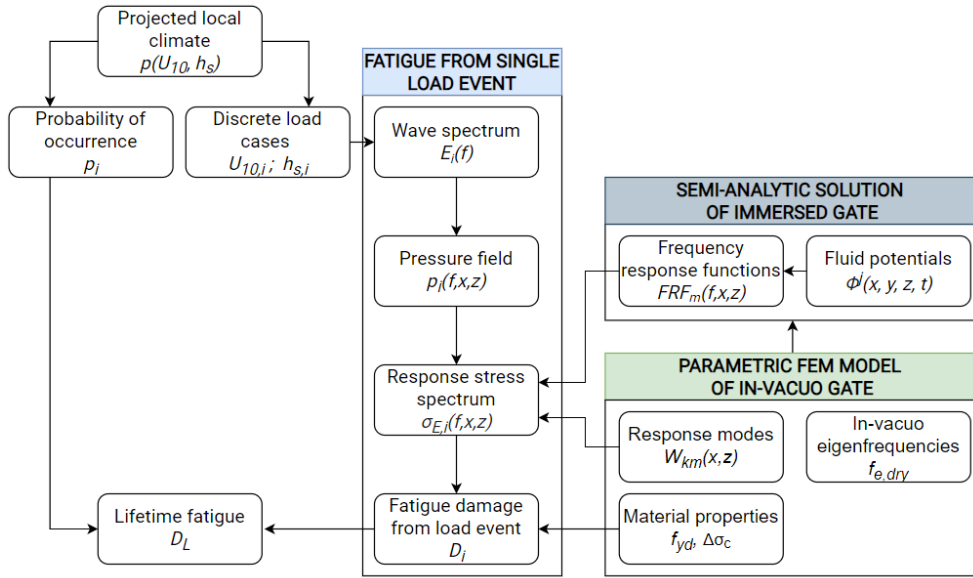


Figure 8.3: Schematic overview of the presented design method

The theory by Bretschneider (1959) is employed to translate the water level (h_s) and wind velocity (u_{10}) to a JONSWAP variance density wave spectrum (Hasselmann, 1973) as a function of the wave frequency f [Hz], given a set of shape parameters and the wind fetch F . More advanced wave models could also be applied within this model routine, for example when considering cases with more complex bathymetries. The waves are assumed to be non-steep and locally generated, and the wave state is considered to be fully developed for all conditions.

The presented model routine is able to evaluate pressure fields which are not uniform over the width of the gate. However, in this study all waves are considered to be long-crested and have a perpendicular angle of approach to the discharge sluice and gate. The wave pressures will therefore be uniform across the width. To account for the shallowness of the sea, the JONSWAP spectrum is modified with a depth correction factor such as the one given by the TMA spectrum from (Hughes, 1984). This adds a dependence on the local water depth and truncates the JONSWAP spectrum to account for the effect of bottom friction on the wave state. Figure 8.4 shows examples of both spectra.

The result is a variance density spectrum $E(f)$ [m^2/Hz], which defines the amount of spectral energy concentrated at every frequency. A time domain wave series may be derived from the spectrum by means of the random phase-amplitude model (Holthuijsen, 2007). For this purpose, realisations $E_i(f)$ of the spectrum are generated by adding a random phase to each frequency. For non-steep linear waves, this phase is uniformly distributed (Holthuijsen, 2007), denoted by $U(0; 2\pi)$.

Because the waves are reflected, the water level at the surface of the gate can be up to twice as high. The strength of the reflection is determined by the reflection coefficient c_r [-

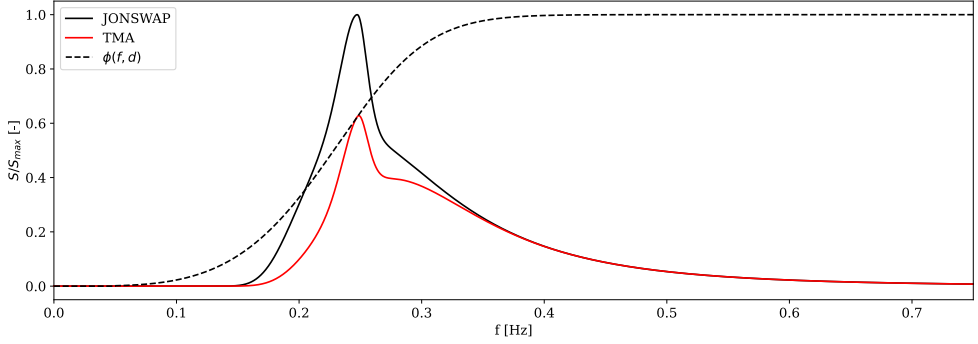


Figure 8.4: Examples of JONSWAP and TMA amplitude spectra for $h_S = 7.5$ m and $u_{10} = 10$ m/s

], which can range from 0 to 1 depending on the geometry of the structure. De Almeida and Hofland (2020b) showed that for vertical gates with an overhang a reflection coefficient of 1 is a reasonable assumption because the incident wave is not influenced by the overhang during the half-period before the wave impact occurs. Therefore $c_r = 1$ will be assumed in this study as well.

$$E_i(f) = (1 + c_r) \cdot E(f) \cdot e^{-iU(0,2\pi)} \quad (8.1)$$

The peak frequency of the resulting spectrum is found by determining the frequency with the highest energy content. The significant wave height follows from $H_{m0} = 4\sqrt{m_0}$, where the spectral moment m_0 [m^2] follows from Equation 8.2 for $m = 0$.

$$m_n = \int_0^\infty f^n E_i(f) df \quad (8.2)$$

8.3.2 HYDROSTATIC AND WAVE PRESSURES

The wave spectrum will now be used to derive a pressure field over the surface of the gate. The pressure is subdivided into three distinct types, visualized in Figure 8.5. The mean water levels at either side of the gate impose a constant hydrostatic pressure on the gate which increases with depth according to Equation 8.3:

$$p_{hs}(x, y = 0, z, t) = \rho g z \quad (8.3)$$

This is represented in the frequency domain as a load with frequency zero. The fluctuations due to quasi-steady wave pressures will be added to this static average by applying linear wave theory (Airy, 1845) (only valid for non-steep waves) to the previously derived wave spectrum at every coordinate on the gate surface.

$$p_{qs}(x, y = 0, z, t) = \rho g a \frac{\cosh k(z + h)}{\cosh kh} \cos \theta \quad (8.4)$$

The pressure due to impulsive wave impacts is very unpredictable, but with the pressure-impulse theory from Wood and Peregrine (1997) it can be probabilistically

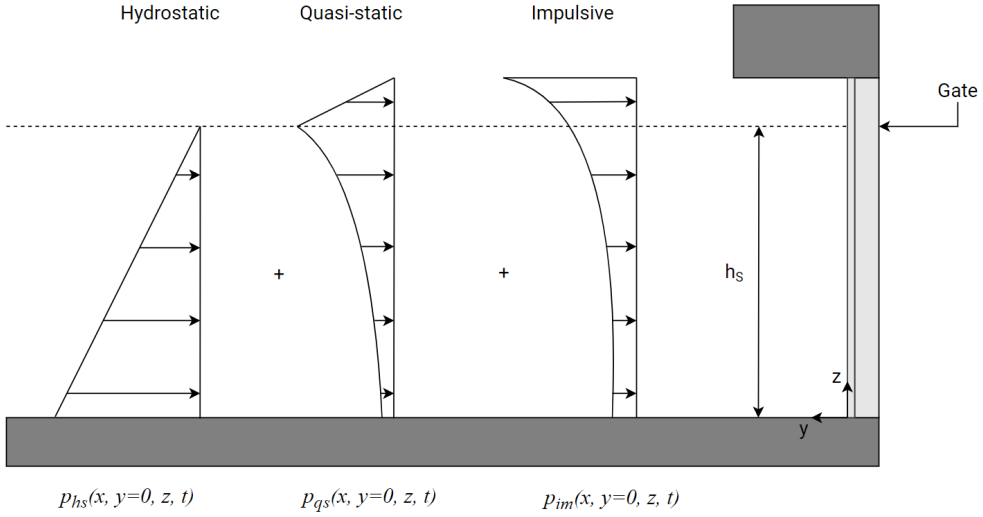


Figure 8.5: Components of total hydraulic pressure.

described. In Equation 8.5 the geometry-dependent dimensionless pressure-impulse shape $\bar{P}(x, y = 0, z)$ [-] is combined with a pressure peak shape, the impact velocity of the water surface U_w [m/s], and a correction factor for the compressibility of entrapped air $1 < \beta_{im} < 2$ [-] (De Almeida and Hofland, 2020b). The result is a pressure distribution over the surface of the gate.

$$\bar{P}(x, y = 0, z) = \frac{P_{im}(x, y = 0, z)}{\beta_{im} \rho_w U_w L_y} = \frac{\int_{t_0}^{t_1} p_{im}(x, z, t) dt}{\beta_{im} \rho_w U_w L_y} \quad (8.5)$$

Four examples of the dimensionless pressure-impulse shape over the height of the gate are plotted in Figure 8.6 for different values of L_y . The integral from Equation 8.5 can be solved by assuming a shape for the pressure impact, which Chen et al. (2019) shows can be represented with reasonable accuracy as a symmetric triangle. The base of this triangle is a probabilistic impact duration $\tau = t_1 - t_0$ [s], which means the peak pressure can be described by:

$$\int_{t_0}^{t_1} p_{im}(x, z, t) dt = \frac{1}{2} \tau p_{peak} \quad (8.6)$$

The experiments of De Almeida and Hofland (2020b) have validated the model for relatively short overhangs relative to the wave length L_w ($12.1 < L_w/L_y < 43.6$), low steepness, and non-breaking conditions.

The upward impact velocities of the water U_w surface are found by taking the derivative of the wave field every time it crosses the elevation of the overhang in the upwards direction. For β_{im} , findings in De Almeida and Hofland (2020b) suggest a normally distributed value with a mean of 1.17 and a standard deviation of 0.11 for standing waves. De Almeida and Hofland (2021) expand this to irregular waves by first

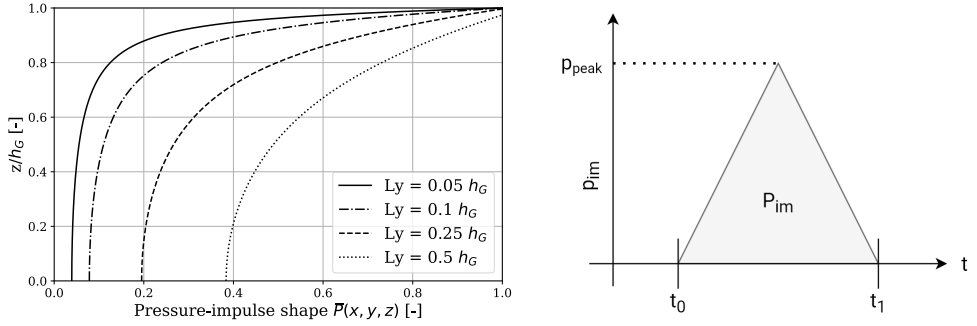


Figure 8.6: Dimensionless pressure impulse shape for different values of L_y (left) and the triangular impact pressure shapes over time (right)

introducing a Γ -factor from which the correction factor β can then be calculated:

$$\Gamma = U_{w,1\%}^2 L_m / g L_y^2 \quad (8.7)$$

$$\beta = 2 - e^{-0.16\Gamma} \quad (8.8)$$

L_m [m] is the mean wave length associated with the mean wave period T_{m02} [s], which is defined in Equation 8.9 based on the spectral parameters from Equation 8.2 (Holthuijsen, 2007).

$$T_{m02} = \sqrt{\frac{m_0}{m_2}} \approx 1,1 T_p \quad (8.9)$$

For the 1%-wave of an irregular wave field, the corresponding impact velocity $U_{w,1\%}$ [m/s] follows from:

$$U_{w,i} = \frac{2\pi}{T} \sqrt{\left((1 + c_r) \frac{H_i}{2} \right)^2 - (h_S - h_G)^2} \quad (8.10)$$

applicable to waves that reach the overhang, such that:

$$\left((1 + c_r) \frac{H_i}{2} \right)^2 - (h_S - h_G)^2 > 0 \quad (8.11)$$

Based on the results shown in Figure 16 of De Almeida and Hofland (2020a), the value for β will be randomly drawn from a normal distribution where the mean is given by Equation 8.8 and whose standard deviation is estimated from the 90% confidence intervals as 0.12. Because this definition of β is based on the highest 1% of wave impacts, it can be used as a conservative estimate for the compressibility correction factors of every wave in the spectrum.

A distribution for the probabilistic impact duration τ of each impact will be based on the findings from the scale experiments by De Almeida and Hofland (2021). For a short overhang ($h_S/L_y = 6$), values for τ were found to be approximately triangularly distributed with a lower limit of 5 ms, a mode of 75 ms, and an upper limit of 200 ms. These values are Froude-scaled to the scale under consideration by a scaling factor of $\gamma^{0.5}$, with

$\gamma = L_y/0.1$ as the overhang in the scale experiments by De Almeida and Hofland (2021) had a length of 0.1 m. It should be noted however that Froude's law is not necessarily accurate here, as near the atmospheric pressure non-linear interactions between the air and water pressures start to play a role. Depending on the way air is entrapped below the overhang, the impact durations can be both shorter or longer than predicted (Ramkema, 1978). Research on the dependence between air entrapment and different wave properties is ongoing based on the results from De Almeida and Hofland (2021). Here, it is assumed the variation for irregular wave conditions can be fully captured in the triangular distribution of the impact duration. Depending on the outcome of further research, it may be necessary to define distributions dependent on the wave conditions.

Evaluating Equation 8.5 for these random variables gives a set of pressure peaks. Adding the all together at their respective moments of impact then results in a single pressure field $p(x, z, t)$ [Pa] over the surface of the gate. Finally, the quasi-static and impulsive pressure fields are combined to give a description of the combined pressure field over the duration of the load event. A random realisation is plotted in Figure 8.7, which shows the impulsive pressure peaks alongside the slower fluctuations from the quasi-static wave pressures.

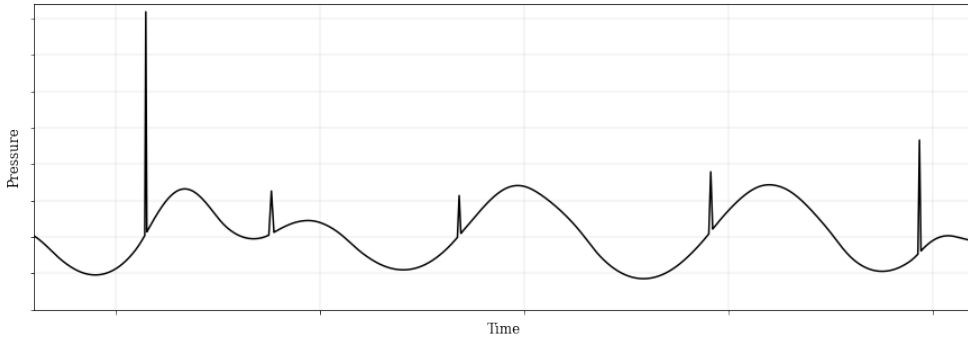


Figure 8.7: Combined depth-integrated pressure time series of all three pressure components: the hydrostatic, and quasi-steady and impulsive wave pressure

8.3.3 DYNAMIC RESPONSE OF THE IMMERSSED GATE

A recently developed hybrid semi-analytical and finite element method by Tieleman et al. (2022b) is employed to predict the response of the gate immersed in fluid. The method of solution is based on a substructuring mode matching technique similar to Tsouvalas and Metrikine (2014, 2016) and Leblond et al. (2009). Tieleman et al. (2022b) derives a semi-analytical solution for the fluid-structure interaction problem. The motion of the in-vacuo gate structure and the corresponding stresses are described in terms of modal

coefficients:

$$\tilde{u}(x, y, z, \omega) = \sum_{k=1}^{\infty} A_k(\omega) U_k(x, y, z) \quad (8.12)$$

$$\tilde{\sigma}_{ij}(x, y, z, \omega) = \sum_{k=1}^{\infty} A_k(\omega) S_{k,ij}(x, y, z) \quad (8.13)$$

in which u [m] denotes the displacement of the gate structure at a certain discretized point, the coefficients A_k [m] denote the amplitudes of the corresponding gate displacement modes U_k [-] and stress modes $S_{k,ij}$ [-], with $i, j = x, y, z, xy, xz, yz$ denoting each of the directional stresses. The motion of the fluid in the domains at either side of the gate is described in a similar matter. The semi-analytical solution then solves the modal coefficients of both the structure and fluid for the joint system in the frequency domain. Any time-domain force can then be applied to the model with the use of a Fourier transform. The main computational advantage of the mode matching technique lies in the ability to store and reuse partial results in contrast to the step-wise calculation in finite element (FE) methods. Even when evaluating a large number of loads, the frequency response function of the gate fluid system only has to be computed once.

The model uses the in vacuo gate modes, fluid modes, and the corresponding frequencies as input. The fluid modes are found by solving the partial differential equation of the fluid motion analytically. A structural finite element model is employed to find the mode shapes and frequencies of in-vacuo gate displacement and corresponding stresses. Any finite element software package which uses the theory of elasticity can be used for this purpose. For this study, SCIA Engineer 2021 is employed. This procedure is straightforward and requires minor computational effort since the interaction with the fluid is not evaluated in the finite element model, but with the semi-analytical approach.

Damping due to fluid compressibility and surface waves is an implicit part of the fluid-structure interaction model. However, for the frequencies and water depths involved with wave impacts on flood gates these damping effects are usually insignificant (Tieleman, 2016; Tieleman et al., 2019a). Furthermore, a material damping factor η [-] can be included directly in the semi-analytical solution. In this study, the application of damping is limited to this material damping factor. However, other types of damping, for instance at the supports of the flood gates, could be modelled within the finite element model of the in-vacuo gate. This would result in complex mode shapes and frequencies as input to the semi-analytical solution.

The wave impact forces or any other time-varying loads are modelled as an external pressure on the surface of the gate. One of the key assumptions of this model approach is therefore that the impact force does not affect the still water level. In Tieleman et al. (2019b) this was discussed to be a reasonable assumption for the time scales involved in impulsive wave impacts. Time series of the wave impact load are Fourier transformed to the frequency domain to determine the frequency response of the system. An inverse Fourier transform is then applied to obtain a time series of the gate response in terms of deflections and stresses.

8.3.4 FATIGUE OF THE STRUCTURE

The final step within the model routine is to predict the fatigue damage. Various methods exist to evaluate the fatigue lifetime of a structure in the time domain, such as peak counting, level-crossing counting, range-mean counting and rainflow counting (RFC) (Benasciutti and Tovo, 2006; Rychlik, 1993). A frequency domain stochastic fatigue analysis is an alternative approach that is often chosen by engineers to avoid numerically costly time-domain simulations. When the stochastic stress process is narrow-banded and Gaussian, its amplitudes follow the Rayleigh distribution. Therefore, the accumulated fatigue can be calculated by integrating the probabilistic function (Zheng et al., 2020; Newland, 2012). For wide-banded processes, an analytic solution does not exist and application of the spectral method is less straightforward.

When sufficiently long stress series are available, the time-domain RFC analysis (Downing and Socie, 1982) for fatigue evaluation is generally the first choice (Zheng et al., 2020). The numerical efficiency of the developed model allows for such an evaluation. The RFC is therefore applied as the cycle counting method in this study. For this purpose, the predicted directional stresses $\tilde{\sigma}_{ij}(x, y, z, \omega)$ [Pa] in the frequency domain are inverse Fourier transformed to obtain the time domain response. These directional stresses are then translated to the type of stress relevant for the fatigue criterium. In this study, fatigue is evaluated by means of the maximum principal stress in accordance with the Eurocode (European committee for Standardization, 2006) in order to preserve direction. The signed Von Mises stress is applied as an alternative in practice as well.

The accumulated fatigue damage is then predicted with the well-known tri-linear logarithmic S-N curve of the material and the Palmgren–Miner rule (Miner, 1945), which compares the stress cycles extracted from the time series with the capacity defined by the S-N curve (See Eq. 8.14). The resistance of a material or connection is typically characterised by its detail category $\Delta\sigma_c$ [MPa] as defined in the Eurocode (European committee for Standardization, 2006), which represents the resistance at $N_c = 2 \cdot 10^6$ [-] and allows the rest of the curve to be calculated.

$$D = \sum_{i=1}^k \frac{n_i}{N_{c,i}} \quad (8.14)$$

where D [-] is the fatigue damage factor, $N_{c,i}$ [-] the allowable amount of a given stress cycle i , and n_i [-] the amount of these stress cycles found in the time series. D indicates how much of the fatigue capacity of the material was depleted by the load event. When D exceeds 1, the element under consideration has failed.

8.4 PROBABILISTIC LIFETIME ANALYSIS

The computational efficiency of the model routine presented in the previous section makes it possible to consider a large number of load events to characterise the stresses in the gate over the lifetime of the structure. This section proposes a probabilistic design method to perform a lifetime fatigue damage assessment of a flood gate subjected to wave impacts utilising this efficiency.

Section 8.4.1 describes how the relevant load cases are derived within this method. A way to further optimise the computational efficiency of the method by filtering irrelevant

load cases and choosing a suitable resolution is presented in 8.4.2. Finally, paragraph 8.4.3 shows how the fatigue lifetime follows from the presented method.

8.4.1 LOAD EVENT DERIVATION

The fluctuations of the water surface relevant for this study can be subdivided into three types:

- Periodic short-term changes, e.g. local wind waves or swell;
- Periodic long-term changes, e.g. tides or storm surge;
- Cumulative long-term changes like sea level rise or land subsidence which change the mean water depth over time.

These fluctuations will be accounted for in different ways within the presented probabilistic method. Historical wind- and water level data of at least hourly intervals are used to generate load cases with representative values for the time-averaged water level h_S and average wind velocity U_{10} . This data is publicly available for many locations along the Dutch coast. The short term water level fluctuations will be determined with the use of a wave spectrum based on these two parameters, as described in paragraph 8.3.1. Because the periods of tides, storm set-up, atmospheric pressure changes, and other long-term effects are generally much longer than an hour, the hourly averages of the mean water level and wind velocity may be employed to predict short-term water level fluctuations.

The long-term periodic changes are expected not to cause fatigue damage due to their quasi-static nature and low cycle count, and are therefore not included in the fatigue assessment. The validity of this assumption can be verified for any specific case. If necessary, the stress cycles caused by these fluctuations can be added to the fatigue damage assessment. Effects that accumulate over time, like climate change or soil settlement, are included separately within this method. These effects are described stochastically by separate probability distributions which define the likelihood that a given relative water level increase occurs at a random point during the lifetime of the gate, and will be combined with the de-trended historical data.

First, probability density functions are fitted to the historical data. When tides are present, sea water levels generally resemble a bi-modal Gaussian distribution. The wind velocities tend to follow a skewed extreme value distribution. The water level distribution is adjusted for long-term effects such as climate change and soil subsidence. If a linear increase over time is assumed the probability distribution of these effects will be uniform. The uniform distribution will range from 0 (at the start of the lifetime) to h_{SLR} [m], which is the expected sea level rise at the end of the lifetime. For coastal structures in the Netherlands, h_{SLR} is generally assigned a fixed value based on a certain climate scenario. More complex distributions that take into account multiple sea level rise scenarios and corresponding probabilities could also be applied within the presented approach however. The design water level probability distribution $f_H(h_S)$ is obtained by performing a convolution of the original fitted distribution f_1 and the climate change distribution f_2 .

$$f_H(h_S) = \int_{-\infty}^{\infty} f_1(t) f_2(h_S - t) dt \quad (8.15)$$

The climate scenarios for the Netherlands do not predict a change in wind climate within this century (van den Hurk et al., 2006). The historical wind data is therefore not adjusted for climate change in this study. However, a similar procedure as for the water levels could be applied to incorporate different scenarios and related probabilities..

Next, the water level and wind distributions are combined into a joint probability density function $f_J(h_S, U_{10})$. The amount of correlation is characterised with the correlation coefficient from Pearson (1895). Depending on the nature of the data independence can be assumed, or a correlation can be applied to either the entire distribution or just the upper tail events.

Next, this continuous joint probability density function will be discretised into a set of two-dimensional segments, each of which will be characterised by a representative load case. After discretisation, the data will look something like Figure 8.8. The representative values $h_{S,j,k}$ and $U_{10,j,k}$ for any segment (j, k) are obtained by calculating the expected value of $f_J(h_S, U_{10})$ over the intervals $(H_j < h_S < H_{j+1}), (U_k < U_{10} < U_{k+1})$:

$$h_{S,j,k} = \frac{\int_{H_j}^{H_{j+1}} \int_{U_k}^{U_{k+1}} h_S \cdot f_J(h_S, U_{10}) dU_{10} dh_S}{\int_{H_j}^{H_{j+1}} \int_{U_k}^{U_{k+1}} f_J(h_S, U_{10}) dU_{10} dh_S} \quad (8.16)$$

$$U_{10,j,k} = \frac{\int_{H_j}^{H_{j+1}} \int_{U_k}^{U_{k+1}} U_{10} \cdot f_J(h_S, U_{10}) dU_{10} dh_S}{\int_{H_j}^{H_{j+1}} \int_{U_k}^{U_{k+1}} f_J(h_S, U_{10}) dU_{10} dh_S} \quad (8.17)$$

The probability associated with that segment is found by integrating the joint probability density function over that interval.

$$p(H_j < h_S < H_{j+1}, U_k < U_{10} < U_{k+1}) = \int_{H_j}^{H_{j+1}} \int_{U_k}^{U_{k+1}} f_J(h_S, U_{10}) dU_{10} dh_S \quad (8.18)$$

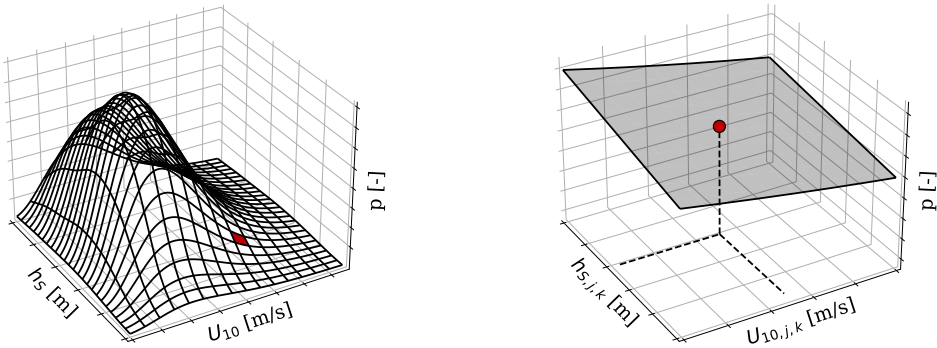


Figure 8.8: Left: Example joint probability density function of historical data for h_S and U_{10} . Grid lines indicate discrete load cases. Right: Single discrete load case and its representative values.

This results in a set of load cases characterised by representative values for h_S and U_{10} as well as a probability of occurrence. The response of the gate to each of these load cases is then predicted based on the model routine presented in Section 8.3.

8.4.2 LOAD CASE RESOLUTION AND FILTERING

This paragraph provides a method to determine the optimal load case resolution based on convergence of the solution. Methods to filter the list of load cases will also be discussed, to increase the efficiency of the lifetime fatigue analysis.

The choice for the size of the segments is a trade-off between required computational effort and accuracy. A smaller segment size results in a larger number of simulated load cases. The resolutions of the two variables are defined as:

$$\Delta_{h_S} = H_{j+1} - H_j \quad (8.19)$$

$$\Delta_{U_{10}} = U_{k+1} - U_k \quad (8.20)$$

The accuracy is assessed with a resolution refinement procedure comparing the standard deviations of a large amount of repetitions randomly picked from within the segments. The resulting error has two sources; variance caused by the probabilistic nature of the wave field and wave impact models applied, and variance caused by the range of possible inputs. For narrower resolutions the randomly picked values will show less divergence. The lower limit for the resolution is zero, in which case only the variance inherent in the model plays a role. This therefore serves as a baseline which can only be asymptotically approached. In order to test convergence, the fatigue analysis is first run N times for the representative values of h_S and U_{10} , which will result in a normally distributed set of fatigue damage values. Then, the fatigue analysis is run N times for random values in a range of Δ_{h_S} [m] by $\Delta_{U_{10}}$ [m/s] around the representative values (i.e. the part of the distribution those values are representing). The standard deviations of these two sets of results are then compared to see how closely the results of the representative values match those of the randomly picked values. This procedure is repeated with increasingly small resolutions until the standard deviations converge. An example of this procedure is given in Section 8.5.

Some load cases can be filtered to further improve the computational speed of the presented method. Certain load cases are highly unlikely to occur and can therefore be discarded, while others cause such small loads such that they do not contribute significantly to the lifetime fatigue damage (i.e. all of the stress cycles are below the cut-off limit of the S-N curve). For these load cases, the wave loads and dynamic response of the gate does not have to be simulated.

The very infrequent cases can be filtered out based on their expected probability of occurrence. A common maximum normative return period for loads on hydraulic structures in the Netherlands is 10.000 years. Cases with a longer expected return period are filtered out. If the lifetime analysis (Section 8.4.3) shows that rare events do contribute significantly this horizon could be extended. This provides the following filtering criterion based on the expected hourly rate of occurrence:

$$p_{\min} < (10.000 \cdot 365.25 \cdot 24)^{-1} = 1.14e^{-8} \quad (8.21)$$

In order to filter cases based on their contribution to fatigue damage, a statistical property of the wave spectrum will be used to avoid running calculations for all of these cases. Load events where the sum of the statistical maximum wave height and the highest water level does not exceed the elevation of the overhang (h_g) will be removed from the data-set.

The statistical maximum wave height produced by a random realisation of a wave spectrum i is $H_{max,i} \approx 2H_{m0,i}$ [m] (Holthuijsen, 2007). Accounting for reflection, this gives a maximum expected water elevation of $\frac{1}{2}H_{max,i}(1 + c_r)$. This results in the following limit for filtering cases that have a low probability of wave impacts occurring:

$$h_s + \frac{1}{2}H_{max,i}(1 + c_r) < h_G \quad (8.22)$$

For these load cases, it is very unlikely that wave impacts on the overhang occur. It is expected that load cases without wave impacts have no or a minor contribution to the fatigue lifetime damage. This assumption is verified for the case study performed in Section 8.5. All load cases which were filtered based on this criterion did not contribute to the fatigue damage.

8.4.3 FATIGUE DAMAGE ACCUMULATION OVER LIFETIME

The model routine described in Section 8.3 is now employed to predict the response of the gate for each load case with associated representative values $U_{10,i}$ and $h_{S,i}$. This results in a fatigue damage factor D_i for every load case i . The associated probability of occurrence $p(D_i)$ [-] follows from the fitted joint probability density function as discussed in paragraph 8.4.1. The expected lifetime fatigue damage factor D_E [-] then follows from:

$$D_E = T_L \cdot \sum_{i=1}^N p(D_i) \cdot D_i \quad (8.23)$$

in which N is the number of distinct discrete load cases following from the discretization of the joint probability density function. T_L [-] is the total number of load events that occurs during the simulation period, which would generally be the lifetime of the structure. Depending on the chosen load case duration and lifetime this is typically in the order of $10^5 - 10^8$ events. The fatigue lifetime of the structure is the duration for which the accumulation of load events leads to fatigue failure ($D = 1$). This lifetime can be found by gradually increasing the simulation period and the corresponding load events.

Above estimate ignores sampling uncertainty: by random chance rarer events can occur more or less frequently than on average in certain lifetime simulations. For a probabilistic assessment that includes this effect, a Monte Carlo analysis is therefore performed. Here, load cases are sampled independently based on their probability of occurrence. The fatigue D associated with the randomly picked load cases is cumulatively added until failure occurs (at $D = 1$). The Monte Carlo simulation repeats this process a certain number of times. Based on the resulting lifetime distribution, a design value for the fatigue lifetime of the structure can be found by determining the lower 95th percentile (or any other desired confidence level). See paragraph 8.5.3 for an example.

The outcome of this simulation is presented in terms of a probability curve of the fatigue lifetime of the flood. However, the same analysis also provides a prediction of the

failure probability due to fatigue in each year over the lifetime of the structure. This failure probability will naturally increase of the lifetime. Such a prediction may be needed for safety assessments of flood gates.

8.5 CASE STUDY OF WAVE-INDUCED FATIGUE OF A FLOOD GATE

The presented method is now applied to a case to demonstrate its purpose and to analyse the results and their implications. This case is hypothetical but based to some extent on the Afsluitdijk renovation project. The Afsluitdijk is a closure dam in the Netherlands that separates the IJsselmeer lake and the Wadden Sea. The water level of the lake is controlled by the two discharge sluices at Den Oever and Kornwederzand. The discharge sluice at Den Oever is located at the south-western side of the Afsluitdijk is being renovated and expanded at the time of writing. The gates considered in this case study have a geometry comparable to the existing gate, but with somewhat more straightforward supporting beam elements. The gates are required to have a design lifetime of 80 years from 2020 to 2100.

Table 8.1 shows the geometry parameters as defined in Figures 8.1 and 8.2 along with the material properties of the gate. The gate is simply supported at its sides ($x = 0$; $x = W$) and unsupported at the top and bottom ($z = 0$; $z = h_G$). The gate has six vertical stiffeners and seven horizontal ones. The in-vacuo modes of this gate were calculated with an eigenvalue analysis of a parametric SCIA Engineer model. Figure 8.9 shows the normalised maximum principal stress distributions for four modes of interest.

Table 8.1: Geometry parameters (deterministic) of the case study

Symbol	Description	Value	Unit	Symbol	Description	Value	Unit
Geometry				Material			
W	Gate width	10	m	ρ_s	Density of steel	7,850	kg/m ³
h_G	Gate height	7.5	m	E_s	Young's Modulus steel	210	GPa
t_G	Skin plate thickness	0.02	m	f_{yd}	Yield strength	355	MPa
t_v	Vert. stiffener thickness	0.02	m	σ_C	Detail category	100	MPa
t_h	Hor. stiffener thickness	0.02	m	ζ	Damping ratio	0.02	-
L_v	Stiffener length	0.65	m	M_G	Gate mass	22,500	kg
h_f	Flange height	0.2	m				
t_f	Flange thickness	0.02	m				
L_y	Overhang length	1	m				

8.5.1 LOAD EVENT DERIVATION

The Wadden Sea experiences tides in addition to atmospheric water level fluctuations. The Wadden Sea has a complex bathymetry with both shoals barely below the mean sea level and gulleys with a depth of about 25 m. However, for the purpose of predicting the generation of local wind waves it is schematised to have a constant average initial depth of 5 m over a fetch of 30 km (roughly the perpendicular distance to the barrier islands). The water level at the lake is constant with a water depth in the sluice of 4 m. It is assumed that the barrier islands and shoals block swell waves generated in the North Sea from reaching the discharge sluices. Only the waves from the sea side are regarded in this case study.

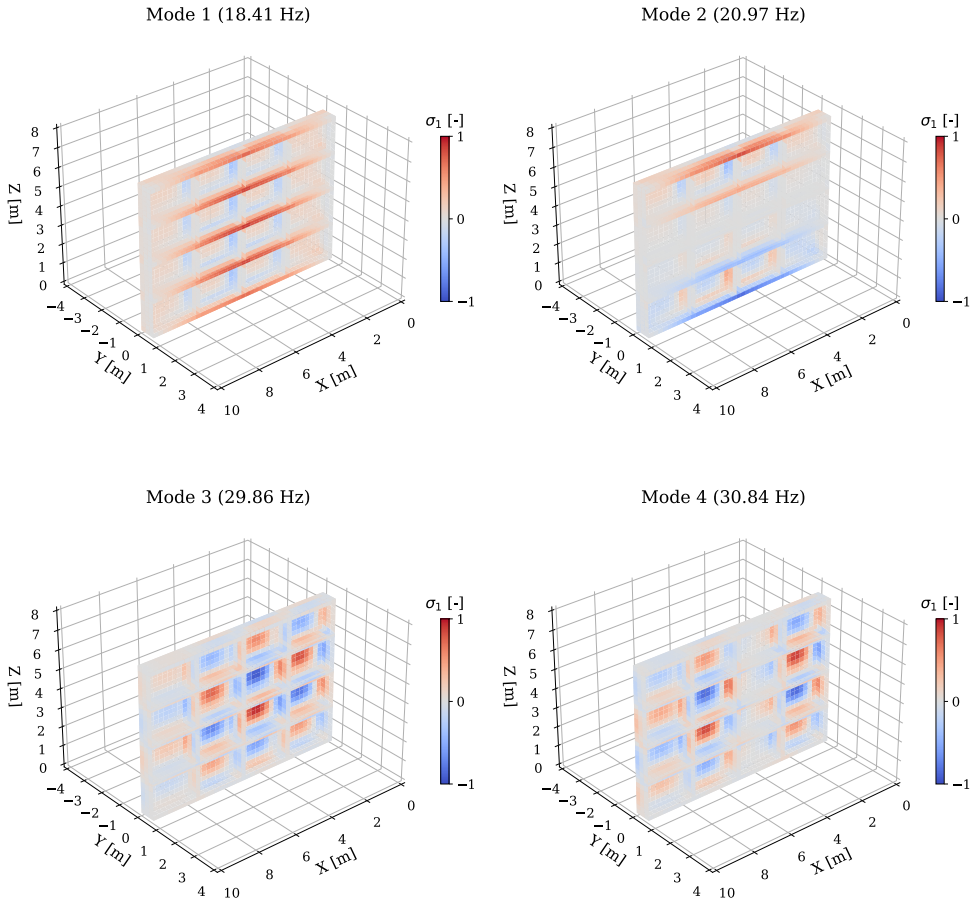


Figure 8.9: Normalised maximum principal stress distributions for four selected in-vacuo modes of the gate

Water level and wind data is obtained from measurement stations operated by Rijkswaterstaat and the Royal Netherlands Meteorological Institute (KNMI). Historical water levels h_S have been measured at the location of sluice complex Den Oever (Rijkswaterstaat, 2020b). Wind data U_{10} is obtained from the measurement station De Kooy, which is located 16.5 km to the west (KNMI, 2020) of the discharge sluice. Both stations have hourly data available over a period of about 50 years (from 1-1-1971 to 1-1-2020).

The correlation between the two data sets is measured with the Pearson correlation coefficient (Pearson, 1895), which can range from -1 (perfect negative linear correlation) to 1 (perfect positive linear correlation). Independent variables will have a value close to zero, though the inverse is not necessarily true.

$$\rho_{h_S, U_{10}} = \frac{\text{cov}(h_S, U_{10})}{\sigma_{h_S} \sigma_{U_{10}}} \quad (8.24)$$

The wind and water data have a positive correlation of 0.158, which is relatively low. Independence of the two parameters is therefore assumed in this case study, though to improve accuracy a correlated copula could be implemented to better represent the historical conditions. Figure 8.10 shows histograms of two variables along with their fitted probability density functions. Based on a least squares analysis a lognormal distribution is found with $\sigma = 0.35$ [-], $\mu = -3.06$ m/s, and $\alpha = 8.34$ m/s:

$$f(U_{10}) = \frac{1}{(U_{10} - \mu) \cdot \sqrt{2\pi\sigma^2}} e^{-\frac{\log(\frac{U_{10}-\mu}{\alpha})^2}{2\sigma^2}} \quad (8.25)$$

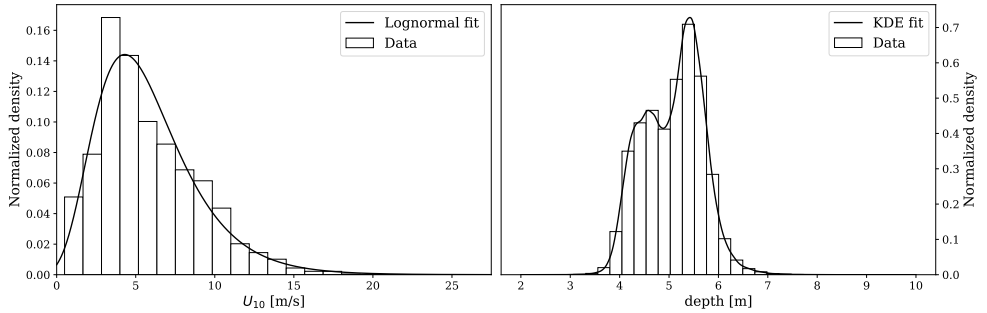


Figure 8.10: Histogram of the historical data h_S and U_{10} and the fitted distributions

The bi-mode shape of the water level distribution caused by the influence of the tides makes a standard distribution fit unsuitable. The water level is therefore modelled by a non-parametric Gaussian Kernel Density Estimate (KDE). Next, the KDE of the water level data is combined with the sea level rise probability distribution according to the method described in paragraph 8.4.1. A climate change scenario of +1 m sea level rise by 2100 is considered, which is the recommended design value according to Klein Tank et al. (2014) for structures along the Dutch coast. It will be modelled as a uniform distribution. The two input distributions and the resulting convoluted distribution are plotted in Figure 8.12.

By applying the previously presented discretisation procedure in total 4480 load cases are obtained. Filtering out the irrelevant load cases based on their probability of occurrence and expected maximum wave height according to Equations 8.21 and 8.22 reduces the amount of load cases by 66% to 1483. For these load cases, the response of the structure is not simulated as no significant contribution to the fatigue damage is expected. Figure 8.11 shows the probability of occurrence of the load cases and the corresponding wave spectrum parameters, and indicates which load cases were filtered out.

Table 8.2: Probabilistic variables used in the case study

Parameter	Symbol	Distribution	Distribution parameters	Unit
Impact peak duration	τ	Triangular	$a = 5; b = 200; c = 75$	ms
Wind velocity	U_{10}	Lognormal	$\sigma = 0.35; \mu = -3.06; \alpha = 8.34$	m/s
Water level measurements	h_s	KDE	Non-parametric fit of data	m
Sea level rise	h_{SLR}	Uniform	$0 \leq h_{SLR} \leq 1$	m
Surface elevation phase shift (per harmonic i)	ϕ_i	Uniform	$0 \leq \phi_i \leq 2\pi$	rad

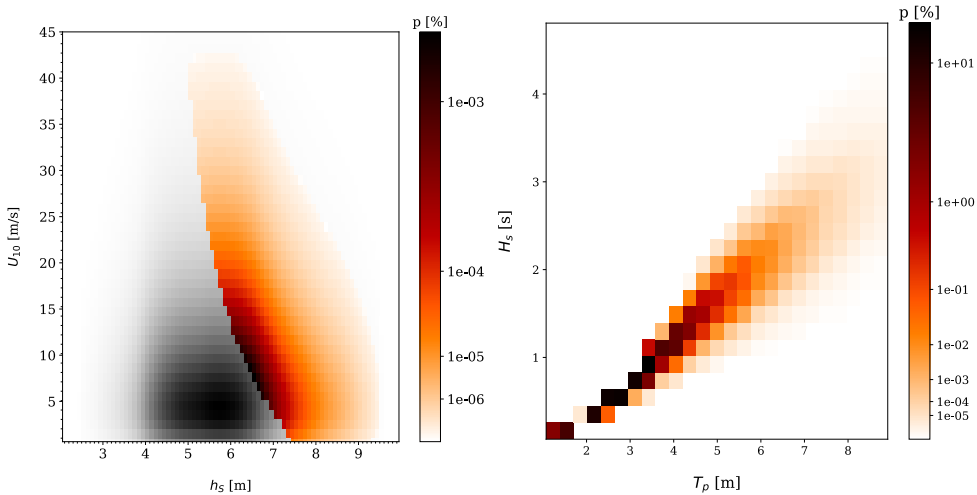


Figure 8.11: Probability of occurrence of the load cases in terms of the wind velocity and water level (left) and the resulting significant wave height and peak period of the remaining load cases (right). The filtered load cases are shown in grey.

8.5.2 FATIGUE DAMAGE DISTRIBUTION

Before proceeding with the lifetime fatigue analysis, the fatigue damage distribution across the gate and the influence of different modes on the final result is discussed. Besides gaining insight in how the structure behaves, identifying which parts of the gate are most strongly affected by fatigue also makes it possible to limit the lifetime fatigue analysis to points of interest rather than the entire surface.

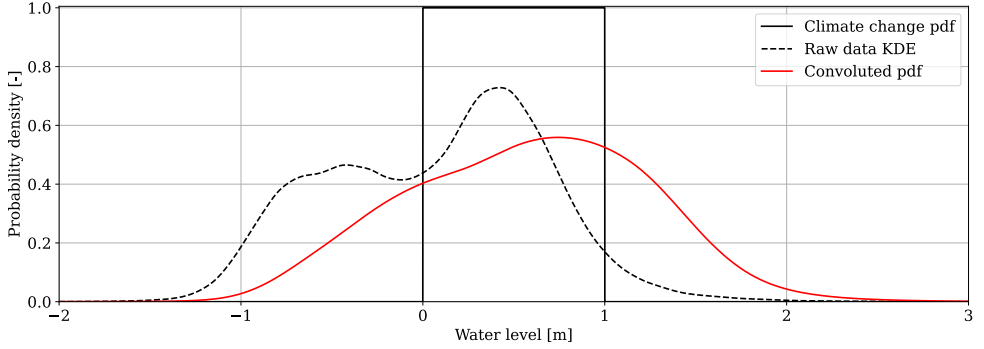


Figure 8.12: Probability density functions of the water level data, a climate change scenario with +1 m sea level rise, and their combined values.

Applying a random hour-long load case to the gate results in a fatigue distribution as shown in Figure 8.13. Due to the asymmetric wave impact shape, the fatigue damage is concentrated at the top and bottom of the middle of the gate. The highest fatigue occurs at coordinate P1 ($x = 5m$; $y = 0.65m$; $z = 7.5m$). The overall distribution suggests a high mobilisation of the second mode from Figure 8.9.

Figure 8.14 shows the relative importance of each mode in the fatigue damage at four points of interest in the gate. The locations of these points were indicated in Figure 8.13. Due to the non-linear relation between stress cycles and fatigue damage, which is logarithmic and includes a cut-off limit, it is not possible to simply simulate the fatigue damage caused by each individual mode. Instead, the ratio R was introduced to measure the relative importance of each mode on the total fatigue damage in each coordinate:

$$R = \frac{D_a - D_{a-m}}{D_a} \quad (8.26)$$

Here, D_a is the fatigue damage factor for a simulation with a modes. D_{a-m} is the fatigue damage factor for the same simulation excluding the response of mode m . Due to the non-linearity of fatigue damage these percentages will not add up to 100%.

The coordinate P1 (5, -0.65, 7.5) was found to be the most heavily loaded part of the gate. The contribution of the second mode is dominant here. The second coordinate, P2 (5, -0.65, 3.75) is located at the centre of the gate. The second mode does not cause significant stresses at this location; virtually all the fatigue damage follows from the first mode. Fatigue damage at coordinate P3 (2.5, -0.65, 3) is dominated by higher modes, especially the seventh and eighth. Finally, P4 (5, -0.65, 0) is located at the bottom middle of the gate and shows a similar pattern as P1.

This result demonstrates the importance of including more than one vibration mode in fatigue analyses of systems similar to the one considered here. The asymmetric load shape over the height and the excitation frequencies of the wave impacts excite higher modes of the gate. At the governing locations, the fatigue damage is dominated by the first and especially second vibration modes. At other locations higher modes were found to be dominant.

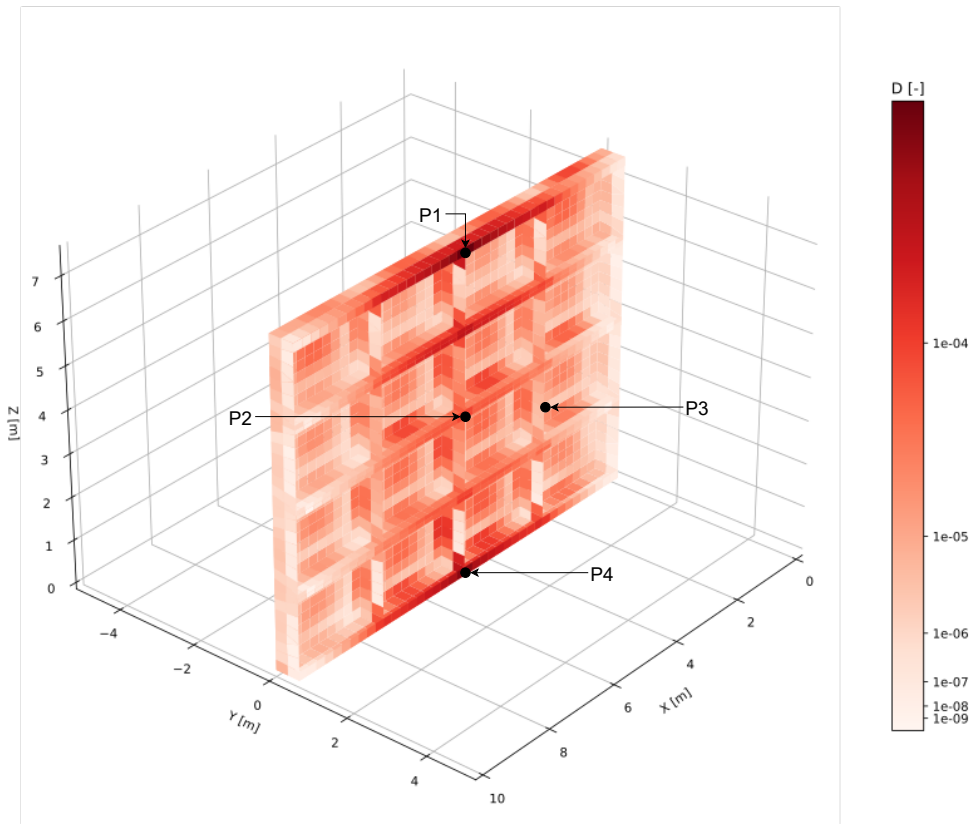


Figure 8.13: D over the surface of the gate after a hour-long load event with $U_{10} = 30$ m/s, $h_S = 7.5$ m, and $h_L = 4$ m. Points of interest are indicated.

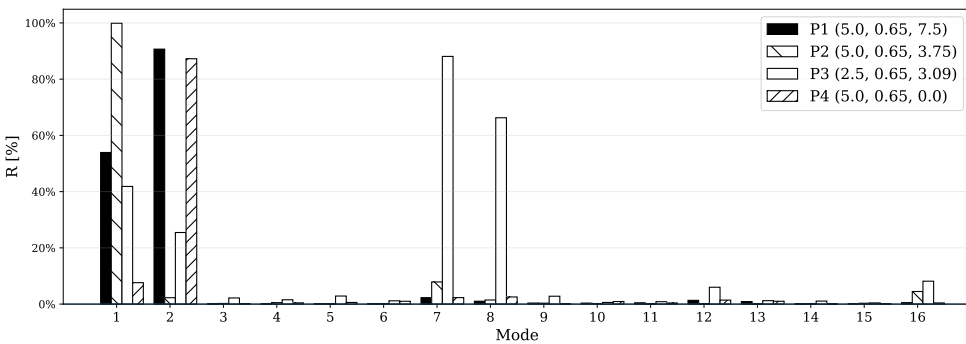


Figure 8.14: Relative importance of the first 16 modes for the fatigue damage at four notable locations.

8.5.3 LIFETIME FATIGUE

The fatigue lifetime analysis described in Section 8.4 is performed to estimate the fatigue lifetime L_D of the gate. This analysis focuses on the most critical point (P1) of the gate identified in the previous paragraph. A Monte Carlo analysis is performed in which the load cases are randomly sampled based on their probability of occurrence until failure occurs (with a maximum simulation period of 100 years). This analysis is repeated 1000 times.

Figure 8.15 shows the resulting accumulation of fatigue damage over time (left) along with the relative importance of the considered load cases (right). The 5th and 95th lower and upper bound of the simulations have been indicated. The distribution in predicted fatigue lifetime can be read along the horizontal line of 100% fatigue damage. The analysis shows that there is a 95% chance that the fatigue lifetime of the gate exceeds 90 years. Vice versa, in the vertical direction, the graph indicates the cumulative failure probability of the gate after a certain time. The probability that the gate has failed due to fatigue after 90 years is approximately 5% and after 98 years approximately 95%. This could also be translated to a failure probability due to fatigue per year, which is often required for safety assessments of flood gates. A higher number of simulations may be desirable to predict minor yearly failure probabilities.

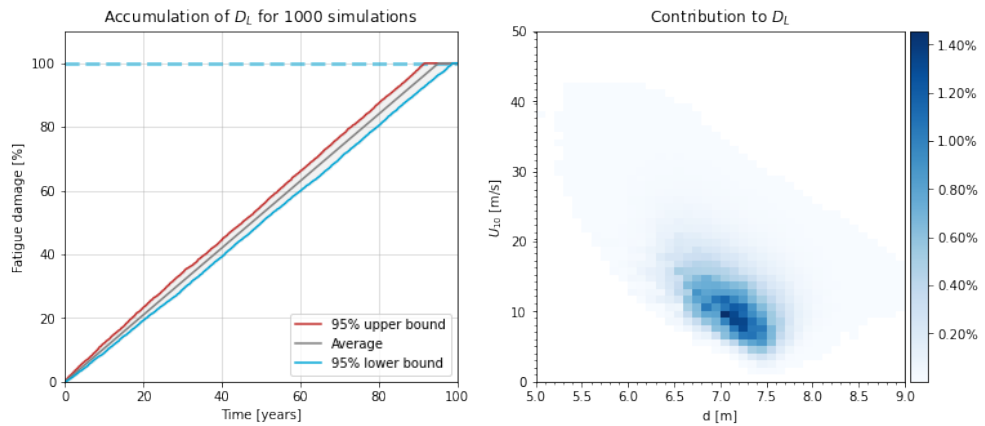


Figure 8.15: Left: Monte Carlo simulations of fatigue accumulation over time. Right: Percentage of total lifetime fatigue damage D_L caused by each load case.

The bandwidth over the simulations is limited. The uncertainty originating from the random phase-amplitude model and the wave impact duration does not lead to a large bandwidth over the high number of load cases and waves over the lifetime over the structure. Sampling uncertainty does lead to some bandwidth: by chance some lifetime simulations will have more or less high-impact events than on average. However, mainly the more commonly occurring load cases with intermediate wave conditions and a water level at the overhang contribute to the fatigue damage. These high frequency of occurrence events lead to less sampling uncertainty than more rare events. Scenario uncertainties like sea level rise could cause larger bandwidths when included in the

analysis. Also, one must note that this analysis only includes the uncertainties on the load side. The uncertainties on the resistance side would lead to a larger and more realistic bandwidth.

Figure 8.15 (right) shows which load cases contributed most to the overall fatigue damage. It stands out that the moderately strong but common load events are much more important than the extreme events. In this case this is likely partly due to the bathymetry of the system which does not allow very large waves to develop.

8.5.4 CONVERGENCE OF THE SOLUTION

Convergence of the solution is discussed both for the number of modes taken into account in the fluid-structure interaction model and the resolution of the load cases considered in the probabilistic fatigue assessment.

CONVERGENCE OF THE FLUID-STRUCTURE RESPONSE

The fluid-structure interaction response model is based on a coupled modal decomposition of the structure and fluid. This solution is exact for the corresponding theoretical formulation of the problem, which is an infinite summation of modes. However, to numerically evaluate the solution, the number of modes should be truncated to a finite number.

Tsouvalas and Metrikine (2016) provides several standard rules for the number of structural modes to take into account. As a rule of thumb, it is sufficient to include all structural mode shapes corresponding to the eigenfrequencies that are up to twice as high as the maximum response frequency of interest. This frequency is not clear-cut in a probabilistic model such as this one however. Convergence of the results for the number of structural mode shapes has been checked in this study by comparing the contribution of higher modes to the total response. Results have sufficiently converged for this case study when the first 16 structural mode shapes are evaluated.

For the fluid modes, Tsouvalas et al. (2015) apply a convergence criterion which matches the obtained amplitude of the displacement of the gate $w_g(x, z)$ [m] with that of the fluid layer at the surface of the gate $w_f(x, y = 0, z)$ [m]. Here, we use a similar method, where we define the average error between the predicted velocity of the gate and the fluid over the interface surface.

$$\delta_u(f) = \left| \frac{\overline{v_g}(x, z, f) - \overline{v_f}(x, y = 0, z, f)}{\overline{v_g}(x, z, f)} \right| \quad (8.27)$$

For the convergence test, the system is excited by a single unit peak load with a relatively short duration (0.05 s) so that a large number of modes is excited. The load is only applied in the upper left quadrant of the gate to excite the anti-symmetric modes over the horizontal as well. The amount of structural modes is kept constant at $k = 16$. The number of fluid modes in the fluid domains in front of the gate are increased from 1 to 225. The results are plotted in Figure 8.16.

Convergence of the results for the number of fluid modes is most critical around a frequency range of 20-25 Hz, where the resonance frequencies of several higher modes are concentrated. The average error $\delta_u(f)$ [-] over all the frequencies falls below 10% with

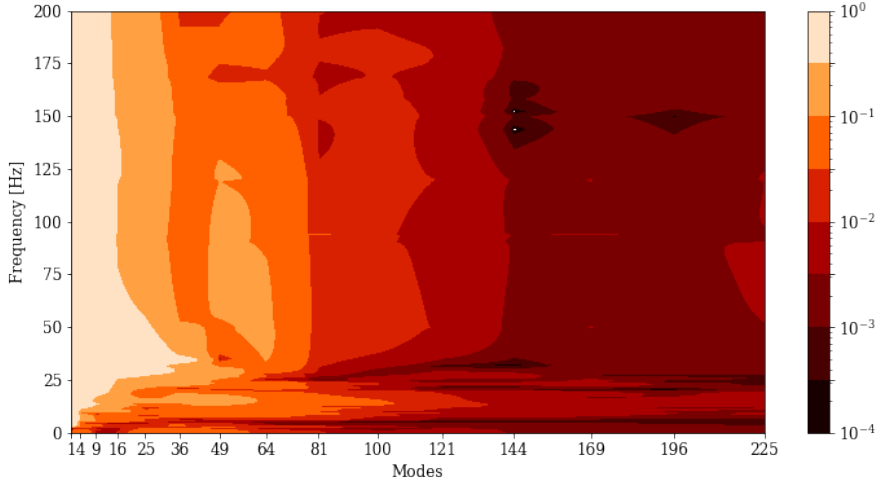


Figure 8.16: The error $\delta_u(f)$ for 1 to 225 fluid modes at a constant number of 16 structural modes.

36 fluid modes and below 1% at 121 fluid modes. A number of 100 fluid modes was chosen, which is deemed sufficiently accurate for the purpose of this case study.

CONVERGENCE FOR THE LOAD CASE RESOLUTION

The historic data in this case study were discretized with a resolution that resulted in 4480 load cases, of which 1066 were included in the fatigue analysis after filtering. Convergence of the solution for this resolution is checked in by varying the bin size according to the routine presented in paragraph 8.4.2. Figure 8.17 shows the standard deviation of the outcome of the fatigue analysis based on random values of h_S and U_{10} in each grid cell versus the chosen representative values.

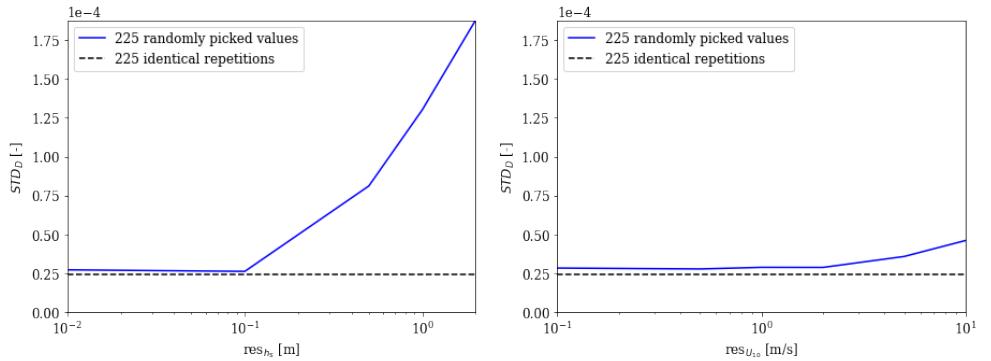


Figure 8.17: Convergence of resolutions to the inherent variance of the model.

As expected, the standard deviation asymptotically approaches a value above zero for increasing resolutions. That value is the variance caused by the random variables within the model, such as the impact duration and randomness of the wave field. For resolutions higher than $\Delta_{hs} = 0.1$ m and $\Delta_{U_{10}} = 1$ the standard deviation of the outcome has converged to this variance. At this point the marginal return in increased accuracy for further narrowing the resolution rapidly diminishes. These resolutions are therefore used in this case study.

8.5.5 COMPARISON WITH METHODS PRESENTLY USED IN ENGINEERING PRACTICE

Presently in engineering practice, the wave climate over the lifetime of the gate is often characterised by a limited set of design storms with defined return periods and significant wave heights. The frequency of different wave heights within such a storm is derived from (modified) Rayleigh distributions like those described in Battjes and Groenendijk (2000). The structural response to each wave is then evaluated individually. The theory of Kolkman and Jongeling (2007a,b) is generally employed for this purpose, which is based on a quasi-static evaluation of the structural stresses. A dynamic amplification factor is then applied to account for dynamic behaviour based on a single degree of freedom (SDOF) representation of the structure. Finally, the fatigue response per individual wave is summed proportional to their probability of occurrence to find the total fatigue damage experienced by the gate during a particular storm.

The presented design method improves on this existing method on several aspects. The response of the structure is explicitly simulated for all load cases relevant to the fatigue lifetime. It is not necessary to simplify the analysis to a limited set of design storms. Furthermore a novel semi-analytical fluid-structure interaction model is employed (Tieleman et al., 2022b) to determine the multi-modal dynamic response of the flood gate in water, rather than a SDOF representation. The following paragraphs investigate the effect of the two above mentioned aspects of the presented design method based on the parameters defined in the case study.

CONSECUTIVE VERSUS INDIVIDUAL WAVES

To investigate the effect of interfering vibrations due to consecutive wave impacts, a comparison will be made between two approaches. First, a random wave state is generated and the individual wave impacts are identified. The sequence of impact velocities is then used to evaluate the response to each impact individually. The structural response to the individual waves will be allowed to fully damp out. In the second analysis the response is derived for the full (identical) time series following the method described in this chapter. Quasi-steady wave fluctuations are ignored in both cases. The fatigue damage of all the isolated waves is summed up and compared to the fatigue damage caused by the time series with consecutive waves. Figure 8.18 gives an example of the structural response of the gate for both analyses.

In the long term, vibrations due to consecutive waves should reinforce and cancel each other out equally often due to their random phase. However, because fatigue damage is logarithmic rather than linearly proportional to the magnitude of stress variations, this does not mean that the impact on the fatigue of the gate will be averaged out as well.

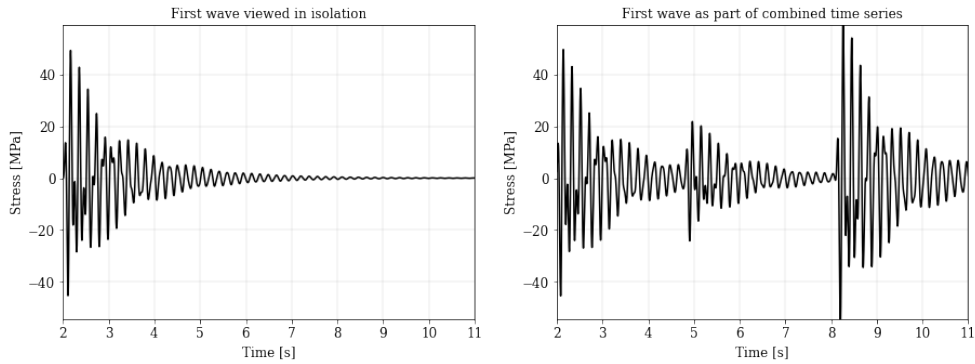


Figure 8.18: The stress response of the gate when a wave is isolated and allowed to damp out vs. the response to the full time series.

The increased fatigue damage from constructively interfering vibrations is larger than the decrease in fatigue due to destructively interfering vibrations.

The effect is stronger when waves follow each other in short succession, where the vibrating gate does not have the time to damp out before the next wave arrives. This suggests a dependence on the mean water level, because if the mean water level h_S is equal to the overhang height h_G virtually every wave will cause an impact. In contrast, wave impacts will be more sporadic when the mean water level is significantly lower. To account for this effect the comparison is repeated for different combinations of environmental conditions. Table 8.3 shows the ratio D_{iso}/D_{full} , where D_{iso} is the predicted fatigue damage by modelling isolated waves and D_{full} the fatigue damage resulting from the entire time series with consecutive wave impacts.

Table 8.3: Average D_{iso}/D_{full} of 15 repetitions for various environmental conditions. The empty cells represent cases where all stress cycles fall below the cut-off limit.

U_{10} [m/s]	h_S [m]						
	$h_G-1.5$	h_G-1	$h_G-0.5$	h_G	$h_G+0.5$	h_G+1	$h_G+1.5$
10	-	82%	81%	78%	79%	82%	-
40	84%	84%	83%	83%	83%	84%	84%

From these results, it follows that the effect of waves reinforcing each other can be very significant. On average the fatigue damage is underestimated by about 18% in these simulations when regarding the response to individual waves. Fatigue analyses of similar systems which regard each wave in isolation therefore risk underestimating the fatigue damage of the structure.

The relative error is slightly higher for lower wind velocities, as these lead to wave spectrum with shorter wave periods and thus less time for vibrations to damp out in between wave impacts. The water level may have some influence on the fluid damping due to surface waves and compressibility. However, this type of damping is usually insignificant for the water levels and vibration frequencies involved with these types of

problems as was discussed in Tieleman et al. (2019a). The relative error therefore shows no clear dependence on the water level.

A relatively high isotropic damping factor ($\eta = 0.02$) was applied in this study. For cases with lower isotropic damping factors the effect of interference due to consecutive impacts is likely to be stronger.

MULTIPLE VERSUS SINGLE DEGREE OF FREEDOM RESPONSE MODEL

The theory of Kolkman and Jongeling (2007a,b) is often employed in practice to determine the response of flood gates for wave impacts. A key element of this approach is that the structural stress distribution over the gate is predicted quasi-statically for the wave impact peak load. A dynamic amplification factor (DAF) is then applied to this stress field to correct for the dynamic behaviour of the structure. This amplification factor is based on a single degree of freedom (SDOF) representation of the structure, whereas the model routine presented in this chapter accounts for multiple degrees of freedom (MDOF) of the gate. Hydrodynamic coefficients or non-dimensionalised added virtual mass incremental factors (Kwak and Kim, 1991; Kwak, 1996) are applied to account for the influence of the fluid.

Several variants of this approach exist. In some cases, only one stress cycle per wave impact is accounted for. The DAF then is a constant for each impact. More advanced analyses do take into account multiple vibrations after each impact by applying a time-varying DAF based on the time response of the single degree of freedom system after each impact. In this analysis, the DAF approach is approximated as follows. First, the full semi-analytical model is used to determine the normalised quasi-static response of the gate to a wave impact peak load. This results in a set of modal coefficients of the gate $A_{k,qs}$ and distributions for each directional stress component $\sigma_{qs,jj}$. Then, the semi-analytical fluid-structure interaction model is applied with only a single structural mode shape to predict the response for a random hour-long load case. The model implicitly includes the hydrodynamic response. This is the same as applying relatively precisely determined hydrodynamic coefficients. This results in a single time domain response signal in terms of the modal coefficient $A_{1,dyn}(t)$. The DAF is then determined by:

$$DAF(t) = \frac{A_{1,dyn}(t)}{A_{1,qs}} \quad (8.28)$$

and subsequently applied to the stress fields corresponding to the quasi-static response as follows:

$$\sigma_{DAF,jj}(t) = DAF(t) \cdot \sigma_{qs,jj} \quad (8.29)$$

The results of the presented design method are compared to this DAF approach. Quasi-steady wave fluctuations are again ignored. The analysis is performed using the DAF approach both for individual and consecutive waves (see paragraph 8.5.5). Based on Figure 8.14, it is expected that a DAF approach based on a single degree of freedom representation of the structure will significantly distort the fatigue damage. Table 8.4 shows the fatigue damage predicted by the semi-analytic approach D_{SA} (which takes higher modes into account), and the fatigue damage predicted by the DAF approach

Table 8.4: Fatigue damage at points of interest on the gate for different methods. Normalised to MDOF results.

Model approach	P1 (5, -0.65, 7.5)	P2 (5, -0.65, 3.75)	P3 (2.5, -0.65, 3)	P4 (5, -0.65, 0)
MDOF (consecutive waves)	100%	100%	100%	100%
DAF (consecutive waves)	121%	147%	0%	0.1%
DAF (individual waves)	111%	133%	0%	0.05%

D_{DAF} (for both consecutive and individually evaluated waves). The locations on the gate correspond to those defined in paragraph 8.5.2.

The DAF approach predicts more fatigue damage at the critical point P1 at the top of the gate and the centre of the gate (P2). Because the quasi-static response to a confined wave impact mainly affects the top middle of the gate, this approach concentrates all energy in this area (See Figure 8.19). Conversely, this different distribution means that the stresses predicted by the DAF method in points P3 and P4 fall almost entirely below the cut-off limit and therefore barely cause any fatigue damage. The presented design method does predict fatigue damage for location P3 en P4 dominated by the seventh and second mode respectively. The difference at P4 is especially noteworthy, as Figure 8.13 demonstrates that significant fatigue will occur here due to second-mode vibrations. For comparison, Figure 8.19 shows the fatigue damage over the entire gate for the DAF approach. The fatigue damage predicted the DAF approach roughly follows the shape of the wave impact pressure over the height, while the fatigue damage predicted by the presented design method is governed by the actual dynamic behaviour of the gate.

Combining the DAF approach with the effect of considering all waves in isolation (as in paragraph 8.5.5) follows the same pattern, but underestimates the response everywhere by omitting the influence of wave reinforcement.

8.6 DISCUSSION

Several key assumptions and potential improvements of the presented design method are discussed in this section. First of all, all waves were considered to approach the flood gate perpendicularly in this study. Perpendicular waves lead to the highest wave impact loads. Accounting for non-perpendicular waves therefore would result in lower overall forces on the gate. However, the resulting loads are non-uniformly distributed over the width of the gate and will therefore excite anti-symmetric modes. This may result in local stress concentrations that differ from the case with perpendicular waves. The response model is fully capable of predicting the response to uniform wave loads. Given a suitable theory to predict non-uniform wave impact loads, the model routine can therefore be adapted relatively straightforwardly to include non-perpendicular waves. For example, De Almeida and Hofland (2021) describe the effects of oblique wave attack in a flume.

Furthermore, a linear wave theory was applied in this chapter to predict the surface elevation time series and resulting wave impact velocities and quasi-steady wave pressures. Especially in shallow waters, waves exhibit non-linear behaviour with steeper peaks and flatter troughs. This leads on average to higher wave impact velocities and thus a shorter fatigue life than what would be predicted based on linear wave theory. To increase the applicability range of the design method, a higher wave order theory could be applied relatively straightforward within the model routine. Sobey (2009) proposes

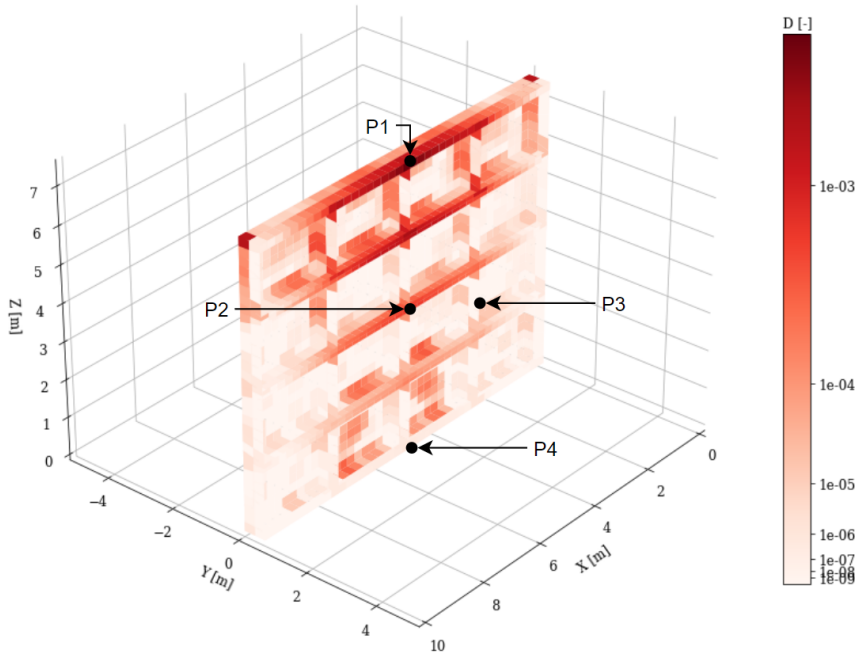


Figure 8.19: D_{DAF} over the surface of the gate after a hour-long load event with $U_{10} = 35$ m/s, $h_S = 7.5$ m, and $h_L = 4$ m. Points of interest indicated.

analytical solutions up to the fifth order. However, based on criteria from Hedges (1995), De Almeida and Hofland (2020b) found that for the largest impacts around the waterline the impact velocities obtained from linear wave theory match non-linear theory well.

Another source of non-linearity can be the presence of entrapped air under the overhang during wave impacts. This may effectively lead to longer impact durations. Research on this topic is ongoing based on the experimental results from De Almeida et al. (2019); De Almeida and Hofland (2020b). Possible ways of accounting for this in the model include adding the air as a separate domain, or modelling the overhang with a certain spring stiffness. On a related note, an effective measure to reduce impact pressures is the application of a ventilation hole. Hofland et al. (2019) showed how this measure can be included in the model to predict impulsive impact pressures. Such a measure would also reduce the presence of air under the overhang during an impact.

Air bubbles in the water column also have an effect on the fluid response to the gate motion. Air bubbles can significantly decrease the sound velocity in the water in front of the gate (Bullock et al., 2007). The sound velocity of water is around $c_p = 1500$ m/s, but could drop as low as 150 m/s for a water-air mixture with 1% air (Gibson, 1970). This may lead to lower resonance frequencies of the fluid due to compressibility and therefore alter the fluid response. Acoustic damping may become more significant as well. Trial runs for the extreme case where $c_p = 150$ m/s suggest the fatigue damage could decrease as much as 50%. To investigate the actual effect on the fatigue assessment a sensitivity analysis

could be performed for various levels of air bubbles, and thus sound velocities, extending over various distances from the gate. The dependence between wave properties and air entrapment could also influence the impact duration. Research on this topic based on the results by De Almeida and Hofland (2021) is still ongoing.

The probability density function of the mean water level and wind velocity have been derived with basic curve fitting methods, as this is not the main focus of this study. A relatively straightforward improvement would be to evaluate the correlation in the upper tail of the probability density function separately, because rare high-impact events are more likely to be correlated than day-to-day water depth and wave statistics. This correlation would likely lead to the prediction of a slightly lower fatigue lifetime, although the fatigue was found to mainly depend on frequent loads. The taken approach is thus conservative. Additionally, a more rigorous estimate based on climate modelling and an improved wave transformation computation based on a realistic bathymetry such as by Groeneweg et al. (2009) is recommended for application in more advanced design stages.

Finally it is noted that although this study focuses on confined wave impacts on an overhang, the presented design method may also be applied for example to breaking wave impacts. An alternative model should then be applied to predict the impulsive part of the wave load. Such theoretical models do exist for breaking wave impacts (Bagnold, 1939; Minikin, 1950; Takashi, 1994; Oumeraci et al., 2001; Cuomo et al., 2010).

8.7 CONCLUSIONS

A novel design approach has been presented to predict the expected fatigue lifetime of a flood gate subjected to confined dynamic wave impacts. The design method takes into account the entire joint probability function of the wind velocity and mean water level based on historical data including an adjustment for sea level rise. This probability function is then translated to a set of discrete load cases and an associated probability of occurrence. A method was suggested to determine the optimal size of this discretization by minimising the internal variance of each interval. Impulse theory is used to predict the wave impact pressures for each load case. The dynamic response of the flood gate is predicted by the fluid-structure interaction developed in this dissertation. The computational efficiency of this semi-analytical model facilitates a much larger number of simulations compared to numerical alternatives. The applied model routine is modular and therefore adaptable to many different situations. The probabilistic approach in this study is simplified, for example by omitting uncertainties on the resistance side. However, the developed model routine is also expected to be applicable within more sophisticated reliability analyses.

The presented design method has been applied to a case study inspired by the situation of the Afsluitdijk in the Netherlands. It was demonstrated that the method is effective in assessing the fatigue accumulation over the lifetime of the gate. For the investigated case with a shallow sea, the mid-sized but common load events were shown to contribute more to the fatigue lifetime than rare events. Furthermore, the non-uniform pressure distribution and excitation frequencies of the wave impacts result in significant higher mode vibrations of the gate. A breakdown of the contribution of the different response modes showed that higher modes have a high contribution to the

fatigue damage in many areas of the gate, including the governing location.

The outcome of the presented method was compared to the dynamic amplification factor (DAF) approach presently used in practice. The DAF approach is based on a single degree of freedom representation of the structure and usually regards the response to individual waves rather than consecutive waves in a design storm. It was shown that the existing design method does not accurately predict the distribution of fatigue damage of the gate. At some points this caused an overestimation of the stresses, while at others it lead to a significant underestimation of the critical fatigue load. This shows that the DAF approach is questionable when the gate response shows a clear participation of higher eigenmodes. Moreover, neglecting the reinforcement effect of vibrations caused by consecutive waves leads to an underestimation of the fatigue damage. The design method presented in this chapter is therefore a significant improvement on existing methods in terms of accuracy, without compromising on computational efficiency.



9

DISCUSSION

This chapter presents a discussion of the results of this thesis. Section 9.1 discusses the key assumptions and relevant phenomena regarding the validity of the developed model and design methods. The validity is elaborated from the perspective of the predictive capabilities of the developed modelling framework. Section 9.2 focuses on the applicability and implementation of these methods from a more broad perspective. Several possibilities for improvement and further research are explored.

9.1 VALIDITY OF THE DEVELOPED METHODS

The following topics are discussed regarding validity of the developed methods: i) interaction between the structure and wave impacts, ii) slack in the gate supports, iii) the influence of air, iv) uncertainties of the responsive system in the probabilistic methods and v) non-linear behaviour of the system.

INTERACTION BETWEEN THE STRUCTURE AND WAVE IMPACT

A model approach has been employed in which the wave impact load is predicted independently from the motion of the flood gate. Pressure impulse theory (Cooker and Peregrine, 1995; De Almeida and Hofland, 2020b) is employed to predict the wave impact load based on a static representation geometry. This impact load is then applied as an external excitation force in the fluid-structure interaction response model. The generation of surface waves due to the motion of the gate is accounted for in the developed method. However, the influence of the incoming wave on the still water level is not accounted for. The interaction of the gate with the surrounding fluid assumes the still water levels on both sides of the gate. The wave impact loads occur over a much shorter period than the wave period of the incoming waves. A separation of the impact process from the water level variation due to the incoming waves is therefore expected to be acceptable to some extent. Hofland et al. (2019) also showed that the water level is almost horizontal during the duration of the wave impact. However, the trailing vibrations after the wave impact may be affected by the change in water level due to the incoming waves. Furthermore, local interaction processes between the wave impact and the motion of the gate may influence the impact force in ways not accounted for in the model. This leads to some uncertainty in the predictions.

The performed scale experiments provide the opportunity to further analyse these detailed interaction processes and reduce this uncertainty. A first comparison was made between the model predictions and the measurements of the dynamic response of a flood gate under regular wave impact loading, which indicated that the developed model is able to predict the dynamic response quite well and this effect may thus be limited. However, this may turn not to be the case when the gate is thinner and or the wave impact alters. Thus, the validity of this assumption needs further investigation. Also research from the field of maritime engineering may provide methods to study the interaction between wave impacts and flexible structures on a more local level. Korobkin (1998); Korobkin and Khabakhpasheva (2006) have for instance studied wave impacts on flexible beams and plates based on the Wagner approach (Wagner, 1932) accounting for the change in shape of the wave during the impact.

On a related note, the prediction of the wave impact velocity and the quasi-steady wave pressures may also be improved by application of higher order wave theories in the

presented design methods. De Almeida and Hofland (2020b) have shown that for water levels at the overhang the impact velocity is predicted well by linear wave theory. For other water levels, higher order wave theories are recommended. Where the local geometry of the structure has a large influence on the incoming waves, computational fluid dynamics simulations may be performed to obtain a more accurate prediction.

SLACK IN THE GATE SUPPORTS

This thesis focused on flood gates with common boundary conditions. The edges of the gate were either assumed clamped, simply supported or free. This matches the way of modelling generally applied in engineering. In practice, various types of supports exist. The developed fluid-structure interaction model is suitable for any type of time-independent boundary condition. Supports of vertical lifting gates such as guiding wheels and sliding supports can in principle be incorporated in the finite element model that is employed to obtain the modal information of the in vacuo gate. However, in some cases the gate sides are situated in recesses in surrounding structure with some slack between the gate and the supports. The possibility of allowing slack in the supports has also been considered for the newly designed gates for the existing discharge sluices in the Afsluitdijk.

The hydrostatic force in those cases initially pushes the flood gate to one side of the recesses. When the wave impact is sufficiently dominant, the gate can be pushed off the supports by the wave impact and hit the supports at the other side, either directly or after a bounce back from the initial response to the wave impact. Figure 9.1 gives a schematic overview of the latter situation with bounce back.

Due to this behaviour, the boundary conditions for the gate become time-dependent. This situation can therefore not be predicted straightforwardly with the developed fluid-structure interaction model. It is recommended to study the behaviour of the flood gate with this type of supports first with a time domain model. Prototype measurements of the existing gate in the Afsluitdijk have been performed in the part by Waterloopkundig Laboratorium (1990), which may provide some data for further research. The results can give an indication to what extent it might be feasible to represent this situation with an adjusted version of the developed fluid-structure interaction model, for instance by modelling a second impact at the supports of the gate.

When possible, it is recommended to avoid slack in the supports of flood gates under wave impact loading. The steel on concrete impacts may lead to high local stresses in the structure. And even with approaches above, the prediction of the behaviour of the immersed gate has a high uncertainty.

THE INFLUENCE OF AIR

The developed model accounts for the interaction between the structure and the surrounding water. However, there are several different phenomena related to the presence of air that could influence the response of the system. First, studies have shown that during wave impacts entrapped air may be present under the overhang depending on the type of impact (De Almeida and Hofland, 2021). This air pocket can undergo vibrations during the impact due to its compressibility (Ramkema, 1978). Research on this topic is ongoing based on the experimental results of (De Almeida and Hofland, 2021). The performed scale experiments in this thesis indicate that the developed model can predict

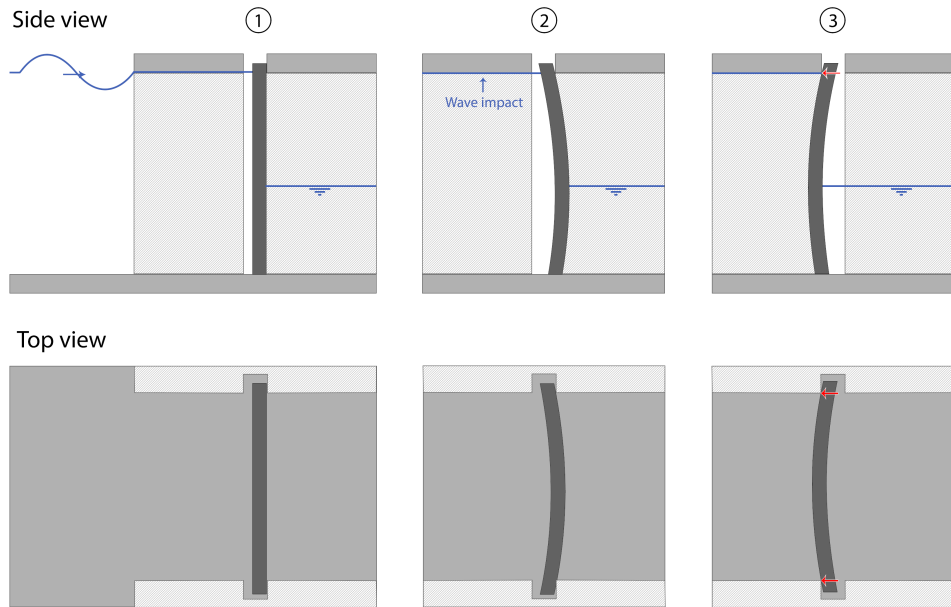


Figure 9.1: Schematic overview of the movement of the gate through the recesses after a wave impact from the high water level side. In the third phase the gate bounces back. At that point secondary impacts of the gate on the concrete structure at the supports can occur, indicated with red arrows.

the dynamic response of a flood gate well for both wave impacts with and without air, as long as the presence of air is accounted for in the wave loading. However, this should be verified in full scale experiments, as the elasticity of air becomes more relevant for larger scales. One hypothesis is that the air pocket effectively only leads to a longer impact duration. Although the effect of air can then have quite a large effect on the peak force, the wave impulse is not affected. Moreover, the effect of air could then be accounted for straightforwardly in the distribution of the impact duration applied in the pressure impulse model of the presented probabilistic design method. However, it might also turn out to be necessary to account for the dynamic behaviour of the air pocket explicitly in the prediction of the response of the system. Another domain or possibly a spring boundary condition at the overhang could then be introduced in the developed model. It is recommended to at least incorporate the uncertainty regarding the effect of air on the impact duration in the probabilistic approaches presented in Chapters 7 and 8. This will also provide an indication of the impact of this uncertainty on the outcome of the safety and fatigue assessments.

On a related note, an effective measure to reduce impact pressures is the application of a ventilation hole, which would also reduce the presence of air under the overhang during an impact. Hofland et al. (2019) showed how the effect of such a measure can be included in the model to predict impulsive impact pressures. A ventilation gap directly between the overhang and the gate with a length of a fifth of the overhang may

already reduce the impact impulse on the gate by 70–95% depending on the height of the overhang.

Also air bubbles in the water column could have an effect on the fluid response to the gate motion. The presence of air bubbles significantly decreases the sound velocity in the water in front of the gate (Bullock et al., 2007). The sound velocity of pure water is around $c_p = 1500$ m/s. This value has been implemented in the case studies throughout the thesis. However, the sound velocity could drop as low as 150 m/s for a water-air mixture with 1% air (Gibson, 1970). This may lead to lower resonance frequencies of the fluid due to compressibility and therefore alter the fluid response. Acoustic damping will become more significant as well, although a large effect on the system is still not expected. A brief sensitivity analysis showed that the sound velocity of the surrounding fluid may also affect the fatigue induced by wave impacts. However, it is not known yet how much air entrainment can be expected in the water column at various distances from the gate during wave impact loading. Experiments or prototype measurements are required to investigate this.

UNCERTAINTIES OF THE RESPONSIVE SYSTEM IN THE PROBABILISTIC METHODS

The probabilistic methods presented in this thesis incorporated the distributions of the most relevant parameters in the prediction of the wave impact loading on the flood gate. Peak pressures and impact durations show large variations for waves with very similar characteristics due to random local perturbations. Wave impacts are therefore expected to be the main contributor to uncertainty in the outcome of the safety and fatigue analyses. Nevertheless, also the structural and fluid properties of the responsive system involve uncertainty that will affect the reliability of the flood gate. This could for instance entail uncertainty in the amount of damping, geometric dimensions of the structure and the yield strength. These parameters are yet included deterministically in the presented methods. Another uncertainty is the effect of sea level rise on water levels. This uncertainty is incorporated in the design method for fatigue assessments, but may also be included in the probabilistic safety assessment. Finally, also the model uncertainty itself could be included in these methods. By including all relevant stochastic variables in the probabilistic methods, it becomes possible to analyse which source of uncertainty contributes most to the overall outcome of the reliability analyses. These are the uncertainties that should be focused on in further research.

The amount of damping in the system is expected to come forward as the most important stochastic variable from such an analysis for two reasons. First, the amount of damping in the system has proved to have a significant impact on the outcome of the safety and fatigue analyses performed in this thesis, especially since the compound effect of vibrations due to consecutive wave impacts has shown to be relevant (see Chapter 7 and 8). Second, the amount of total damping in the responsive system has proved difficult to predict. Damping due to compressibility of the fluid and surface waves is part of the developed model. Chapter 6 showed this type of damping is often negligible for the frequencies and water depths involved with the problem considered in this thesis, at least for water without entrained air ($c_p = 1500$ m/s). A material damping factor was also included in the model. This type of damping can be predicted relatively well. The theoretical prediction of the total amount of damping originating from various sources in

the structure and fluid, such as friction in joints, turbulence in the fluid, air entrapment in the fluid or heat transfer, is much more uncertain however. The damping from these sources may therefore in practice need to be determined experimentally. When the amount of damping is known, plenty of methods are available to model various types of damping for fluid-structure interaction problems. An overview is for example given by Adhikari (2000). Also during the design of the flood gates for the Afsluitdijk, the amount of damping has been a topic of discussion. The experiments showed that likely more damping may be expected in these type of problems than applied in the case studies in this thesis. Further analysis of the experimental data in this thesis may provide more insights in the amount of damping that can be expected. However, the experimental setup concerns a simplification of the real structure focused on validating the fluid-structure interaction process. One aspects that may be relevant for damping in real structures may for instance be the interaction between the fluid and the subsoil. Prototype measurements of the dynamic response (displacements, accelerations or strains) of flood gates under wave impacts are therefore preferred. The Afsluitdijk provides an interesting opportunity for such measurements.

NON-LINEAR BEHAVIOUR OF THE SYSTEM

The developed semi-analytical model is based on linear dynamics of the structure and fluid. It provides a solution in the frequency domain. Results showed to be in good agreement with the results of a conventional non-linear time domain finite element model (COMSOL). However, it was not studied explicitly to what extent non-linear dynamics can play a role for certain gate designs or fluid domain geometries and water levels.

Non-linearity may originate from complex interactions between the wave impact or the non-linear elasticity of air on large scales. Non-linearity can also originate from the fluid response, which has been linearised in the model. It is therefore recommended to study to what extend non-linearity may influence the governing response of flood gates under wave impacts. Furthermore, when one wants to include the plastic behaviour of the gate in the analysis, this leads to non-linearity. Rijkswaterstaat however applies the yield stress as a critical design limit for flood gates in the Netherlands, thus avoid plastic deformations.

As a first step, the outcome of the developed model could be compared more extensively to the conventional non-linear finite element models that also explicitly model the incoming wave motion and impact on the structure for various geometries. However, the prediction of these phenomena with finite element models also knows large uncertainties. Experimental studies may therefore be necessary.

When non-linearities prove significant, a coupled modal analysis may still be applied to solve the fluid-structure interaction of the gate-fluid system. However, this analysis must then be performed in the time domain. This has an impact on the numerical efficiency of the model. Kwak (1996), Amabili and Kwak (1996); Amabili et al. (1996) have for instance applied the Rayleigh-Ritz method to rectangular, circular, and annular plates in fluid.

9.2 OTHER APPLICATIONS AND IMPLEMENTATION

A fluid-structure interaction model was developed to predict the vibrations of a flood gate. The employed method of solution was shown to solve the fluid-structure interaction much more efficiently than coupled finite element models. On the other hand, finite element models have a very wide applicability range, while the analytical solution of the developed fluid-structure interaction model is derived for a specific situation. The applicability of this model therefore has its limitations. The most important applications and limitations are discussed. Also the implementation of the methods in engineering practice is explored.

APPLICATION FIELDS OF THE DEVELOPED METHODS

The developed model is primarily aimed at predicting the dynamic behaviour of a vertical flood gate situated in a discharge sluice. The model accounts for the presence of an overhang causing confined wave impacts. The case studies in this thesis were inspired by the situation at the Afsluitdijk, both the existing and to be built discharge sluices. Many similar hydraulic structures with vertical gates and an overhang exist however. Many of these hydraulic structures also border a discharge sluice or canal with limited width.

The applied method of solution in the model can also be suitable for other types of gates and situations. That mainly depends on the geometry of the fluid domain and the interface between the gate and the fluid. The motion of the fluid is solved analytically. This is one of the reasons the method is computationally efficient. However, it also means that the applicability of this method is limited to relatively straightforward fluid and interface geometries. The sector gates of the Haringvlietsluizen (NL) for instance have relatively flat vertical surface when in closed position and thus in contact with the water. Sliding gates of locks, such as in the sea lock IJmuiden (NL), are also an interesting type of application of the developed model. The developed methods may be applied to such cases relatively straightforwardly. In contrast, gates such as the Maeslant Barrier (NL) have a complete different shape. Moreover, mostly vertical vibrations of the arms of the Maeslant Barrier in floating position have shown to be relevant (Kolkman and Jongeling, 2007a). The interface with the fluid therefore differs strongly from the cases investigated in this thesis. Also for such a situation it may still be possible to derive an analytical solution of the interaction of these gates with the surrounding for this case by introducing geometrical simplifications. The more global dynamic behaviour of the system is expected to generally be governing. More straightforward schematisations may therefore still lead to acceptable results for some of such cases. The same applies to complex bathymetries. Wave propagation models used to deduce the hydraulic boundary conditions may include such bathymetries in detail. For the hydrodynamic response during vibrations, simplifications may be acceptable however. This should be verified for the specifics of the case of interest.

The examples of structures in the first chapter show various sluice lengths and shapes. Moreover, some are located in an inlet of limited width while others directly border a wide lake or sea. The applied method of solution can in principle deal with all of such fluid geometries. However, for situations where the discharge sluice is very short, or for example only pillars present, and the adjacent fluid body is very wide, a specific analytical solution should be derived to obtain the mode shapes of the fluid. A wave radiation

condition could in that case be employed to deal with domains that have to be modelled as infinite in multiple direction.

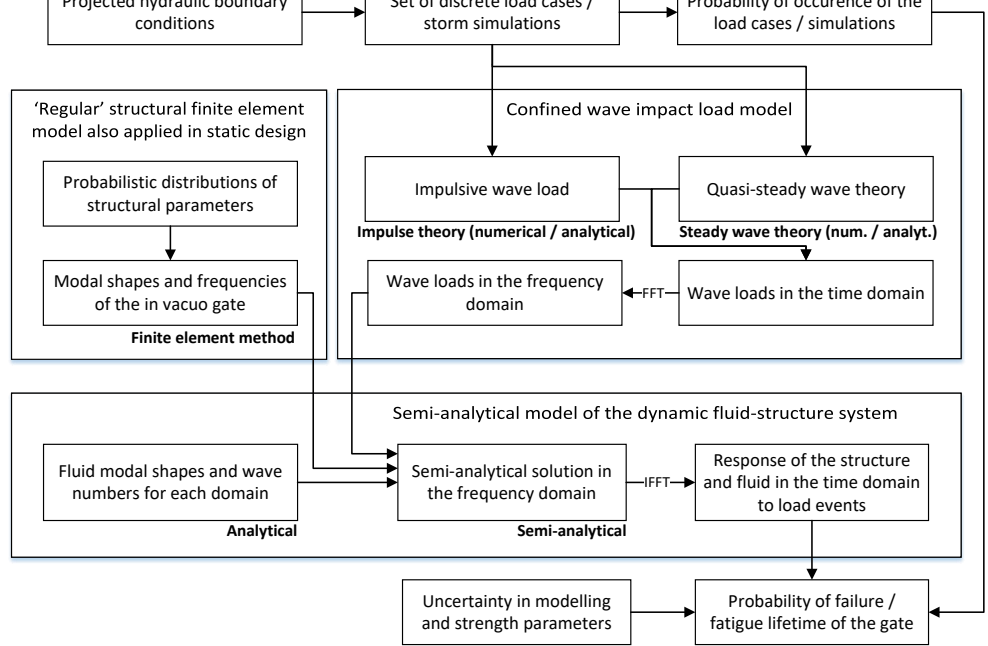
Furthermore, it is noted that the developed model can deal with any external excitation force that is not a function of the dynamic response of the system. The presented design methods are specifically aimed at flood gate vibrations induced by confined wave impacts. Also the case of breaking wave impacts has been considered in the case study in Chapter 2. Applications with other types of loads are also possible. Also debris impacts may for instance give a dynamic response of gates. This method of solution has also been applied to predict vibrations of a pump gate (Tieleman, 2016), which is a flood gate that also houses one or more pumps. A pump gate allows to discharge water also during times of negative head by pumping, while lifting it allows for maximum discharge when free flow is possible. The motion of the pumps and the interaction with the flow may then be a source of dynamic excitation. This concept has also been considered for the Afsluitdijk in earlier stages of the renovation project.

Finally, the developed design methods may also be of interest in other fields of engineering. Confined wave impacts for example also occur under the deck of offshore platforms as for instance studied by De Sonnevile et al. (2015). Semi-analytical methods have been more common in the field of offshore engineering to predict the dynamic behaviour of structure in fluid (Tsouvalas and Metrikine, 2016). The combination with methods to probabilistically predict wave impacts may be useful in this field. Also sloshing in tanks of LNG carriers may lead to violent wave impacts (Abrahamsen and Faltinsen, 2011; Dias and Ghidaglia, 2018). In that field, it is more common than in hydraulic engineering to experimentally test designs for thousands of wave impacts. A probabilistic design method combining a semi-analytical fluid-structure interaction model with an impulsive wave impact model may present opportunities to predict the reliability of such designs completely theoretically.

IMPLEMENTING THE PRESENTED METHODS IN DESIGN PRACTICE

Existing design approaches for flood gates under wave impacts that make use of a dynamic amplification factor were shown to both underestimate and overestimate the stress and fatigue damage of gates depending on the location and case specifics. Two novel methods were presented that include several aspects that the existing approaches lack, such as the multiple mode behaviour of the structure and the effect of consecutive wave impacts. In principle, it is therefore recommended to implement the presented methods in design practice.

Figure 9.2 gives an overview of the different model components that are applied within these design methods. A wave impact model is applied that combines regular linear or higher order wave theory with impulse theory. For large scale hydraulic structures it is likely profitable to perform experiments aimed at the the specific situation to reduce the uncertainty in the prediction of the wave loads. The semi-analytical model then predicts the response of the flood gate immersed in fluid. The semi-analytical model requires the mode shapes and frequencies of the in vacuo gate as input. A finite element model can be applied for this purpose (see Chapter 4). Structural engineers generally set up a finite element to design flood gates for (quasi-)static loads. This entails hydrostatic loads and quasi-steady wave loading, but also impulsive wave loading after application of a



been included in the presented methods.

The presented design methods explicitly predict the response to all wave impacts in a governing design storm or even over the entire lifetime of the structure. Defining a single or set of governing waves may reduce the amount of simulations required to a level where more conventional finite elements methods become computationally feasible. However,

predicting the governing sequence of waves is much less obvious for the dynamic than for the (quasi-)static behaviour of the gate. Moreover, this will also differ for fatigue and the ultimate stress. Nevertheless, it is expected that there are some opportunities to simplify the design method on this aspect. One approach could for example be to define a design value (for instance the 0.1% exceedance value) of the impulsive impact of a single or two consecutive wave impacts for the given design storm. The impact duration may then be varied systematically within the range of possible values to find the governing dynamic response of the flood gate. Moreover, the relevance of consecutive wave impacts may be captured in an formula that includes both the amount of damping in the system and the peak wave period in the spectrum, which determines the time periods in between wave impacts. The developed semi-analytical fluid-structure interaction now provides the possibility to study these opportunities and compare the resulting design response to the outcome of the complete reliability analysis.

Capturing the dynamic response of the flood gate in more simplified methods with the required accuracy for design is more challenging. Applying a general coefficient in the dynamic amplification factor approach to account for higher mode behaviour is not recommended. Apart from leading to suboptimal designs, such a coefficient will not be very effective in terms of safety as some parts of the gate where stress occur due to higher modes are completely overlooked in the single mode representation. Models that incorporate higher mode behaviour such as the one developed in this thesis or coupled finite elements are then necessary. Moreover, the amount of involved variables (types of supports, reinforcement beam arrangement, front plate thickness, ratios between width and height of the gate, water levels, and more) makes it impossible to derive design tables that are practically relevant. Representing the gate as a multi degree of freedom system in combination with an assumed mode approach for the interaction with the fluid might be possible for some cases. The hydrodynamic coefficients could then be derived numerically and applied separately to each relevant mode shape, such that it is not necessary to derive an analytical solution for the interaction. Also the feasibility of this simplification could be studied by comparing results to the developed semi-analytical solution.

10

CONCLUSIONS AND RECOMMENDATIONS

10.1 CONCLUSIONS

A model has been developed in this thesis to predict the dynamic behaviour of a flood gate immersed in fluid. An experimental study has been performed to validate the model and provide further insight on the phenomena involved with wave impacts on flood gates. The model has then been applied as the basis of a novel design method to assess the safety and fatigue life of flood gates subjected to wave impact loading. The main conclusions of the thesis are presented below, grouped based on the three main topics of the thesis.

MODELLING WORK

It has been shown that the fluid-structure interaction involved with vertical flood gate vibrations can be modelled successfully by a semi-analytical mode matching approach. Within the mode matching method, the gate vibrations are first expressed in terms of in-vacuo modes while the liquid motion is described as a superposition of linear potentials. A semi-analytical solution is then derived for the response of the coupled system to any time-varying force. The situation at the Afsluitdijk of a vertical gate in a discharge sluice forms the basis for the geometry considered in the developed model.

The fluid-structure interaction model has been made suitable for situations of increasing levels of complexity in several development steps. In the most basic form, the gate was modelled as a thin plate and assumed to be situated in an infinitely long discharge sluice (Chapter 2). The mode shapes and frequencies of the in vacuo gate were found analytically. It was shown that also composite fluid domains can be represented accurately by extending the analytical fluid-structure interaction solution (Chapter 3). This makes it possible to accurately represent the situation of a gate in a discharge sluice of limited length with an overhanging structure in front that may cause confined wave impacts. This situation might for example occur when culverts or bridge decks are situated on top of discharge sluices. The wave impacts on the flood gates in the Afsluitdijk in the Netherlands are of this type. Finally, coupling the semi-analytical method to a finite element model proved to enable a detailed prediction of the structural stresses for more realistic gate designs (Chapter 4). A gate design consisting of a front plate supported by horizontal and vertical stiffeners was considered. The finite element model is employed to retrieve the in vacuo mode shapes and frequencies of this design. The final version of the developed fluid-structure interaction model has been made available on the 4TU repository (Tieleman, 2022, [link](#)).

The model improves the existing analytical methods on several aspects. The two-way fluid-structure interaction is implicitly considered in the model without simplifications, such as assuming the shape of the in vacuo modes of the gate unaltered by the presence of fluid (the ‘assumed modes approach’). Both the effect of surface waves and compressibility on the hydrodynamic response are taken into account in the approach. In this way, the hydrodynamic fluid pressure exerted on the gate is predicted accurately in both low and high frequency regimes. Moreover, the fluid-structure interaction model includes higher mode behaviour of the structure. By means of a design optimization case study it was demonstrated that the model can be effectively applied in the design of flood gates under wave impact loading. A substantially different optimal design was found compared to what would be expected based on existing quasi-static methods, in which the stiffeners were located in the middle of the gate instead of the top and bottom

where the highest fluid pressures occurred. This confirms the relevance of the described improvements.

The main benefit of the developed model approach compared to existing finite element methods is its computational efficiency in solving the two way fluid-structure interaction. The developed model proved to give similar results as conventional FE software at only a fraction of the computational time of the latter (Chapter 2-4). This makes the model particularly effective in performing preliminary design studies in which many parameters are varied or fatigue calculations and probabilistic assessments in which many load cases over long periods must be considered. This benefit has been utilized in the design methods presented in this thesis.

EXPERIMENTAL WORK

Experiments of confined wave impacts on flexible gate structures with an overhang have been carried out. These experiments entailed regular and irregular test conditions for various water levels. Additionally, supporting static loading and hammer impact tests were carried out. Two gate designs were tested: a plain gate of which the flexible part consists of a solid steel plate, and a reinforced gate in which reinforcement beams additionally support the front plate. The experimental approach is an extension of previous experiments of wave impacts on a rigid wall (De Almeida and Hofland, 2020b, 2021). This allows a direct comparison with the results of those studies, isolating the effect of the flexibility of the structure.

A preliminary validation of the developed fluid-structure interaction model was performed. The first few resonance frequencies of the gate in fluid predicted by the model were within 3–6% of the experimental results for the generally governing water level at the overhang. Compared to the models commonly applied in design, the developed model thus is able to accurately predict the higher resonance frequencies of the immersed gate. The predicted response to wave impact loading was compared the measurements in the regular wave impact tests. The aim of this validation was to obtain an indication whether all relevant physical phenomena that govern the response of flood gates to wave impacts are covered in the developed model. One of the main assumptions of the developed modelling framework is that the wave impact may be modelled as an external load. In the validation study, the force input was based on previous experiments of confined wave impacts on a rigid vertical wall with overhang. Some differences between the predictions and measurements were found regarding the dominant response frequencies and the magnitude and damping of the higher mode response. However, overall the predictions showed good agreement with the measurement results, providing a first verification that modelling the wave impact as an external force is acceptable. The validation study showed no reduction in accuracy of the predictions for wave impacts with air entrapment under the overhang. This indicates that it is possible to account for the presence of air in the prediction of the wave load instead of explicitly modelling it as a domain in the fluid-structure interaction response model.

The model predictions best matched the measurements for a structural damping factor of $\eta = 0.035$. Although applied as structural damping in the model, this amount of damping is higher than would be expected based on material damping alone and must thus originate from other sources such as friction in the supports and the loss of energy

through the surrounding flume structure. This provides some indication of the amount of damping for these type of phenomena. More research is needed however to be able to better predict the amount of damping from various sources for practical applications.

The experiments additionally resulted in a valuable dataset, made publicly available for research on the 4TU repository (Tieleman et al., 2022a, [link](#)), that can be used to further study wave impacts on flexible structures. The data may for instance be used to study the effect of phenomena such as air entrapment and air entrainment on the response of the fluid-structure system in more detail. The irregular wave tests closely match realistic conditions and can for example be used to further validate the probabilistic design approaches presented in this thesis.

IMPROVED DESIGN METHODS FOR FLOOD GATES SUBJECTED TO WAVE IMPACTS

Flood gates are generally designed based on a quasi-static approach in present engineering practice. A dynamic amplification factor is then applied to account for the effect of the vibrations, which is derived from a single degree of freedom representation of the structure. The fluid-structure interaction is not explicitly solved but included by using hydrodynamic coefficients. These hydrodynamic coefficients are usually derived from a linear potential flow model with an fluid assumed incompressible and excluding surface waves.

This thesis studied the effect of compressibility and surface waves on the response of the fluid to gate vibrations based on an exact analytical solution of the schematised system (Chapter 6). Ranges were derived in terms of excitation frequencies and water depths for which compressibility and surface waves have a significant effect on the magnitude of the hydrodynamic pressure and must thus be taken into account. Results show that for typical flood gate dimensions and excitation frequencies both surface waves and compressibility are important. However, only compressibility plays a role for the excitation frequencies involved with wave impacts and typical vertical flood gate dimensions. A first theoretical analysis showed that a small amount air present in the surrounding fluid can even result in compressibility effects at much lower excitation frequencies than otherwise expected. More research is needed however to obtain insight in the amount of entrained air for wave impact problems. Neglecting the effect of compressibility and surface waves in existing approaches may be a conservative assumption in terms of damping but not necessarily for the overall response of the structure. Furthermore, dimensionless values for the added mass and damping including the effect of compressibility and surface waves have been presented for gates of various boundary conditions. These coefficients can for example be applied in a finite element model of the in vacuo gate, however only when the problem under consideration allows for such a simplified representation of the interaction between the structure and fluid.

Two methods have been presented in this thesis for the design or assessment of flood gates subjected to wave impacts. The first method regards the ultimate limit state safety of the flood gate based on the failure criterion of exceeding the maximum yield stress in the structure (Chapter 7), while the second method is aimed at predicting the fatigue lifetime of the flood gate (Chapter 8). Both failure mechanisms proved to be relevant based on the performed case studies. The method regarding the safety in relation to the critical yield stress criterion was employed in a simplified reliability analysis that explicitly quantifies the failure probability of the flood gate for a given design storm. For this purpose, the

response of the gate is predicted for a large number of storm simulations in a Monte Carlo type analysis, in which each storm could have a duration of several hours and involve thousands of wave impacts. Recently validated pressure-impulse theory is employed to predict the wave impact loads on the gate. The free surface elevation, wave impact duration and impact impulse are all considered stochastically. The resulting maximum stress in the gate showed a large variation over the storm simulations in the case study even though thousands of waves occurred in each storm. These results may ultimately be utilized to derive more accurate safety factors in semi-probabilistic design methods. The method for assessing the fatigue lifetime of the flood gate defines a joint probability function of the wind velocity and mean water level based on historical data adjusted for long term effects such as climate change. This probability function is then translated to a set of discrete load cases and an associated probability of occurrence. For each load case, the wave loads are predicted probabilistically taking into account uncertainties in for example the durations of the wave impacts. A Monte Carlo analysis can be performed for each load case as in the first design method. However, in contrast to the variation in the ultimate stress response over simulations of a single governing design storm, the variation in predicted fatigue lifetime showed to be limited over the simulations. Predicting the dynamic response to every single wave during a governing design storm or over the lifetime of the structure is a novelty within the field of hydraulic engineering. At least when no concessions are made on the accuracy of the physical modelling of the involved fluid-structure interaction processes. The computational efficiency of the developed semi-analytical model has enabled this. Predicting the response of the flood gate to each storm simulation using existing time-domain finite element models would computationally be an impossible mission.

The developed design methods and underlying fluid-structure interaction model have been applied to several case studies inspired by the situation at the Afsluitdijk. Several aspects that are not captured in common existing design methods turned out to be crucial in the design of flood gates. First, higher modes show to have a significant impact on the maximum stress occurring for typical flood gates subjected wave impacts. For fatigue damage, the higher modes even turned out to be governing. In the case study, a dynamic amplification factor (DAF) approach based on a single degree of freedom representation of the structure substantially overestimated the fatigue damage at some points of the gate (by about 20-50%) and underestimated it at other points (up to 100%). This makes such an approach much less reliable in the design of these type of flood gates under wave impact loading. Second, the wave impact with the highest peak pressure is often assumed to be governing in present design practice. However, the governing response of the flood gate showed to be dominated mainly by the magnitude of the pressure impulse of the wave impact. The pressure impulse of a wave impact links the magnitude of the peak pressure to the duration of the impact and can be predicted better. This assumption therefore leads to an underestimation of the maximum response of the structure. Third, gate vibrations may not fully damp out between wave impacts depending on the time between impacts and the amount of damping in the system. The sequence and exact moment of wave impacts then influence the maximum response of the flood gate. This effect is not included in the conventional design methods, but is captured well within the presented methods. In the performed case study, the dynamic amplification factor method underestimated the

fatigue damage with approximately 10–15% due to this specific effect. Above findings show the relevance of the implementation of the developed method in the design or assessment of the reliability of flood gates under wave impacts.

10.2 RECOMMENDATIONS

Based on the findings in this thesis and the discussion presented in this chapter, the following recommendations are made:

1. Implement the presented methods as an alternative of the dynamic amplification factor approach for the design of flood gates subjected to wave impacts. For cases outside of the applicability range of the developed underlying fluid-structure interaction model (Tieleman, 2022, [link](#)), resort to other methods that capture higher mode vibrations of the structure and as much as possible of the fluid-structure interaction process. The likely higher computational effort required by alternative methods may be partially countered by implementing measures such as selective sampling in the presented probabilistic design methods.

Incorporate this philosophy also in the design guidelines. The guideline for water retaining structures in the Netherlands (Van Breem et al., 2018) now references Kolkman and Jongeling (2007a) in which the dynamic amplification approach is described to predict the response of flexible structures under wave impact loading. Many other guidelines only describe the Goda–Takahashi formula for wave loads implicitly including the dynamic behaviour of the structure, which is not applicable to impulsive impact loads on vertical slender hydraulic structures (Kortenhaus et al., 1999; Meinen et al., 2020).

2. Monitor the dynamic behaviour of the existing or new gates at the Afsluitdijk during a storm with wave impacts. The overhanging structure at both the existing and newly designed discharge locks of the Afsluitdijk are situated such that wave impacts can occur relatively frequently. This makes monitoring the behaviour of the gates under impact loading feasible and provides an interesting opportunity to measure the dynamic response of a real life flood gate under wave impact loads. Such measurements are expected to be effective in investigating uncertainties such as slack in the supports and damping in the system.
3. Perform full scale laboratory measurements on flood gates to further study the local wave and structure interaction and the effect of air entrapment and entrainment. Laboratory experiments are more suitable for this purpose than prototype measurements as testing these phenomena requires accurate control of the test conditions. Laboratory experiments of wave impacts on a flexible flood gate were performed as part of this thesis. Valuable data is provided to study these phenomena (Tieleman et al., 2022a, [link](#)). However, especially regarding the characteristics of wave impacts and phenomena where air is involved, scale effects will play a role. Full scale experiments are therefore a valuable addition in further research (see also previous recommendation).
4. Include also the uncertainties of the responsive system and model uncertainty in the probabilistic design methods in addition to the variation in the wave loading. By including all relevant stochastic variables in the probabilistic methods, it becomes

possible to analyse which source of uncertainty contributes most to the overall outcome of the reliability analyses. These are the uncertainties that should be focused on in further research. The amount of damping in the system, from sources such as friction in the supports, entrapped and entrained air, and interaction with the surrounding structure, is expected to be the most relevant aspect for further inquiry.

5. Prevent the occurrence of confined wave impacts in the design by avoiding overhanging elements or by measures such as breakwaters, rather than dimensioning the gate to withstand these loads. When the occurrence of wave impacts cannot be completely avoided, reduce the loads by implementing measures such as venting gaps (Hofland et al., 2019). The occurrence of impacts will generally have a large impact on the design of flood gates as these lead to higher loads than for example the hydrostatic head difference and quasi-steady waves. Moreover, even though the research performed here, predicting the dynamic response to these impacts still goes accompanied with quite some uncertainty. This makes measures to prevent impact loads less costly than dimensioning the structure to withstand these loads.

REFERENCES

- Abrahamsen, B.C., Faltinsen, O.M., 2011. The effect of air leakage and heat exchange on the decay of entrapped air pocket slamming oscillations. *Physics of Fluids* 23, 102107. doi:[10.1063/1.3638612](https://doi.org/10.1063/1.3638612).
- Adhikari, S., 2000. Damping Models for Structural Vibration. Ph.D. thesis.
- Airy, G.B., 1845. Tides and waves.
- Amabili, M., Frosali, G., Kwak, M., 1996. Free vibrations of annular plates coupled with fluids. *Journal of Sound and Vibration* 191, 825–846. doi:[10.1006/jsvi.1996.0158](https://doi.org/10.1006/jsvi.1996.0158).
- Amabili, M., Kwak, M.K., 1996. Free vibrations of circular plates coupled with liquids: Revising the lamb problem. *Journal of Fluids and Structures* 10, 743–761. doi:[10.1006/jfls.1996.0051](https://doi.org/10.1006/jfls.1996.0051).
- Anami, K., Ishii, N., Knisely, C., 2004. Field vibration tests and dynamic stability analysis of a full-scaled tainter-gate, in: American Society of Mechanical Engineers, Pressure Vessels and Piping Division (Publication) PVP, pp. 81–88. doi:[10.1115/PVP2004-3008](https://doi.org/10.1115/PVP2004-3008).
- Anami, K., Ishii, N., Knisely, C.W., 2012. Added mass and wave radiation damping for flow-induced rotational vibrations of skinplates of hydraulic gates. *Journal of Fluids and Structures* 35, 213–228. doi:[10.1016/j.jfluidstructs.2012.07.008](https://doi.org/10.1016/j.jfluidstructs.2012.07.008).
- Bagnold, R.A., 1939. Interim Report on Wave-Pressure Research. Technical Report 7. Institution of Civil Engineers. doi:[10.1680/ijoti.1939.14539](https://doi.org/10.1680/ijoti.1939.14539).
- Battjes, J.A., Groenendijk, H.W., 2000. Wave height distributions on shallow foreshores. *Coastal Engineering* 40. doi:[10.1016/S0378-3839\(00\)00007-7](https://doi.org/10.1016/S0378-3839(00)00007-7).
- Benasciutti, D., Tovo, R., 2006. Comparison of spectral methods for fatigue analysis of broad-band Gaussian random processes. *Probabilistic Engineering Mechanics* 21, 287–299. doi:[10.1016/j.probengmech.2005.10.003](https://doi.org/10.1016/j.probengmech.2005.10.003).
- Bretschneider, C.L., 1959. Wave variability and wave spectra for wind-generated gravity waves. Beach Erosion Board, Tech. Memo. US Army Corps of Engineers, N° 113.
- Brincker, R., Zhang, L., Andersen, P., 2001. Modal identification of output-only systems using frequency domain decomposition. *Smart Materials and Structures* 10, 441–445. doi:[10.1088/0964-1726/10/3/303](https://doi.org/10.1088/0964-1726/10/3/303).
- Bullock, G., Crawford, A., Hewson, P., Walkden, M., Bird, P., 2001. The influence of air and scale on wave impact pressures. *Coastal Engineering* 42, 291–312. doi:[10.1016/S0378-3839\(00\)00065-X](https://doi.org/10.1016/S0378-3839(00)00065-X).

- Bullock, G., Obhrai, C., Peregrine, D., Bredmose, H., 2007. Violent breaking wave impacts. Part 1: Results from large-scale regular wave tests on vertical and sloping walls. *Coastal Engineering* 54, 602–617. doi:[10.1016/j.coastaleng.2006.12.002](https://doi.org/10.1016/j.coastaleng.2006.12.002).
- Chen, X., Hofland, B., Altomare, C., Suzuki, T., Uijttewaal, W., 2015. Forces on a vertical wall on a dike crest due to overtopping flow. doi:[10.1016/j.coastaleng.2014.10.002](https://doi.org/10.1016/j.coastaleng.2014.10.002).
- Chen, X., Hofland, B., Molenaar, W., Capel, A., Van Gent, M.R., 2019. Use of impulses to determine the reaction force of a hydraulic structure with an overhang due to wave impact. *Coastal Engineering* 147, 75–88. doi:[10.1016/j.coastaleng.2019.02.003](https://doi.org/10.1016/j.coastaleng.2019.02.003).
- Chen, X., Hofland, B., Uijttewaal, W., 2016. Maximum overtopping forces on a dike-mounted wall with a shallow foreshore. *Coastal Engineering* 116, 89–102. doi:[10.1016/j.coastaleng.2016.06.004](https://doi.org/10.1016/j.coastaleng.2016.06.004).
- Chen, X., Jonkman, S.N., Pasterkamp, S., Suzuki, T., Altomare, C., 2017. Vulnerability of Buildings on Coastal Dikes due to Wave Overtopping. *Water* 9, 394. doi:[10.3390/w9060394](https://doi.org/10.3390/w9060394).
- Clausen, W.E., Hopper, A.T., Hulbert, L.E., Leissa, A.W., 1969. A comparison of approximate methods for the solution of plate bending problems. *AIAA Journal* 7, 920–928.
- COMSOL, 2018. COMSOL Multiphysics Reference Manual, version 5.3. Technical Report. URL: www.comsol.com.
- Cooker, M.J., Peregrine, D.H., 1995. Pressure-impulse theory for liquid impact problems. *Journal of Fluid Mechanics* 297, 193–214. doi:[10.1017/S0022112095003053](https://doi.org/10.1017/S0022112095003053).
- Cuomo, G., 2007. Wave impacts on vertical seawalls and caisson breakwaters. *Bulletin of the International Navigation Association* 127, 25–38.
- Cuomo, G., Allsop, W., Bruce, T., Pearson, J., 2010. Breaking wave loads at vertical seawalls and breakwaters. *Coastal Engineering* 57, 424–439. doi:[10.1016/j.coastaleng.2009.11.005](https://doi.org/10.1016/j.coastaleng.2009.11.005).
- van Dalen, K.N., Tsouvalas, A., Metrikine, A.V., Hoving, J.S., 2015. Transition radiation excited by a surface load that moves over the interface of two elastic layers. *International Journal of Solids and Structures* 73-74, 99–112. doi:[10.1016/j.ijsolstr.2015.07.001](https://doi.org/10.1016/j.ijsolstr.2015.07.001).
- De Almeida, E., Hofland, B., 2020a. Experimental Observations on Impact Velocity and Entrapped Air for Standing Wave Impacts on Vertical Hydraulic Structures with Overhangs. *Journal of Marine Science and Engineering* 8, 857. doi:[10.3390/jmse8110857](https://doi.org/10.3390/jmse8110857).
- De Almeida, E., Hofland, B., 2020b. Validation of pressure-impulse theory for standing wave impact loading on vertical hydraulic structures with short overhangs. *Coastal Engineering* 159, 103702. doi:[10.1016/j.coastaleng.2020.103702](https://doi.org/10.1016/j.coastaleng.2020.103702).

- De Almeida, E., Hofland, B., 2021. Standing wave impacts on vertical hydraulic structures with overhangs for varying wave fields and configurations. *Journal of Coastal and Hydraulic Structures* 1, 1–24. doi:[10.48438/jchs.2021.0010](https://doi.org/10.48438/jchs.2021.0010).
- De Almeida, E., Hofland, B., Jonkman, S.N., 2019. Wave Impact Pressure-Impulse on Vertical Structures with Overhangs, in: *Coastal Structures*, pp. 86–96. doi:[10.18451/978-3-939230-64-9_010](https://doi.org/10.18451/978-3-939230-64-9_010).
- De Almeida, E., Hofland, B., Tieleman, O.C., Antonini, A., Jonkman, B., 2022. Hydraulic design loads for confined wave impacts. *Journal of Coastal and Hydraulic Structures* (to be submitted) .
- De Sonnevile, B., Hofland, B., Mowinkel, A., Paulsen, B.T., 2015. Wave impact loads on offshore gravity based structure. *Proceedings of the International Conference on Offshore Mechanics and Arctic Engineering - OMAE* 1, 1–10. doi:[10.1115/OMAE201541879](https://doi.org/10.1115/OMAE201541879).
- Dias, F., Ghidaglia, J.M., 2018. Slamming: Recent Progress in the Evaluation of Impact Pressures. *Annual Review of Fluid Mechanics* 50, 243–273. doi:[10.1146/annurev-fluid-010816-060121](https://doi.org/10.1146/annurev-fluid-010816-060121).
- Downing, S., Socie, D., 1982. Simple rainflow counting algorithms. *International Journal of Fatigue* 4, 31–40. doi:[10.1016/0142-1123\(82\)90018-4](https://doi.org/10.1016/0142-1123(82)90018-4).
- Erdbrink, C.D., 2014. Modelling flow-induced vibrations of gates in hydraulic structures. Ph.D. thesis. University of Amsterdam.
- Ergin, A., Ugurlu, B., 2003. Linear vibration analysis of cantilever plates partially submerged in fluid. *Journal of Fluids and Structures* 17, 927–939. doi:[10.1016/S0889-9746\(03\)00050-1](https://doi.org/10.1016/S0889-9746(03)00050-1).
- European committee for Standardization, 2006. Eurocode 3: Design of steel structures. Technical Report.
- Fu, Y., Price, W.G., 1987. Interactions between a partially or totally immersed vibrating cantilever plate and the surrounding fluid. *Journal of Sound and Vibration* 118, 495–513. doi:[10.1016/0022-460X\(87\)90366-X](https://doi.org/10.1016/0022-460X(87)90366-X).
- Gibson, F.W., 1970. Measurement of the Effect of Air Bubbles on the Speed of Sound in Water. *The Journal of the Acoustical Society of America* 48. doi:[10.1121/1.1912260](https://doi.org/10.1121/1.1912260).
- Goda, Y., 2000. Random seas and design of maritime structures. World Scientific Publishing Co. Pte. Ltd 15, 1–462.
- Gorman, D.G., Horáček, J., 2007. Analysis of the free vibration of a coupled plate/fluid interacting system and interpretation using sub-system modal energy. *Engineering Structures* 29, 754–762. doi:[10.1016/j.engstruct.2006.06.017](https://doi.org/10.1016/j.engstruct.2006.06.017).

- Groeneweg, J., Geerse, C., Gautier, C., van Haaren, D., Camarena Calderon, A., Vuik, V., 2013. Hydraulische randvoorwaarden voor het ontwerp van de versterking van de Afsluitdijk. Technical Report. Deltares.
- Groeneweg, J., van der Westhuysen, A., van Vledder, G., Jacobse, S., Lanssen, J., van Dongeren, A., 2009. WAVE MODELLING IN A TIDAL INLET: PERFORMANCE OF SWAN IN THE WADDEN SEA. doi:[10.1142/9789814277426_0035](https://doi.org/10.1142/9789814277426_0035).
- Harris, D.A., 1991. Noise Control Manual. Van Nostrand Reinhold. doi:[10.1007/978-1-4757-6009-5](https://doi.org/10.1007/978-1-4757-6009-5).
- Hasselmann, K., 1973. Measurements of wind-wave growth and swell decay during the Joint North Sea Wave Project (JONSWAP). Technical Report.
- Hattori, M., Tsujioka, N., 1997. Dynamic Response of Vertical Elastic Walls to Breaking Wave Impact, in: Coastal Engineering 1996, American Society of Civil Engineers, New York, NY. pp. 2456–2469. doi:[10.1061/9780784402429.190](https://doi.org/10.1061/9780784402429.190).
- Hedges, T.S., 1995. Regions of validity of analytical wave theories. Proceedings of the Institution of Civil Engineers: Water, Maritime and Energy 112. doi:[10.1680/iwtme.1995.27656](https://doi.org/10.1680/iwtme.1995.27656).
- Helsdingen, M., 2021. Experimental modal validation of a semi-analytical method for assessing dynamic behaviour of flood gates (MSc thesis).
- Hofland, B., Kaminski, M., Wolters, G., 2011. LARGE SCALE WAVE IMPACTS ON A VERTICAL WALL. Coastal Engineering Proceedings 1, 15. doi:[10.9753/icce.v32.structures.15](https://doi.org/10.9753/icce.v32.structures.15).
- Hofland, B., Passos, M., de Almeida, E., 2019. Effect of Venting Holes to Relieve Wave Impact Pressures on Flood Gates with Overhangs, in: Coastal Structures Conference 2019, pp. 190–199. doi:[10.18451/978-3-939230-64-9_020](https://doi.org/10.18451/978-3-939230-64-9_020).
- Holthuijsen, L.H., 2007. Waves in Oceanic and Coastal Waters. volume 1. Cambridge University Press, Cambridge. doi:[10.1017/CB09780511618536](https://doi.org/10.1017/CB09780511618536).
- Horáček, J., Trnka, J., Veselý, J., Gorman, D.G., 1995. Vibration analysis of cylindrical shells in contact with an annular fluid region. Engineering Structures 17, 714–724. doi:[10.1016/0141-0296\(95\)00003-P](https://doi.org/10.1016/0141-0296(95)00003-P).
- Huang, J., Chen, G., 2022. Experimental study of wave impact on a vertical wall with overhanging horizontal cantilever slab and structural response analysis. Ocean Engineering 247, 110765. doi:[10.1016/j.oceaneng.2022.110765](https://doi.org/10.1016/j.oceaneng.2022.110765).
- Hughes, S.A., 1984. TMA Shallow-water spectrum: description and applications. Technical Report.
- van den Hurk, B., Tank, A.K., Lenderink, G., van Ulden, A., van Oldenborgh, G.J., Katsman, C., van den Brink, H., Keller, F., Bessembinder, J., Burgers, G., Komen, G., Hazeleger, W., Driffhout, S., 2006. KNMI Climate Change Scenarios 2006 for the Netherlands. KNMI Scientific Report WR 2006-01 .

- Ishii, N., Knisely, 1992. Flow-induced vibration of shell-type long-span gates. *Journal of Fluids and Structures*, 681–703.
- Jensen, F.B., Kuperman, W.A., Porter, M.B., Schmidt, H., 2011. *Computational Ocean Acoustics*. Springer New York, New York, NY. doi:[10.1007/978-1-4419-8678-8](https://doi.org/10.1007/978-1-4419-8678-8).
- Jongejan, R.B., Maaskant, B., 2015. Quantifying Flood Risks in the Netherlands. *Risk Analysis* 35, 252–264. doi:[10.1111/risa.12285](https://doi.org/10.1111/risa.12285).
- Jonkman, S.N., Steenbergen, R.D.J.M., Morales-Nápoles, O., Vrouwenvelder, A.C.W.M., Vrijling, J.K., 2016. Probabilistic Design: Risk and Reliability Analysis in Civil Engineering. Technical Report. Delft University of Technology.
- Kerboua, Y., Lakis, A.A., Thomas, M., Marcouiller, L., 2008. Vibration analysis of rectangular plates coupled with fluid. *Applied Mathematical Modelling* 32, 2570–2586. doi:[10.1016/j.apm.2007.09.004](https://doi.org/10.1016/j.apm.2007.09.004).
- Kidger, J., 2012. ANSYS - Fluid-Structure Interaction (FSI) with System Coupling System Coupling. Technical Report. ANSYS UK Ltd.
- Kirkgöz, S., 1990. An experimental investigation of a vertical wall response to breaking wave impact. *Ocean Engineering* 17, 379–391. doi:[10.1016/0029-8018\(90\)90030-A](https://doi.org/10.1016/0029-8018(90)90030-A).
- Kisacik, D., Troch, P., Van Bogaert, P., Caspeele, R., 2014. Investigation of uplift impact forces on a vertical wall with an overhanging horizontal cantilever slab. *Coastal Engineering* 90, 12–22. doi:[10.1016/j.coastaleng.2014.04.011](https://doi.org/10.1016/j.coastaleng.2014.04.011).
- Kleiberg, T.N.J., Tieleman, O.C., Versluis, M., Hofland, B., Kortlever, W., Ten Oever, E., 2022. A novel design method for wave-induced fatigue of flood gates. To be submitted to *Journal of Coastal and Hydraulic Structures*.
- Klein Tank, A., Beersma, J., Bessembinder, J., Van den Hurk, B., Lenderink, G., 2014. KNMI 14: Klimaatscenario's voor Nederland. Technical Report.
- KNMI, 2020. Daily historical weather data of the Netherlands. URL: <http://projects.knmi.nl/klimatologie/daggegevens/selectie.cgi>.
- Kolkman, P., 1988. A simple scheme for calculating the added mass of hydraulic gates. *Journal of Fluids and Structures* 2, 339–353. doi:[10.1016/S0889-9746\(88\)90051-5](https://doi.org/10.1016/S0889-9746(88)90051-5).
- Kolkman, P.A., Jongeling, T.H.G., 2007a. Dynamic behaviour of hydraulic structures - Part A. WL | Delft Hydraulics.
- Kolkman, P.A., Jongeling, T.H.G., 2007b. Dynamic behaviour of hydraulic structures - Part B. WL | Delft Hydraulics.
- Korobkin, A.A., 1998. Wave Impact on the Center of an Euler Beam. *Journal of Applied Mechanics and Technical Physics Prikladnaya Mekhanika i Tekhnicheskaya Fizika* 39, 134–147.

- Korobkin, A.A., Khabakhpasheva, T.I., 2006. Regular wave impact onto an elastic plate. *Journal of Engineering Mathematics* 55, 127–145. doi:[10.1007/s10665-005-0191-8](https://doi.org/10.1007/s10665-005-0191-8).
- Kortenhaus, A., Oumeraci, H., Allsop, N., McConnell, K., Van Gelder, P., Hewson, P., Walkden, M., Müller, G., Calabrese, M., Vicinanza, D., 1999. Wave impact loads - pressures and forces, in: *Final Proceedings, 693 MAST III, PROVERBS-Project. chapter IIa: Hydro*, pp. 1–44.
- Kvalsvold, Faltinsen, O.M., 1993. Hydroelastic modelling of slamming against wetdecks, in: *8th International Workshop on Water Waves and Floating Bodies*, pp. 57–60.
- Kwak, M.K., 1996. Hydroelastic Vibration of Rectangular Plates. *Journal of Applied Mechanics* 63, 110–115. doi:[10.1115/1.2787184](https://doi.org/10.1115/1.2787184).
- Kwak, M.K., Kim, K.C., 1991. Axisymmetric vibration of circular plates in contact with fluid. *Journal of Sound and Vibration* 146, 381–389. doi:[10.1016/0022-460X\(91\)90696-H](https://doi.org/10.1016/0022-460X(91)90696-H).
- Kwak, M.K., Yang, D.H., 2013. Free vibration analysis of cantilever plate partially submerged into a fluid. *Journal of Fluids and Structures* 40, 25–41. doi:[10.1016/j.jfluidstructs.2013.03.005](https://doi.org/10.1016/j.jfluidstructs.2013.03.005).
- Lamb, H., 1921. On the vibrations of an elastic plate in contact with water. *Proceedings of the Royal Society of London. Series A, Containing Papers of a Mathematical and Physical Character* 98, 205–216.
- Leblond, C., Sigrist, J., Auvity, B., Peerhossaini, H., 2009. A semi-analytical approach to the study of an elastic circular cylinder confined in a cylindrical fluid domain subjected to small-amplitude transient motions. *Journal of Fluids and Structures* 25, 134–154. doi:[10.1016/j.jfluidstructs.2008.04.004](https://doi.org/10.1016/j.jfluidstructs.2008.04.004).
- Leissa, A.W., 1969. *Vibration of plates*. NASA; United States, Washington, D.C.
- Matsuishi, M., Endo, T., 1968. Fatigue of metal subjected to varying stress. *Japan Society of Mechanical Engineers, Fukuoka, Japan* 68, 37—40.
- Meinen, N.E., Steenbergen, R.D.J.M., Hofland, B., Jonkman, S.N., 2020. Applicability of the Goda–Takahashi Wave Load Formula for Vertical Slender Hydraulic Structures. *Journal of Marine Science and Engineering* 8, 868. doi:[10.3390/jmse8110868](https://doi.org/10.3390/jmse8110868).
- Mindlin, R.D., 1951. Influence of Rotatory Inertia and Shear on Flexural Motions of Isotropic, Elastic Plates. *Journal of Applied Mechanics* 18. doi:[10.1115/1.4010217](https://doi.org/10.1115/1.4010217).
- Miner, M., 1945. Cumulative fatigue damage. *Journal of Applied Mechanics* 12, A159–A164.
- Minikin, R., 1950. *Winds, Waves, and Maritime Structures: Studies in Harbour Making and in the Protection of Coasts*. Griffin. URL: <https://books.google.nl/books?id=wAghAAAAAAAJ>.

- Naudascher, E., Rockwell, D., 1994. Flow-Induced Vibrations: An Engineering Guide. *Journal of Fluid Mechanics* doi:[10.1017/S0022112095230180](https://doi.org/10.1017/S0022112095230180).
- Newland, D.E., 2012. An introduction to random vibrations, spectral & wavelet analysis. Courier Corporation.
- Oumeraci, H., Kortenhaus, A., Allsop, W., De Groot, M., Couch, R., Vrijling, H., Voortman, H., 2001. Probabilistic Design Tools for Vertical Breakwater.
- Pastor, M., Binda, M., Harčarik, T., 2012. Modal Assurance Criterion. *Procedia Engineering* 48, 543–548. doi:[10.1016/j.proeng.2012.09.551](https://doi.org/10.1016/j.proeng.2012.09.551).
- Pearson, K., 1895. Notes on Regression and Inheritance in the Case of Two Parents. *Proceedings of the Royal Society of London* 58, 240–242.
- Powell, J.H., Roberts, J.H.T., 1922. On the Frequency of Vibration of Circular Diaphragms. *Proceedings of the Physical Society of London* 35, 170–182. doi:[10.1088/1478-7814/35/1/321](https://doi.org/10.1088/1478-7814/35/1/321).
- Ramkema, C., 1978. A model law for wave impacts on coastal structures. *Coastal Engineering Proceedings* 16, 2308–2327.
- Reissner, E., 1945. The Effect of Transverse Shear Deformation on the Bending of Elastic Plates. *Journal of Applied Mechanics* 12. doi:[10.1115/1.4009435](https://doi.org/10.1115/1.4009435).
- Rijkswaterstaat, 2020a. Project overview Afsluitdijk. URL: <https://www.rijkswaterstaat.nl/water/projectenoverzicht/afsluitdijk>.
- Rijkswaterstaat, 2020b. Rijkswaterstaat Waterinfo. URL: <https://waterinfo.rws.nl/>.
- Rychlik, I., 1993. On the ‘narrow-band’ approximation for expected fatigue damage. *Probabilistic Engineering Mechanics* 8, 1–4. doi:[10.1016/0266-8920\(93\)90024-P](https://doi.org/10.1016/0266-8920(93)90024-P).
- Schmidt, H., Tango, G., 1986. Efficient global matrix approach to the computation of synthetic seismograms. *Geophysical Journal International* 84, 331–359. doi:[10.1111/j.1365-246X.1986.tb04359.x](https://doi.org/10.1111/j.1365-246X.1986.tb04359.x).
- Schweckendiek, T., Kanning, W., Jonkman, S.N., 2014. Advances in reliability analysis of the piping failure mechanism of flood defences in the Netherlands. *Heron* 59, 101–127.
- Sobey, R.J., 2009. Analytical solutions for steep standing waves. *Proceedings of the Institution of Civil Engineers: Engineering and Computational Mechanics* 162. doi:[10.1680/eacm.2009.162.4.185](https://doi.org/10.1680/eacm.2009.162.4.185).
- Tadjbakhsh, I., Keller, J.B., 1960. Standing surface waves of finite amplitude. *Journal of Fluid Mechanics* 8, 442. doi:[10.1017/S0022112060000724](https://doi.org/10.1017/S0022112060000724).
- Takashi, S., 1994. A proposal of impulsive pressure coefficient for design of composite breakwater, in: *Proceedings of the International Conference on Hydrotechnical Engineering for Port and Harbor Construction*, pp. 489–504.

- Tanrikulu, A., Kirkgöz, M., DüNDAR, C., 2002. Theoretical and experimental investigation of a vertical wall response to wave impact. *Ocean Engineering* 29, 769–782. doi:[10.1016/S0029-8018\(01\)00052-X](https://doi.org/10.1016/S0029-8018(01)00052-X).
- Technische Adviescommissie voor de Waterkeringen, 2003. Leidraad Kunstwerken. Technical Report.
- Tieleman, O.C., 2016. The dynamic behaviour of pump gates in the Afsluitdijk (MSc thesis).
- Tieleman, O.C., 2022. Fluid-structure interaction model to predict bending vibrations of flood gates (software). doi:<https://doi.org/10.4121/19204788>.
- Tieleman, O.C., De Almeida, E., Hofland, B., Lourens, E., Helsdingen, M., 2022a. Experimental data of confined wave impacts on flexible gates with an overhang (dataset). doi:<https://doi.org/10.4121/18865796>.
- Tieleman, O.C., Hofland, B., Jonkman, S.N., 2018. Bending Vibrations of the Afsluitdijk Gates Subjected to Wave Impacts: A Comparison of Two Design Methods, in: *Proceedings of the 34th PIANC World Congress*.
- Tieleman, O.C., Hofland, B., Tsouvalas, A., de Almeida, E., Jonkman, S.N., 2021. A fluid–structure interaction model for assessing the safety of flood gate vibrations due to wave impacts. *Coastal Engineering* 170, 104007. doi:[10.1016/j.coastaleng.2021.104007](https://doi.org/10.1016/j.coastaleng.2021.104007).
- Tieleman, O.C., Tsouvalas, A., Hofland, B., 2019a. Effect of Compressibility and Surface Waves on the Hydrodynamic Pressures for a Vertical Flood Gate. *Proceedings of the Twenty-ninth (2019) International Ocean and Polar Engineering Conference*, 3349–3356.
- Tieleman, O.C., Tsouvalas, A., Hofland, B., Peng, Y., Jonkman, S.N., 2019b. A three dimensional semi-analytical model for the prediction of gate vibrations immersed in fluid. *Marine Structures* 65, 134–153. doi:[10.1016/j.marstruc.2018.12.007](https://doi.org/10.1016/j.marstruc.2018.12.007).
- Tieleman, O.C., Vorderregger, R., Hofland, B., Tsouvalas, A., Jonkman, S.N., 2022b. A hybrid semi-analytical and finite element model to predict flood gate vibrations. To be published.
- Timoshenko, S., Woinowsky-krieger, S., 1959. *Theory of Plates and Shells*. McGraw-Hill.
- Tsouvalas, A., 2015. Underwater noise generated by offshore pile driving. Ph.D. thesis. Delft University of Technology. doi:[10.4233/uuid:55776f60-bbf4-443c-acb6-be1005559a98](https://doi.org/10.4233/uuid:55776f60-bbf4-443c-acb6-be1005559a98).
- Tsouvalas, A., van Dalen, K.N., Metrikine, A.V., 2015. The significance of the evanescent spectrum in structure-waveguide interaction problems. *The Journal of the Acoustical Society of America* 138, 2574–2588. doi:[10.1121/1.4932016](https://doi.org/10.1121/1.4932016).

- Tsouvalas, A., Metrikine, A., 2013. A semi-analytical model for the prediction of underwater noise from offshore pile driving. *Journal of Sound and Vibration* 332, 3232–3257. doi:[10.1016/j.jsv.2013.01.026](https://doi.org/10.1016/j.jsv.2013.01.026).
- Tsouvalas, A., Metrikine, A., 2014. A three-dimensional vibroacoustic model for the prediction of underwater noise from offshore pile driving. *Journal of Sound and Vibration* 333, 2283–2311. doi:[10.1016/j.jsv.2013.11.045](https://doi.org/10.1016/j.jsv.2013.11.045).
- Tsouvalas, A., Metrikine, A., 2016. Noise reduction by the application of an air-bubble curtain in offshore pile driving. *Journal of Sound and Vibration* 371, 150–170. doi:[10.1016/j.jsv.2016.02.025](https://doi.org/10.1016/j.jsv.2016.02.025).
- Tsouvalas, A., Molenkamp, T., Canny, K., Kroon, D., Versluis, M., Peng, Y., Metrikine, A., 2020. A mode matching technique for the seismic response of liquid storage tanks including soil-structure interaction, pp. 1–14. doi:[10.47964/1120.9001.18621](https://doi.org/10.47964/1120.9001.18621).
- Tubaldi, E., Amabili, M., 2013. Vibrations and stability of a periodically supported rectangular plate immersed in axial flow. *Journal of Fluids and Structures* 39, 391–407. doi:[10.1016/j.jfluidstructs.2013.03.003](https://doi.org/10.1016/j.jfluidstructs.2013.03.003).
- Tubaldi, E., Amabili, M., Alijani, F., 2015. Nonlinear vibrations of plates in axial pulsating flow. *Journal of Fluids and Structures* 56, 33–55. doi:[10.1016/j.jfluidstructs.2015.03.021](https://doi.org/10.1016/j.jfluidstructs.2015.03.021).
- US Army Corps of Engineers, 2002. Coastal Engineering Manual.
- Van Breem, B., Delhez, R., Jongejan, R., Casteleijn, A., 2018. Werkwijzer Ontwerpen Waterkerende Kunstwerken – Ontwerpverificaties voor de hoogwatersituatie. Rijkswaterstaat WVL Waterkeringen.
- Van der Wal, R.J., de Boer, G., 2004. Downtime Analysis Techniques for Complex Offshore and Dredging Operations, in: 23rd International Conference on Offshore Mechanics and Arctic Engineering, Volume 2, ASMEDC. pp. 93–101. doi:[10.1115/OMAE2004-51113](https://doi.org/10.1115/OMAE2004-51113).
- Vorderegger, R., 2019. Optimization of gate design in the Afsluitdijk based on dynamic wave impact (MSc thesis).
- Vrijling, J., 2001. Probabilistic design of water defense systems in The Netherlands. *Reliability Engineering & System Safety* 74, 337–344. doi:[10.1016/S0951-8320\(01\)00082-5](https://doi.org/10.1016/S0951-8320(01)00082-5).
- Wagner, H., 1932. Über Stoss- und Gleitvorgänge an der Oberfläche von Flüssigkeiten. *Zeitschrift für Angewandte Mathematik und Mechanik* 12.
- Wang, S., Garbatov, Y., Chen, B., Guedes Soares, C., 2016. Dynamic structural response of perforated plates subjected to water impact load. *Engineering Structures* 125, 179–190. doi:[10.1016/j.engstruct.2016.05.011](https://doi.org/10.1016/j.engstruct.2016.05.011).

- Waterloopkundig Laboratorium, 1990. Spuisluizen Afsluitdijk Den Oever: dynamisch gedrag hefschuiven bij golfklappen (verslag prototypemetingen). Technical Report.
- Westergaard, H.M., 1933. Water Pressure on Dams During Earthquaks. Transactions of the American Society of Civil Engineers 95, 418–433.
- Wood, D., Peregrine, D., 1997. Wave Impact Beneath a Horizontal Surface, in: Coastal Engineering 1996, American Society of Civil Engineers, New York, NY. pp. 2573–2583. doi:[10.1061/9780784402429.199](https://doi.org/10.1061/9780784402429.199).
- Zheng, X., Gao, S., Huang, Y., 2020. Cross-mode couplings for the fatigue damage evaluation of trimodal Gaussian processes. Ocean Engineering 202, 107177. doi:[10.1016/j.oceaneng.2020.107177](https://doi.org/10.1016/j.oceaneng.2020.107177).

LIST OF PUBLICATIONS

- [1] **O. C. Tieleman**, Hofland, B., Jonkman, S. N., Bending Vibrations of the Afsluitdijk Gates Subjected to Wave Impacts: A Comparison of Two Design Methods, Proceedings of the 34th PIANC World Congress (2018).
- [2] **Tieleman, O.C.**, Tsouvalas, A., Hofland, B., Peng, Y., Jonkman, S. N., A three dimensional semi-analytical model for the prediction of gate vibrations immersed in fluid, Marine Structure 65 (2019) 134-153.
- [3] **Tieleman, O.C.**, Tsouvalas, A., Hofland, B., Effect of Compressibility and Surface Waves on the Hydrodynamic Pressures for a Vertical Flood Gate, Proceedings of the Twenty-ninth International Ocean and Polar Engineering Conference (2019) 3349–3356.
- [4] **Tieleman, O.C.**, Hofland, B., Tsouvalas, A., De Almeida, E., Jonkman, S. N., A fluid-structure interaction model for assessing the safety of flood gate vibrations due to wave impacts, Coastal Engineering 170 (2021) 104007.
- [5] T. N. J. Kleiberg, **Tieleman, O.C.**, M. Versluis, Hofland, B., Kortlever, W., Ten Oever, E., A novel design method for wave-induced fatigue of flood gates, Submitted to the Journal of Coastal and Hydraulic Structures (2022).
- [6] **Tieleman, O.C.**, Vorderegger, R., Hofland, B., Tsouvalas, A., Jonkman, S. N., A hybrid semi-analytical and finite element parametric model to predict flood gate vibrations, Submitted to Engineering Structures (2022).

CURRICULUM VITAE

12-09-1991	Born in Amsterdam, The Netherlands
2003 – 2009	Barlaeus Gymnasium
2009 – 2013	Bachelor Civil Engineering Delft University of Technology
2013 – 2016	Master Civil Engineering (cum laude) Delft University of Technology Track Hydraulic Engineering
2016 – 2022	PhD Research Delft University of Technology Faculty Civil Engineering and Geosciences, Section of Hydraulic Structures and Flood Risk
2016 –	Consultant Horvat & Partners

ACKNOWLEDGEMENTS

Working on this thesis has been a great experience. One that I would not want to have missed, but would not repeat either. I would like to take this opportunity to thank everyone that has supported me over the last years.

Starting with my supervisory team, Bas Hofland, Apostolos Tsouvalas and Bas Jonkman. Without your guidance and seemingly unlimited scientific knowledge I could not have written this thesis. The discussions with Bas Hofland were not only productive, but also a boost for morale due to his unwavering enthusiasm and positivity. If not for Apostolos, I would now still be puzzling with some of the equations in this thesis. With his practical view, Bas Jonkman helped me to keep an eye on the end result and to navigate the bureaucracy of the university.

I would also like to express my gratitude to Rijkswaterstaat for providing the financial support for this research and for the opportunity to relate my thesis to relevant practical challenges. And to all other supporters of the DynaHicS research programme, amongst which Deltares, PT Structural and Witteveen+Bos.

My colleagues have made my time at the university an unforgettable experience. A special thanks to Ermano, Ece, Erik, Job and Stephan, with whom I shared the office for many years. The covid years have underlined how great this time really was. The experience of Ermano has made the experimental study in this thesis a success. And his research on wave impacts have been the basis for an important part of the presented design methods. I have also enjoyed the interaction with master students at the university. Thanks to Joachim Kleiberg, Ruben Vorderegger and Martijn Helsdingen, who have contributed directly to parts of this thesis. And I want to acknowledge my colleagues at Horvat & Partners, whose flexibility made it possible to combine two interesting positions over these years.

Last, but not least, I want to thank my family, Wouter, Paola and Joia, for the opportunities they have given me and their encouragement. And of course, Annebelle, for designing the beautiful cover of this thesis and her love and support all these years.

*Orson Cosmo Tieleman
Amsterdam, June 2022*